spatiotemporal cats
or, try herding 6 cats

siminos/spatiotemp, rev. 6188: last edit by Predrag Cvitanović, 01/20/2018

Predrag Cvitanović, Boris Gutkin, Li Han,
Rana Jafari, Han Liang, and Adrien K. Saremi

April 10, 2018

Contents

This is a project of many movable parts, so here is a guide where to blog specific topics (or where to find them)

Blog fearlessly: this is your own lab-book, a chronology of your learning and research that you might find invaluable years hence.

Chapter 1

Cat map

> If space is infinite, we are in no particular point in space.
> If time is infinite, we are in no particular point in time.
> — The Book of Sand, by Jorge Luis Borges

What is a natural way to cover the torus, in such a way that the dynamics and the partition borders are correctly aligned? You are allowed to coordinatize the unit torus by any set of coordinates that covers the torus by a unit area. The origin is fixed under the action of $\mathbf{A}$, and straight lines map into the straight lines, so Adler and Weiss did the natural thing, and used parallelograms (following Bowen [29] we shall refer to such parallelograms as 'rectangles') with edges parallel to the two eigenvectors of $\mathbf{A}$. Adler and Weiss observed that the torus in the new eigen-coordinates is covered by two rectangles, labelled A and B in figure 1.1. [1]

1.1 Adler-Weiss partition of the Thom-Arnol'd cat map

Figure 1.1 for the canonical Thom-Arnol'd cat map

remark 1.4

$$A = \begin{bmatrix} 2 & 1 \\ 1 & 1 \end{bmatrix} . \tag{1.1}$$

Note that [6]

$$\begin{bmatrix} 2 & 1 \\ 1 & 1 \end{bmatrix} = \begin{bmatrix} 1 & 1 \\ 1 & 0 \end{bmatrix}^2 , \tag{1.2}$$

so each of equivalence classes with respect to centralizer is split into two equivalence classes with respect to the group $\{\pm A^n \mid n \in \mathbb{Z}\}$.

[1] Predrag 2018-02-09: (1) motivate Manning multiples by doing the 1D circle map first. Maybe Robinson [86] does that.
(2) motivate spatiotemporal cat map by recent Gutkin *et al.* many-body paper

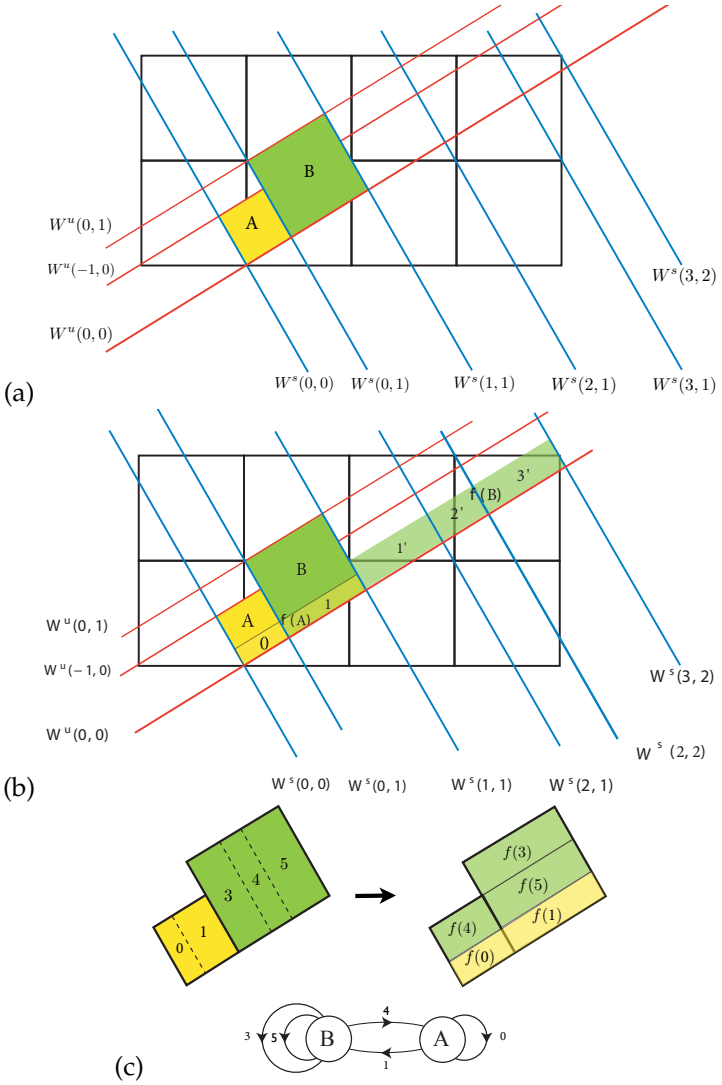

Figure 1.1: (a) Two-rectangles Adler-Weiss generating partition for the canonical Arnol'd cat map (1.1), with borders given by stable-unstable manifolds of the unfolded cat map lattice points near to the origin. (b) The first iterate of the partition. (c) The iterate pulled back into the generating partition, and the corresponding 5-letter transition graph. In (b) and (c) I have not bothered to relabel Crutchfield partition labels with our shift code. This is a "linear code," in the sense that for each square on can count how many side-lengths are needed to pull the overhanging part of $f(x)$ back into the two defining squares. (Figure by Crutchfield [37])

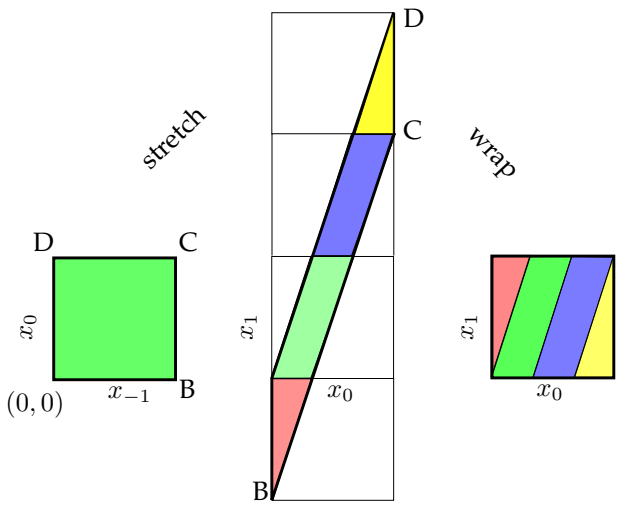

Figure 1.2: (Color online) The $s = 3$ Percival-Vivaldi cat map matrix (1.5) stretches the unit square into a parallelogram. Translations by m_0 from alphabet $\mathcal{A} = \{-1, 0, 1, 2\} = \{$red, green, blue, yellow$\}$ bring stray regions back onto the torus.

As another example, with $s = 4$, Manning [75] discusses a Markov partition for the cat map (also discussed by Anosov, Klimenko and Kolutsky [6])

$$A = \begin{bmatrix} 3 & 1 \\ 2 & 1 \end{bmatrix} . \tag{1.3}$$

2CB

In order to count all admissible walks, one associates with the transition graph such as the one in figure 1.1 (c) the *connectivity* matrix

$$C = \begin{bmatrix} 1 & 1 \\ 1 & 2 \end{bmatrix} , \tag{1.4}$$

where C_{ij} is the number of ways (number of links) of getting to i from j.

1.2 Adler-Weiss partition of the Percival-Vivaldi cat map

As illustrated in figure 1.2, the action of the cat map in the Percival-Vivaldi [83] "two-configuration representation" is given by the antisymmetric area preserving $[2\times2]$ matrix

$$\mathbf{A} = \begin{bmatrix} 0 & 1 \\ -1 & s \end{bmatrix} \tag{1.5}$$

For the Arnol'd value $s = 3$, in one time step the map stretches the unit square into a parallelogram, and than wraps it around the torus 3 times, as in figure 1.2. Visualise the phase space as a bagel, with x_0 axis a circle on the outside of the bagel. This circle is divided into three color segments, which map onto each other as you got in the x_1 axis direction. Now apply the inverse map - you get 3 strips intersecting the the above strips, for 9 rectangles in all: a full shift, i.e., a ternary Smale horseshoe. So on the torus there are only 3 strips - there is no distinction between the two outer letters $\mathcal{A}_1 = \{-1, 2\} = \{$red, yellow$\}$, it is the same third strip. The division into 2 triangles is an artifact of plotting the torus as a unit square. All complicated pruning of (the current draft of) Gutkin *et al.* [52] is a red herring, due to over-partitioning of the torus with a 4-letter alphabet.

This is stupid.

How do Adler and Weiss coordinates work out for the Arnol'd cat map in the Percival-Vivaldi representation (1.5) used here? First one needs to construct the eigen-coordinates.

example 1.3 p. 60

For $s > 2$ the stability multipliers $(\Lambda^+, \Lambda^-) = (\Lambda\,,\ \Lambda^{-1})$ are real,

$$\Lambda^{\pm} = \frac{1}{2}(s \pm D)\,, \qquad \Lambda = e^{\lambda}\,, \tag{1.6}$$

where $s = \Lambda + \Lambda^{-1}$, $\sqrt{D} = \Lambda - \Lambda^{-1}$, discriminant $D = s^2 - 4$, with a positive Lyapunov exponent $\lambda > 0$, and the right, left eigenvectors:

$$\begin{aligned} \{\mathbf{e}^{(+)}, \mathbf{e}^{(-)}\} &= \left\{ \begin{bmatrix} \Lambda^{-1} \\ 1 \end{bmatrix}, \begin{bmatrix} \Lambda \\ 1 \end{bmatrix} \right\} \\ \{\mathbf{e}_{(+)}, \mathbf{e}_{(-)}\} &= \left\{ [-\Lambda^{-1}, 1], [\Lambda, -1] \right\}, \end{aligned} \tag{1.7}$$

(where the overall scale is arbitrary). As the matrix is not symmetric, the $\{\mathbf{e}^{(j)}\}$ do not form an orthogonal basis.

What does this do to the partition of figure 1.2? The origin is still the fixed point. For a state space point in the new, dynamically intrinsic right eigenvector Adler-Weiss coordinate basis x'

$$\begin{pmatrix} x'_{t-1} \\ x'_t \end{pmatrix} = \begin{pmatrix} -\Lambda x_t + x_{t-1} \\ -\Lambda^{-1} x_t + x_{t-1} \end{pmatrix}.$$

the abscissa (x_{t-1} direction) is not affected, but the ordinate (x_t direction) is flipped and stretched/shrunk by factor $-\Lambda$, $-\Lambda^{-1}$ respectively,

$$\begin{pmatrix} x'_t \\ x'_{t+1} \end{pmatrix} = \begin{bmatrix} \Lambda^{-1} & 0 \\ 0 & \Lambda \end{bmatrix} \begin{pmatrix} x'_{t-1} \\ x'_t \end{pmatrix} - \begin{pmatrix} 0 \\ m_t \end{pmatrix},$$

preserving the vertical strip nature of the partition of figure 1.2. In the Adler-Weiss right eigenbasis, $\mathbf{A}$ acts by stretching the $\mathbf{e}^{(+)}$ direction by Λ, and shrinking the $\mathbf{e}^{(-)}$ direction by Λ^{-1}, without any rotation of either direction.

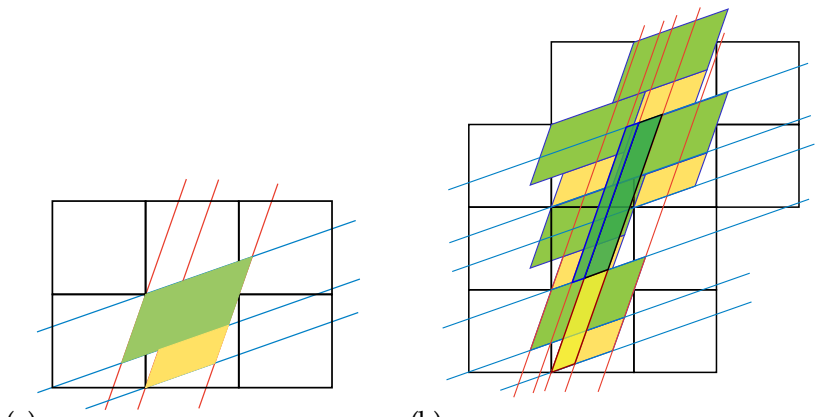

Figure 1.3: (a) The two-rectangle Adler-Weiss generating partition for the Percival-Vivaldi cat map (1.5), with borders given by cat map stable-unstable manifolds. (b) An abandoned attempt to identify the finite partition, since superseded by the partition of figure 1.6 (b) and figure 1.9.

Thus the Adler-Weiss coordinates preserve the convenient feature of the Percival-Vivaldi cat map, figure 1.2: the torus 'rewrapping' translations remain all vertical, specified by a single integer.

The angles of stable / unstable manifolds are irrational respective to the lattice, and they never hit another vertex (and so they do not close onto themselves under quotienting of translations).

Note that from figure 1.4 (a) to figure 1.4 (b) we have used the continuous translation invariance to center the large tile A within the unit square. That makes the time reversal invariance more explicit. It might not be obvious that the two parallelograms of figure 1.3 (a) tile the square lattice, but they do, as illustrated in figure 1.4 (a). Such tilings are known as 'Pythagorean'.

remark 1.5

Given the stable/unstable eigenvectors, the natural eigen-coordinates are given. I had first constructed a 2-rectangle generating partition for the Percival-Vivaldi [83] two-configuration representation (1.5) - it is a squashed and rotated version of figure 1.1 (a) drawn in figure 1.3 (a). The point is, after a linear change of coordinates one has finite grammar Adler-Weiss symbolic dynamics, and the symbolic dynamics is a linear code in sense of Boris, but this time with all admissible sequences generated as walks on a transition graph isomorphic to the one in figure 1.1 (c).

I actually like better the three-rectangle, time reversal symmetric generating partition of figure 1.5 and figure 1.6.

Thus we have constructed Percival-Vivaldi cat map coordinate transformation from the square to the intrinsic Adler-Weiss eigencoordinate basis. This is a LINEAR transformation. As this has been falling on deaf ears for last few years, let me say it again:

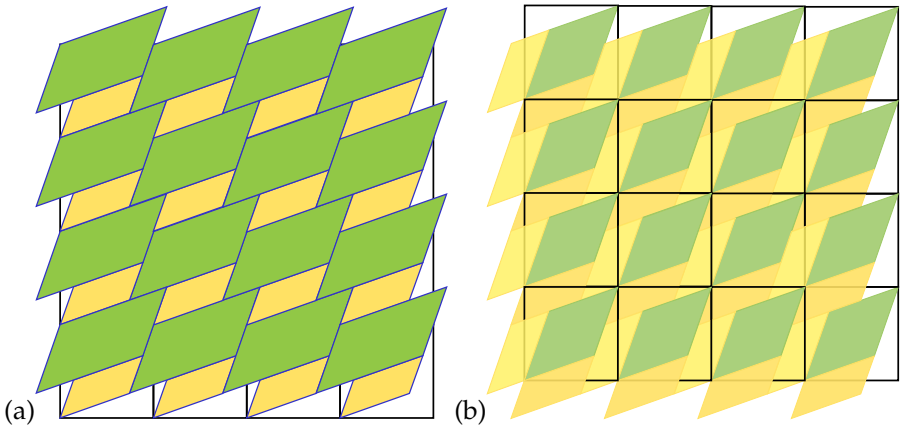

Figure 1.4: (a) [Abandoned] Tiling of the square lattice by the two-rectangle Adler-Weiss generating partition of figure 1.3 (a) for the Percival-Vivaldi cat map (1.5). (b) Tiling of the square lattice by the three-rectangle, time reversal symmetric generating partition. Note that we have used the continuous translation invariance to center the large tile A within the unit square (continued in figure 1.5 (a)).

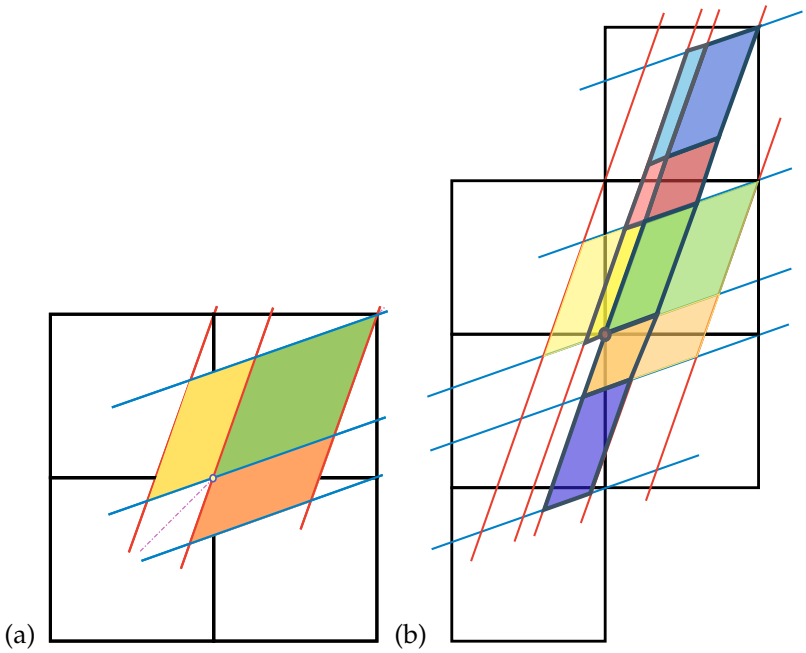

Figure 1.5: (a) The three-rectangle, time reversal symmetric generating partition for the Percival-Vivaldi cat map (1.5), with borders given by cat map stable-unstable manifolds. (b) The three-rectangle mapped one step forward in time.

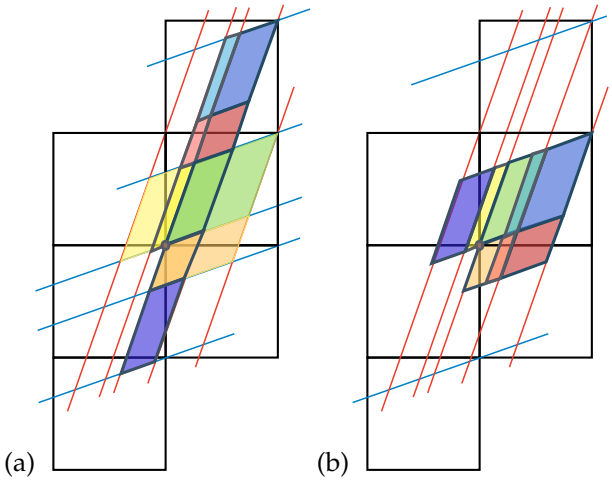

Figure 1.6: (a) The three-rectangle mapped one step forward in time. (b) The three-rectangle wrapped back onto the torus, along the unstable direction, yields 8-letter alphabet generating partition, with three-nodes transition graph. One could have kept the two-rectangle Adler-Weiss generating partition of figure 1.3 (a), in which case the alphabet is the standard 5 letters.

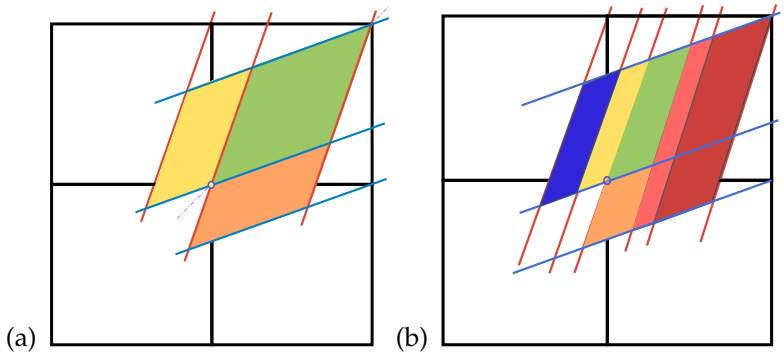

Figure 1.7: Figure 1.6 continued. (a) The three-rectangle, time reversal symmetric generating partition for the Percival-Vivaldi cat map (1.5), with borders given by cat map stable-unstable manifolds. (b) The three-rectangle subpartition, one step forward in time. A into three strips, B into three strips, B' into two strips, for a total of 8 forward links in the graph continue with a sensible coloring of these regions). Label the graph links by translations that bring these pieces back into the unit square. Under time reversal, interchange B and B', get the same partition going backwards in time. Then make it Lagrangian, meaning the combined graph should have undirected links (?).

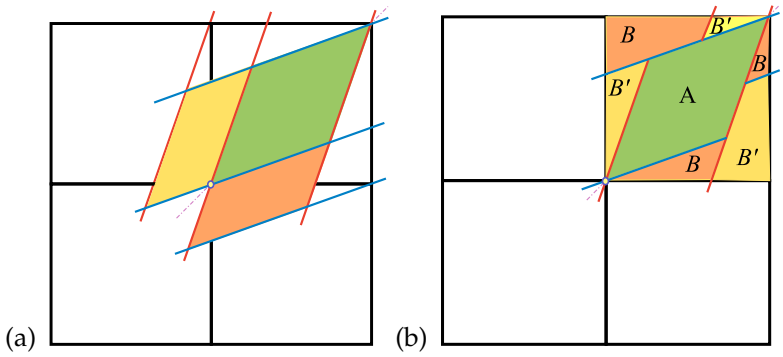

Figure 1.8: (a) The three-rectangle, time reversal symmetric generating partition for the Percival-Vivaldi cat map (1.5), with borders given by cat map stable-unstable manifolds. (b) The three-rectangle partition of the unit square (torus laid out). In this partition A already lies entirely within the unit square, while B and B' are wrapped around the torus, and only seem to consist of three pieces each, an artifact of the wrapping. The unit square borders have no physical meaning.

This is a LINEAR code,

as is every code in ChaosBook, as illustrated by the examples of sect. 1.10 that I worked out for feline pleasure some years back. Got that?

As Adler-Weiss partition is generating, there is noting for Dirichlet boundary conditions Green's functions to accomplish - all admissible symbol blocks are known. The problem is now *trivial*, in the Soviet sense (i.e., after a few years of work, I understand it).

What is wrong with the argument so far? I used Newtonian, evolution-in-time thinking to generate the $d = 1$ partition. That will not work in higher dimensions, so the above argument has to be recast in the Lagrangian form.

The cat map 2-step difference, Lagrangian form equation (1.51) can be written as

$$sx_t = x_{t+1} + x_{t-1} + m_t \,, \tag{1.8}$$

with $0 \geq x_1 < 1$ leading to the two inequalities ssp_{t+1}, x_{t-1} have to satisfy,

$$-m \leq x_0 + x_2 < s - m \,.$$

Be my guest - I'm going to bed:)

A few side, symmetry related remarks: we *must* quotient translation symmetries, do calculations in the elementary cell or, better still, the fundamental domain.

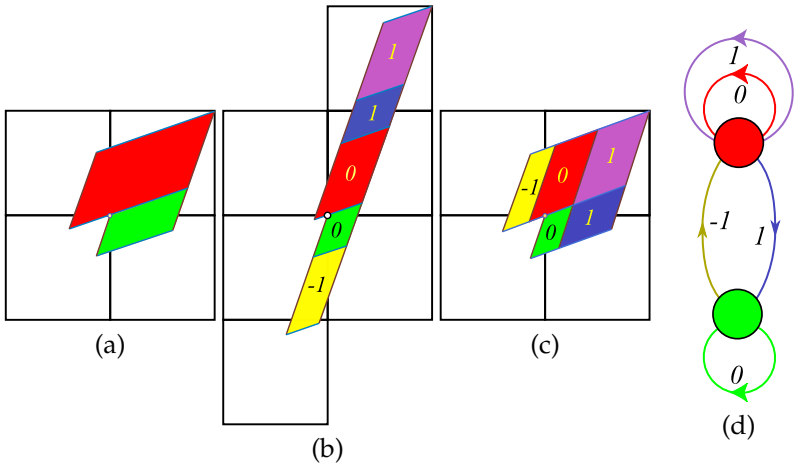

Figure 1.9: (Color online) (a) An Adler-Weiss generating partition of the unit torus with rectangles $\mathcal{M}_A$ (red) and $\mathcal{M}_B$ (green) for the Percival-Vivaldi cat map (1.5), with borders given by the cat map stable (blue) and unstable (dark red) manifolds. (b) Mapped one step forward in time, the rectangles are stretched along the unstable direction and shrunk along the stable direction. Sub-rectangles $\mathcal{M}_j$ that have to be translated back into the partition are indicated by color and labeled by their lattice translation $m_j \in \mathcal{A} = \{\underline{1}, 0, 1\}$, which also doubles as the 3-letter alphabet $\mathcal{A}$. (c) The sub-rectangles $\mathcal{M}_j$ translated back into the unit square yield a generating partition, with (d) the finite grammar given by the transition graph for this partition. The nodes refer to the rectangles A and B, and the five links correspond to the five sub-rectangles induced by one step forward-time dynamics. (Compare with figure 1.2. For details, see ChaosBook [38]).

1.2.1 Adler–Weiss linear code partition of the phase space

There are many ways to skin a cat. For example, due to the space reflection symmetry of the Percival-Vivaldi cat map, it is natural (especially in studies of deterministic diffusion on periodic lattices [10, 38]) to center the phase space unit interval [83] as $x \in [-1/2, 1/2)$. In that case the Arnol'd cat map of figure 1.2 has a 5-letter linear code $\mathcal{A} = \{\underline{2}, \underline{1}, 0, 1, 2\}$ in which the spatial reflection symmetry (**??**) is explicit (the "conjugate" of a symbol $m \in \mathcal{A}$ is simply $\bar{m} = -m$), with phase space partitions and pruning rules taking a symmetric form.

However, the deep problem with the Percival-Vivaldi linear code is that it does not yield a generating partition (for a glossary, see appendix **??**); the x_1, x_2 axis borders of the unit-square partition in figure 1.2 do not map onto themselves, resulting in the infinity of pruning rules (see table **??**). This problem has been elegantly resolved in 1967 by Adler and Weiss [2, 3, 7] who

utilized the stable / unstable manifolds of the fixed point at the origin in order to partition the torus into a two-rectangles generating partition (for details see, for example, Robinson [86] or Devaney [41]; Siemaszko and Wojtkowski [90] refer to such partitions as the 'Berg partitions', and Creagh [36] generalizes them to weakly nonliner mappings). For the Arnol'd cat map in the Percival-Vivaldi [83] "two-configuration representation" (1.5), such partition [38] is given in figure 1.9; following Bowen [29] one refers to parallelograms in the figure as 'rectangles'. Symbolic dynamics on this partition is a subshift of finite type, with the 3-letter alphabet

$$\mathcal{A} = \{\underline{1}, 0, 1\}\,, \tag{1.9}$$

that indicates the translation needed to return the given sub-rectangle $\mathcal{M}_j$ back into the two-rectangle partition $\mathcal{M} = \mathcal{M}_A \cup \mathcal{M}_B$. All admissible itineraries are generated by all walks on the transition graph of figure 1.9 (d). Rational and irrational initial coordinates generate periodic and ergodic orbits, respectively [65, 84], with phase space orbits uniquely labeled by the admissible bi-infinite itineraries of symbols from $\mathcal{A}$.

Note that this code is a linear code, as we are using the same "Lagrangian" cat map equation (**??**)

$$(\Box + 2 - s)\, x_t = -m_t\,, \tag{1.10}$$

but the integer translation m_t is now enforcing that the orbit $\{x_t\}$ always stays in the two-rectangle partition $\mathcal{M} = \mathcal{M}_A \cup \mathcal{M}_B$, in the sequence dictated by the itinerary $\{x_t\}$. Indeed, the only difference from the Percival-Vivaldi formulation is that we have traded in the arbitrary, unit-square cover of the torus of figure 1.2 for the dynamically intrinsic two-rectangles cover of figure 1.9, but the effect is magic - now for each admissible itinerary $\{m_t\}$ the same Green's functions as those introduced above yield the unique phase space orbit $\{x_t\}$. While Percival and Vivaldi [83] were well aware of Adler-Weiss partitions, they believed that their "coding is less efficient in requiring more symbols, but it has the advantage of linearity." This paper is first to construct a generating cat map partitions with a linear code.

The five sub-rectangles $\mathcal{M}_j$ of the two-rectangle partition $\mathcal{M} = \cup\mathcal{M}_j$ of figure 1.9 (c) motivate introduction of an alternative, 5-letter (colors) alphabet:

$$\bar{\mathcal{A}} = \{1, 2, 3, 4, 5\} = \{A^0A, B^1A, A^1A, B^0B, A^{\underline{1}}B\}\,, \tag{1.11}$$

which encodes the links of the transition graph of figure 1.9 (d).

The loop expansion of the determinant of the transition graph of figure 1.10 (b) is given by all non-intersecting walks on the graph [38]

$$\det(1 - zL) = 1 - z(t_1 + t_3 + t_4) - z^2(t_{25} - (t_1 + t_3)t_4)\,, \tag{1.12}$$

where t_p are traces over prime cycles, the three fixed points $t_1 = T_{A^0A}, t_3 = T_{A^1A}, t_4 = T_{B^0B}$, and the 2-cycle $t_{25} = T_{B^1AT_{A^1B}}$.

As the simplest application, consider counting all admissible cat map periodic orbits. This is accomplished by setting the non-vanishing links of the

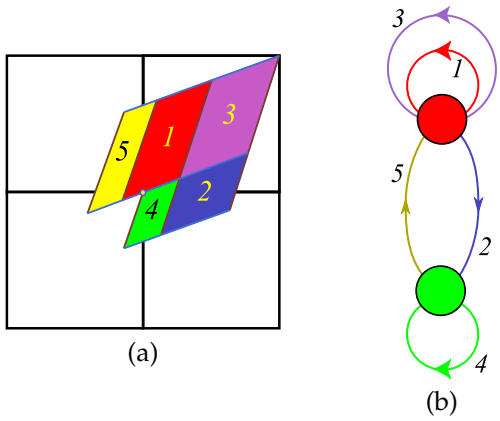

Figure 1.10: (Color online) (a) The sub-rectangles $\mathcal{M}_j$ of figure 1.9 (c), labeled by the compact 5-letter alphabet (1.11). (b) Admissible orbits correspond to walks on the transition graph of figure 1.9 (d), now labeled by alphabet $\bar{\mathcal{A}}$. For examples, see the loop expansion (1.12).

transition graph to $T_{ji} = 1$, and counting all periodic walks on the graph. This yields the cat maps topological zeta function [38, 62] (for the example at hand, $s = 3$),

$$1/\zeta(z) = \frac{1 - sz + z^2}{(1-z)^2}\,, \tag{1.13}$$

where the numerator $(1-z)^2$ corrects the overcounting of the fixed point at the origin due to assigning it to both $\mathcal{M}_A$ (twice) and $\mathcal{M}_B$ rectangles [74].

However, for our purposes, Adler–Weiss codes still have one fatal shortcoming, and are therefore not used in this paper: for L coupled cat maps the size of the alphabet $|\mathcal{A}|$ (the number of partitions of the phase space, a $2L$-dimensional unit hypercube) grows exponentially with L. [2] The Percival and Vivaldi [83] linear code that we utilize here currently appears to be the only bridge from a single cat map (**??**) to the coupled multi-particle spatial lattice (5.29).

1.3 Perron-Frobenius operators and periodic orbits theory of cat maps

[3]

[2] Predrag 2018-02-09: add Howie Weiss Bowen reference somewhere?

[3] Predrag 2017-08-28: "Average coordinate" depends on b.c.'s. Average coordinate (**??**) is computed for the the very unphysical Dirichlet boundary condition $x_z = 0$ for $z \in \mathcal{R}$ which breaks translation invariance. If one takes the much gentler, translationally invariant doubly periodic b.c., the "average coordinate" $\bar{x}_z$ is the invariant 2-torus periodic point, a more natural choice.

An extensive analysis of the periodic orbits of the cat map, following Percival and Vivaldi [83, 84] has been carried out by Keating [64].

Periodic boundary conditions: The Green's function for periodic lattice of period T is obtained by summing (**??**) over period T:

$$\tilde{g}_n = \sum_{j=-\infty}^{\infty} g_{n-j,T} = \frac{\Lambda^{-|n|} + \Lambda^{-|n-T|}}{(1-\Lambda^{-T})(\Lambda - \Lambda^{-1})} \,. \tag{1.14}$$

[4]

In practice one can supply only symbol sequences of finite length, in which case the truncated (**??**) returns a finite trajectory x_t, with a finite accuracy. However, a periodic orbit p of period n (an n-cycle) is infinite in duration, but specified by a finite admissible block $p = [m_1 m_2 \cdots m_n]$. To generate all admissible n-cycles for a given n, list all prime symbol sequences $[m_1 m_2, \cdots m_n]$, (one string per its n cyclic permutations, not composed from repeats of a shorter cycle), apply (**??**) with cyclic $[n \times n]$ $g_{tt'}$, and then apply modulus one to all points in the cycle,

$$x_t = \sum_{t'=t}^{n+t-1} g_{tt'} m_{t'} \qquad \mod 1 \,. \tag{1.15}$$

If the cycle is admissible, $\mod 1$ does not affect it. If it is inadmissible, add the string to the list of pruned symbol strings. One can even start with any random sequence $[m_1 m_2 \cdots m_n]$, have $\mod 1$ corral back the stray x_t's into the unit interval, and in this way map any inadmissible symbol sequence into an admissible trajectory of the same duration.

[5]

[4] Predrag 2017-08-03: please recheck: do you want to refer to (**??**) or (**??**) in the above?

[5] Predrag 2016-11-15: **Homework for all cats**: Write the correct (1.15) for an n-cycle. For inspiration: check ChaosBook.org discussion of the kneading theory, where such formula is written down for unimodal maps. Might require thinking.
Hint: the answer is in the paper:)

1.4 Generating functions; action

2CB

To understand the relation between the Hamiltonian and Lagrangian formulations, one needs to understand the discrete mapping generating function, such as (1.37). What follows is (initially) copied from Li and Tomsovic [70], *Exact relations between homoclinic and periodic orbit actions in chaotic systems* arXiv source file, then merged with the MacKay-Meiss-Percival action principle refs. [73, 77].

The main point is that in symplectic dynamics, the distance between two orbits is not measured by Euclidean distance (which is not invariant under symplectic transformations, and thus meaningless in the Hamiltonian phase space): *the (symplectic) distance between a pair of shadowing orbits is given by the difference of their actions.*

Consider a symplectic ("area preserving") map

$$x_{n+1} = M(x_n)\,, \qquad x_n = (q_n, p_n)$$

that maps x_n to x_{n+1} while preserving the symplectic area. If it satisfies the twist condition,

$$\partial p_{n+1}/\partial q_n \neq 0 \text{ for all } p_{n+1}, q_n\,, \tag{1.16}$$

then there exists a *generating function* $L(q_n, q_{n+1})$ such that [73, 77] the momenta can be computed from its derivatives

$$p_n = -\partial L(q_n, q_{n+1})/\partial q_n\,, \quad p_{n+1} = \partial L(q_n, q_{n+1})/\partial q_{n+1}\,. \tag{1.17}$$

The twist condition (1.16) ensures that

$$\frac{\partial^2 L}{\partial q_n \partial q_{n+1}} \neq 0\,. \tag{1.18}$$

We have to distinguish a *path*, which is any set of successive points $\{x_n\}$ in the phase space, from the unique *orbit segment* (in the ChaosBook convention, a trajectory) $M^k(x_n)$ from x_n to x_{n+k} generated by the *action*

$$W_{n,n+k} \equiv \sum_{i=n}^{n+k-1} L(q_i, q_{i+k})\,, \tag{1.19}$$

with momenta given by (1.17). In other words, not only q_n, but also p_n have to align from phase space point to phase space point,

$$\frac{\partial}{\partial q_n}\left(L(q_{n-1}, q_n) + L(q_n, q_{n+1})\right) = 0\,. \tag{1.20}$$

The orbit segment is a path that satisfies a variational principle, i.e., the stationarity of the action (1.19) at each orbit point q_i between the end points q_n

and q_{n+k}. For 1-dof systems, the geometrical interpretation of $W_{n,n+k}$ is that $L(q_n, q_{n+1})$ is, up to an overall constant, the phase-space area below the x_n to x_{n+1} path in the (q, p) phase plane.

example 1.1 p. 59

example 1.1

[6] For prime periodic orbit p of period $|p|$, the *action* of the orbit is:

$$W_p \equiv \sum_{n=0}^{|p|-1} L(q_n, q_{n+1}) \,. \tag{1.21}$$

W_p is the generating function that maps a point along the orbit for one primitive period. For the case of a fixed point p of period $|p| = 1$, the action is

$$W_p = L(q_p, q_p) \,, \tag{1.22}$$

where the generating function $L(q_p, q_p)$ maps x_p into itself in one iteration. For an aperiodic orbit $\{x_0\}$ going through the point x_0, the action, evaluated as the sum over an infinity of successive mappings,

$$W_{\{x_0\}} \equiv \lim_{N\to\infty} \sum_{n=-N}^{N-1} L(q_n, q_{n+1}) = \lim_{N\to\infty} W_{-N,N} \,, \tag{1.23}$$

is not necessarily convergent. However, the MacKay-Meiss-Percival action principle [73, 77] can be applied to obtain well defined action differences between pairs of orbits. For example, the *relative action* $\Delta W_{\{h_0\}\{x\}}$ between a fixed point x_p and its homoclinic orbit $\{h_0\}$, where $h_{\pm\infty} \to x_p$:

$$\begin{aligned} \Delta W_{\{h_0\}\{x_p\}} &\equiv \lim_{N\to\infty} \sum_{i=-N}^{N-1} [L(h_i, h_{i+1}) - L(x_p, x_p)] \\ &= \int_{U[x_p,h_0]} p\mathrm{d}q + \int_{S[h_0,x_p]} p\mathrm{d}q = \oint_{US[x_p,h_0]} p\mathrm{d}q \\ &= \mathcal{A}^{\circ}_{US[x_p,h_0]} \end{aligned} \tag{1.24}$$

where $U[x_p, h_0]$ is the segment of the unstable manifold from x_p to h_0, and $S[h_0, x_p]$ the segment of the stable manifold from h_0 to x_p. The $\circ$ superscript on the last line indicates that the area is interior to a path that forms a closed loop, and the subscript indicates the path: $US[x_p, h_0] = U[x_p, h_0] + S[h_0, x_p]$. The clockwise enclosure of an area is positive, counterclockwise negative. $\Delta W_{\{h_0\}\{x_p\}}$ gives the action difference between the homoclinic orbit segment $[h_{-N}, \cdots, h_N]$ and the length-$(2N + 1)$ fixed point orbit segment $[x_p, \cdots, x_p]$ in the limit

[6] Predrag 2018-01-21: Is this true? To go from the Hamiltonian (x_t, p_t) phase space formulation to the Newtonian (or Lagrangian) (x_{t-1}, x_t) *state space* formulation, replace p_t by $p_t = (x_t - x_{t-1})/\Delta t$, where $\Delta t = 1$.

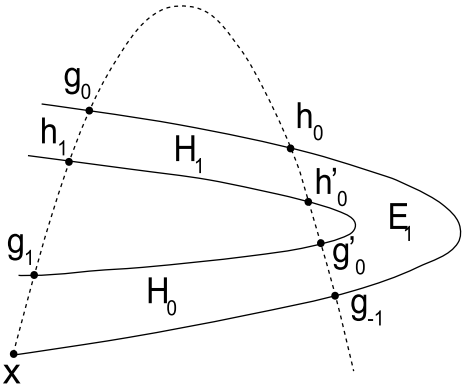

Figure 1.11: A sketch of a partial homoclinic tangle which forms a complete horseshoe structure. The unstable (stable) manifold of x is the solid (dashed) curve. There are two primary homoclinic orbits $\{h_0\}$ and $\{g_0\}$. $\mathcal{R}$ is the closed region bounded by loop $\mathcal{L}_{USUS[x,g_{-1},h_0,g_0]}$. (From ref. [70])

$N \to \infty$. In later sections, upon specifying the symbolic code of the homoclinic orbit $\{h_0\} \Rightarrow \overline{0}\gamma\overline{0}$, we also denote $\Delta W_{\{h_0\}\{x_p\}}$ alternatively as

$$\Delta W_{\{h_0\}\{x_p\}} = \Delta W_{\overline{0}\gamma\overline{0},\overline{0}} \tag{1.25}$$

by replacing the orbits in the subscript with their symbolic codes.

Likewise, a second important case is for the relative action between a pair of homoclinic orbits $\{h'_0\} \Rightarrow \overline{0}\gamma'\overline{0}$ and $\{h_0\} \Rightarrow \overline{0}\gamma\overline{0}$, which results in

$$\begin{aligned}
\Delta W_{\{h'_0\}\{h_0\}} &\equiv \lim_{N\to\infty} \sum_{i=-N}^{N-1} \left[L(h'_i, h'_{i+1}) - L(h_i, h_{i+1})\right] \\
&= \lim_{N\to\infty} \left[L(h'_{-N}, h'_N) - L(h_{-N}, h_N)\right] \\
&= \int_{U[h_0,h'_0]} p\mathrm{d}q + \int_{S[h'_0,h_0]} p\mathrm{d}q = \mathcal{A}^{\circ}_{US[h_0,h'_0]} \\
&= \Delta W_{\overline{0}\gamma'\overline{0},\overline{0}\gamma\overline{0}}
\end{aligned} \tag{1.26}$$

where $U[h_0, h'_0]$ is the segment of the unstable manifold from h_0 to h'_0, and $S[h'_0, h_0]$ the segment of the stable manifold from h'_0 to h_0. Due to the fact that the endpoints approach x_p forward and backward in time, one can also write

$$\begin{aligned}
\Delta W_{\{h'_0\}\{h_0\}} &= \lim_{N\to\infty} \Big[L(h'_{-(N+n)}, h'_{N+m}) - L(h_{-N}, h_N)\Big] \\
&\quad -(n+m)\mathcal{F}_0\,.
\end{aligned} \tag{1.27}$$

1.4.1 Linear stability

The 2016-11-11 draft of this section is based on excerpts from Mackay and Meiss [72] *Linear stability of periodic orbits in Lagrangian systems*, and Bolotin

and Treschev [27] *Hill's formula*.

Bolotin and Treschev write: [7] " In his study of periodic orbits of the three-body problem, Hill obtained a formula connecting the characteristic polynomial of the monodromy matrix of a periodic orbit with the infinite determinant of the Hessian of the action functional. A proof of Hill's formula was given by Poincaré [??]. Here two multidimensional generalizations of Hill's formula are given: for discrete Lagrangian systems (symplectic twist maps) and for continuous Lagrangian systems. Additional aspects appearing in the presence of symmetries or reversibility are discussed. Also studied is the change of the Morse index of a periodic trajectory upon reduction of order in a system with symmetries. "

In a Lagrangian system each path of finite length in the configuration space is assigned an action. For example, in a discrete-time one-degree-of-freedom Lagrangian system with coordinate x and Lagrangian $L(x, x')$, the finite paths are sequences (x_i), $m \leq i \leq n$, and the action of such a path is [8]

$$W = \sum_{i=m}^{n-1} L(x_i, x_{i+1}) \tag{1.28}$$

Any finite path for which the action is stationary with respect to variations of the segment keeping the endpoints fixed is called an orbit segment. Infinite paths for which each finite segment is an orbit segment are called orbits.

For discrete-time one-degree-of-freedom Lagrangian systems satisfying a periodicity condition (i.e., cat map):

$$L(x + 1, x' + 1) = L(x, x') + C \,, \tag{1.29}$$

one can consider generalised periodic paths, with

$$x_{i+q} = x_i + p \tag{1.30}$$

for some integers p, q. They are called periodic paths of type (p, q) (PC: presumably they relative periodic orbits, or pre-periodic orbits, with a rational winding number p/q). Orbits satisfying (1.30) are called periodic orbits of type (p, q), and are given by stationary points of the action

$$W = \sum_{i=0}^{q-1} L(x_i, x_{i+1}) \tag{1.31}$$

in the space of periodic paths of type (p, q).

If the constant C (the Calabi invariant [33]) in the periodicity condition (1.29) is zero, and the Lagrangian satisfies a convexity condition

$$L_{12}(x, x') < 0 \,, \tag{1.32}$$

[7] Predrag 2016-11-12: eventually move to remark 2.1

[8] Predrag 2018-02-11: merge with (1.19)

where subscript k refers to the derivative with respect to the kth argument, then the action of periodic paths of type (p, q) is bounded below, so there is a minimising path. Since its action is stationary, it gives a periodic orbit of type (p, q). There can be more than one minimising path. In particular, translating one minimising path by an integer in time or space or both gives another. This implies existence of saddle points of the action in between the minima, with one downward direction [1-3]. They are called minimax points, and give rise to minimax periodic orbits of type (p, q). The statement of the existence of at least two periodic orbits of each type (p, q) is known as the Poincaré-Birkhoff theorem.

The linear stability of a periodic orbit is determined by its multipliers, the eigenvalues of the derivative of the return map round the orbit. While the first variation of the action is by definition zero for an orbit, it seems reasonable that the multipliers of a penodic orbit might be obtained from the second variation of the action in the space of periodic paths. This has been shown in various cases. Hill derived a formula for the multipliers in the case of one-degree-of-freedom systems of the form kinetic minus potential [4], using a Fourier representation for periodic paths. Bountis and Helleman [28] and Greene [50] treated the case of discrete-time one-degree-of-freedom systems with

$$L_{12}(x, x') = -1\,. \tag{1.33}$$

Schmidt [89] finds n-tupling bifurcations by the criterion that the matrix of second variations of the action with respect to periodic paths of n times the period have a zero eigenvalue. In this note, we derive a formula (17) for the multipliers of a periodic orbit for general discrete-time one-degree-of-freedom systems.

As a corollary, we derive the old result that when the convexity condition is satisfied, the multipliers of a minimising orbit are a reciprocal pair of positive reals, and those of a minimax orbit are either a complex conjugate pair on the unit circle, or a reciprocal pair of negative reals. The result for minimising orbits was shown by Poincaré [9] for two-degree-of-freedom continuous-time systems, and Birkhoff [1] discusses the minimax case. Allroth [5] has found some partial results for higher-dimensional discrete-time systems. Stationarity of the action for an orbit of a discrete-time one-degree-of-freedom system implies that

$$L_2(x_{i-1}, x_i) + L_1(x_i, x_{i+1}) = 0\,. \tag{1.34}$$

Thus the tangent orbits δx_i satisfy [...]. The multipliers Λ of a periodic orbit of period q are defined by existence of a tangent orbit satisfying [...] residue of a periodic orbit one can easily solve for multipliers. [... losing steam]

Now $D(1)$ is the determinant of the matrix $M(1)$ of second variations of the action in the space of periodic paths of period q. So we have related the multipliers of a periodic orbit to the second variations of the action about the orbit. Our claims about the multipliers of minimising and minimax orbits follow directly. Under the convexity condition (1.32), the denominator is positive. At a

minimum of action (whether local or global):

$$D(1) \leq 0\,, \tag{1.35}$$

so the multipliers are real and positive. At a minimax with one downward direction:

$$D(1) \geq 0\,, \tag{1.36}$$

so the multipliers are on the unit circle or the negative real axis.

1.4.2 Generating function literature

The latest entry at the bottom for this blog

2016-11-11 Predrag I still cannot get over how elegant the Gutkin and Osipov [53] spatiotemporal cat map is. It is *linear*! ($\mod 1$, that is - the map is continuous for integer s). A 1-dimensional cat map has a Hamiltonian (1.50), and they have written down the 2-dimensional Lagrangian, their Eq. (3.1) (or the "generating function", as this is a mapping). Their spatiotemporal cat map generating function is defined on a spatiotemporal cylinder, infinite in time direction,

$$\begin{aligned} W(q_t, q_{t+1}) = &-\sum_{n=1}^{N} q_{nt} q_{1+n,t} - \sum_{n=1}^{N} q_{nt}(q_{n,t+1} + m^q_{n,t+1}) + \\ &+ \frac{a}{2}\sum_{n=1}^{N} q_{nt}^2 + \frac{b}{2}\sum_{n=1}^{N}(q_{n,t+1} + m^q_{n,t+1})^2 - m^p_{n,t+1} q_{n,t+1}\,, \end{aligned} \tag{1.37}$$

where $q_t = \{q_{nt}\}_{n=1}^{N}$ is a spatially periodic state at time t, with q_{nt} being the coordinate of nth "particle" $n = 1 \dots N$ at the moment of time $t \in \mathbb{Z}$, and $m^q_{n,t+1}, m^p_{n,t+1}$ are integer numbers which stand for winding numbers along the q and p directions of the 2N-torus. Note that $q_{1+n,t} = q_{1+(n \bmod N),t}$. The coefficients a, b, $s = a + b$ are integers which they specify. Gutkin and Osipov refer to the map generated by the action (1.37) as non-perturbed *coupled cat map*, and to an invariant 2-torus p as a "many-particle periodic orbit" (MPO) if q_{nt} is doubly-periodic, or "closed," i.e.,

$$q_{nt} = q_{n+L,t+T}\,, \quad n = 1, 2, \cdots, L\,, \quad t = 1, 2, \cdots, T\,.$$

Action of an invariant 2-torus p is

$$W_p = -\frac{1}{2}\sum_{t=1}^{T}\sum_{n=1}^{L} m_{nt} q_{nt} \tag{1.38}$$

2D symbolic representation Encode each invariant 2-torus (many-particle periodic orbit) p by a two dimensional (periodic) lattice of symbols a_{nt},

$(nt) \in \mathbb{Z}^2$, where symbols a_{nt} belong to some alphabet $\mathcal{A}$ of a small size. Each invariant 2-torus p is represented by $L \times T$ toroidal array of symbols:

$$\bar{\mathcal{A}}_p = \{a_{nt} | \, (nt) \in \mathbb{Z}^2_{LT}\} \, .$$

The Hamiltonian equations of motion can be generated using (1.17) but who needs them? Remember, a field theorist would formulate a spacetime symmetric field theory in a Lagrangian way, with the invariant action.

2016-11-11 Predrag "mean action" = the action divided by the period

Percival and Vivaldi [83] state the Lagrangian variational principle in Sect. 6. *Codes, variational principle and the static model*: [9]

The Lagrangian variational principle for the sawtooth map on the real line states that the action sum (1.79) is stationary with respect to variations of any finite set of configurations x_t. Their discussion of how "elasticity" works against the "potential" is worth reading. For large values of stretching parameter s, the potential wins out, and the state x_t falls into the m_tth well: "the code may be considered as a labelling of the local minima of the Lagrangian variational principle."

Dullin and Meiss [43] *Stability of minimal periodic orbits* does the calculations in great detail.

1.5 Noether's theorem

2016-11-23 Predrag A variational principle (such as the action (1.37) in case at hand) together with a continuous symmetry implies

> **Noether's theorem**: To every one-parameter, continuous group of symmetries of a Lagrangian dynamical system there corresponds a scalar, real-valued conserved quantity.

Is there is a version of it for discrete translations? What is the conserved quantity for a single cat map? What is it for the lattice? Internet says many contradictory things:

"The fact that a Lagrangian is unchanged by a discrete transformation is of no significance. There is no conserved quantity associated with the transformation."

"For infinite symmetries like lattice translations the conserved quantity is continuous, albeit a periodic one. So in such case momentum is conserved modulo vectors in the reciprocal lattice. The conservation is local just as in the case of continuous symmetries."

Read about it here.

[9] Predrag 2016-11-12: eventually move to remark 2.1

Mansfield [76] in proceedings here and in her talk defines *total difference* and says " Just as an integral of a total divergence depends only on the boundary data, so does the sum over lattice domain of a total difference."

She states the discrete Noether's Theorem, and in her Example 1.3.7 she shows that for a discretization of a standard mechanical Lagrangian, time invariance yields "energy" as a the conserved quantity.

Hydon and Mansfield [61].

Capobianco and Toffoli [34] *Can anything from Noether's Theorem be salvaged for discrete dynamical systems?* is fun to read (but ultimately unsatisfactory):

" we take the Ising spin model with both ferromagnetic and antiferromagnetic bonds. We show that –and why– energy not only acts as a generator of the dynamics for this family of systems, but is also conserved when the dynamics is time-invariant."

The *microcanonical Ising model* is strictly deterministic and invertible: on a given step, a spin will flip (that is, reverse its orientation) if and only if doing so will leave the sum of the potential energies of the four surrounding bonds unchanged. The Ising dynamics is a second-order recurrence relation. They define "energy" as the length of the boundary between 'up' and 'down' domains. While the magnetization—number of spins up minus number of spins down—may change with time, that length, and thus the energy, remains constant. The total energy of a system may be defined as

1. A real-valued function of the system's state,
2. that is additive,
3. and is a generator of the dynamics.

In a discrete Hamiltonian dynamics, a state is no longer a "position/momentum" pair $< q, p >$ as in the continuous case, but an ordered pair of configurations $< q_0, q_1 >$.

A second-order dynamical system has an evolution rule of the form

$$x_{t+1} = g(x_t, x_{t-1}) \,.$$

1.6 Cat map literature

1.6.1 Adler / Adler98

Predrag 2017-10-02 excerpts from or notes on
Adler [1] *Symbolic dynamics and Markov partitions*, (click here) an excellent overview

of symbolic dynamics techniques.

$$A = \begin{pmatrix} a & b \\ c & d \end{pmatrix} , \tag{1.39}$$

where a, b, c, d and $\det A = 1$. The row vectors

$$\{\mathbf{e}_{(+)}, \mathbf{e}_{(-)}\} = \left\{[c, \Lambda - a] , [c, \Lambda^{-1} - a]\right\} \tag{1.40}$$

are the left expanding / contracting eigenvectors. The matrix (1.39) is in general not symmetric, so $\{\mathbf{e}_{(j)}\}$ do not form an orthogonal basis. For matrix (1.5) the left eigenvectors are 2CB

$$\{\mathbf{e}_{(+)}, \mathbf{e}_{(-)}\} = \left\{[-1, \Lambda] , [-1, \Lambda^{-1}]\right\} , \tag{1.41}$$

in agreement with (1.7). I prefer the right eigenvectors basis $\{\mathbf{e}^{(j)}\}$, as it lies in the first quadrant.

1.6.2 Percival and Vivaldi / PerViv

Predrag 2016-05-29 excerpts from or notes on
Percival and Vivaldi [83] *A linear code for the sawtooth and cat maps* (click here)

"Completely chaotic systems are comparatively well understood, but they have been neglected as a starting point for the study of systems with divided phase space. It is the purpose of this and related papers to remedy this." 2CB

"When one starts with an integrable system, and perturbs it to introduce some chaos, new orbits and new classes of orbits keep on appearing by bifurcation processes, and they are very difficult to follow or to classify. It is better to start with a purely chaotic system and then reduce the chaos by *removing* orbits." [10]

"In this paper we present the symbolic dynamics of the sawtooth maps, and in the companion paper [84] *Arithmetical properties of strongly chaotic motions* the number theory for the periodic orbits of the automorphisms of the torus, including the cat maps."

"we start with the simplest systems that show the phenomena of interest-area preserving maps. The sawtooth maps are piecewise linear systems. They depend on a parameter K and for positive K they are completely chaotic. For positive *integer* K they are automorphisms of the torus, of which the simplest is the Arnol'd-Sinai cat map, with K = 1. We shall refer to all such toral automorphisms, with positive integer K, as cat maps. They are Anosov systems, continuous on the torus. On the other hand, when K is not an integer, the sawtooth map is discontinuous."

"Most of this paper is concerned with a 'linear code' for the symbolic dynamics of the sawtooth maps, including the cat maps. This code is chosen for its convenience in practice, and differs from the usual codes for the Arnol'd-Sinai cat."

[10] Predrag 2016-05-29: totally agree - they say it well

"In section 3 a practical problem of stabilisation is considered, that provides a concrete model for the sawtooth and cat maps, and a natural introduction to the linear codes. An explicit linear transformation from the itinerary to the orbit is given."

[11] Every Anosov diffeomorphism of the torus is topologically conjugate to a hyperbolic automorphism. These are represented by $[2 \times 2]$ matrices with integer entries (for continuity), unit determinant (for area preservation) and real eigenvalues (for hyperbolicity), and are known as cat maps.

In order to describe certain collective properties of cat map orbits Hannay and Berry [55] introduced a function closely related to the least common multiple of their periods.

1.6.3 Isola / Isola90

Predrag 2016-06-02 excerpts from or notes on
S. Isola [62] *ζ-functions and distribution of periodic orbits of toral automorphisms*

Bellissard's friend Isola gives counting formulas of the usual type - could easily be turned into examples/exercises for ChaosBook. But I am looking for symbolic dynamics - not even mentioned here.

We consider canonical automorphisms of the torus T^2, i.e. maps of the form

$$T(x, y) = (ax + by, cx + dy) \quad (\mod 1)$$

which are implemented by the group of [2x2] matrices with integer entries, determinant 1, and eigenvalues (2.12).

To study the properties of this dense set of unstable periodic orbits, observe that the periodic orbits of T consist precisely of those points having rational coordinates $(p_l/q_l, p_1/q_2)$. If p_1, q_1 are coprime and g is the least common multiple of q_1 and q_z, then the square lattice of size l/g is invariant under T.

In this direction, Percival and Vivaldi [18, 83, 84] have constructed a nice translation of the dynamical problem into the language of modular arithmetic, allowing a profound understanding of the structure of periodic orbits. Here, however, we follow another approach where a general expression for the N,'s is derived through a simple iterative scheme. Consider the numbers

$$u_n = \frac{\Lambda^n - \Lambda^{-n}}{\sqrt{D}} \,. \tag{1.42}$$

The first two terms of the series are $u_0 = 0$, $u_1 = 1$ and each term after is given by

$$u_n = k u_{n-1} - u_{n-2} \,. \tag{1.43}$$

[stuff to work out: Isola has nice figures that illustrate the partitions of the 2-torus]

For the number of periodic points he finds, for any integer $s > 2$

$$N_n = \Lambda^n + \Lambda^{-n} - 2 \,, \tag{1.44}$$

[11] Predrag 2016-06-02: verbatim from Keating [64]

in agreement with the numerics of ref. [82]. Walters [104] defines the topological entropy as

$$h = \lim_{n\to\infty} \frac{1}{n} \ln N_n \,, \tag{1.45}$$

This yields $h = \log \Lambda$, i.e., the Sinai theorem for the entropy of an automorphism [7, 93].

The topological ζ-function for cat-map class of models is

$$1/\zeta(z) = \frac{(1-\Lambda z)(1-\Lambda^{-1} z)}{(1-z)^2} = \frac{1-sz+z^2}{(1-z)^2} \,. \tag{1.46}$$

The denominator $(1-z)^2$ takes care of the over-counting of the fixed point at the origin due to the 2-periodicity on the torus.

I wonder whether the fact that this is quadratic in z has something to do with the time-reversibility, and the unsigned graph's Ihara zeta functions, see chapter 4.

He also gives the number of prime cycles of period n, which is as usual given in terms of the Moebius function $\mu(m)$,

$$P_n = \frac{1}{n} \sum_{m|n} \mu(m) N_{n/m} \,. \tag{1.47}$$

1.6.4 Creagh / Creagh94

Predrag 2016-06-02 excerpts from or notes on
Creagh [36], *Quantum zeta function for perturbed cat maps* (click here), who says: " The behavior of semiclassical approximations to the spectra of perturbed quantum cat maps is examined as the perturbation parameter brings the corresponding classical system into the nonhyperbolic regime. The approximations are initially accurate but large errors are found to appear in the traces and in the coefficients of the characteristic polynomial after nonhyperbolic structures appear. Nevertheless, the eigenvalues obtained from them remain accurate up to large perturbations. "

Thom-Arnol'd cat map

$$A = \begin{pmatrix} 1 & 1 \\ 1 & 2 \end{pmatrix} \,, \qquad \det A = 1 \,. \tag{1.48}$$

This system can be written as:

$$\begin{pmatrix} q_{t+1} \\ p_{t+1} \end{pmatrix} = A \begin{pmatrix} q_t \\ p_t \end{pmatrix} \mod 1 \tag{1.49}$$

It is possible to construct a symbolic coding with finite grammar, as described in Devaney [41]. Robinson [86] goes through the construction clearly, step by step. The coding is constructed for an antisymplectic map whose double iteration is (1.49) - orbits of the cat map are then coded by sequences

whose length is even. A brief summary of the construction follows (see Devaney [41] for figures and details). The stable and unstable manifolds coming from the fixed point at $(q, p) = (0, 0)$ are used to divide the phase space into 3 rectangles R_1, R_2 and R_3. Under iteration of the antisymplectic map, R_1 is mapped into $R_2 \cup R_3$, R_2 into $R_1 \cup R_3$ and R_3 is mapped completely into R_2. Therefore orbits of the antisymplectic map are coded by sequences of 3 symbols (1,2,3), where 1 must be followed by 2 or 3, 2 is followed by 1 or 3, and 3 must be followed by 2. The full cat map is coded by even sequences of symbols following the same grammar. We can alternatively code orbits of the full map with 5 symbols denoting the admissible pairs of the symbols above: $(a, b, c, d, e) = (12, 13, 21, 23, 32)$.

The integers that must be subtracted from the phase space coordinates following application of the linear map in (1.49) in order to take the point back into the unit torus are fixed for each pair of symbols. The equation defining a periodic orbit can be written out as an explicit affine equation and solved for each itinerary. In this way a complete list of primitive periodic orbits is obtained for the unperturbed map.

1.6.5 Keating / Keating91

Keating [65] *The cat maps: quantum mechanics and classical motion*.

the action of map on the vector (p, q) can be described as the motion in the phase space specified by the Hamiltonian [65]

$$H(p, q) = (k^2 - 4)^{-1/2} \sinh^{-1}[(k^2 - 4)^{-1/2}/2][m_{12}p^2 - m_{21}q^2 + (m_{11} - m_{22})pq] \,. \tag{1.50}$$

Here, (p, q) are taken modulo 1 at each observation (the integer part is ignored), and observations occur at integer points of time.

The paper has a nice discussion of (possible discrete symmetries of cat maps.

Keating and F. Mezzadri [66] *Pseudo-symmetries of Anosov maps and spectral statistics*. [12]

Siemaszko and Wojtkowski [90] *Counting Berg partitions* describe symmetries of Adler-Weiss partitions. They are present for reversible toral automorphisms. The full symmetry group of a toral automorphism was studied by Baake and Roberts [11].

Earlier work: Rykken [88] constructed new types of Markov partitions. Snavely [97] studied the connectivity matrices of Markov partitions for hyperbolic automorphisms of T^2. He found that for Berg partitions the connectivity matrices are conjugated to the dynamics. He also found a way to list all such matrices and hence to classify the shapes of Berg partitions. He relied on the result of Adler [1] that such partitions are indeed present for any toral automorphism. Manning [75] gave a powerful generalization of this to T^n.

2CB

Anosov, Klimenko and Kolutsky [6] give an introduction to Anosov diffeomorphisms, ways to represent their chaotic properties and some historical

[12] Predrag 2016-08-29: not useful for the deterministic case

remarks on this subject: " As far as we know, the first example of such kind was pointed out by J. Hadamard about 1900. A couple of decades earlier H.Poincaré discovered the "homoclinic points" which now serve as the main "source" of "chaoticity"; however, Poincaré himself spoke only that the "phase portrait" (i. e., the qualitative picture of trajectories' behaviour in the phase space) near such points is extremely complicated. A couple of decades after Hadamard, E. Borel encountered a much simpler example of the "chaoticity" where it is easy to understand the "moving strings" of this phenomenon. We shall begin with a description of his example. About 100 years later it remains the simplest manifestation of the fact that a dynamical system (which, by definition, is deterministic) can somehow resemble a stochastic process."

1.7 Green's function for 1-dimensional lattice

Cat map is a 2-step difference equation

$$x_{t+1} - s\, x_t + x_{t-1} = -m_t\,, \tag{1.51}$$

with the unique integer "winding number" m_t at every time step t ensuring that x_{t+1} lands in the unit interval. This is a 1-dimensional linear discrete Poisson equation of form

$$\mathcal{D}x = m\,, \tag{1.52}$$

where x_t are lattice states, and m_t are the 'sources'. Since $(\mathcal{D}_\ell)_{tt'}$ is of a tridiagonal form, its inverse, or its Green's discrete matrix g on infinite lattice satisfies

$$(\mathcal{D}\mathsf{g})_{t0} = \delta_{t0}\,, \qquad t \in \mathbb{Z} \tag{1.53}$$

with a point source at $t = 0$. By time-translation invariance $\mathsf{g}_{tt'} = \mathsf{g}(t'-t)$, and by time-reversal invariance $\mathsf{g}(t'-t) = \mathsf{g}(t-t')$. In this simple, tridiagonal case, g can be evaluated explicitely [78, 83],

$$\mathsf{g}_{tt'} = \frac{1}{\Lambda^{|t'-t|}}\,\frac{1}{\Lambda - \Lambda^{-1}}\,, \tag{1.54}$$

where, in the hyperbolic $s > 2$ case, the cat map "stretching" parameter s is related to the 1-time step cat map eigenvalues $\{\Lambda, \Lambda^{-1}\}$ by

$$s = \Lambda + \Lambda^{-1} = e^{\lambda} + e^{-\lambda} = 2\cosh\lambda\,, \quad \lambda > 0\,. \tag{1.55}$$

While the "Laplacian" matrix $\mathcal{D}_\ell$ is sparse, it is non-local (i.e., not diagonal), and its inverse is the full matrix g, whose key feature, however, is the prefactor $\Lambda^{-|t'-t|}$ which says that the magnitude of the matrix elements falls off exponentially with their distance from the diagonal. For this it is crucial that the $\mathcal{D}$ eigenvalues (1.55) are hyperbolic. In the elliptic, $-2 < s < 2$ case, the sinh's and cosh's are replaced by sines and cosines, $s = 2\cos\theta = \exp(i\theta) + \exp(-i\theta)$, and there is no such decay of the off-diagonal matrix elements.

For a finite-time lattice with T sites we can represent $\mathcal{D}$ by a symmetric tridiagonal $[T\times T]$ Toeplitz matrix. The matrix

$$\mathcal{D}_T = \begin{pmatrix} s & -1 & 0 & 0 & \dots & 0 & 0 \\ -1 & s & -1 & 0 & \dots & 0 & 0 \\ 0 & -1 & s & -1 & \dots & 0 & 0 \\ \vdots & \vdots & \vdots & \vdots & \ddots & \vdots & \vdots \\ 0 & 0 & \dots & \dots & \dots & s & -1 \\ 0 & 0 & \dots & \dots & \dots & -1 & s \end{pmatrix} \tag{1.56}$$

satisfies *Dirchlet boundary conditions*, in the sense that the first and the last site do not have a left (right) neighbor to couple to. We distinguish it from the circulant matrix (1.61) by emphasising that $(\mathcal{D}_T)_{0,T-1} = (\mathcal{D}_T)_{T-1,0} = 0$. As the time-translation invariance is lost, the matrix elements of its inverse, the Green's $[T\times T]$ matrix $\mathsf{g}_{tt'}$, with a delta-function source term and the Dirichlet boundary conditions

$$\begin{aligned} (\mathcal{D}\mathsf{g})_{tt'} &= \delta_{tt'} \qquad t,t' \in 0,1,2,\cdots,T-1 \\ 0 &= \mathsf{g}_{-1,t'} = \mathsf{g}_{t,-1} = \mathsf{g}_{Tt'} = \mathsf{g}_{tT} \end{aligned} \tag{1.57}$$

depend on the point source location t, and no formula for its matrix elements as simple as (1.112) is to be expected. In general, a finite matrix inverse is of the form

$$\mathcal{D}^{-1} = \frac{1}{\det \mathcal{D}} (\text{cofactor matrix of } \mathcal{D})^T \,.$$

While the cofactor matrix might be complicated, the key here is, as in formula (1.112), the prefactor $1/\det\mathcal{D}$, falls off exponentially, and for Toeplitz matrices can be computed recursively.

Associated with this simple tridiagonal matrix are the Chebyshev polynomials of the first and the second kind

$$T_j(s/2) = \cosh(j\lambda)\,, \qquad U_j(s/2) = \sinh(j+1)\lambda \,/\, \sinh(j\lambda)\,,$$

generated by a three-term recursion relation.

The inverse of the Dirichlet boundary conditions matrix $\mathcal{D}_T$ (1.56) can be determined explicitly, in a number of different ways [59, 91, 96, 98]. Here we find it convenient to write the inverse of $\mathcal{D}_T$ in the Chebyshev polynomial form [106]. The determinant of $\mathcal{D}_T$, i.e., the Jacobian of the linear transformation (1.52) is well known [49]

$$\det \mathcal{D}_T = U_T(s/2)\,, \tag{1.58}$$

and the matrix elements of the Green's function in the Chebyshev polynomial form [59, 106] are explicitly

$$\mathsf{g}_{ij} = \frac{1}{\det \mathcal{D}_T} \times \begin{cases} U_{i-1}(s/2)\, U_{T-j}(s/2) & \text{for } i \le j \\ U_{j-1}(s/2)\, U_{T-i}(s/2) & \text{for } i > j. \end{cases} \,. \tag{1.59}$$

It follows from the recurrence relation $x_{i+1} = sx_i - x_{i-1}\,, \mod 1$, that $U_n(s/2)$ Chebyshev polynomials have the generating function

$$\begin{aligned}\sum_{n=0}^{\infty} U_n(s/2)t^n &= \frac{1}{1-st+t^2} \\ &= 1 + st + (s^2-1)t^2 + (s^3-2s)t^3 + \cdots\,, \end{aligned} \tag{1.60}$$

with $U_n(s/2) \approx s^n \approx \Lambda^n$, and for a hyperbolic system the off-diagonal matrix elements $\mathsf{g}_{tt'}$ are again falling off exponentially with their separation $|t'-t|$, as in (1.112), but this time only in an approximate sense.

[13] Alternatively, for finite time T we can represent $\mathcal{D}$ by a symmetric tridiagonal $[T\times T]$ circulant matrix with *periodic boundary conditions*

$$\mathcal{D}_T = \begin{pmatrix} s & -1 & 0 & 0 & \dots & 0 & -1 \\ -1 & s & -1 & 0 & \dots & 0 & 0 \\ 0 & -1 & s & -1 & \dots & 0 & 0 \\ \vdots & \vdots & \vdots & \vdots & \ddots & \vdots & \vdots \\ 0 & 0 & \dots & \dots & \dots & s & -1 \\ -1 & 0 & \dots & \dots & \dots & -1 & s \end{pmatrix}. \tag{1.61}$$

Now the discrete matrix Green's function $\mathsf{g}_{tt'}$ satisfies periodic boundary conditions

$$\begin{aligned}(\mathcal{D}\mathsf{g})_{t1} &= \delta_{t1}, \qquad\qquad t = 1, 2, \cdots, T \\ \mathsf{g}_{T+1,t'} &= \mathsf{g}_{1t'}\,, \qquad \mathsf{g}_{t,T+1} = \mathsf{g}_{t1}\,. \end{aligned} \tag{1.62}$$

Note that the Green's matrix is strictly negative for both the periodic and Dirichlet boundary conditions.

Left over from Boris version: Consider the single cat map equation with a delta-function source term

$$(-\Box + s - 2)\mathsf{g}_t = \delta_{t,0}, \qquad t \in \mathbb{Z}^1\,. \tag{1.63}$$

An alternative way to evaluate $\mathsf{g}_{i,j}$ is to use Green's function g and take antiperiodic sum (similar method can be used for periodic and Neumann boundary conditions)

$$\mathsf{g}_{i,j} = \sum_{n=-\infty}^{\infty} \mathsf{g}_{i,j+2n(T+1)} - \mathsf{g}_{i,-j+2n(T+1)}\,.$$

This approach has an advantage of being extendable to the $\mathbb{Z}^2$ case. After substituting g and taking the sum one obtains (1.59)

[13] Predrag 2017-09-20: Probably should do circulants first, then the complicated Dirichlet case next, in the spirit of starting out with the infinite lattice case (1.112).

1.8 Green's blog

2017-08-24,2017-09-09 Predrag This to all curious cats, but mostly likely only Boris might care: OK now I see why Chebyshevs...

Chebyshev expansions are used here because of the recurrence relations
2CB that they satisfy.

A *Toeplitz matrix*, T, is a matrix that is constant along each diagonal, i.e., $T_{jk} = t_{j-k}$. A *Hankel matrix*, H, is a matrix that is constant along each anti-diagonal, i.e., $H_{jk} = h_{j+k}$. There is also the *Laurent matrix* or *doubly infinite Toeplitz matrix*.

R. M. Gray (2009) Toeplitz and Circulant Matrices: A Review focuses on bounds of sums of eigenvalues - I see nothing here that is of immediate use to us, with maybe the exception of the discussion of the diagonalization
2CB of circulant matrices (discrete Fourier series).

A look at a Toeplitz matrix evokes time evolution of a periodic orbit symbolic block: it looks like successive time shifts stacked upon each other, every entry is doubly periodic on a torus of size $[|p| \times |p|]$. Does that have to do something with Chebyshev polynomials (rather than with the usual discrete Fourier series)? One uses Chebyshev polynomials of the first, second, third, and fourth kind, denoted by T_n, U_n, V_n, W_n, if, as an example, on looks at a pentadiagonal symmetric Toeplitz matrix, a generalization of the 3rd order spatial derivative.

Maybe some of the literature cited here illuminates this:

2017-09-09 Predrag The eigenvalues and eigenvectors for the finite symmetric tridiagonal Toeplitz matrix were obtained by Streater [98] *A bound for the difference Laplacian*. They seem to also be given in Smith [96] *Numerical Solution of Partial Differential Equations: Finite Difference Methods*.

Hu and O'Connell [59] *Analytical inversion of symmetric tridiagonal matrices* " present an analytical formula for the inversion of symmetrical tridiagonal matrices. As an example, the formula is used to derive an exact analytical solution for the one-dimensional discrete Poisson equation (DPE) with Dirichlet boundary conditions. " The T eigenvalues and orthonormal T-dimensional eigenvectors of $\mathcal{D}$ are [14]

$$\begin{aligned} \gamma_k &= s + 2\cosh\frac{k\pi}{T+1}\,, \qquad k = 1, 2, \cdots, T \\ e_n^{(k)} &= \sqrt{\frac{2}{T+1}}\sinh\frac{kn\pi}{T+1} \end{aligned} \tag{1.64}$$

(see, for example, refs. [59, 106]). This is a typical inverse propagator, see ChaosBook [9]

$$(\varphi_k^\dagger \cdot \Delta \cdot \varphi_{k'}) = \left(-2\cos\left(\frac{2\pi}{N}k\right) + 2\right)\delta_{kk'} \tag{1.65}$$

[14] Predrag 2017-09-09: recheck!

The inverse (the Green's function) $\mathsf{g}\mathcal{D} = 1$ is [59] [15]

$$\mathsf{g}_{jk} = \frac{\cosh(T+1-|k-j|)\lambda \; - \; \cosh(T+1-j-k)\lambda}{2\sinh\lambda \, \sinh(T+1)\lambda} \tag{1.66}$$

The above paper is applied to physical problems in Hu and O'Connell [57] *Exact solution for the charge soliton in a one-dimensional array of small tunnel junctions*, and in Hu and O'Connell [58] *Exact solution of the electrostatic problem for a single electron multijunction trap*. The erratum is of no importance for us, unless the - sign errors affect us.

A cute fact is that they also state the solution for $s = 2$, which, unlike (1.66) has no exponentials - it's a power law.

Eigenvalues, eigenvectors and inverse for $[T \times T]$ matrix $\mathcal{D}$ (1.56), $-2 < s < 2$,

$$\begin{aligned}
\lambda_k &= -s + 2\cos\frac{k\pi}{T+1} \\
e_k &= \sqrt{\frac{2}{T+1}}\left(\sin\frac{k\pi}{T+1}, \sin\frac{2k\pi}{T+1}, \cdots, \sin\frac{Tk\pi}{T+1}\right) \\
(\mathcal{D}^{-1})_{kT} &= \frac{2}{T+1}\sum_{m=1}^{T}\frac{\sin\frac{km\pi}{T+1}\sin\frac{Tm\pi}{T+1}}{-s+2\cos\frac{k\pi}{T+1}}
\end{aligned} \tag{1.67}$$

are computed in Meyer [79] *Matrix Analysis and Applied Linear Algebra*.

Yamani and Abdelmonem [106] *The analytic inversion of any finite symmetric tridiagonal matrix* rederive Hu and O'Connell [59], using the theory of orthogonal polynomials in order to write down explicit expressions for the polynomials of the first and second kind associated with a given infinite symmetric tridagonal matrix H.

The matrix representation of many physical operators are tridiagonal, and some computational methods, are based on creating a basis that renders a given system Hamiltonian operator tridiagonal. The advantage lies in the connections between tridiagonal matrices and the orthogonal polynomials, continued fractions, and the quadrature approximation which can be used to invert the tridiagonal matrix by finding the matrix representation of the Green's functions.

The Green's function $G(z)$ associated with the matrix H is defined by the relation

$$(H - zI)G = I\,. \tag{1.68}$$

It is more convenient to calculate the inverse of the matrix $(H - zI)$ instead of the inverse of the matrix H. Note that in this formulation G is the *resolvent* of H.

[15] Predrag 2017-09-09: It is shown in ref. [106] that is the same as the formula (1.59) Boris uses (without a source citation).

Simons [91] *Analytical inversion of a particular type of banded matrix* rederives Hu and O'Connell [59] by a "a simpler and more direct approach". The structure of equation (1.68) is that of a homogeneous difference equation with constant coefficients and therefore one looks for a solution of the form

$$G_{pq} = A_q e^{p\lambda} + A_q e^{-p\lambda} ,$$

with appropriate boundary conditions. This leads to the Hu and O'Connell formulas for the inverses of G.

How to invert a very regular banded Toeplitz matrix.

Yueh [107] *Explicit inverses of several tridiagonal matrices* has a bunch of fun tri-diagonal Toeplitz matrix inverses, full of integers - of no interest to us.

Dow [42] *Explicit inverses of Toeplitz and associated matrices*: " We discuss Toeplitz and associated matrices which have simple explicit expressions for their inverses. We first review existing results and generalize these where possible, including matrices with hyperbolic and trigonometric elements. In Section 4 we invert a tridiagonal Toeplitz matrix with modified corner elements. A bunch of fun tri-diagonal Toeplitz matrix inverses, full of integers - of no interest to us.

Noschese, Pasquini and Reichel [81] *Tridiagonal Toeplitz matrices: properties and novel applications* use the eigenvalues and eigenvectors of tridiagonal Toeplitz matrices to investigate the sensitivity of the spectrum. Of no interest to us.

Berlin and Kac [17] *The spherical model of a ferromagnet* use bloc-circulant matrices; see also

Davis [40] *Circulant Matrices*

2017-09-09 Predrag Gover [48] *The Eigenproblem of a Tridiagonal 2-Toeplitz Matrix* seems less useful: " The characteristic polynomial of a tridiagonal 2-Toeplitz matrix is shown to be closely connected to polynomials which satisfy the three point Chebyshev recurrence relationship. This is an extension of the well-known result for a tridiagonal Toeplitz matrix. When the order of the matrix is odd, the eigenvalues are found explicitly in terms of the Chebyshev zeros. The eigenvectors are found in terms of the polynomials satisfying the three point recurrence relationship. "

Gover [48] motivates his paper by reviewing a tridiagonal 1-Toeplitz, or Toeplitz matrix, referring to the original literature. Consider a tridiagonal $[\ell \times \ell]$ Toeplitz matrix with Dirchlet boundary conditions (1.56), with eigenvalues (1.64).

Kübra Duru and Bozkurt [67] *Integer powers of certain complex pentadiagonal 2-Toeplitz matrices*

Elouafi [45] *On a relationship between Chebyshev polynomials and Toeplitz determinants*: "Explicit formulas are given for the determinants of a band

symmetric Toeplitz matrix T_n with bandwidth $2r+1$. The formulas involve $r \times r$ determinants whose entries are the values of Chebyshev polynomials on the zeros of a certain rth degree q which is independent of n."

2017-09-09 Predrag Felsner and Heldt *Lattice paths* seem to be all on graphs - I see no 2-dimensional lattice here.

Spectral asymptotics in one-dimensional periodic lattices with geometric interaction

1.9 $C_2 = D_1$ factorization

As the simplest example of implementing the above scheme consider the $C_2 = D_1$ symmetry. For our purposes, all that we need to know here is that each orbit or configuration is uniquely labeled by an infinite string $\{s_i\}$, $s_i = +, -$ and that the dynamics is invariant under the $+ \leftrightarrow -$ interchange, i.e., it is C_2 symmetric. The C_2 symmetry cycles separate into two classes, the self-dual configurations $+-$, $++--$, $+++---$, $+--+-++-$, $\cdots$, with multiplicity $m_p = 1$, and the asymmetric configurations $+$, $-$, $++-$, $--+$, $\cdots$, with multiplicity $m_p = 2$. For example, as there is no absolute distinction between the "up" and the "down" spins, or the "left" or the "right" lobe, $t_+ = t_-$, $t_{++-} = t_{+--}$, and so on.

exercise ??

The symmetry reduced labeling $\rho_i \in \{0, 1\}$ is related to the standard $s_i \in \{+, -\}$ Ising spin labeling by

$$\begin{array}{lllll} \text{If} & s_i & = & s_{i-1} & \text{then} \quad \rho_i = 1 \\ \text{If} & s_i & \neq & s_{i-1} & \text{then} \quad \rho_i = 0 \end{array} \tag{1.69}$$

For example, $\overline{+} = \cdots+++\cdots$ maps into $\cdots 111 \cdots = \overline{1}$ (and so does $\overline{-}$), $\overline{-+} = \cdots-+-+\cdots$ maps into $\cdots 000 \cdots = \overline{0}$, $\overline{-++-} = \cdots--++--++\cdots$ maps into $\cdots 0101 \cdots = \overline{01}$, and so forth. A list of such reductions is given in table **??**.

Depending on the maximal symmetry group $\mathcal{H}_p$ that leaves an orbit p invariant (see sects. ?? and ?? as well as example **??**), the contributions to the dynamical zeta function factor as

⇓PRIVATE

⇑PRIVATE

$$\begin{array}{rlcll} & & & A_1 & A_2 \\ \mathcal{H}_p = \{e\}: & (1-t_{\hat{p}})^2 & = & (1-t_{\hat{p}}) & (1-t_{\hat{p}}) \\ \mathcal{H}_p = \{e,\sigma\}: & (1-t_{\hat{p}}^2) & = & (1-t_{\hat{p}}) & (1+t_{\hat{p}}) \ , \end{array} \tag{1.70}$$

For example:

$$\begin{array}{rlcll} \mathcal{H}_{++-} = \{e\}: & (1-t_{++-})^2 & = & (1-t_{001}) & (1-t_{001}) \\ \mathcal{H}_{+-} = \{e,\sigma\}: & (1-t_{+-}) & = & (1-t_0) & (1+t_0), \quad t_{+-} = t_0^2 \end{array}$$

This yields two binary cycle expansions. The A_1 subspace dynamical zeta function is given by the standard binary expansion (**??**). The antisymmetric A_2 subspace dynamical zeta function ζ_{A_2} differs from ζ_{A_1} only by a minus sign for cycles with an odd number of 0's:

$$\begin{aligned} 1/\zeta_{A_2} &= (1+t_0)(1-t_1)(1+t_{10})(1-t_{100})(1+t_{101})(1+t_{1000}) \\ &\quad (1-t_{1001})(1+t_{1011})(1-t_{10000})(1+t_{10001}) \\ &\quad (1+t_{10010})(1-t_{10011})(1-t_{10101})(1+t_{10111})\dots \\ &= 1+t_0-t_1+(t_{10}-t_1t_0)-(t_{100}-t_{10}t_0)+(t_{101}-t_{10}t_1) \\ &\quad -(t_{1001}-t_1t_{001}-t_{101}t_0+t_{10}t_0t_1)-\dots\dots \end{aligned} \tag{1.71}$$

Note that the group theory factors do not destroy the curvature corrections (the cycles and pseudo cycles are still arranged into shadowing combinations).

If the system under consideration has a boundary orbit (*cf.* sect. **??**) with group-theoretic factor $h_p = (e+\sigma)/2$, the boundary orbit does not contribute to the antisymmetric subspace

$$\begin{aligned} & & A_1 \quad & A_2 \\ \text{boundary:} \quad (1-t_p) &= (1-t_{\hat{p}})(1-0t_{\hat{p}}) \end{aligned} \tag{1.72}$$

This is the $1/\zeta$ part of the boundary orbit factorization discussed in example **??**, where the factorization of the corresponding spectral determinants for the 1-dimensional reflection symmetric maps is worked out in detail.

1.10 Any piecewise linear map has "linear code"

2CB

For reasons unbeknownst to me, it is below the dignity of any cat to work out any problem in ChaosBook, or in the online course, no matter how often I point out that it is easier to understand what we do for cat maps if you first work it out for 1-dimensional maps.

So I have to do these exercises myself - I'm forced to it, so Li Han can be motivated to re-derive his polynomials (as described in Bird and Vivaldi [18], see my notes of **2016-05-21, -12-12** below), rather than to fit them to Mathematica grammar rule counts for integer s.

Basically, I am baffled by why should "linear code" be such a big deal that it has to go into the title of our paper [52]. *Every* example of symbolic dynamics worked out in ChaosBook is a "linear code." The strategy is always the same - find a topological conjugacy from your map to a piecewise linear map, and then use the fact that any piecewise linear map has "linear code." The pruning theory is always the same - kneading orbit separates admissible from the inadmissible, also in the infinite 1-dimensional discrete lattice case worked out in the *Diffusion* chapter in the ChaosBook, and the appendix (chapter 2 reproduced here) that no one wants to read either.

A tent map is a 1-dimensional example (the next would be Bernoulli, and its sawtooth generalizations). The 2-dimensional examples are the Belykh map,

example 1.9, and the Lozi map, example 1.10. Belykh map is of particular interest to us, as it is in form very close to the cat map. Both maps have the pruning front conjecture is proven for them, for a some sets of parameters.

example 1.7 p. 63
example 1.8 p. 64
example 1.9 p. 65
example 1.10 p. 66

1.11 Symbolic dynamics, a glossary

2017-08-05 Predrag Consult ChaosBook.org Chapter *Charting the state space* (source file knead.tex) or the Appendix of ref. [52].

to Predrag: check that all this is in ChaosBook, then erase:

The set of all bi-infinite itineraries that can be formed from the letters of the alphabet $\mathcal{A}$ is called the *full shift* (or *topological Markov chain*)

Here we refer to this set of all conceivable itineraries as the *covering* symbolic dynamics.

A bar over a finite block of symbols denotes a periodic itinerary with infinitely repeating basic block; we shall omit the bar whenever it is clear from the context that the orbit is periodic. [16]

Orbit that starts out as a finite block followed by infinite number of repeats of another block $p = (m_1 m_2 m_3 \cdots m_T)$ is said to be *heteroclinic* to the cycle p. An orbit that starts out as p^∞ followed by a different finite block followed by $(p')^\infty$ of another block p' is said to be a *heteroclinic connection* from cycle p to cycle p'.

Suppose that the grammar can be stated as a finite number of pruning rules, each forbidding a block of finite length,

$$\mathcal{G} = \{b_1, b_2, \cdots b_k\} \ , \tag{1.73}$$

where a *pruned block* b is a sequence of symbols $b = m_1 m_2 \cdots m_{|b|}$, $m \in \mathcal{A}$, of finite length $|b|$.

Subshifts of finite type. A topological dynamical system (Σ, σ) for which all admissible itineraries are generated by a finite transition matrix

$$\Sigma = \left\{(m_k)_{k\in\mathbb{Z}} \ : \ T_{s_k s_{k+1}} = 1 \quad \text{for all } k\right\} \tag{1.74}$$

is called a subshift of *finite type*.

1.12 Cat map blog

2CB

2016-05-18 Predrag I start with our 2011 *Notes for cat map*
(former *appendStatMnotes.doc* in *dasbuch/book/notes*),
to be eventually merged with *chapter/appendStatM.tex*.

[16] Predrag : eliminate $\_m_{-m+1}\cdots m_0\_$ and $[m_{-m+1}\cdots m_0.]$ notation in favor a single convention

2011-05-14 Jean-Luc Thiffeault I figured out that the grouping of periodic orbits is crucial, and moreover that there is something delicate with the fixed point of the cat map, which lies on the boundary of Markov boxes.

2011-05-14 Predrag For Anosov (linear Anosov?) - Arnol'd cat map - it should work like ton of rocks, but you have to note that because of the periodicity there is one fixed point, not two. If you screw up an early term in the series, then it converges very slowly. I think the Stephen Creagh [36] tested it on weakly nonlinearly perturbed cat map (weakly, so golden-mean grammar is working) and it converged super-exponentially (you know the grammar, flow has bounded hyperbolicity, so weight-truncated cycle expansions are not needed - they perform less well).

2011-05-14 Jean-Luc Thiffeault I know how to do it with the Markov partition now, and it works much better. Keep in mind this is a warmup problem: what I really have in mind (with my collaborator Erwan Lanneau [68]) is to compute periodic orbits for Teichmuller flow, where the periodic orbits themselves are actually now pseudo-Anosovs!

2011-05-16 Hans-Henrik Rugh The situation as I recall it is roughly as follows:

When you construct the symbolic dynamics you may start by picking one periodic orbit, typically the fixed point $p = f(p)$ (but the following depends on the choice). You then cut the torus into pieces following s/u-manifolds until you get a small collection of N rectangles.

$$R_1, \cdots, R_N$$

Associated to this collection you have a transition matrix (for SINGLE rectangles). Now, you also need to construct a transition matrix for PAIRS of rectangles, e.g. $(R_1, R_2) \to (R_2, R_1)$ and then TRIPLES of rectangles ... $(R_1, R_2, R_3) \to (R_2, R_1, R_3)$, etc.... These k'th - order transitions comes from the fact that there is a fixed point/periodic cycle on the boundary of the Markov partition elements.

You get determinants $d_k(z)$ for each of these k'th–order transition matrices. NB : $(R_1, R_2) \to (R_2, R_1)$ is a periodic orbit of prime length 2 even if it represents a fixed point of f. I think (but is not sure?) that the weights in the determinant are calculated in the same way...

The final determinant is $d(z) = d_1(z)d_3(z).../(d_2(z)d_4(z)...)$ if I am not mistaken. This is related to the so-called Manning trick [74] for counting real orbits related to

$$\det(1 - s) = 1 - \mathrm{tr}\, s + \mathrm{tr}\, s \wedge s - \cdots$$

where s is a permutation. What is not obvious is that $d(z)$ is entire, but it is!

It's a kind of model problem anyway. In more realistic systems I suppose that one may run into the problem of having several orbits on boundaries.

One of the tricky points is to see how such an orbit in the 'higher' order zeta-functions/Fredholm-det.

As mentioned in e.g. $d_1(z)$ a 'physical' fixed point may appear zero times, or twice, or,...? In $d_2(z)$ a fixed point may actually appear as a period two orbit, so should be treated as such when looking for cancelling terms.

Great, if you have managed to make it work in practice. I don't think that one can call it a standard trick but one may perhaps get it implicitly from the paper of Ruelle [87]. But it is difficult to digest and even more difficult to convert into computable formulae.

2018-02-10 Predrag Manning [74] writes: " According to Bowen [29], a Markov partition is a finite cover of state space by closed subsets called *rectangles*. The rectangles are pairwise disjoint except possibly for the intersection of their boundaries. [...] At the boundaries of the rectangles, that is where they intersect, several periodic points individual rectangles may be mapped to the same periodic point in the full state space. "

" Counting the periodic points involves also certain auxiliary subshifts of finite type to remedy overcounting of points in the boundaries of the rectangles. "

2011-05-18 Jean-Luc Thiffeault emailed to Predrag pdf file *Notes on periodic orbit expansions for Teichmüller flow* (saved as *POexp.pdf* in *dasbuch/book/notes/*). which maybe figures out cat map symbolic dynamics. He writes:

" Updated notes: on page 4-5 I used the Markov boxes to compute the PO expansion. I used a trick to deal with the orbit on the boundary: include several copies of the orbit, but divide by the correct factor. It makes the series very nicely convergent. I don't know if this is a standard trick but it seems to work well. "

2011-05-17 Predrag It is standard, it is in ChaosBook.org Chapter *Counting*, Sect *Counting cycles*. I introduced it in Roberto Artuso, Erik Aurell and Predrag Cvitanović [8], *Recycling of strange sets: II. applications*, see eq. (4) and Fig. 6, but Manning [74] did it it in 1971 (if that's what he did), and Ruelle [87] at the same time, according to Hans Henrik. ChaosBook says: "Smale [95] conjectured rationality of the zeta functions for Axiom A diffeomorphisms, later proved by Guckenheimer [51] and Manning [74]," and ChaosBook cannot be wrong.

The rule of thumb is that all credit should go to old white male mathematicians whose names one knows how to spell.

The argument is something like this: the correct object, the Fredholm determinant, can be written as ratios of products of skew products (AKA determinants of different dimensions), each one being the not correct object, but historically the first thing written down (dynamical or Ruelle zeta function).

The ones on partition boundaries (what I currently call 'ridges') are of lower dimensions, either downstairs or upstairs in these rations. They account for overcounting of the boundary fixed and periodic points.

ChaosBook does something of that when explaining the relation between Fredholm determinants and dynamical zeta functions, but is so far silent on explicit examples of the Manning multiples. That is why I would really like us to write up the cat map symbolic dynamics simply and elegantly. Jean-Luc is not the only person who has gotten lost here, anybody mathematician who thinks that Arnol'd is the simplest exercise to try sinks precisely at this spot (physicists train on unimodal maps and the 3-disk system, remaining blissfully ignorant of the Manning multiples)

Hans Henrik might have more elegant way of saying this. Vivianne still more elegant.

2012-03-01 Predrag I've been dreaming about this forever, see for example my post of **[2012-03-01]**, `pipes` repository, *A letter to our experimental friends*:

" For large aspect systems I imagine we fit local templates whose 2-dimensional or 3-dimensional volume is concentrated on a region big enough to capture interaction of close-by structures, but small enough not to track weakly interacting ones.

In other words, cover 3-dimensional volume with a finite-size template that tracks a neighborhood for a finite time. It's OK to make it spatially periodic, as long as distance is measured in finite size spatiotemporal windows. That is what we already do when we use unstable periodic orbits - we use temporally-infinite periodic solution (that cannot be seen in experiment) to identify a finite-time neighboring segment of a chaotic trajectory.

It has not been tried, so I might be wrong (again). "

2016-05-04 Predrag I am not suggesting that we should study this, but it's something to maybe keep in mind: Slipantschuk, Bandtlow and Just [94], *Complete spectral data for analytic Anosov maps of the torus*, construct a family of analytic hyperbolic diffeomorphisms of the torus (of which Arnol'd cat map is a special case) for which the spectral properties of the associated transfer operator acting on a suitable Hilbert space can be computed explicitly. They introduce an example of an analytic hyperbolic diffeomorphism on the complex unit torus, of which the cat map is a special, linear case. the real representation of the map, Eq. (2) is area-preserving and thus provides an example of a chaotic Hamiltonian system. Unlike the situation for one-dimensional non-invertible maps, here is no distinction between Perron-Frobenius and Koopman operators as diffeomorphism is area-preserving.

Note that the eigenvalues of the evolution (transfer) operators come in doublets or quadruplets, presumably because of the discrete symmetries of the unit square.

Just looking at their Figs. 1 is inspirational.

The cat map can always be written as a composition of area preserving orientation reversing linear automorphisms. They define a two-parameter area-preserving family, Eq. (85), and show that measures for such maps, where the determinant of the Jacobian varies, may have fractal properties, see Fig. 2.

2016-05-16 PC Weirdly, Wolfram's Weisstein [105] is wrong: what he calls "Lyapunov characteristic exponents" for Arnol'd cat map are certainly not "exponents" but multipliers. Maybe you guys could alert him, ask him to fix it.

The eigenvectors are correct. They are the same for all periodic points and thus parallel: cat map is uniformly hyperbolic (the same stability exponents for all orbits), a nice example of the Anosov Axim A system, with the stable and unstable manifolds transverse everywhere, at the same intersection angle.

2016-05-16 PC The boyscout version of ChaosBook Appendix N *Statistical mechanics applications*, Artuso's Sect. N.1 *Diffusion in sawtooth and cat maps* sure merits a read. The pruning rules are given there. Exercise e-Per-P-Cats gives the exact number of T–periodic points of the cat map.

2016-05-17 Predrag I have added for the time being chapter 2 *Statistical mechanics applications* from ChaosBook to this blog. Note that there are yet more references to read in the Commentary to the chapter 2.

2016-05-21 Predrag I had included Percival and Vivaldi [18, 83, 84] among the papers to read (search for **2016-05-16 PC**; see remark 2.1). Percival and Vivaldi [84] *Arithmetical properties of strongly chaotic motions* is about cat maps. ChaosBook material included in sect. 2.3 might be based on that, but I do not remember now, I had last worked on that section in 1996 :)

Maybe working out exercise 2.1 to exercise 2.5 is the fastest way to make sure one understands this symbolic dynamics...

2016-05-17 Li Han Uploaded to `siminos/mathematica` two Mathematica notebooks. *CatMap - single cat map symbolic dynamics and statistics* counts the single cat map symbols and determines their statistics. It is interactive and one can modify the parameters and play with it. *CatMap - single cat map periodic orbits and zeta functions* verifies the number of periodic orbits and the topological zeta functions for a single cat map.

2016-05-21 Predrag Adrien and Rana wondered why are (9.2) and (9.3) the same equation. Have a look at the two forms of the Hénon equation in the ChaosBook Example 3.6. Or see (2.3) (eq. (2.2) in Percival and Vivaldi [83]). Does that help in understanding the relation? Once you do, write it up in your reports.

2016-06-01 Predrag As no one has written anything down, I am not sure what happened in the rest of the WebEx session, but my impression is that perhaps we should step a step back back and first work through some more introductory material for cat-map dynamics to start making sense. Do not be discouraged - it is all very different in flavor from what one learns in most traditional physics courses (though once you learn the stuff, deep connections to statistical mechanics emerge). My recommendation is that Rana and Adrien work through week 9, week 10, and at least parts of week 12 (skip Chap. 23. Cycle expansions).

Could one of you focus on understanding the cat-map 'the linear code' part of Percival and Vivaldi [83] - perhaps just complete sect. 1.6.2 started by me.

The other one could describe the 'standard' generating partition code allegedly given in Arnol'd and Avez [7] and in most of the references in remark 2.1, so we all understand what Boris means when he says that code is not good for a study of spatiotemporal chaos.

2016-07-01 Li Han :

code: *mathematica/Catmap - single cat map symbol diagram and symbol frequencies.nb*

Single cat map symbol diagram and symbol frequencies. Analytical results of 2-symbol frequencies, up to a gap of 5. Great thanks to the new geometry package in Mathematica 10.

2016-07-06 Li Han :

code: *mathematica/Catmap - single cat map symbol diagram and symbol frequencies v2.nb*
Modified the form of matrix A so that area calculation is easier;
Added sections for 3-7 symbol frequencies (joint probability).

Total pruning rules for consecutive n symbols of single Arnol'd cat map, $s = \mathrm{tr}\,[A] = 3$, see table 1.1. Compare with Rana's table 6.2: the number of inadmissible sequences that she found for $|a| = 7$ differs.

It would take 12 core*hours to run all (up to 6 symbols: 1 core*hour)

2016-07-10 Rana I agree with Li Han table 1.1 on the numbers of pruned blocks.

2016-07-20 Li Han :

code: *mathematica/Catmap - single cat map symbol diagram and symbol frequencies v3.nb*

Total pruning rules for consecutive n symbols of single Arnol'd cat map, $s = \mathrm{tr}\,[A] = 3$ up to length 12, see table 1.1. Compare with Rana's table 6.2: the number of inadmissible sequences that she found for $|a| = 7$ differs.

For $s = 3$ up to ...:
length 7: ≈ 1 Core*hour
length 10: ≈ 3 Core*days
length 12: $\approx 15 - -20$ Core*days

2016-08-01 Predrag : According to table 1.1, there is a single new pruning rule for each prime-number period. Li Han lists it as 2, but by the reflection symmetry there is only one. One should really quotient the symmetry, and it is not just by removing overall factor 2 in the table: there are pruning blocks that map into each other by the reflection symmetry, and there are pruning blocks that are self-dual under reflection, giving one pruning rule rather than two in the not-desymmetrized listing of this table.

- Is this surmise something proved by Dyson [44]? Or does Behrends [15, 16] explain it?
- Does this new rule have a simple geometric interpretation, in terms of the inequalities? What is the code of the pruned block?

None of

0, 2, 22, 132, 684, 3164, 13894, 58912, 244678, 1002558, 4073528, 16460290
= 2 (1, 11, 66, 342, 1582, 6947, 29456, 122339, 501279, 2036764, 8230145)

0, 2, 8, 2, 30, 2, 70, 16, 198, 2, 528, 2, $\cdots$
= 2 (1, 4, 1, 15, 1, 35, 8, 99, 1, 264, 1, $\cdots$)

sequences is in the On-Line Encyclopedia of Integer Sequences, which is bad news. It means that not only this is a number-theoretic problem that has to do with prime factorization (bad news) but in addition it is not one of the standard number-theoretic problems. Means this is an undoable problem, unlikely to have any simple explanation. Do not waste any more time on it.

2016-08-15 Predrag : I need this stupid Arnol'd cat map in ChaosBook.org, because an example of a tractable Hamiltonian system is useful, and because so many people refer to it.

I say "stupid" because it is very seductive (as much of number theory is), and totally useless as physics. The moment one goes away from the piece-wise linear (and integer!) cat map to any physical nonlinear flow, all this symbol counting falls apart, and one needs cycle expansions (ChaosBook.org/course1, the 2nd course) to describe the physics. I had wasted too much time on number theory in my life to be ever dragged into that again. You have to be very smart, as sooner or later you discover you are assuming the Riemann Hypothesis holds true :)

2017-09-27 Predrag For counting orbits, Baake *et al.* [12] *Periodic orbits of linear endomorphisms on the 2-torus and its lattices*, might be useful.

2016-10-15 Predrag Boris is thinking about temporal and spatial correlations in spatiotemporal cat maps. Here is some literature on the topic, just for cat maps:

Brini *et al.* [31] *Decay of correlations for the automorphism of the torus* T^2

García-Mata and Saraceno [47] *Spectral properties and classical decays in quantum open systems* (who study the Arnol'd cat map with a small sinusoidal perturbation write that Blank, Keller and Liverani [21] and Nonnenmacher [80] provide a rigorous theoretical underpinning to their calculations for quantum and classical maps on the torus.

Blank, Keller and Liverani [21] *Ruelle-Perron-Frobenius spectrum for Anosov maps* extend a number of results from one-dimensional dynamics based on spectral properties of the Ruelle–Perron–Frobenius transfer operator to Anosov diffeomorphisms on compact manifolds.

Nonnenmacher [80] studies classical and quantum maps on the torus phase space, in the presence of noise. We focus on the spectral properties of the noisy evolution operator, and prove that for any amount of noise, the quantum spectrum converges to the classical one in the semiclassical limit.

2016-11-11 Predrag For fun and games with the cat map, check out Hunt, and B. D. Todd [60, 101] *On the Arnol'd cat map and periodic boundary conditions for planar elongational flow*

2016-12-12 Predrag Percival and Vivaldi [83] write: "The linear code described here may be considered as a development of the code used by Bullett [32] for the piecewise linear tent map." But Bullett mentions no tent map, I see nothing there... :) His piecewise linear standard map is the simplest possible area preserving piecewise linear twist homeomorphism of zero flux.

Beardon, Bullett and Rippon [14] *Periodic orbits of difference equations* might be of interest.

2016-12-12 Predrag Pondering Li Han's undisputable polynomial fits in s to the (new) pruned blocks $\tilde{N}_n$. Li Han now has a set of polynomials that counts the number of pruning rules $\tilde{N}_n(s)$ for small finite n, but any s. (table 1.1 lists them only for $s = 3$, but Li Han has new tables, not included in the blog as yet).

What's so unique about primes? I think that if cycle period $n-1 = p$ is a prime, there is always one "most monotone $(p+1)$-cycle" such that cycle points order themselves monotonically along the spatial coordinate q,

$$q_{1/(p+1)} < q_{2/(p+1)} < \cdots < q_{p/(p+1)} \,,$$

and one would have to show that this forces $1 < q_{p/(p+1)}$, so that one $(p+1)$-cycle is pruned, but all the rest are somehow protected and fall

n	N_n	$\tilde{N}_{n-1}$
2	2	0
3	22	2
4	132	$8 = 2 \cdot 2 \cdot 2$
5	684	2
6	3164	$30 = 2 \cdot 3 \cdot 5$
7	13894	2
8	58912	$70 = 2 \cdot 5 \cdot 7$
9	244678	$16 = 2 \cdot 2 \cdot 2 \cdot 2$
10	1002558	$198 = 2 \cdot 3 \cdot 3 \cdot 11$
11	4073528	2
12	16460290	$528 = 2 \cdot 2 \cdot 2 \cdot 2 \cdot 3 \cdot 11$
13	??	2

Table 1.1: N_n is the total number of pruned blocks of length $n = |a|$ for the $s = 3$ Arnol'd cat map. $\tilde{N}_n$ is the number of *new* pruned blocks of length $|a|$, with all length $|a|$ blocks that contain shorter pruned blocks already eliminated. Note that (empirically) there is a single new pruning rule for each prime-number period (it is listed as 2 rules, but by the reflection symmetry there is only one).

within the unit interval. Keating [64] is all about prime cycles, so maybe this is explained there - of if not there, maybe in Percival and Vivaldi [84]? Percival and Vivaldi [83] and Boris' Green's functions are polynomial functions of s, so maybe the answer is there already.

What about non-prime periods $n = p_1 p_2 \cdots p_m$? Perhaps on has to replace the cat map f by the commuting set of maps $f_{p_\ell} = f^{p_\ell}$, one for each prime, and argue about pruning rules for $f^n = f_{p_1} \circ f_{p_2} \circ \cdots \circ f_{p_m}$. Will be messy. But while cat map f is linear in s, f_p are polynomial in s, and that might lead to Li Han's polynomials for $\tilde{N}_n(s)$.

2016-05-21, -12-12 Predrag I had included Bird and Vivaldi [18] *Periodic orbits of the sawtooth maps* among the papers to read, but the paper remained woefully unread. Now Li Han has no choice but to read it :)

They assert that for the Arnol'd cat map there are 11 440 548 orbits of period 20.

Percival and Vivaldi [83] refer to the discrete Laplacian as the "central difference operator."

The special case $s = 2$ corresponds to an unperturbed twist map, for which orbits represent uniform motions of a free rotor.

The one-parameter s family of sawtooth maps (of the 2-torus), within which reside infinitely many Anosov diffeomorphisms. Sawtooth maps are piecewise linear, and for this reason we are able to construct the parameter dependence of the sawtooth orbits explicitly in terms of rational functions with integer coefficients.

(i) for integral s the sawtooth map reduces to a toral automorphism, and the structure of periodic orbits of such maps is known [84]. They are found to coincide with points having rational coordinates, and can be dealt with using arithmetical techniques, one can locate and count all periodic orbits.

(ii) if an orbit is known for one value of s, it can be computed for any other value.

We represent orbits as doubly infinite sequences of integers (words), where the integers are drawn from a finite set (alphabet). An orbit is written in terms of the configuration coordinate x_t alone and is denoted by (x_t). The word we denote by (m_t). For $s > 2$ the code is an isomorphism. For a given s, the possible values of the m_t are bounded in magnitude by $|m_t| \leq Int(1 + s/2)$. The itinerary of a given orbit is independent of the parameter. The orbit is recovered by Green's function (1.112):

$$q_t = \frac{1}{\sqrt{D}} \sum_{s\in\mathbb{N}} \Lambda^{-|t-s|} b_s \quad , \tag{1.75}$$

The leading eigenvalue of the cat map Jacobian matrix M is given by (1.6). For an n-cycle x_t are rational functions of Λ, given by the quotient of two reflexive polynomials (for example, $P_t(\Lambda) = \Lambda^n P_t(1/\Lambda)$),

$$\begin{aligned} x_t &= \Lambda\, P_t(\Lambda)/Q(\Lambda) \\ P_t(\Lambda) &= \sum_{\tau=1}^{n-1} \Lambda^{n-\tau}(\Lambda\, m_{t+\tau-1} + m_{t-\tau}) \\ Q(\Lambda) &= (\Lambda^2 - 1)\,(\Lambda^n - 1) \end{aligned} \tag{1.76}$$

Bird and Vivaldi [18] then discuss pruning, give formulas for the numbers of prime cycles for integer s, etc.. Most likely Li Han's polynomials are implicit in these formulas.

2016-12-15 Predrag to Roberto, **Going catty**: What is the main question? **My Question of the Day** is:

In ChaosBook Diffusion chapter we show that whenever the critical point of the 1D sawtooth map (the rightmost highest point) is pre-periodic, we have finite grammar and an analytic cycle expansion formula (essentially the topological zeta function, with the uniform expansion rate stuck into z^n) for the diffusion constant.

As far as I can tell, both you and Boris ignore the issues of the grammar, get some long-time limit estimate of the diffusion constant.

Usually in 2D there is a fractal set of critical points (AKA pruning front) - we had worked it out for the Lozi map and the Henon map. If the strange set is a strange repeller, there we have infinitely many examples of finite grammars. But it never happens for non-repelling sets, like the cat map

for integer trace s. There there is a new (only one!) pruning rule for each prime period set of cycles (ie, are we on the way to prove Riemann conjecture?) and a messy set of rules for non-prime periods (which can be described by a polynomial in s.

The Question: Is the cat map pruning front a fractal set? Is there a systematic set of formulas for the diffusion constant, one for each set of grammar rules? Is this implicit in papers of Vivaldi and/or Keating?

I'm a attaching the list of table 1.1, generated by Li Han. He (and not only he) operates on a different astral plane, so getting him to commit his results to our blog or draft of the paper is harder than pulling teeth . He has the grammar rules count to length 17 and the polynomials in s, but that I have only seen on his laptop screen.

PS - I am throwing in for a good measure a tent map, sect. 1.10, to illustrate what these polynomials in the stretching rate (s for cat, Λ for tent) are.

Now, what was YOUR main question that is still blowing in the wind?

2016-12-12 Roberto Artuso The main question, as I thought of it in my work of many years ago [10] (see ChaosBook.org Appendix *Statistical mechanics applications*, included in this blog as chapter 2), was to understand the behavior of D as $K \to 0$, since it seems to get an extra factor $D \sim K^{2.5}$, while $D \sim K^2$ is the usual quasilinear result. The Percival-Vivaldi linear code seemed to me appealing since it selects allowed itineraries within a sort of rhombus in many dimensions, and the symbols are directly linked to transport, while usual Markov partitions for integer K are not. My thought was that non-integer K behavior could be linked to the number of lattice points within the "rhombus", and that the K correction (as well as oscillations with respect to quasilinear estimate), could be related to estimates of errors in volumes *vs.* number of lattice points (something like Dyson-Bleher [22–25] work for ellipses).

2017-09-29 Predrag Vaienti [102] *Ergodic properties of the discontinuous sawtooth map* might be worthy of a read.

2017-09-27 Predrag Vallejos and Saraceno [103] *The construction of a quantum Markov partition* (1999), present in Figure 6 the 5-rectangles Markov partition of the Arnol'd cat map of Adler and Weiss [3] *Similarity of automorphisms of the torus*. Work it out for our A'.

The three regions partition of the cat map is explained at length in Tabrizian's notes.

Chernov (see his Fig. 1) writes: "If the matrix A' is not symmetric, the stable and unstable lines for on the torus may not be orthogonal. Then, the atoms of Markov partitions are, geometrically, parallelograms rather than rectangles. In early works on Markov partitions [92], the term 'parallelogram' was used instead of 'rectangle'.

Check also Nonnenmacher notes, and the Sect. 5 of Huntsman's paper.

From math stockexchange: A reference would be the Handbook of dynamical systems by Hasselblatt and Katok [56], Volume 1, starting on page 324. The cat map example is on pages 327-328. Another good source is the original paper by Adler and Weiss [2] from 1967 and R. Bowen's paper on Axiom A from 1970. Constructing Markov partitions for higher dimensional tori is much more complicated, as the borders of their atoms are fractal and not differentiable, hence the nice rectangles only happen to exist in 2 dimensions.

The two and M regions partition of the cat map are drawn in Vorobets' lecture.

Here is a beautifully laid out problem set.

For a cat map, the SRB measure is just the Lebesgue measure, which also serves as a probability measure.

Bruin, in his Sect. 12 discussion of *Toral automorphisms*, asserts that Arnol'd didn't seem to like cats. So, never ever forget to blame the cat. Whatever you do, the cat will be back.

2018-02-11 Predrag Ignore the following cryptic remark about symbolic dynamics intrinsic to being in the stable / unstable manifolds coordinates: The symbolic dynamics is 2-dimensional: a partition can be {left,right} $= \{L, R\}$ with respect to the unstable eigendirection through the origin, and {up,down} $= \{U, D\}$ with respect to the stable eigendirection, so partitions are labeled by pairs of symbols (the canonical Arn 3-letter alphabet)

$$\{h_j, v_j\} \in \{RU, LU, RD\}\,,$$

with $\{LD\}$ forbidden.

2018-02-11 Predrag I had left it as an exercise to any and every cat who wished to be a coauthor of the forthcoming paper [52] to construct the transition graph for the generating partition of figure 1.6 (b), and show that its topological zeta function is indeed the one given by Isola [62] (here equation (1.46) in sect. 1.6.3; there is a chapter on topological zeta functions in ChaosBook). But not one putative author responded by a single word, so I had to do the whole thing - here sect. 1.2.1. Adler–Weiss partition.

Look ma - no pruning!

Commentary

Remark 1.1. Anosov maps. Exposition of sect. 2.1 is taken from the excellent and influential paper of Percival and Vivaldi [83]. Anosov maps have been extensively analyzed as examples of genuine Hamiltonian chaotic evolution: in particular they admit simple Markov partitions [7, 41], which lead to simple analytic expressions for topological zeta functions [62]. Behrends [15, 16] *The ghosts of the cat* is fun - he uncovers

various regular patterns in the iterates of the cat map. Barash and Shchur [13] give an algorithm for determining certain sets periodic orbits in the context of using cat maps as pseudorandom number generators. The linear code of sect. 2.3 was introduced and worked out in detail by Percival and Vivaldi [18, 83]. However, digesting Percival and Vivaldi [84] will require some pencil and paper.

An extensive analysis of the periodic orbits of the cat map, following Percival and Vivaldi [83] has been carried out by Keating [64]. The fact that even Dyson [44] counts cat map periods should give you pause - clearly, some nontrivial number theory is afoot. Problems with the discretization of Arnol'd cat map were pointed out in refs. [19, 20]. Ref. [20] discusses two partitions of the cat map unit square.

There is a whole strain of mathematical literature that refers to the cat map as the 'Thom's toral automorphism', or 'Thom-Anosov diffeomorphism'.

[17] (Continued in remark **??**)

Remark 1.2. Cat map quantization. Hannay and Berry [55] *Quantization of linear maps on a torus – Fresnel diffraction by a periodic grating* might be the first to use Arnol'd cat map [7] in the quantization context. They exhibit various periodic orbits (cycles) and rules for constructing them. [18] An extensive analysis of the use of the periodic orbits of the cat map in quantization has been performed by Keating [65].*The cat maps: quantum mechanics and classical motion*. Jin and Zworski [63] write down the classical trace formula for Anosov flows. [19] Creagh [36] studies semiclassical approximations to the spectra of smoothly perturbed quantum cat maps. Boasman and Keating [26] study semiclassical asymptotics of perturbed cat maps. García-Mata and Saraceno [47] study the Arnol'd cat map with a small sinusoidal perturbation and note that its Lyapunov exponent $\lambda = \ln[(3+\sqrt{5})/2]$ is almost independent of the week nonlinearity, while the Ruelle-Pollicot resonances are very sensitive to it. Rivas [85] derives an exact expression for a (linear) cat map. Faure [46] investigates resonances of a "prequantum" cat map.

Remark 1.3. Phase space. The cylinder phase is $[-1/2, 1/2) \times \mathbb{R}$: the map is originally defined definition in $[-1/2, 1/2)^2$, and is generalized over the cylinder by symmetry requirements. [20]

Remark 1.4. Cat map.

Adler [1] *Symbolic dynamics and Markov partitions*, is an excellent overview of symbolic dynamics techniques. Adler writes: "The decimal expansion of real numbers, familiar to us all, has a dramatic generalization to representation of dynamical system orbits by symbolic sequences. The natural way to associate a symbolic sequence with an orbit is to track its history through a partition. But in order to get a useful symbolism, one needs to construct a partition with special properties, by means of so-called Markov partitions. We apply the results to one of the more tractable examples: namely, hyperbolic automorphisms of the two dimensional torus."

"The first use of infinite sequences of symbols to describe orbits is attributed to a nineteenth century work of Hadamard [54]. However the present work is rooted in something very much older and familiar to us all: namely, the representation of real numbers by infinite binary expansions. Markov partitions for hyperbolic automorphisms acting on the two dimensional torus have come to play a pervasive role

[17] Predrag 2016-08-03: not sure whether this leads to symbolic dynamics.

[18] Predrag 2016-08-03: though, at a very superficial glance, the cat map seems to be excluded form these considerations.

[19] Predrag 2016-08-03: but I do not see them actually computing any periodic orbits.

[20] Predrag 2016-08-03: missing eq. refeqtra-sym reference.

in understanding the dynamics of general hyperbolic systems, e.g., Anosov diffeomorphisms, axiom A diffeomorphisms, and pseudo-Anosov diffeomorphisms. Sinai [92] constructed Markov partitions for Anosov diffeomorphisms (a simpler treatment can be found in Bowen [30]). This class of maps includes hyperbolic automorphisms of n-dimensional tori, $n > 2$. "

example 1.1

Area-preserving maps that describe kicked rotors subject to a discrete time sequence of angle-dependent impulses (1.77) play important role in the theory of chaos in Hamiltonian systems, from the Taylor, Chirikov and Greene standard map [35, 71], to the cat maps.

Cat maps have been extensively analyzed as particularly simple examples of chaotic Hamiltonian dynamics. There are many good expositions - in particular we enjoyed Robinson [86]. They exhibit ergodicity, mixing, exponential sensitivity to variation of the initial conditions (the positivity of the Lyapunov exponent), and the positivity of the Kolmogorov-Sinai entropy [99]. They admit simple Markov partitions [7, 41], which lead to simple analytic expressions for topological zeta functions [62]. Detailed understanding of dynamics of cat maps is important also for the much richer world of nonlinear hyperbolic toral automorphisms, see refs. [36, 47, 94] for examples.

We refer here to (1.3), with $s = 3$ the least unstable of the cat maps, as the "Arnol'd", or "Thom-Arnol'd-Sinai cat map" [7, 41], and to general maps with integer $s \geq 3$ as "cat maps".

The "linear code" [18, 83] for temporal evolution of a single cat map was introduced in the beautiful 1987 paper by Percival and Vivaldi.

Percival and Vivaldi give a clear discussion of the "two-configuration cat map representation" (1.5) in Sect. 4. *Geometry of the linear code* of their paper [83], well worth reading. Their alphabet is different, as their map acts on the centered unit interval $[-1/2, 12)$.

Circulant matrix are discussed in ref. [4].

Jim Crutchfield [37] online course lect. 13 illustrates nicely the action of Thom-Arnol'd cat map (1.1). The course is thoughtfully put together, with notes and videos, a valuable resource.

Remark 1.5. Pythagorean tiling or *two squares tessellation* is a tiling of a Euclidean plane by squares of two different sizes, in which each square touches four squares of the other size on its four sides (see wikipedia.org/wiki/Pythagorean_tiling). This tiling has four-way rotational symmetry around each of its squares. When the ratio of the side lengths of the two squares is an irrational number such as the golden ratio, its cross-sections form aperiodic sequences with a Fibonacci-type recursive structure. It has a cyclic set of symmetries around the corresponding points, giving it **p4** symmetry: square lattice, point group C_4, two rotation centres of order four (90^0), and one rotation centre of order two (180^0). It has no reflections or glide reflections. It is a chiral pattern, meaning that it is impossible to superpose it on top of its mirror image using only translations and rotations; a Pythagorean tiling is not symmetric under mirror reflections. Although a Pythagorean tiling is itself periodic (it has a square lattice of translational symmetries) its cross sections can be used to generate one-dimensional aperiodic sequences.

Remark 1.6. XXX.

References

[1] R. L. Adler, "Symbolic dynamics and Markov partitions", Bull. Amer. Math. Soc. **35**, 1–56 (1998).

[2] R. L. Adler and B. Weiss, "Entropy, a complete metric invariant for automorphisms of the torus", Proc. Natl. Acad. Sci. USA **57**, 1573–1576 (1967).

[3] R. L. Adler and B. Weiss, *Similarity of automorphisms of the torus*, Vol. 98, Memoirs Amer. Math. Soc. (Amer. Math. Soc., Providence RI, 1970).

[4] A. Aitken, *Determinants & Matrices* (Oliver & Boyd, Edinburgh, 1939).

[5] E. Allroth, "Ground state of one-dimensional systems and fixed points of 2n-dimensional map", J. Phys. A **16**, L497 (1983).

[6] D. V. Anosov, A. V. Klimenko, and G. Kolutsky, On the hyperbolic automorphisms of the 2-torus and their Markov partitions, 2008.

[7] V. I. Arnol'd and A. Avez, *Ergodic Problems of Classical Mechanics* (Addison-Wesley, Redwood City, 1989).

[8] R. Artuso, E. Aurell, and P. Cvitanović, "Recycling of strange sets: II. Applications", Nonlinearity **3**, 361–386 (1990).

[9] R. Artuso and P. Cvitanović, "Deterministic diffusion", in *Chaos: Classical and Quantum*, edited by P. Cvitanović, R. Artuso, R. Mainieri, G. Tanner, and G. Vattay (Niels Bohr Inst., Copenhagen, 2017).

[10] R. Artuso and R. Strepparava, "Reycling diffusion in sawtooth and cat maps", Phys. Lett. A **236**, 469–475 (1997).

[11] M. Baake and J. A. G. Roberts, "Reversing symmetry group of Gl(2,z) and PGl(2,z) matrices with connections to cat maps and trace maps", J. Phys. A **30**, 1549 (1997).

[12] M. Baake, J. A. G. Roberts, and A. Weiss, "Periodic orbits of linear endomorphisms on the 2-torus and its lattices", Nonlinearity **21**, 2427 (2008).

[13] L. Barash and L. N. Shchur, "Periodic orbits of the ensemble of Sinai-Arnold cat maps and pseudorandom number generation", Phys. Rev. E **73**, 036701 (2006).

[14] A. F. Beardon, S. R. Bullett, and P. J. Rippon, "Periodic orbits of difference equations", Proc. Roy. Soc. Edinburgh Sect. A **125**, 657–674 (1995).

[15] E. Behrends, "The ghosts of the cat", Ergod. Theor. Dynam. Syst. **18**, 321–330 (1998).

[16] E. Behrends and B. Fielder, "Periods of discretized linear Anosov maps", Ergod. Theor. Dynam. Syst. **18**, 331–341 (1998).

[17] T. H. Berlin and M. Kac, "The spherical model of a ferromagnet", Phys. Rev. **86**, 821–835 (1952).

[18] N. Bird and F. Vivaldi, "Periodic orbits of the sawtooth maps", Physica D **30**, 164–176 (1988).

[19] M. . Blank, *Discreteness and Continuity in Problems of Chaotic Dynamics* (Amer. Math. Soc., Providence RI, 1997).

[20] M. Blank and G. Keller, "Random perturbations of chaotic dynamical systems: stability of the spectrum", Nonlinearity **11**, 1351–1364 (1998).

[21] M. Blank, G. Keller, and C. Liverani, "Ruelle-Perron-Frobenius spectrum for Anosov maps", Nonlinearity **15**, 1905–1973 (2002).

[22] P. M. Bleher and F. J. Dyson, "Mean square limit for lattice points in a sphere", Acta Arith. **68**, 383–393 (1994).

[23] P. M. Bleher and F. J. Dyson, "Mean square value of exponential sums related to representation of integers as sum of two squares", Acta Arith. **68**, 71–84 (1994).

[24] P. M. Bleher and F. J. Dyson, "The variance of the error function in the shifted circle problem is a wild function of the shift", Commun. Math. Phys. **160**, 493–505 (1994).

[25] P. Bleher, "Trace formula for quantum integrable systems, lattice-point problem, and small divisors", in *Emerging Applications of Number Theory*, edited by D. A. Hejhal, J.Friedman, M. C. Gutzwiller, and A. M. Odlyzko (Springer, 1999), pp. 1–38.

[26] P. A. Boasman and J. P. Keating, "Semiclassical asymptotics of perturbed cat maps", Proc. Roy. Soc. Ser A **449**, 629–653 (1995).

[27] S. V. Bolotin and D. V. Treschev, "Hill's formula", Russ. Math. Surv. **65**, 191 (2010).

[28] T. Bountis and R. H. G. Helleman, "On the stability of periodic orbits of two-dimensional mappings", J. Math. Phys **22**, 1867–1877 (1981).

[29] R. Bowen, "Markov partitions for Axiom A diffeomorphisms", Amer. J. Math. **92**, 725–747 (1970).

[30] R. Bowen, *Equilibrium States and the Ergodic Theory of Anosov Diffeomorphisms* (Springer, Berlin, 1975).

[31] F. Brini, S. Siboni, G. Turchetti, and S. Vaienti, "Decay of correlations for the automorphism of the torus T^2", Nonlinearity **10**, 1257–1268 (1997).

[32] S. Bullett, "Invariant circles for the piecewise linear standard map", Commun. Math. Phys. **107**, 241–262 (1986).

[33] E. Calabi, "On the group of automorphisms of a symplectic manifold", in *Problems in Analysis: A Symposium in Honor of Salomon Bochner* (Princeton Univ. Press, Princeton NJ, 1970), pp. 1–26.

[34] S. Capobianco and T. Toffoli, Can anything from Noether's theorem be salvaged for discrete dynamical systems?, in *Unconventional computation: 10th international conference, uc 2011, turku, finland*, edited by C. S. Calude, J. Kari, I. Petre, and G. Rozenberg (Springer, Berlin, Heidelberg, 2011), pp. 77–88.

[35] B. V. Chirikov, "A universal instability of many-dimensional oscillator system", Phys. Rep. **52**, 263–379 (1979).

[36] S. C. Creagh, "Quantum zeta function for perturbed cat maps", Chaos **5**, 477–493 (1995).

[37] J. Crutchfield, Roadmap for Natural Computation and Self-Organization, tech. rep., Physics 256A course (U. California, Davis, 2017).

[38] P. Cvitanović, R. Artuso, R. Mainieri, G. Tanner, and G. Vattay, *Chaos: Classical and Quantum* (Niels Bohr Inst., Copenhagen, 2017).

[39] P. Cvitanović, R. Artuso, L. Rondoni, and E. A. Spiegel, "Transporting densities", in *Chaos: Classical and Quantum*, edited by P. Cvitanović, R. Artuso, R. Mainieri, G. Tanner, and G. Vattay (Niels Bohr Inst., Copenhagen, 2017).

[40] P. J. Davis, *Circulant matrices*, 2nd ed. (Amer. Math. Soc., New York, 1979).

[41] R. L. Devaney, *An Introduction to Chaotic Dynamical systems*, 2nd ed. (Westview Press, 2008).

[42] M. Dow, "Explicit inverses of Toeplitz and associated matrices", ANZIAM J. **44**, E185–E215 (2003).

[43] H. R. Dullin and J. D. Meiss, "Stability of minimal periodic orbits", Phys. Lett. A **247**, 227–234 (1998).

[44] F. J. Dyson and H. Falk, "Period of a discrete cat mapping", Amer. Math. Monthly **99**, 603–614 (1992).

[45] M. Elouafi, "On a relationship between Chebyshev polynomials and Toeplitz determinants", Appl. Math. Comput. **229**, 27–33 (2014).

[46] F. Faure, "Prequantum chaos: Resonances of the prequantum cat map", Phys. Rev. Lett. **1**, 255–285 (1987).

[47] I. García-Mata and M. Saraceno, "Spectral properties and classical decays in quantum open systems", Phys. Rev. E **69**, 056211 (2004).

[48] M. J. C. Gover, "The eigenproblem of a tridiagonal 2-Toeplitz matrix", Linear Algebra Appl. **197**, 63–78 (1994).

[49] I. S. Gradshteyn and I. M. Ryzhik, *Tables of integrals, series and products* (Academic, New York, 1980).

[50] J. M. Greene, "A method for determining a stochastic transition", J. Math. Phys. **20**, 1183–1201 (1979).

[51] J. Guckenheimer, "On the bifurcation of maps of the interval", Inv. Math. **39**, 165–178 (1977).

[52] B. Gutkin, L. Han, R. Jafari, A. K. Saremi, and P. Cvitanović, Linear encoding of the spatiotemporal cat map, In preparation, 2018.

[53] B. Gutkin and V. Osipov, "Classical foundations of many-particle quantum chaos", Nonlinearity **29**, 325–356 (2016).

[54] J. Hadamard, "Les surfaces à courbures opposées et leurs lignes géodésique", J. Math. Pures Appl. **4**, 27–73 (1898).

[55] J. H. Hannay and M. V. Berry, "Quantization of linear maps on a torus – Fresnel diffraction by a periodic grating", Physica D **1**, 267–290 (1980).

[56] B. Hasselblatt and A. Katok, *Handbook of Dynamical Systems* (Elsevier, New York, 2002).

[57] G. Y. Hu and R. F. O'Connell, "Exact solution for the charge soliton in a one-dimensional array of small tunnel junctions", Phys. Rev. B **49**, 16773–16776 (1994).

[58] G. Y. Hu and R. F. O'Connell, "Exact solution of the electrostatic problem for a single electron multijunction trap", Phys. Rev. Lett. **74**, 1839–1842 (1995).

[59] G. Y. Hu and R. F. O'Connell, "Analytical inversion of symmetric tridiagonal matrices", J. Phys. A **29**, 1511 (1996).

[60] T. A. Hunt and B. D. Todd, "On the Arnold cat map and periodic boundary conditions for planar elongational flow", Molec. Phys **101**, 3445–3454 (2003).

[61] P. E. Hydon and E. L. Mansfield, "Extensions of Noether's Second Theorem: from continuous to discrete systems", Proc. R. Soc. London A **467**, 3206–3221 (2011).

[62] S. Isola, "ζ-functions and distribution of periodic orbits of toral automorphisms", Europhys. Lett. **11**, 517–522 (1990).

[63] L. Jin and M. Zworski, A local trace formula for Anosov flows, 2014.

[64] J. P. Keating, "Asymptotic properties of the periodic orbits of the cat maps", Nonlinearity **4**, 277 (1991).

[65] J. P. Keating, "The cat maps: quantum mechanics and classical motion", Nonlinearity **4**, 309–341 (1991).

[66] J. P. Keating and F. Mezzadri, "Pseudo-symmetries of Anosov maps and spectral statistics", Nonlinearity **13**, 747–775 (2000).

[67] H. Kübra Duru and D. Bozkurt, Integer powers of certain complex pentadiagonal 2-Toeplitz matrices, 2017.

[68] E. Lanneau and J.-L. Thiffeault, "On the minimum dilatation of pseudo-Anosov homeomorphisms on surfaces of small genus", Ann. Inst. Fourier **61**, 105–144 (2011).

[69] D. Li and J. Xie, "Symbolic dynamics of Belykh-type maps", Appl. Math. Mech. **37**, 671–682 (2016).

[70] J. Li and S. Tomsovic, "Exact relations between homoclinic and periodic orbit actions in chaotic systems", Phys. Rev. E **97**, 022216 (2017).

[71] A. J. Lichtenberg and M. A. Lieberman, *Regular and Chaotic Dynamics*, 2nd ed. (Springer, New York, 2013).

[72] R. S. Mackay and J. D. Meiss, "Linear stability of periodic orbits in Lagrangian systems", Phys. Lett. A **98**, 92–94 (1983).

[73] S. MacKay, J. D. Meiss, and I. C. Percival, "Transport in Hamiltonian systems", Physica D **13**, 55–81 (1984).

[74] A. Manning, "Axiom A diffeomorphisms have rational zeta function", Bull. London Math. Soc. **3**, 215–220 (1971).

[75] A. Manning, "A Markov partition that reflects the geometry of a hyperbolic toral automorphism", Trans. Amer. Math. Soc. **354**, 2849–2864 (2002).

[76] E. L. Mansfield, Noether's theorem for smooth, difference and finite element schemes, in Foundations of computational mathematics, santander 2005, Vol. 331, London Math. Soc. Lect. Notes (2006), pp. 230–254.

[77] J. D. Meiss, "Symplectic maps, variational principles, and transport", Rev. Mod. Phys. **64**, 795–848 (1992).

[78] B. D. Mestel and I. Percival, "Newton method for highly unstable orbits", Physica D **24**, 172 (1987).

[79] C. Meyer, *Matrix Analysis and Applied Linear Algebra* (SIAM, Philadelphia, 2000).

[80] S. Nonnenmacher, "Spectral properties of noisy classical and quantum propagators", Nonlinearity **16**, 1685–1713 (2003).

[81] S. Noschese, L. Pasquini, and L. Reichel, "Tridiagonal Toeplitz matrices: properties and novel applications", Numer. Linear Algebra Appl. **20**, 302–326 (2013).

[82] A. M. Ozorio de Almeida and J. H. Hannay, "Periodic orbits and a correlation function for the semiclassical density of states", J. Phys. A **17**, 3429 (1984).

[83] I. Percival and F. Vivaldi, "A linear code for the sawtooth and cat maps", Physica D **27**, 373–386 (1987).

[84] I. Percival and F. Vivaldi, "Arithmetical properties of strongly chaotic motions", Physica D **25**, 105–130 (1987).

[85] A. M. F. Rivas, "Semiclassical matrix elements for a chaotic propagator in the scar function basis", J. Phys. A **46** (2013) 10.1088/1751-8113/46/14/145101.

[86] R. C. Robinson, *An Introduction to Dynamical Systems: Continuous and Discrete* (Amer. Math. Soc., New York, 2012).

[87] D. Ruelle, "An extension of the theory of Fredholm determinants", Inst. Hautes Études Sci. Publ. Math. **72**, 175–193 (1990).

[88] E. Rykken, "Markov partitions for hyperbolic toral automorphisms of T^2", Rocky Mountain J. Math. **28**, 1103–1124 (1998).

[89] G. Schmidt, "Hamilton's principle and the splitting of periodic orbits", in *Statistical Physics and Chaos in Fusion Plasmas*, edited by C. W. Horton Jr. and L. E. Reichl (John Wiley and Sons, 1984), p. 57.

[90] A. Siemaszko and M. P. Wojtkowski, "Counting Berg partitions", Nonlinearity **24**, 2383–2403 (2011).

[91] S. Simons, "Analytical inversion of a particular type of banded matrix", J. Phys. A **30**, 755 (1997).

[92] Y. G. Sinai, "Construction of Markov partitions", Funct. Anal. Appl. **2**, 245–253 (1968).

[93] Y. G. Sinai, *Introduction to Ergodic Theory* (Princeton Univ. Press, Princeton, 1976).

[94] J. Slipantschuk, O. F. Bandtlow, and W. Just, "Complete spectral data for analytic Anosov maps of the torus", Nonlinearity **30**, 2667 (2017).

[95] S. Smale, "Generalized Poincaré's conjecture in dimensions greater than four", Ann. Math. **74**, 199 (1961).

[96] G. D. Smith, *Numerical Solution of Partial Differential Equations: Finite Difference Methods* (Clarendon Press, Oxford UK, 1985).

[97] M. R. Snavely, "Markov partitions for the two-dimensional torus", Proc. Amer. Math. Soc. **113**, 517–517 (1991).

[98] R. F. Streater, "A bound for the difference Laplacian", Bull. London Math. Soc. **11**, 354–357 (1979).

[99] R. Sturman, J. M. Ottino, and S. Wiggins, *The Mathematical Foundations of Mixing* (Cambridge Univ. Press, 2006).

[100] T. Tél, "Fractal dimension of the strange attractor in a piecewise linear two-dimensional map", Phys. Lett. A **97**, 219–223 (1983).

[101] B. D. Todd, "Cats, maps and nanoflows: some recent developments in nonequilibrium nanofluidics", Molec. Simul. **31**, 411–428 (2005).

[102] S. Vaienti, "Ergodic properties of the discontinuous sawtooth map", J. Stat. Phys. **67**, 251–269 (1992).

[103] R. O. Vallejos and M. Saraceno, "The construction of a quantum Markov partition", J. Phys. A **32**, 7273 (1999).

[104] P. Walters, *An Introduction to Ergodic Theory* (Springer, New York, 1981).

[105] E. W. Weisstein, Arnold's Cat Map, MathWorld–A Wolfram Web Resource.

[106] H. A. Yamani and M. S. Abdelmonem, "The analytic inversion of any finite symmetric tridiagonal matrix", J. Phys. A **30**, 2889 (1997).

[107] W.-C. Yueh, "Explicit inverses of several tridiagonal matrices", Appl. Math. E-Notes **6**, 74–83 (2006).

1.13 Examples

Example 1.1. ***Kicked rotor action.*** *Area-preserving maps that describe kicked rotors subject to a discrete time sequence of angle-dependent impulses $P(x_n)$, $t \in \mathbb{Z}$,*

$$x_{n+1} = x_n + p_{n+1} \mod 1, \tag{1.77}$$
$$p_{n+1} = p_n + P(x_n)\,, \tag{1.78}$$

play important role in the theory of chaos in Hamiltonian systems, from the Taylor, Chirikov and Greene standard map [35, 71], to the cat maps that we study here. Here $2\pi x$ is the angle of the rotor, p is the momentum conjugate to the configuration coordinate x, $P(x) = P(x+1)$ is periodic pulse with period 1, and the time step has been set to $\Delta t = 1$. Area-preserving maps that describe kicked rotors subject to a discrete time sequence of angle-dependent impulses $P(x_n)$ of form (1.77), (1.78) have a generating function

$$F(q_n, q_{n+1}) = \frac{1}{2}(q_n - q_{n+1})^2 - V(q_n)^2\,, \qquad P(q) = -\frac{dV(q)}{dq}\,. \tag{1.79}$$

This generating function is the discrete time Lagrangian for a particle moving in potential $V(x)$. Eq. (1.77) says that in one time step Δt the configuration trajectory starting at x_n reaches $x_{n+1} = x_n + p_{n+1}\Delta t$, and (1.78) says that at each kick the angular momentum p_n is accelerated to p_{n+1} by the force pulse $P(x_n)\Delta t$. As the values of x differing by integers are identified, and the momentum p is unbounded, the phase space is a cylinder. However, to analyse the dynamics, one can just as well compactify the state space by folding the momentum dynamics onto a circle, by adding " $\mod 1$ *" to (1.78). This reduces the dynamics to a toral automorphism acting on a $(0,1] \times (0,1]$ square of unit area, with the opposite sides identified.*

click to return: p. 20

Example 1.2. ***Cat map.*** *The simplest example of (1.77,1.78) is a rotor subject to a force $F(x) = Kx$ linear in the displacement x. The $\mod 1$ added to (1.78) makes this a discontinuous "sawtooth," unless K is an integer. In that case the map (1.77,1.78) is a continuous automorphism of the torus, or a "cat map" [7], a linear symplectic map on the unit 2-torus state space, $(x \mapsto Ax \,|\, x \in \mathbb{T}^2 = \mathbb{R}^2/\mathbb{Z}^2\,;\ A \in SL(2,\mathbb{Z}))$, with coordinates $x = (x_n, p_n)$ interpreted as the angular position variable and its conjugate momentum at time instant t. Explicitly:*

$$\begin{pmatrix} x_{n+1} \\ p_{n+1} \end{pmatrix} = A \begin{pmatrix} x_n \\ p_n \end{pmatrix} \mod 1\,, \qquad A = \begin{pmatrix} a & c \\ d & b \end{pmatrix}\,, \tag{1.80}$$

where a, b, c, d are integers whose precise values do not matter, as long as $\det A = 1$, so that the map is symplectic (area preserving). In that case the map is characterized by only one invariant parameter, $s = \operatorname{tr} A$, so consider a linear, phase space (area) preserving map of a 2-torus onto itself

$$\begin{pmatrix} x_{n+1} \\ p_{n+1} \end{pmatrix} = A \begin{pmatrix} x_n \\ p_n \end{pmatrix} \mod 1\,, \qquad A = \begin{pmatrix} s-1 & 1 \\ s-2 & 1 \end{pmatrix}\,, \tag{1.81}$$

where both x_n and p_n belong to the unit interval. For integer $s = \operatorname{tr} A > 2$ the map is referred to as a cat map [7]. It is a fully chaotic Hamiltonian dynamical system, which, rewritten as a 2-step difference equation in (x_{n-1}, x_n) takes a particularly simple form [83]

$$x_{n+1} - s\,x_n + x_{n-1} = -m_n\,, \tag{1.82}$$

with the unique integer "winding number" m_n at every time step n ensuring that x_{n+1} lands in the unit interval. While the dynamics is linear, the nonlinearity comes through the $\mod 1$ operation, encoded in $m_n \in \mathcal{A}$, where $\mathcal{A}$ is finite alphabet of possible values for m_n.

A cat map is a fully chaotic Hamiltonian dynamical system if its stability multipliers $(\Lambda^+, \Lambda^-) = (\Lambda\,,\ \Lambda^{-1})$

$$\Lambda^{\pm} = \frac{1}{2}(s \pm \sqrt{D})\,, \qquad \Lambda = \frac{1}{2}(s + \sqrt{(s-2)(s+2)}) = e^{\lambda}\,, \tag{1.83}$$

are real, where $s = \operatorname{tr} A = \Lambda + \Lambda^{-1}$, $\sqrt{D} = \Lambda - \Lambda^{-1}$, discriminant $D = s^2 - 4$, with a positive Lyapunov exponent $\lambda > 0$. The eigenvalues are functions of the "stretching" parameter s, and the map is chaotic if and only if $|s| > 2$.

We refer here to the least unstable of the cat maps (1.80), with $s = 3$, as the "Arnol'd", or "Thom-Arnol'd-Sinai cat map" [7, 41], and to general maps with integer $s \geq 3$ as "cat maps". Cat maps have been extensively analyzed as particularly simple examples of chaotic Hamiltonian dynamics. They exhibit ergodicity, mixing, exponential sensitivity to variation of the initial conditions (the positivity of the Lyapunov exponent), and the positivity of the Kolmogorov-Sinai entropy [99]. Detailed understanding of dynamics of cat maps is important also for the much richer world of nonlinear hyperbolic toral automorphisms, see refs. [36, 47, 94] for examples.

Example 1.3. ***Projection operator decomposition of the cat map:*** *Let's illustrate how the decomposition works for the Percival and Vivaldi [83] "two-configuration representation" of the Arnol'd cat map by the $[2\times 2]$ matrix*

$$\mathbf{A} = \begin{bmatrix} 0 & 1 \\ -1 & s \end{bmatrix}\,. \tag{1.84}$$

To interpret m_n's, consider the action of the this map (1.90) on a 2-dimensional state space point (x_{n-1}, x_n),

$$\begin{pmatrix} x_n \\ x_{n+1} \end{pmatrix} = \mathbf{A} \begin{pmatrix} x_{n-1} \\ x_n \end{pmatrix} - \begin{pmatrix} 0 \\ m_n \end{pmatrix}\,. \tag{1.85}$$

In Percival and Vivaldi [83] this representation of cat map is referred to as "the two-configuration representation". As illustrated in figure 1.2, in one time step the area preserving map A' stretches the unit square into a parallelogram, and a point (x_0, x_1) within the initial unit square in general lands outside it, in another unit square m_n steps away. As they shepherd such stray points back into the unit torus, the integers m_n can be interpreted as "winding numbers" [65], or "stabilising impulses" [83]. The m_n translations reshuffle the state space, thus partitioning it into $|\mathcal{A}|$ regions $\mathcal{M}_m$, $m \in \mathcal{A}$.

Associated with each root Λ^i in (1.83) is the projection operator *$\mathbf{P}^i = \prod(\mathbf{A} - \Lambda^j\mathbf{1})/(\Lambda^i - \Lambda^j)\,,\ j \neq i$,*

$$\mathbf{P}^+ = \frac{1}{\sqrt{D}}(\mathbf{A} - \Lambda^{-1}\mathbf{1}) = \frac{1}{\sqrt{D}} \begin{bmatrix} -\Lambda^{-1} & 1 \\ -1 & \Lambda \end{bmatrix} \tag{1.86}$$

$$\mathbf{P}^- = -\frac{1}{\sqrt{D}}(\mathbf{A} - \Lambda\,\mathbf{1}) = \frac{1}{\sqrt{D}} \begin{bmatrix} \Lambda & -1 \\ 1 & -\Lambda^{-1} \end{bmatrix}\,. \tag{1.87}$$

Matrices $\mathbf{P}^{\pm}$ are orthonormal and complete. The dimension of the ith subspace is given by $d_i = \operatorname{tr}\mathbf{P}_i$; in case at hand both subspaces are 1-dimensional. From the characteristic equation it follows that $\mathbf{P}^{\pm}$ satisfy the eigenvalue equation $\mathbf{A}\,\mathbf{P}^{\pm} = \Lambda^{\pm}\mathbf{P}^{\pm}$,

with every column a right eigenvector, and every row a left eigenvector. Picking –for example– the first row/column we get the right and the left eigenvectors:

$$\begin{aligned}\{\mathbf{e}^{(+)},\mathbf{e}^{(-)}\} &= \left\{\frac{1}{\sqrt{D}}\begin{bmatrix}-\Lambda^{-1}\\ -1\end{bmatrix},\frac{1}{\sqrt{D}}\begin{bmatrix}\Lambda\\ 1\end{bmatrix}\right\}\\ \{\mathbf{e}_{(+)},\mathbf{e}_{(-)}\} &= \left\{\frac{1}{\sqrt{D}}[-\Lambda^{-1},1],\frac{1}{\sqrt{D}}[\Lambda,-1]\right\},\end{aligned} \tag{1.88}$$

with overall scale arbitrary. [21] *The matrix is not symmetric, so* $\{\mathbf{e}^{(j)}\}$ *do not form an orthogonal basis. The left-right eigenvector dot products* $\mathbf{e}_{(j)}\cdot\mathbf{e}^{(k)}$*, however, are orthogonal,* 2CB

$$\mathbf{e}_{(i)}\cdot\mathbf{e}^{(j)} = c_j\,\delta_{ij}\,.$$

What does this do to the partition figure 1.2? The origin is still the fixed point. A state space point in the new, dynamically intrinsic right eigenvector Adler-Weiss [3] coordinate basis is

$$\begin{aligned}\begin{pmatrix}x_{n-1}\\ x_n\end{pmatrix} &= (\mathbf{P}^+ + \mathbf{P}^-)\begin{pmatrix}x_{n-1}\\ x_n\end{pmatrix}\\ = \frac{1}{\sqrt{D}}\begin{bmatrix}-\Lambda^{-1} & 1\\ -1 & \Lambda\end{bmatrix}\begin{pmatrix}x_{n-1}\\ x_n\end{pmatrix} &+ \frac{1}{\sqrt{D}}\begin{bmatrix}\Lambda & -1\\ 1 & -\Lambda^{-1}\end{bmatrix}\begin{pmatrix}x_{n-1}\\ x_n\end{pmatrix}\\ = \frac{1}{\sqrt{D}}\begin{pmatrix}x_n-\Lambda^{-1}x_{n-1}\\ \Lambda x_n - x_{n-1}\end{pmatrix} &+ \frac{1}{\sqrt{D}}\begin{pmatrix}-x_n+\Lambda x_{n-1}\\ -\Lambda^{-1}x_n + x_{n-1}\end{pmatrix}\\ = -(\Lambda x_n - x_{n-1})\frac{1}{\sqrt{D}}\begin{bmatrix}-\Lambda^{-1}\\ -1\end{bmatrix} &+ (-\Lambda^{-1}x_n + x_{n-1})\frac{1}{\sqrt{D}}\begin{bmatrix}\Lambda\\ 1\end{bmatrix}\\ = (-\Lambda x_n + x_{n-1})\,\mathbf{P}^+ &+ (-\Lambda^{-1}x_n + x_{n-1})\,\mathbf{P}^-\,.\end{aligned}$$

The abscissa (x_{n-1} *direction) is not affected, but the ordinate* (x_n *direction) is flipped and stretched/shrunk by factor* $-\Lambda$, $-\Lambda^{-1}$ *respectively, preserving the vertical strip nature of the partition figure 1.2. In the Adler-Weiss right eigenbasis,* $\mathbf{A}$ *acts by stretching the* $\mathbf{e}^{(+)}$ *direction by* Λ*, and shrinking the* $\mathbf{e}^{(-)}$ *direction by* Λ^{-1}*, without any rotation of either direction.*

Example 1.4. ***A linear cat map code.*** *Eqs. (1.77,1.78) are the discrete-time Hamilton's equations, which induce temporal evolution on the 2-torus* (x_n, p_n) phase space*. For the problem at hand, it pays to go from the Hamiltonian* (x_n, p_n) *phase space formulation to the Newtonian (or Lagrangian)* (x_{n-1}, x_n) state space *formulation [83], with* p_n *replaced by* $p_n = (x_n - x_{n-1})/\Delta t$*. Eq. (1.78) then takes the 2-step difference form (the discrete time Laplacian* $\Box$ *formula for the second order time derivative* d^2/dt^2*, with the time step set to* $\Delta t = 1$*),*

$$\Box\, x_n \equiv x_{n+1} - 2x_n + x_{n-1} = P(x_n) \qquad \mod 1\,, \tag{1.89}$$

i.e., Newton's Second Law: "acceleration equals force." For a cat map, with force $P(x)$ *linear in the displacement* x*, the Newton's equation of motion (2.3) takes form*

$$(\Box + 2 - s)\,x_n = -m_n\,, \tag{1.90}$$

with $\mod 1$ *enforced by* m_n*'s, integers from the alphabet*

$$\mathcal{A} = \{\underline{1}, 0, \ldots s-1\}\,, \tag{1.91}$$

[21] Predrag 2017-10-02: compare with (1.40)

necessary to keep x_n for all times t within the unit interval $[0,1)$. The genesis of this alphabet is illustrated by figure 1.2. We have introduced here the symbol $\underline{|m_n|}$ to denote m_n with the negative sign, i.e., '$\underline{1}$' stands for symbol '-1'.

Example 1.5. ***Perron-Frobenius operator for the Arnol'd cat map.*** *For a piecewise linear maps acting on a finite generating partition the Perron-Frobenius operator takes the finite, transfer matrix form (see ref. [39]).*

$$\mathbf{L}_{ij} \;=\; \frac{|\mathcal{M}_i \cap f^{-1}(\mathcal{M}_j)|}{|\mathcal{M}_i|}\,, \quad \rho' = \rho\mathbf{L} \tag{1.92}$$

The two rectangles and five sub-rectangle areas $|\mathcal{M}_j|$ are given by inspection of figure 1.10 (a): [22]

$$\begin{aligned}
|\mathcal{M}_A| &= \Lambda/(\Lambda+1)\,, \quad |\mathcal{M}_B| = 1/(\Lambda+1)\,, \\
|\mathcal{M}_1| &= |\mathcal{M}_A|/\Lambda\,, \quad |\mathcal{M}_2| = (\Lambda-1)|\mathcal{M}_B|/\Lambda\,, \quad |\mathcal{M}_3| = |\mathcal{M}_A|/\Lambda\,, \\
|\mathcal{M}_4| &= |\mathcal{M}_B|/\Lambda\,, \quad |\mathcal{M}_5| = (\Lambda-2)|\mathcal{M}_A|/\Lambda\,,
\end{aligned} \tag{1.93}$$

where Λ and D are given in (1.83), and we are considering the $s=3$ Arnol'd cat map case (the generalization to $s>3$. is immediate) The areas are symplectic invariants, and thus the same in any choice of cat-map coordinates. As in the ChaosBook example exam:FP_eigs_Ulam *(currently 19.1), the Adler-Weiss partitioned Percival-Vivaldi cat map is an expanding piecewise-linear map, so we can construct the associated transfer matrix explicitly, by weighing the links of transition graph figure 1.10 (a) by the ratios of out-, in-rectangle areas $T_{kj} = |\mathcal{M}_{m_k}|/|\mathcal{M}_{m_j}|$:* [23]

$$\begin{bmatrix} \phi'_1 \\ \phi'_2 \\ \phi'_3 \\ \phi'_4 \\ \phi'_5 \end{bmatrix} = \mathbf{T}\phi = \frac{1}{\Lambda} \begin{bmatrix} 1 & \Lambda-2 & 1 & 0 & 0 \\ 0 & 0 & 0 & \Lambda-1 & 1 \\ 1 & \Lambda-2 & 1 & 0 & 0 \\ 0 & 0 & 0 & 1 & \Lambda-1 \\ 1 & \Lambda-1 & \frac{\Lambda-2}{\Lambda-1} & 0 & 0 \end{bmatrix} \begin{bmatrix} \phi_1 \\ \phi_2 \\ \phi_3 \\ \phi_4 \\ \phi_5 \end{bmatrix} \tag{1.94}$$

The probability for starting in initial state j is conserved, $\sum_k L_{kj} = 1$, as it should be. Such non-negative matrix whose columns conserve probability is called Markov, probability *or* stochastic *matrix. Thanks to the same expansion everywhere, and a finite transition graph, the Fredholm determinant is the characteristic polynomial of the transfer matrix (currently ChaosBook Eq. (18.13)) defined by the transition graph of figure 1.1 (c), expanded in non-intersecting loops $t_A = T_{A^0A}, t'_A = T_{A^1A}, t_B = T_{B^0B}, t_{AB} = T_{A^{\underline{1}}B}T_{B^1A}$:*

$$\det(1-z\mathbf{T}) = 1-z(t_A+t'_A+t_B)-z^2t_{AB}+z^2(t_A+t'_A)t_B = 1-3\frac{z}{\Lambda}-(\Lambda-3)\frac{z^2}{\Lambda}\,, \tag{1.95}$$

$$\det(1-z\mathbf{T}) = 1-3\frac{z}{\Lambda}-(\Lambda-3)\frac{z^2}{\Lambda}\,, \tag{1.96}$$

in agreement with (1.12). This counts the fixed point at the origin thrice (it lives in the invariant subspace spanned by stable and unstable manifolds, the border) so that has to be divided out.

[22] Predrag 2018-02-16: to Han: PLEASE RECHECK

[23] Predrag 2018-02-11: the matrix is NOT CORRECT yet, FIX!

Due to probability (unit area) conservation, $\mathbf{T}$ *has a unit eigenvalue* $z = 1 = e^{s_0}$*, with constant density eigenvector* $\rho_0 = \rho_1$*.*

In the orbit-counting case one retrieves Isola's ζ*-function [62] (1.46).*

This simple explicit matrix representation of the Perron-Frobenius operator is a consequence of the piecewise linearity of the time-forward map, and the restriction of the densities ρ *to the space of piecewise constant functions.*

Example 1.6. ***XXX.***

Example 1.7. ***Tent map linear code.*** *The simplest example of a piece-wise linear unimodal map with a binary (in general, pruned) symbolic dynamics is the* tent map*,*

$$f(x) = \begin{cases} f_0(x) = \Lambda x & \text{if } x < 1/2 \\ f_1(x) = \Lambda(1-x) & \text{if } x > 1/2 \end{cases} , \tag{1.97}$$

with $1 < \Lambda < \infty$ *and* $x \in \mathcal{M} = [0,1]$*. (Everything would go through for a skew tent map with* $\Lambda_0 \neq -\Lambda_1$*, but there is no need here for that complication.) For this family of unimodal maps the coarse (covering) partition of the unit interval* $\mathcal{M} = \mathcal{M}_0 \cap C \cap \mathcal{M}_1$ *is given by intervals* $\mathcal{M}_0 = [0, 1/2)$*,* $\mathcal{M}_1 = (1/2, 1]$*, and the critical point* $C = 1/2$*. Let's rewrite this as a linear first-order difference equation, in the manner of cat lovers enamoured of matters feline:*

$$\frac{1}{\Lambda}\, x_{t+1} + (2m_t - 1)x_t = m_t \,, \qquad \begin{cases} m_t = 0 & \text{if } x_t < 1/2 \\ m_t = 1 & \text{if } x_t > 1/2 \end{cases} . \tag{1.98}$$

That every such code is a 'linear code' is best understood by computing a periodic orbit for a specified itinerary. The fixed point condition $f^n(x) = x$ *for* n*-cycle* $\overline{m_1 m_2 m_3 \cdots m_{n-1} m_n}$ *is a linear relation between the finite alphabet* $m_t \in \{0,1\}$ *code, and the* $x_t \in \mathbb{R}$ *orbit*

$$\Delta(m) q(m) = m(m) \tag{1.99}$$

with orbit-dependent inverse propagator $\Delta(m) =$

$$\begin{pmatrix} 2m_n - 1 & 0 & 0 & \dots & 0 & \Lambda^{-1} \\ \Lambda^{-1} & 2m_{n-1} - 1 & 0 & \dots & 0 & 0 \\ 0 & \Lambda^{-1} & 2m_{n-2} - 1 & \dots & 0 & 0 \\ \vdots & \vdots & \vdots & \ddots & \vdots & \vdots \\ 0 & 0 & 0 & \dots & 2m_2 - 1 & 0 \\ 0 & 0 & 0 & \dots & \Lambda^{-1} & 2m_1 - 1 \end{pmatrix} ,$$

$$q(m) = \begin{pmatrix} x_n \\ x_{n-1} \\ x_{n-2} \\ \vdots \\ x_2 \\ x_1 \end{pmatrix} , \qquad m(m) = \begin{pmatrix} m_n \\ m_{n-1} \\ m_{n-2} \\ \vdots \\ m_2 \\ m_1 \end{pmatrix} ,$$

and $m(m)$ *is needed to fold the stretched orbit back into the unit interval. While the off-diagonal "1"s do generate cyclic shifts, the diagonal* $\pm\Lambda$ *terms are not shift invariant, so I do not believe this can be diagonalized by a discrete Fourier transform. I had worked*

it out for $\Lambda = 2$ in ChaosBook, but not sure if there are elegant tricks for arbitrary $\Lambda \neq 2$. For an orbit

$$q(m) = \Delta(m)^{-1} m(m) \tag{1.100}$$

to be admissible, no point should be to the right of the kneading value $x_\kappa = f(C)$. It follows from the kneading theory for unimodal maps (dike map with slope $\Lambda = 2$ being the canonical example) that if a periodic orbit exists for a given Λ, it exists for all larger Λ, and that all orbits exist for $\Lambda \geq 2$.

In other words, Λ is the "stretching parameter" for this problem, and the rational polynomial expressions in Λ for x_t correspond to Li Han's polynomials for cat maps.

click to return: p. 39

Example 1.8. ***Periodic points of a tent map.***

Exercise *Check (1.100) for fixed point(s).*

Exercise *Check (1.100) for the 2-cycle $\overline{01}$.*

$$\Delta(m) = \begin{pmatrix} -\Lambda & 1 \\ 1 & \Lambda \end{pmatrix}, \qquad m(m) = \Lambda \begin{pmatrix} 0 \\ 1 \end{pmatrix}.$$

$$\Delta^{-1} = \frac{1}{\Lambda^2+1} \begin{pmatrix} -\Lambda & 1 \\ 1 & \Lambda \end{pmatrix}, \qquad \det \Delta(m) = -(\Lambda^2+1)$$

$$\begin{pmatrix} x_{01} \\ x_{10} \end{pmatrix} = \frac{\Lambda}{\Lambda^2+1} \begin{pmatrix} -\Lambda & 1 \\ 1 & \Lambda \end{pmatrix} \begin{pmatrix} 0 \\ 1 \end{pmatrix} = \frac{\Lambda}{\Lambda^2+1} \begin{pmatrix} 1 \\ \Lambda \end{pmatrix}.$$

For the Ulam tent map this yields the correct periodic points $\{x_{01}, x_{10}\} = \{2/5, 4/5\}$. In the $\Lambda \to 1$ limit, this 2-cycle collapses into the critical point $C = 1/2$.

Exercise *Check (1.100) for the two 3-cycles. For the Ulam tent map case, the periodic points are*

$$\begin{aligned} \{\gamma_{001}, \gamma_{010}, \gamma_{100}\} &= \{2/9, 4/9, 8/9\} \\ \{\gamma_{011}, \gamma_{110}, \gamma_{101}\} &= \{2/7, 4/7, 6/7\}. \end{aligned}$$

Exercise *Check (1.100) for $\Lambda =$ golden mean. The $\overline{001} \to \overline{0C1}$ as $\Lambda \to$ golden mean from above. Do you get all admissible cycles? That is worked out in ChaosBook, but not in this formulation.*

Exercise *Is there a systematic solution to (1.100) for arbitrary n-cycle? The $\Lambda = 2$ case has the elegant solution described in ChaosBook; whatever polynomials you find, they should agree with that particular factorization. In other words, think of the sums (1.101) and (1.102) as the expansion of a real number in terms of the digits w_t in the nonintegral base Λ. As the symbolic dynamics of a cycle is independent of Λ, the Ulam tent map calculation, in the familiar base 2 clinches the arbitrary tent map case.*

The rest of the section might even be right - has to factorize in agreement with my Ulam tent map computations. Please fix at your leisure, if I am wrong.

2CB *If the repeating string $m_1 m_2 \dots m_n$ contains an even number of '1's, the repating*

string of well ordered symbols $w_1 w_2 \dots w_n$ is of the same length. The cycle-point x is a geometrical sum which we can rewrite as the odd-denominator fraction

$$\begin{aligned} x(\overline{m_1 m_2 \dots m_n}) &= \sum_{t=1}^{n} \frac{w_t}{\Lambda^t} + \frac{1}{\Lambda^{-n}} \sum_{t=1}^{n} \frac{w_t}{\Lambda^t} + \cdots \\ &= \frac{1}{\Lambda^n - 1} \sum_{t=1}^{n} w_t \Lambda^{n-t} \end{aligned} \tag{1.101}$$

If the repeating string $m_1 m_2 \dots m_n$ contains an odd number of '1's, the string of well ordered symbols $w_1 w_2 \dots w_{2n}$ has to be of the double length before it repeats itself. The cycle-point x is a geometrical sum which we can rewrite as the odd-denominator fraction

$$\begin{aligned} x(\overline{m_1 m_2 \dots m_n}) &= \sum_{t=1}^{2n} \frac{w_t}{\Lambda^t} + \frac{1}{\Lambda^{-2n}} \sum_{t=1}^{2n} \frac{w_t}{\Lambda^t} + \cdots \\ &= \frac{1}{(\Lambda^n - 1)(\Lambda^n + 1)} \sum_{t=1}^{2n} w_t \Lambda^{2n-t} \end{aligned} \tag{1.102}$$

click to return: p. 39

Example 1.9. ***Belykh map linear code.*** *Li and Xie [69]* Symbolic dynamics of Belykh-type maps*: " The symbolic dynamics of a Belykh-type map (a two-dimensional discontinuous piecewise linear map) is investigated. The pruning front conjecture (the admissibility condition for symbol sequences) is proved under a hyperbolicity condition. Using this result, a symbolic dynamics model of the map is constructed according to its pruning front and primary pruned region. "*

The Belykh map is a piecewise linear map given by

$$\begin{pmatrix} x_{n+1} \\ y_{n+1} \end{pmatrix} = \begin{pmatrix} \sigma_n - a x_n + b y_n \\ x_n \end{pmatrix} = \begin{pmatrix} \sigma_n \\ 0 \end{pmatrix} + \begin{pmatrix} -a & b \\ 1 & 0 \end{pmatrix} \begin{pmatrix} x_n \\ y_n \end{pmatrix} .$$

where

$$\sigma_n = \begin{cases} 1 & \text{if} \quad x_n \geq 0 \\ -1 & \text{if} \quad x_n < 0 \end{cases} .$$

The two branches of the map are

$$f_\pm = \begin{cases} \pm 1 - a x + b y \\ x \end{cases} .$$

In the 2-step difference formulation (the linear code), the map is an asymmetric tridiagonal Toeplitz matrix

$$x_{n+1} + a x_n - b x_{n-1} = \sigma_n \, ,$$

or

$$\Box x_n + (2 + a) x_n - (1 + b) x_{n-1} = \sigma_n \, . \tag{1.103}$$

For $b = -1$ (the Hamiltonian, time-reversible case) this is almost the cat map, with $a = -s$, except that the single sawtooth discontinuity is across $x = 0$, there is no $\mod 1$ condition.

Li and Xie consider the $a, b > 0$ case. The strange attractor (for example, for $a = 1.5$ and $b = 0.3$) looks like a fractal set of parallel lines. They define the pruning

front, the primary pruned region, plot them in the symbol plane, and prove the pruning front conjecture for this map. In the symbol plane there is a symmetry under rotation by π, but they do not seem to exploit that.

They call the past and the future itineraries of the tail and the head, and start the head with s_0.

Tél [100] Fractal dimension of the strange attractor in a piecewise linear two-dimensional map *computes the box-counting dimension of this map (which he does not call Belykh map).*

Example 1.10. ***Lozi map linear code.*** *The Lozi map*

$$x_{n+1} = 1 - \sigma_n a x_n + b x_{n-1} \,.$$

written as a 2-step recurrence relation

$$x_{n+1} - 2x_n + x_{n-1} + (2 + \sigma_n a)x_n - (b+1)x_{n-1} = 1 \,. \tag{1.104}$$

That has the same nonlinear term $\sigma_n x_n$ as (1.98), so maybe we can figure out the pruning front as well, in this formulation.

click to return: p. 39

1.14 *

Exercises boyscout

1.1. **Cat map Green's function, infinite lattice.**
(a) Show that the eigenvalues of the cat map M are given by

$$\Lambda^{\pm} = \frac{1}{2}(s \pm \sqrt{D}) \,, \qquad \Lambda = e^{\lambda} \,, \tag{1.105}$$

where $\Lambda \equiv \Lambda^{+}$, $s = \Lambda + \Lambda^{-1}$, $\sqrt{D} = \Lambda - \Lambda^{-1}$, and the discriminant is $D = s^2 - 4$.
(b) Verify by substitution that the Green's function is given by

$$\mathsf{g}_{nn'} = \frac{1}{\sqrt{D}} \frac{1}{\Lambda^{|n'-n|}} \,. \tag{1.106}$$

(c) Show that the orbit is then recovered by

$$x_n = \frac{1}{\sqrt{D}} \sum_{n' \in \mathbb{Z}} \Lambda^{-|n-n'|} m_{n'} \,. \tag{1.107}$$

1.2. **Cat map Green's function for a periodic orbit.** Show that the Green's function for a periodic orbit of period $|p|$ is obtained by summing (1.106) over period $|p|$:

$$g^p_{nn'} = \sum_{j=-\infty}^{\infty} g_{n-n',j|p|} = \frac{1}{\sqrt{D}} \frac{\Lambda^{-|n-n'|} + \Lambda^{-|p|+|n-n'|}}{1 - \Lambda^{-|p|}} \,. \tag{1.108}$$

Verify this formula by explicit matrix inversion for a few periodic points of cycles p of periods $|p| = 1, 2, 3, 4, \cdots$.

1.3. $d = 2$ **cat map guess Green's function, infinite lattice.** Show by substitution that a $d = 2$ "Green's function" guess given by

$$\mathsf{g}_{zz'} = \frac{1}{2}\frac{1}{\sqrt{D}}\,\frac{1}{\Lambda^{|\ell'-\ell|+|t'-t|}}\,, \tag{1.109}$$

(and similarly, in arbitrary dimension $d > 1$) *does not* satisfy the Green's function conditions

$$(\mathcal{D}\mathsf{g})_{zz'} = \delta_{zz'} = \delta_{ll'}\delta_{tt'}\,, \tag{1.110}$$

Here the eigenvalues of the cat map M are

$$\Lambda^{\pm} = \frac{1}{2}(s/2 \pm \sqrt{D})\,, \qquad \Lambda = e^{\lambda}\,, \tag{1.111}$$

where $\Lambda \equiv \Lambda^{+}$, $s/2 = \Lambda + \Lambda^{-1}$, $\sqrt{D} = \Lambda - \Lambda^{-1}$, and the discriminant is $D = (s/2)^2 - 4$.

Hint: the check works just like for exercise 1.1.

1.4. **Periodic orbits of Arnol'd cat map.**

(a) Describe precisely how you actually pick "random q_1 and q_2"

(b) Explain what happens if q_1 and q_2 are rational

(c) Can you get a periodic orbit if q_1 and q_2 are irrational?

(d) What do you mean by period 0?

(e) Does the Arnol'd cat map have periodic orbits of any period?

(f) Derive analytically that $m_j \in \{-1, 0, 1, 2\}$ (you can continue the exposition that I started in sect. 1.6.2, if that helps). Does you result agree with Percival and Vivaldi [83]?

Chapter 1. Cat map

Solution 1.1 - Cat map Green's function, infinite lattice.
(a) It's just the roots of a quadratic equation, with $s = \Lambda + \Lambda^{-1}$ *, and* $\sqrt{D} = \Lambda - \Lambda^{-1}$ *.*
(b) The Green's function (1.106)

$$\mathsf{g}_{tt'} = \frac{1}{\sqrt{D}}\,\frac{1}{\Lambda^{|t'-t|}} \tag{1.112}$$

for the discrete damped Poison equation (1.52) was first computed explicitly by Percival and Vivaldi [83], using the methods introduced in Mestel and Percival [78]. It should satisfy

$$(\mathcal{D}\mathsf{g})_{ij} = \sum_k \mathcal{D}_{ik}\mathsf{g}_{kj} = \delta_{ij}\,. \tag{1.113}$$

Since we are considering infinite $1D$ lattice, we do not need to specify the boundary conditions. $\mathcal{D}$ is a Toeplitz matrix

$$\mathcal{D}_{ik} = s\delta_{ik} - \delta_{i-1,k} - \delta_{i+1,k} \tag{1.114}$$

Substituting (1.114) into (1.113)

$$\sum_k \mathcal{D}_{ik}\mathrm{g}_{kj} = s\mathrm{g}_{ij} - \mathrm{g}_{i-1,j} - \mathrm{g}_{i+1,j} = \delta_{ij}\,, \tag{1.115}$$

and substituting (1.106)

$$\mathrm{g}_{ij} = \frac{1}{\sqrt{D}}\,\frac{1}{\Lambda^{|j-i|}} = \begin{cases} \frac{1}{\sqrt{D}}\,\frac{1}{\Lambda^{i-j}} & \text{if } j < i \\ \frac{1}{\sqrt{D}} & \text{if } j = i \\ \frac{1}{\sqrt{D}}\,\frac{1}{\Lambda^{j-i}} & \text{if } j > i \end{cases}\,. \tag{1.116}$$

into (1.115), one verifies that (1.106) is indeed the Green's function for the infinite lattice. By translational invariance, for $i = j$ consider

$$s\mathrm{g}_{00} - \mathrm{g}_{-1,0} - \mathrm{g}_{10} = \frac{1}{\sqrt{D}}\left(s - \frac{2}{\Lambda}\right) = \frac{1}{\sqrt{D}}\left(\Lambda - \frac{1}{\Lambda}\right) = 1\,. \tag{1.117}$$

For $i > j$ consider

$$s\mathrm{g}_{10} - \mathrm{g}_{00} - \mathrm{g}_{20} = \frac{1}{\sqrt{D}}\left(\frac{s}{\Lambda} - 1 - \frac{1}{\Lambda^2}\right) = \frac{1}{\sqrt{D}}\,\frac{1}{\Lambda}\left(s - \Lambda - \frac{1}{\Lambda}\right) = 0\,. \tag{1.118}$$

(c) The orbit is recovered by:

$$x_n = \sum_{n'\in\mathbb{Z}} \mathrm{g}_{nn'} m_{n'} = \frac{1}{\sqrt{D}} \sum_{n'\in\mathbb{Z}} \Lambda^{-|n-n'|} m_{n'}\,. \tag{1.119}$$

(Han Liang)

Solution 1.2 - Cat map Green's function for a periodic orbit. *Express the periodic orbit Green's function in terms of the infinite lattice by using a periodic source $m_{n'} = m_{n'} + |p|$,*

$$\begin{aligned} \sum_{n'=-\infty}^{\infty} \mathrm{g}_{nn'} m_{n'} &= \sum_{r=-\infty}^{\infty} \sum_{n'=r|p|}^{r|p|+|p|-1} \mathrm{g}_{nn'}\, m_{n'} = \sum_{r=-\infty}^{\infty} \sum_{n'=0}^{|p|-1} \mathrm{g}_{n,n'+r|p|}\, m_{n'+r|p|} \\ &= \sum_{r=-\infty}^{\infty} \sum_{n'=0}^{|p|-1} \mathrm{g}_{n-n',r|p|}\, m_{n'} \end{aligned} \tag{1.120}$$

Comparing with the expression for the Green's function of a periodic orbit:

$$\sum_{n'=0}^{|p|-1} \mathrm{g}^{|p|}_{nn'} m_{n'} \tag{1.121}$$

we see that

$$\mathrm{g}^{|p|}_{nn'} = \sum_{r=-\infty}^{\infty} \mathrm{g}_{n-n',r|p|} \tag{1.122}$$

Substituting (1.106) into (1.122) we have:

$$\begin{aligned}
\mathrm{g}^{|p|}_{nn'} &= \frac{1}{\sqrt{D}} \sum_{r=-\infty}^{\infty} \frac{1}{\Lambda^{|n-n'-r|p||}} \\
&= \frac{1}{\sqrt{D}} \left(\frac{1}{\Lambda^{|n-n'|}} + \sum_{r=1}^{\infty} \frac{1}{\Lambda^{r|p|-(n-n')}} + \sum_{r=-1}^{-\infty} \frac{1}{\Lambda^{(n-n')-r|p|}} \right) \\
&= \frac{1}{\sqrt{D}} \left(\frac{1}{\Lambda^{|n-n'|}} + \frac{1}{\Lambda^{-|n-n'|}} \frac{1}{\Lambda^{|p|}-1} + \frac{1}{\Lambda^{|n-n'|}} \frac{1}{\Lambda^{|p|}-1} \right) \\
&= \frac{1}{\sqrt{D}} \frac{1}{1-\Lambda^{-|p|}} (\Lambda^{-|n-n'|} + \Lambda^{-|p|+|n-n'|}) \qquad (1.123)
\end{aligned}$$

This verifies (3.39).

Bird and Vivaldi [18] show that for an n-cycle $x_{n'}$ are rational functions of Λ, given by the quotient of two reflexive polynomials (for example, $P_t(\Lambda) = \Lambda^n P_t(1/\Lambda)$),

$$\begin{aligned}
x_t &= \Lambda\, P_t(\Lambda)/Q(\Lambda) \\
P_t(\Lambda) &= \sum_{\tau=1}^{n-1} \Lambda^{n-\tau} (\Lambda\, m_{t+\tau-1} + m_{t-\tau}) \\
Q(\Lambda) &= (\Lambda^2 - 1)\,(\Lambda^n - 1) \qquad (1.124)
\end{aligned}$$

Bird and Vivaldi [18] then discuss pruning, give formulas for the numbers of prime cycles for integer s, etc..

(Han Liang)

Solution 1.3 - $d = 2$ cat map guess Green's function, infinite lattice. *The Green's function g for the Toeplitz matrix (tensor) in 2 dimensions*

$$\begin{aligned}
\mathcal{D}_{lt,l't'} &= [-\Box + 2\,(s/2-2)]_{lt,l't'} \\
&= \left(\frac{s}{2}\delta_{ll'} - \delta_{l-1,l'} - \delta_{l+1,l'}\right) \delta_{tt'} \\
&\quad + \delta_{ll'} \left(\frac{s}{2}\,\delta_{tt'} - \delta_{t-1,t'} - \delta_{t+1,t'}\right) . \qquad (1.125)
\end{aligned}$$

should satisfy (1.110), or, substituting (1.125) into (1.110),

$$\begin{aligned}
2\,\delta_{ll'}\delta_{tt'} &= \frac{s}{2}\mathrm{g}_{ll',tt'} - \mathrm{g}_{l-1,l',tt'} - \mathrm{g}_{l+1,l',tt'} \\
&\quad + \frac{s}{2}\mathrm{g}_{ll',tt'} - \mathrm{g}_{ll',t-1,t'} - \mathrm{g}_{ll',t+1,t'} \,. \qquad (1.126)
\end{aligned}$$

Let's check this. By translational invariance, need to look only at different values of $l - l'$ and $t - t' = 0$. For $l = l'$ and $t = t'$ it suffices that we consider the $l = l' = t = t' = 0$ case. Using (1.111) we have

$$\begin{aligned}
&\frac{s}{2}\mathrm{g}_{00,00} - \mathrm{g}_{-1,0,00} - \mathrm{g}_{10,00} \\
&+ \frac{s}{2}\mathrm{g}_{00,00} - \mathrm{g}_{00,-1,0} - \mathrm{g}_{00,10} \\
&= \frac{2}{\sqrt{D}} \left(\frac{s}{2} - \frac{2}{\Lambda}\right) = \frac{2}{\sqrt{D}} \left(\Lambda - \frac{1}{\Lambda}\right) = 2\,, \qquad (1.127)
\end{aligned}$$

verifies (1.125).

For $l > l'$ and $t = t'$ it suffices to consider $l = 1, l' = 0$, $t = t' = 0$ case.

$$\begin{aligned}
&\frac{s}{2}\mathrm{g}_{10,00} - \mathrm{g}_{00,00} - \mathrm{g}_{20,00} \\
&+\frac{s}{2}\mathrm{g}_{10,00} - \mathrm{g}_{10,-1,0} - \mathrm{g}_{10,10} \\
&= \frac{1}{2\sqrt{D}}\left(\frac{s/2}{\Lambda} - 1 - \frac{1}{\Lambda^2}\right) + \frac{1}{2\sqrt{D}}\left(\frac{s/2}{\Lambda} - \frac{2}{\Lambda^2}\right) \\
&= \frac{1}{2\Lambda\sqrt{D}}\left(\frac{s}{2} - \frac{2}{\Lambda}\right) = \frac{1}{2\Lambda\sqrt{D}}\left(\Lambda - \frac{1}{\Lambda}\right) = \frac{1}{2\Lambda}\,.
\end{aligned} \tag{1.128}$$

So, the guess (1.109) already does not work.

Substitute (1.109) into (1.126) we get:

$$\sum_{z''}\mathcal{D}_{zz''}\mathrm{g}_{z''z'} = \begin{cases} \frac{1}{\sqrt{D}}\frac{1}{\Lambda^{|l'-l|+|t'-t|}}(s - 2\Lambda - 2\Lambda^{-1}) & \text{if } l \neq l' \text{ and } t \neq t' \\ \frac{1}{\sqrt{D}}(s - 4\Lambda^{-1}) & \text{if } l = l' \text{ and } t = t' \end{cases}\,. \tag{1.129}$$

To satisfy (1.110), s, $\sqrt{D}$ and Λ must satisfy:

$$\begin{cases} s = 2\Lambda + 2\Lambda^{-1} \\ \sqrt{D} = 2\Lambda - 2\Lambda^{-1} \end{cases}\,. \tag{1.130}$$

So we will have:

$$\begin{cases} \Lambda = \frac{1}{4}(s + \sqrt{s^2 - 16}) \\ \Lambda^{-1} = \frac{1}{4}(s - \sqrt{s^2 - 16}) \end{cases}\,. \tag{1.131}$$

Now the problem is, if $l \neq l'$ but $t = t'$, (1.129) become:

$$\sum_{z''}\mathcal{D}_{zz''}\mathrm{g}_{z''z'} = \frac{1}{\sqrt{D}}\frac{1}{\Lambda^{|l'-l|+|t'-t|}}(s - \Lambda - 3\Lambda^{-1}) \tag{1.132}$$

and this is not satisfied by (1.131). So (1.109) does not work for the 2-dimensional case. I haven't figured out the correct Green's function for the 2 dimensions.

(Han Liang)

Solution 1.3 - $d = 2$ cat map guess Green's function, infinite lattice. *The guess Green's function (1.109) doesn't work. For $l = 2$, $l' = 0$ and $t = t' = 0$, the correct form of (1.128) is:*

$$\begin{aligned}
&\frac{s}{2}\mathrm{g}_{10,00} - \mathrm{g}_{00,00} - \mathrm{g}_{20,00} \\
&+\frac{s}{2}\mathrm{g}_{10,00} - \mathrm{g}_{10,10} - \mathrm{g}_{10,-10} && (1.133)\\
&= \frac{1}{2\sqrt{D}}\left(\frac{s}{2\Lambda} - 1 - \frac{1}{\Lambda^2}\right) + \frac{1}{2\sqrt{D}}\left(\frac{s}{2\Lambda} - \frac{1}{\Lambda^2} - \frac{1}{\Lambda^2}\right) && (1.134)\\
&= \frac{1}{2\sqrt{D}}\frac{1}{\Lambda}\left(\frac{s}{2} - \Lambda - \frac{1}{\Lambda}\right) + \frac{1}{2\sqrt{D}}\frac{1}{\Lambda}\left(\frac{s}{2} - \frac{1}{\Lambda} - \frac{1}{\Lambda}\right) && (1.135)\\
&= 0 + \frac{1}{2\Lambda}\,. && (1.136)
\end{aligned}$$

As in (1.128), this does not work .

(Han Liang)

Solution 1.4 - Periodic orbits of Arnol'd cat map. *No solution available.*

Chapter 2

Statistical mechanics applications

2.1 Cat map

HERE WE WILL DEAL WITH the prototype example of chaotic Hamiltonian maps, *hyperbolic toral automorphisms*, (subspecies of which, known as the as the 'Arnol'd cat map', you have most likely already encountered), acting on a cylinder or over $\mathbb{R}^2$. Their dynamics restricted to the elementary cell involves maps on $\mathbf{T}^2$ (two–dimensional torus). On such torus an action of a matrix in $SL_2(\mathbb{N})$ with unit determinant and absolute value of the trace bigger than 2 is known as the Anosov map.

2.2 New example: Arnol'd cat map

the Arnol'd-Sinai cat is a practical cat
— Ian Percival and Franco Vivaldi [16]

The 'standard' generating partition code of Arnol'd and Avez [2] is rather simple - it is described in Devaney [9]. [1] It relies on a 3-rectangles complete partition of the torus. It is a subshift of finite type - it is well suited to the generation and counting of periodic orbits on the torus, see Isola [12] rational topological ζ function in sect. 1.6.3.

However, the Arnol'd–Avez alphabet has no easy translation to the integers shift on the unfolded torus (on the lattice, most of torus periodic orbits are relative periodic orbits). Furthermore, for N coupled cat maps the number of such rectangles would grow exponentially [11]. [2]

[1] Predrag 2016-08-03: I do not have either monograph at hand, but Creagh [7] summary in sect. 1.6.4 is pretty clear.

[2] Predrag 2016-08-03: Have not checked that, or whether this is explained in ref. [11].

There is a general consensus in the cat map community [13] that the 'linear code' of Percival and Vivaldi [16] (here sect. 1.6.2) is deeper and more powerful. For deterministic diffusion developed in ChaosBook (chapter 2 here) that is the only choice, as one needs to convert symbolic dynamics of an relative periodic orbit to the integer shift (translation) on the lattice. [3] The downside is that the Markov/generating partition is infinite, meaning that for longer and longer orbits there are more and more new pruning (inadmissible blocks) rules, ad infinitum.

[4] Iterated area preserving maps of the form

$$p' = p + F(x) \tag{2.1}$$
$$x' = x + p' \qquad \mod 1, \tag{2.2}$$

where F(x) is periodic of period 1, are widely studied because of their importance in dynamics. They include the standard map of Taylor, Chirikov and Greene [5, 14], and also the sawtooth and cat maps that we describe here. Because values of x differing by integers are identified, whereas the corresponding values of p are not, the phase space for these equations is a cylinder.

These maps describe 'kicked' rotors that are subject to a sequence of angle-dependent impulses F(x), with $2\pi x$ as the configuration angle of the rotor, and p as the momentum conjugate to the configuration coordinate x. The time step has been set to $\Delta t = 1$. Eq. (2.1) says that the momentum p is accelerated to p' by the force pulse $F(x)\Delta t$, and eq. (2.2) says in that time the trajectory x reaches $x' = x + p'\Delta t$.

The phase space of the rotor is a cylinder, but it is often convenient to extend it to the plane or contract it to a torus. For the former case the " $\mod 1$" is removed from (2.2) and for the latter it is included in (2.1).

Eqs. (2.1,2.2) are a discrete time form of Hamilton's equations. But for many purposes we are only interested in the values of the configuration coordinate x, which satisfy the second difference equation (the discrete Laplacian in time)

$$\delta^2 x_t \equiv x_{t+1} - 2x_t + x_{t-1} = F(x_t) \qquad \mod 1 \tag{2.3}$$

where t is a discrete time variable that takes only integer values. This equation may be considered as the Lagrangian or Newtonian equation corresponding to the Hamiltonian form (2.1), with $p_t = x_t + x_{t-1}$.

Rewrite (2.3) as

$$x_{t+1} = 2x_t + F(x_t) - x_{t-1} \qquad \mod 1 \tag{2.4}$$

Call the 1-step configuration point forward in (2.2) $x_t = y$, and the next configuration point $x_{t+1} = y'$. This recasts the dynamical equation in the form of an area preserving map in which only configurations at different times appear,

$$x' = y$$
$$y' = 2y + F(y) - x \qquad \mod 1\,. \tag{2.5}$$

[3] Predrag 2016-08-03: I do not know why this symbolic dynamics is natural for extensions to N nearest-neighbor coupled maps.

[4] Predrag 2016-06-02: verbatim from Percival and Vivaldi [16]

This they call the 'two-configuration representation'.

The sawtooth map represents a rotor subject to an impulse F(x) that is linear in x, except for a single discontinuity. The impulse is standardised to have zero mean, the origin of x is chosen so that F(0)= 0, so

$$F(x) = Kx \quad (-1/2 \le x < 1/2) \tag{2.6}$$

With these conventions Hamilton's equations for the sawtooth are

$$\begin{aligned} x' &= y && \mod 1 \\ y' &= -x + sy && \mod 1 \end{aligned} \tag{2.7}$$

in the two-configuration representation, where

$$s = K + 2\,. \tag{2.8}$$

For $s > 2$ the map is unstable. In the two-configuration representation, Hamilton's equations can be written in matrix form as

$$\begin{pmatrix} x' \\ y' \end{pmatrix} = M \begin{pmatrix} x \\ y \end{pmatrix} \qquad \mod 1 \tag{2.9}$$

with

$$M = \begin{pmatrix} 0 & 1 \\ -1 & s \end{pmatrix}, \tag{2.10}$$

characteristic polynomial

$$\Lambda^2 - s\Lambda + 1\,. \tag{2.11}$$

and eigenvalues

$$\Lambda = (s + \sqrt{D})/2\,, \qquad \Lambda' = (s - \sqrt{D})/2\,, \tag{2.12}$$

where $D = s^2 - 4$. When s is an integer, then the map (2.9) is continuous on the torus, because the discontinuity of the sawtooth is an integer absorbed into the modulus. The map is then continuous; it is a toral automorphism, of a class called *cat maps*, of which the Arnol'd-Sinai cat map [2] with $s = 3$ is a special case,

$$M = \begin{pmatrix} 0 & 1 \\ -1 & 3 \end{pmatrix}. \tag{2.13}$$

If instead of (2.4) dynamics on a torus, one considers motion on a line (no $\mod 1$), one can land in any unit interval along the q-axis. Let then $-b_t$ be the sequence of integer shifts that ensures that for all t the dynamics

$$x_{t+1} = 2x_t + F(x_t) - x_{t-1} - b_t \tag{2.14}$$

stays confined to the elementary cell $x_t \in [-1/2, 1/2)$. The Newton equation (2.3) then takes the form

$$(\delta^2 - K)x_t = -b_t \tag{2.15}$$

The linear operator or infinite tridiagonal matrix on the left of (2.15) has a Green's function or inverse matrix given by the unique bounded solution g_{ts} of the inhomogeneous equation [5]

$$g_{t+1,t'} - s\, g_{tt'} + g_{t-1,t'} = \delta_{tt'} \,, \tag{2.16}$$

which is given by

$$g_{tt'} = -\Lambda^{-|t-t'|}/\sqrt{D} \,. \tag{2.17}$$

This solution is obtained by a method that is directly analogous to the method used for second order linear differential equations [15](click here). The solution of (2.15) for the orbit is therefore [6]

$$t_t = \sum_t{}' g_{tt'}(-b_t) = \frac{1}{\sqrt{D}} \sum_t{}' \Lambda^{-|t-t'|} b_{t'} = \delta_{tt'} \,, \tag{2.18}$$

defining the orbit uniquely in terms of the symbol sequence. That is to say that the code is complete. We shall refer to an integer code such as $\{b_t\}$ for a linear system as a *linear code*: the orbit and the code are related to one another by a linear transformation. Clearly, a shift in the symbol sequence $\{b_t\}$ corresponds to an equivalent time shift of the orbit.

The past and the future sums in (2.18) resembles the expression for a real number in terms of the digits b_t, using a representation of the reals in the non-integral base Λ, in contrast with the past and future coordinates for the baker's transformation, which have a similar form, to base 2. The 'present' symbol b_0 is incorporated with the past in our convention.

2.3 Diffusion in Hamiltonian sawtooth and cat maps

(R. Artuso) [7]

In this section we will study deterministic diffusion that arises in the prototype example of chaotic Hamiltonian maps, the *Anosov maps*. Diffusive properties will arise in considering such maps acting on a cylinder or over $\mathbb{R}^2$, while the dynamics restricted to the elementary cell involves maps on $\mathbf{T}^2$ (two–dimensional torus). On such torus an action of a matrix in $SL_2(\mathbb{N})$ with unit determinant and absolute value of the trace bigger than 2 is known as the Anosov map.

Maps of this kind are as the simplest examples of Hamiltonian chaotic dynamics, with finite Markov partitions, and simple symbolic dynamics. Within

chapter ??

[5] Predrag 2016-05-29: still have to check this calculation

[6] Predrag 2018-03-11: Mestel and Percival [15] is very systematic, with Wronskians, etc., but I do not see this solution there. Percival and Vivaldi [16] state it, say it can be derived by the method of Mestel and Percival [15], and say "as may be verified by substitution."

[7] Predrag 2016-06-16: return eventually to ChaosBook

the framework of Hamiltonian dynamical systems, hyperbolic linear automorphisms play the role of piecewise linear Markov maps: their symbolic dynamics can be encoded in a grammatically simple way, and their linearity leads to uniformity of cycle stabilities.

Following Percival and Vivaldi [16], we will consider linear hyperbolic toral automorphisms in the "two-configuration representation,"

$$\begin{bmatrix} x' \\ y' \end{bmatrix} = M \begin{bmatrix} x \\ y \end{bmatrix}$$

with

$$M = \begin{bmatrix} 0 & 1 \\ -1 & K+2 \end{bmatrix}$$

which allows considering their extension on a cylinder phase space ($[-1/2, 1/2)\times \mathbb{R}$) in a natural way. So it is natural to study diffusion properties along the y direction.

Though Markov partitions encode the symbolic dynamics in the simplest possible way, they are not well suited to deal with diffusion, as the jumping number is not related in a simple way to the induced symbol sequence. To this end the "linear code" is quite natural. We start by a few notational conventions: χ will denote the trace of M, $\chi = K+2$. The leading eigenvalue of the Jacobian matrix M will be denoted by $\Lambda = (\chi + \sqrt{D})/2$, where $D = \chi^2 - 4$. In principle the code (and the problem of diffusion) can be also considered for non-integer K (thus losing continuity of the torus map when K): we will remark in what follows that results which are exact for $K \in \mathbb{N}$ are only approximate for generic K.

The the alphabet is determined by the parameter K: the letters are integer numbers, whose absolute values does not exceed Int$(1 + \chi/2)$ (see figure 2.1 for the case $K = 2$). The code is linear, as, given a bi-infinite sequence $\{x_i\}_{i\in\mathbb{N}}$

$$b_t \stackrel{\text{def}}{=} \left[(K+2)x_t - x_{t-1} + \frac{1}{2}\right] \quad , \tag{2.19}$$

$[\dots]$ denoting the integer part, while the inversion formula (once a bi-infinite symbolic string $\{b_i\}_{i\in\mathbb{N}}$ is given), reads

$$x_t = \frac{1}{\sqrt{D}} \sum_{s\in\mathbb{N}} \Lambda^{-|t-s|} b_s \quad , \tag{2.20}$$

As the x coordinate lives in the interval $[-1/2, 1/2)$, (2.20) induces a condition of admissible symbol sequences: $\{b_i\}_{i\in\mathbb{N}}$ will be an admissible orbit if

$$-\frac{1}{2} \le \frac{1}{\sqrt{D}} \sum_{s\in\mathbb{N}} \Lambda^{-|t-s|} b_s < \frac{1}{2} \quad . \tag{2.21}$$

By (2.19) and (2.20) it is easy to observe that periodic orbits and admissible periodic symbol sequences are in one-to-one correspondence. From (2.21) we

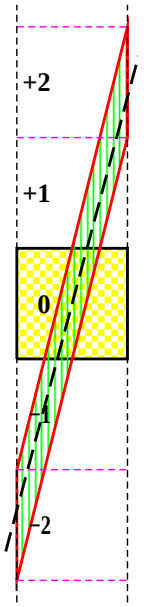

Figure 2.1: The elementary cell for the torus map $[-1/2, 1/2]$ (checkered yellow) together with its image for $K = 2$, in green: symbols refer to the linear code. The dashed line through the origin gives the direction of the unstable manifold. Note that the unstable manifold is not parallel to the image borders.

get the condition that a $\{b_i\}_{i=1,\dots,T}$ sequence corresponds to a T–periodic orbit of the map

$$|A_n b_t + A_{n-1}(b_{t+1} + b_{t-1}) + \cdots + A_0(b_{t+n} + b_{t-n})| < \frac{B_n}{2} \quad \forall t = 1, \dots, T$$

when $T = 2n + 1$, and

$$|C_n b_t + C_{n-1}(b_{t+1} + b_{t-1}) + \cdots + C_0(b_{t+n})| < \frac{D_n}{2} \quad \forall t = 1, \dots, T \tag{2.22}$$

when $T = 2n$ where

exercise 2.1
exercise 2.2

$$\begin{aligned} B_k &= \Lambda^k(\Lambda - 1) + \Lambda^{-k}(\Lambda^{-1} - 1) & A_k &= \frac{\Lambda^{k+1} + \Lambda^{-k}}{\Lambda + 1} \\ D_k &= (\Lambda^k - \Lambda^{-k})(\Lambda - \Lambda^{-1}) & C_k &= \Lambda^k + \Lambda^{-k}\,. \end{aligned} \tag{2.23}$$

The pruning rules (2.22) admit a simple geometric interpretation: a lattice point $\boldsymbol{b} \in \mathbb{N}^T$ identifies a T–periodic point of the map if $\boldsymbol{b} \in \mathcal{P}_T$ where

$$\mathcal{P}_T \stackrel{\text{def}}{=} \{\boldsymbol{x} \in \mathbb{R}^T : \quad \left\{ \begin{array}{c} |a_1 x_1 + \cdots + a_T x_T| < e_T \\ \vdots \\ |a_2 x_1 + \cdots + a_1 x_T| < e_T \end{array} \right\} \tag{2.24}$$

and

$$\begin{aligned} a_1 \dots a_T &= A_0 A_1 \dots A_{n-1} A_n A_{n-1} \dots A_0 & e_T &= B_n/2 \\ a_1 \dots a_T &= C_1 \dots C_{n-1} C_n C_{n-1} \dots C_1 C_0 & e_T &= D_n/2 \end{aligned} \tag{2.25}$$

for $T = 2n+1$ or $T = 2n$, respectively. Thus $\mathcal{P}_T$ is a measure polytope [6], obtained by deforming a T–cube. This is the key issue of this appendix: though the map is endowed with a most remarkable symbolic dynamics, the same is hardly fit to deal with transport properties, as the rectangles that define the partition are not directly connected to translations once the map is unfolded to the cylinder. The partition connected to the linear code (see figure 2.1) on the other side is most natural when dealing with transport, though its not being directly related to invariant manifolds leads to a multitude of pruning rules (which in the present example bear a remarkable geometric interpretation, which is not to be expected as a generic feature). exercise 2.3

We will denote by $\mathcal{N}_{n,s}$ the number of periodic points of period n with jumping number s. By taking (**??**) into account we can easily see that for cat maps a way to compute D is provided by

$$D = \lim_{n\to\infty} D_n \qquad D_n = \frac{1}{n\mathcal{N}_n} \sum_{k=1}^{p(n)} k^2 \mathcal{N}_{n,k} \tag{2.26}$$

where $\mathcal{N}_n$ is the number of periodic points of period n, $p(n)$ is the highest jumping number of n–periodic orbits and we employed

$$\left|\det\left(\mathbf{1} - \boldsymbol{J}_x^{(n)}\right)\right| = (\Lambda^n - 1)(1 - \Lambda^{-n}) = \mathcal{N}_n$$

which is valid for cat maps.

Sums can be converted into integrals by using Poisson summation formula: we define

$$f_T(n) = \begin{cases} (n_1 + \cdots + n_T)^2 & n \in \mathcal{P}_T \bigcap \mathbb{N}^T \\ 0 & otherwise \end{cases}$$

and

$$\tilde{f}_T(\xi) = \int_{\mathbb{R}^T} dx\, e^{i(x,\xi)}\, f_T(x)$$

From Poisson summation formula we have that

$$D_T = \frac{1}{T\mathcal{N}_T} \sum_{n\in\mathbb{N}^T} \tilde{f}_T(2\pi n) \tag{2.27}$$

The quasilinear estimate for D_T amounts to considering the $n = 0$ contribution to (2.27):

$$D_T^{(q.l.)} = \int_{\mathcal{P}_T} dx\, (x_1 + x_2 + \cdots + x_T)^2 \tag{2.28}$$

The evaluation of (2.28) requires introducing a coordinate transformation in symbolic space in which $\mathcal{P}_T$ is transformed in a T–cube. This is equivalent to finding the inverse of the matrix A:

$$A \stackrel{\text{def}}{=} \begin{pmatrix} a_1 & a_2 & \cdots & a_{T-1} & a_T \\ a_T & a_1 & \cdots & a_{T-2} & a_{T-1} \\ \vdots & \vdots & \ddots & \vdots & \vdots \\ a_3 & a_4 & \cdots & a_1 & a_2 \\ a_2 & a_3 & \cdots & a_T & a_1 \end{pmatrix} . \tag{2.29}$$

First of all let us observe that A is a circulant matrix, so that its determinant is the product of T factors, each of the form $f(\epsilon_j) = a_1 + \epsilon_j a_2 + \cdots + a_T \epsilon_j^{T-1}$, where ϵ_j is a Tth root of unity. By using (2.23) it is possible to see that

$$f(\epsilon_j) = \begin{cases} \frac{\epsilon_j^{n+1} B_n}{(\Lambda\epsilon_j - 1)(1-\Lambda^{-1}\epsilon_j)} & T = 2n+1 \\ \frac{\epsilon_j^{n} D_n}{(\Lambda\epsilon_j - 1)(1-\Lambda^{-1}\epsilon_j)} & T = 2n \end{cases}$$

so that

$$|\det A| = \frac{(2e_T)^T}{\Lambda^T + \Lambda^{-T} - 2} \tag{2.30}$$

exercise 2.4 By using the results coming from the former exercise we can finally express A^{-1} via

$$\tilde{C} A^{-1} = \frac{1}{B_n^T} \begin{pmatrix} \chi & -1 & \cdots & 0 & -1 \\ -1 & \chi & \cdots & 0 & 0 \\ \vdots & \vdots & \ddots & \vdots & \vdots \\ 0 & 0 & \cdots & \chi & -1 \\ -1 & 0 & \cdots & -1 & \chi \end{pmatrix} \tag{2.31}$$

where

$$\tilde{C} = \begin{pmatrix} \mathbf{0} & \mathbf{1}_{n+1} \\ \mathbf{1}_n & \mathbf{0} \end{pmatrix} \quad .$$

if $T = 2n+1$ and

$$\tilde{K} A^{-1} = \frac{1}{D_n^T} \begin{pmatrix} \chi & -1 & \cdots & 0 & -1 \\ -1 & \chi & \cdots & 0 & 0 \\ \vdots & \vdots & \ddots & \vdots & \vdots \\ 0 & 0 & \cdots & \chi & -1 \\ -1 & 0 & \cdots & -1 & \chi \end{pmatrix} \tag{2.32}$$

where

$$\tilde{K} = \begin{pmatrix} \mathbf{0} & \mathbf{1}_n \\ \mathbf{1}_n & \mathbf{0} \end{pmatrix} \quad .$$

if $T = 2n$. As a first check of quasilinear estimates let's compute the volume of $\mathcal{P}_T$:

$$\begin{aligned} Vol(\mathcal{P}_T) &= \int_{\mathcal{P}_T} dx_1\, dx_2 \ldots dx_T = \frac{1}{|\det A|} \int_{-e_T}^{e_T} \cdots \int_{e_T}^{e_T} d\xi_1 \ldots d\xi_T \\ &= \Lambda^T + \Lambda^{-T} - 2 \end{aligned} \tag{2.33}$$

exercise 2.5 In an analogous way we may compute the quasilinear estimate for $\mathcal{N}_{T,k}$

$$\begin{aligned} \mathcal{N}_{T,k}^{(q.l.)} &= \int_{\mathcal{P}_T} dx_1 \ldots dx_T\, \delta(x_1 + \ldots x_T - k) \\ &= \frac{\Lambda^T + \Lambda^{-T} - 2}{(2e_T)^T} \int_{-\infty}^{\infty} d\alpha\, e^{-2\pi i \alpha k} \int_{-e_T}^{e_T} \cdots \int_{-e_T}^{e_T} d\xi_1 \ldots d\xi_T\, e^{\frac{2\pi i \alpha \chi}{2e_T}(\xi_1 + \cdots + \xi_T)} \\ &= \frac{2}{\pi\chi}(\Lambda^T + \Lambda^{-T} - 2) \int_0^{\infty} dy\, \cos\left(\frac{2qy}{\chi}\right) \left(\frac{\sin y}{y}\right)^T \end{aligned} \tag{2.34}$$

where we have used $x_1 + \cdots + x_T = (\chi/(2e_T))(\xi_1 + \cdots + \xi_T)$ (cfr. (2.31),(2.32)).

We are now ready to evaluate the quasilinear estimate fo the diffusion coefficient

$$D_T^{(q.l.)} = \frac{1}{\pi\chi T}\int_{-T\chi/2}^{T\chi/2} dz\, z^2 \int_0^\infty dy\, \cos\left(\frac{2zy}{\chi}\right)\left(\frac{\sin y}{y}\right)^T \tag{2.35}$$

(where the bounds on the jumping number again come easily from (2.31),(2.32)). By dropping terms vanishing as $T \mapsto \infty$, and using [10]

$$\int_0^\infty dx\, \left(\frac{\sin x}{x}\right)^n \frac{\sin(mx)}{x} = \frac{\pi}{2}\ \ m \geq n$$

we can obtain

$$D^{(q.l.)} = \frac{\chi^2}{24}\,. \tag{2.36}$$

Note that for cat maps (2.36) is not just the quasilinear estimate, but it is actually the exact value of the diffusion coefficient.

exercise 2.6

Commentary

Remark 2.1. Deterministic diffusion in Hamiltonian maps. (Continued from remark **??**) The quasilinear estimate (2.28) was given in ref. [4] and evaluated in refs. [3, 17]. Circulant matrices are discussed in ref. [1]. The result (2.36) agrees with the saw-tooth result of ref. [4]; for the cat maps (2.36) is the exact value of the diffusion coefficient. This result was also obtained, by using periodic orbits, in ref. [8], where Gaussian nature of the diffusion process is explicitly assumed. Measure polytopes are discussed in ref. [6].

Exercises boyscout

2.1. **Recursion relations.** Verify that the following recursion relations are satisfied

$$u_{k+2} = \chi u_{k+1} - u_k$$

where $u_k = A_k, B_k, C_k, D_k$.

2.2. **Arnol'd cat map.** Show that for $\chi = 3$, $A_k = F_{2k+1}$, $B_k = L_{2k+1}$, $C_k = L_{2k}$ and $D_k = 5F_{2k}$, where F_n and L_n are the Fibonacci and Lucas numbers..

2.3. **Pruning rules for substrings of length 2.** Take $K = 8$ and draw the region determined by (2.22).

2.4. **Diagonalization of A.** Show that A can be diagonalized by considering the auxiliary matrix U

$$U \stackrel{\text{def}}{=} \begin{pmatrix} 1 & 1 & \cdots & 1 & 1 \\ \epsilon_0 & \epsilon_1 & \cdots & \epsilon_{T-2} & \epsilon_{T-1} \\ \vdots & \vdots & \ddots & \vdots & \vdots \\ \epsilon_0^{T-2} & \epsilon_1^{T-2} & \cdots & \epsilon_{T-2}^{T-2} & \epsilon_{T-1}^{T-2} \\ \epsilon_0^{T-1} & \epsilon_1^{T-1} & \cdots & \epsilon_{T-2}^{T-1} & \epsilon_{T-1}^{T-1} \end{pmatrix} .$$

In fact $U^{-1}AU$ is a diagonal matrix (the diagonal elements coinciding with $f(\epsilon_j)$).

2.5. **Periodic points of cat maps.** Verify that (2.33) is exactly the number of T–periodic points of the map when K is an integer.

2.6. **Probability distribution.** Higher order moments can be computed easily for integer K (or generic K within the quasilinear approximation), by generalizations of (2.35): show that the results prove that, given a period T, the distribution of periodic orbits with respect to their jumping number is asymptotically Gaussian, with parameter $D^{(q.l.)}$.

References

[1] A. Aitken, *Determinants & Matrices* (Oliver & Boyd, Edinburgh, 1939).

[2] V. I. Arnol'd and A. Avez, *Ergodic Problems of Classical Mechanics* (Addison-Wesley, Redwood City, 1989).

[3] R. Artuso and R. Strepparava, "Reycling diffusion in sawtooth and cat maps", Phys. Lett. A **236**, 469–475 (1997).

[4] J. R. Cary and J. D. Meiss, "Rigorously diffusive deterministic map", Phys. Rev. A **24**, 2664–2668 (1981).

[5] B. V. Chirikov, "A universal instability of many-dimensional oscillator system", Phys. Rep. **52**, 263–379 (1979).

[6] H. S. M. Coxeter, *Regular Polytopes* (Dover, New York, 1948).

[7] S. C. Creagh, "Quantum zeta function for perturbed cat maps", Chaos **5**, 477–493 (1995).

[8] Dana, "Hamiltonian transport on unstable periodic orbits", Physica D **39**, 205 (1989).

[9] R. L. Devaney, *An Introduction to Chaotic Dynamical systems*, 2nd ed. (Westview Press, 2008).

[10] I. S. Gradshteyn and I. M. Ryzhik, *Tables of integrals, series and products* (Academic, New York, 1980).

[11] B. Gutkin and V. Osipov, "Classical foundations of many-particle quantum chaos", Nonlinearity **29**, 325–356 (2016).

[12] S. Isola, "ζ-functions and distribution of periodic orbits of toral automorphisms", Europhys. Lett. **11**, 517–522 (1990).

[13] J. P. Keating, "Asymptotic properties of the periodic orbits of the cat maps", Nonlinearity **4**, 277 (1991).

[14] A. J. Lichtenberg and M. A. Lieberman, *Regular and Chaotic Dynamics*, 2nd ed. (Springer, New York, 2013).

[15] B. D. Mestel and I. Percival, "Newton method for highly unstable orbits", Physica D **24**, 172 (1987).

[16] I. Percival and F. Vivaldi, "A linear code for the sawtooth and cat maps", Physica D **27**, 373–386 (1987).

[17] R. Strepparava, Laurea thesis, MA thesis (Universitá degli Studi di Milano, 1995).

Chapter 3

Spatiotemporal cat map

2016-09-09 PC I have added this chapter with intention to include it as several examples in ChaosBook.org.

Diffusive coupled map lattices (CML) were introduced by Kaneko [67, 68]:

$$x_{n,t+1} = g(x_{n,t}) + \frac{\epsilon}{2}[g(x_{n-1,t}) - 2g(x_{n,t}) + g(x_{n+1,t})] = (1 + \epsilon\,\Box)g(x_{n,t}) \quad (3.1)$$

where the individual site dynamical system $g(x)$ is a 1D map such as the logistic map.

In the discretization of a spacetime field $q(x,t)$ on lattice points (x_n, t_j), the field is replaced by its lattice point value $q_{n,j} = q(x_n, t_j)$. For a Hamiltonian set of fields we also have $p_{n,j} = p(x_n, t_j)$. In the spatiotemporal cat map, a cat map at each periodic lattice site is coupled diffusively to its nearest neighbors:

$$q_{n,j+1} = p_{n,j} + (s-3)q_{n,j} - (q_{n+1,j} - 2q_{n,j} + q_{n-1,j}) - m^q_{n,j+1}$$

$$p_{n,j+1} = p_{n,j} + (s-4)q_{n,j} - (q_{n+1,j} - 2q_{n,j} + q_{n-1,j}) - m^p_{n,j+1}$$

The spatiotemporal symbols follow from the Newtonian equations in d spatiotemporal dimensions

$$\begin{aligned} m_{n,j} &= (q_{n,j+1} - 2q_{n,j} + q_{n,j-1}) + (q_{n+1,j} - 2q_{n,j} + q_{n-1,j}) - (s-4)q_{n,j} \\ \mathsf{m} &= [\Box + 2d1 - s1]\ \mathsf{q}\,. \end{aligned} \quad (3.2)$$

The $\Box + 2d1$ part is the standard statistical mechanics diffusive inverse propagator that counts paths on a d-dimensional lattice [34], and $-s1$ is the on-site cat map dynamics. For $d = 1$ lattice, $s = 3$ is the the usual Arnol'd cat map.

3.1 Elastodynamic equilibria of 2D solids

In his MIT course, Lecture 23, Mehran Kardar discusses two dimensional solids. Consider a perfect solid at $T = 0$. The equilibrium configuration of

atoms forms a lattice,

$$\vec{r}_0(m,n) = m\vec{e}_1 + n\vec{e}_2 \,,$$

where $\vec{e}_1$ and $\vec{e}_2$ are basis vectors, $a = |\vec{e}_j|$ is the lattice spacing, and $\{m, n\}$ are integers. At finite temperatures, the atoms fluctuate away from their equilibrium position, moving to

$$\vec{r}(m,n) = \vec{r}_0(m,n) + \vec{u}(m,n) \,,$$

As the low temperature distortions do not vary substantially over nearby atoms, one can define a coarse-grained distortion field $\vec{u}(\vec{x})$, where $\vec{x} = (x_1, x_2)$ is treated as continuous, with an implicit short distance cutoff of the lattice spacing a. Due to translational symmetry, the elastic energy depends only on the strain matrix,

$$u_{ij}(\vec{x}) = \tfrac{1}{2}\left(\partial_i u_j + \partial_j u_i\right) \,.$$

Kardar picks the triangular lattice, as its elastic energy is isotropic, (invariant under lattice rotations, see Landau and Lifshitz [80]). In terms of the Lamé coefficients λ and μ,

$$\begin{aligned} \beta H &= \frac{1}{2}\int d^2\vec{x}\,(2\mu\, u_{ij}u_{ij} + \lambda\, u_{ii}u_{jj}) \\ &= -\frac{1}{2}\int d^2\vec{x}\, u_i[2\mu\,\Box\,\delta_{ij} + (\mu+\lambda)\,\partial_i\partial_j]\, u_j \,. \end{aligned} \tag{3.3}$$

(here we have assumed either infinite or doubly periodic lattice, so no boundary terms from integration by parts), with the equations of motion something like (FIX!)

$$\partial_t^2 u_i = [2\mu\,\Box\,\delta_{ij} + (\mu+\lambda)\,\partial_i\partial_j]\, u_j \,. \tag{3.4}$$

The symmetry of a square lattice permits an additional term proportional to $\partial_x^2 u_x^2 + \partial_y^2 u_y^2$. In general, the number of independent elastic constants depends on the dimensionality and rotational symmetry of the lattice in question. In two dimensions, square lattices have three independent elastic constants, and triangular lattices are "elastically isotropic" (i.e., elastic properties are independent of direction and thus have only two [80]).

The Goldstone modes associated with the broken (PC: why "broken"?) translational symmetry are *phonons*, the normal modes of vibrations. Eq. (3.4) supports two types of lattice normal modes, transverse and longitudinal.

The order parameter describing broken translational symmetry is

$$\rho_{\vec{G}}(\vec{x}) = e^{i\vec{G}\cdot\vec{r}(\vec{x})} = e^{i\vec{G}\cdot\vec{u}(\vec{x})} \,,$$

where $\vec{G}$ is any reciprocal lattice vector. Since, by definition, $\vec{G}\cdot\vec{r_0}$ is an integer multiple of 2π, $\rho_{\vec{G}} = 1$ at zero temperature. Due to the fluctuations,

$$\langle\rho_{\vec{G}}(\vec{x})\rangle = \langle e^{i\vec{G}\cdot\vec{u}(\vec{x})}\rangle$$

decreases at finite temperatures, and its correlations decay as $\langle \rho_{\vec{G}}(\vec{x})\rho^*_{\vec{G}}(\vec{0})\rangle$. This is the order parameter ChaosBook (chapter 2 here) and Gaspard use in deriving formulas for deterministic diffusion. Kardar computes this in Fourier space by approximating $\vec{G}\cdot\vec{q}$ with its angular average $G^2q^2/2$, ignoring the rotationally symmetry-breaking term $\cos\vec{q}\cdot\vec{x}$, and getting only the asymptotics of the correlations right (the decay is algebraic).

The translational correlations are measured in diffraction experiments. The scattering amplitude is the Fourier transform of $\rho_{\vec{G}}$, and the scattered intensity at a wave-vector q is proportional to the structure factor. At zero temperature, the structure factor is a set of delta-functions (Bragg peaks) at the reciprocal lattice vectors.

The orientational order parameter that characterizes the broken rotational symmetry of the crystal can be defined as

$$\Psi(\vec{x}) = e^{6i\theta(\vec{x})}\,,$$

where $\theta(\vec{x})$ is the angle between local lattice bonds and a reference axis. The factor of 6 accounts for the equivalence of the 6 possible C_{3v} orientations of the triangular lattice. (Kardar says the appropriate choice for a square lattice is $\exp(4i\theta(\vec{x}))$ - shouldn't the factor be 8, the order of C_{4v}?) The order parameter has unit magnitude at $T = 0$, and is expected to decrease due to fluctuations at finite temperature. The distortion $u(\vec{x})$ leads to a change in bond angle given by

$$\theta(\vec{x}) = -\tfrac{1}{2}\left(\partial_x u_y - \partial_y u_x\right)\,.$$

(This seems to be dimensionally wrong? For detailed calculations, see the above Kardar lecture notes.)

So, we may perhaps think of the spatiotemporal cat map equation (3.5) as a linearization of the equilibrium condition for an unstable 2D solid, with "inverse-harmonic" springs.

3.2 Spatiotemporal cat map symmetries

There are 2 distinct square lattices discussed in these notes:

1. Unfolding of a single cat map unit torus (or cylinder in time direction) into a square lattice.

2. Spatiotemporal cat map d-dimensional lattice (with a cat map at each node).

Consider the d-dimensional spatiotemporal cat map (3.2), first studied in ref. [53]:

$$(\Box + (2d-s)\mathbf{1})_{zz'}x_{z'} = m_z\,, \qquad x_z \in \mathbb{T}^1\,, \quad m_z \in \mathcal{A}^1\,, \quad z \in \mathbb{Z}^d\,, \tag{3.5}$$

where $\Box$ is the Euclidean discrete space-time Laplacian, so there is no need to distinguish "time" from "space" directions.

In the continuum limit, on an infinite $\mathbb{R}^2$ domain, in the absence of any boundary conditions, the "imaginary mass" oscillator (3.5) equations are equivariant under d translations, SO(d) rotations, and $x_z \to -x_z$ inversion through the origin. In $d = 2$ dimensions the inversion is the same as rotation by π. In spatiotemporal cat map square lattice, the lattice restricts the rotation symmetry to rotations by $\pi/2$ in d lattice planes. We denote this rotation by σ_x and the inversion through the origin by σ_{xy}. The suffixes indicate which of the homogeneous directions x, z change sign and might simplify the notation for the group algebra of translations, rotations, and inversion.

There is lots of literature on time-reversal invariant dynamical systems. We need (eventually) to take care of that and other symmetries, because spatiotemporal cat map has all the symmetries of the square lattice (the remnants of the Euclidean symmetry $E(2)$ after discretization):

- 2 discrete translation symmetries
- rotations by $\pi/2$:
$$C_4 = \{E, C_{4z}^+, C_{4z}^-, C_{2z}\}\,. \tag{3.6}$$
- reflection across x-axis, y-axis, diagonal a, diagonal b:
$$C_{4v} = \{E, C_{4z}^+, C_{4z}^-, C_{2z}, \sigma_y, \sigma_x, \sigma_{da}, \sigma_{db}, \}\,. \tag{3.7}$$

In the international crystallographic notation [37], this square lattice is referred to as $p4mm$. It is symmorphic, with point group $p4mm$.

3.2.1 Square lattice space group

Dresselhaus *et al.* textbook [37] (click here) is good on discrete and space groups. The MIT course 6.734 online version contains much of the same material.

Chapter *9. Space Groups in Real Space* is quite clear on matrix representation of space groups. The translation group T is a normal subgroup of G and defines the Bravais lattice. The cosets by translation T (set all all group elements obtained by all translations) form a factor group G/T, isomorphic to the point group g (rotations). All irreducible representations of G can be compounded from irreducible representations of g and T.

Section *9.3 Two-Dimensional Space Groups*: In the international crystallographic notation, our square lattice #11 is called $p4mm$, symmorphic, with point group $p4mm$. The group elements are listed in (3.7). The largest invariant subgroup of C_{4v} is C_4, listed in (3.6). In that case, the space group is $p4$, or #10. Prefix p indicates that the unit cell is primitive (not centered). This is a simple or *symmorphic* group, which makes calculations easier. The Bravais lattice 'unit cell' is a square, and the ChaosBook's 'fundamental domain' makes an appearance as the Brilloun zone in figure 3.1.

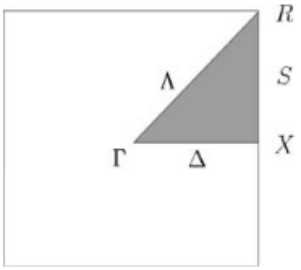

Figure 3.1: The shaded triangle $\Gamma\Lambda RSX\Delta\Gamma$ which constitutes $1/8$ of the Brillouin zone for the 2D square lattice and contains the basic wave vectors and high symmetry points (Fig. 10.2 from ref. [37]).

The Brillouin zone is a unit cell of the reciprocal lattice. The particular unit cell that is conventionally used is the Wigner-Seitz cell which is bounded by planes of the form $\vec{k}\cdot\vec{G} = \frac{1}{2}|\vec{G}|^2$ where $\vec{G}$ is a vector of the reciprocal lattice.

The main trick in quantum-mechanical calculations is to go to the *reciprocal* space, in our case with the full Γ point, $k = 0$, wave vector symmetry (see Table 10.1 of ref. [37]), and 'Large Representations'. This is something we have not tried in deriving the zeta functions for the spatiotemporal cat map.

Sect. *10.5 Characters for the Equivalence Representation* look like those for the point group, sort of. We should probably work out problem 10.1.

We had worked out this space group in Exercise 8.2 of our Spring 2016 group theory course.

The lattice unit is always a *generating region*, but a generating region (fundamental domains) may be smaller than the lattice units.

The $d = 2$ spatiotemporal cat map has **p4m** symmetry: square lattice, point group D_4, two rotation centres of order four (90^0), and reflections in four distinct directions (horizontal, vertical, and diagonals). This corresponds to a straightforward grid of rows and columns of equal squares with the four reflection axes.

The $d = 2$ Lorentz gas has **p6m** symmetry: hexagonal lattice, point group D_6. A pattern with this symmetry can be looked upon as a tessellation of the plane with equal triangular tiles with D3 symmetry, or equivalently, a tessellation of the plane with equal hexagonal tiles with D6 symmetry (with the edges of the tiles not necessarily part of the pattern). Thus the simplest examples are a triangular lattice with or without connecting lines, and a hexagonal tiling with one color for outlining the hexagons and one for the background.

There are five lattice types or Bravais lattices, corresponding to the five possible wallpaper groups of the lattice itself. The wallpaper group of a pattern with this lattice of translational symmetry cannot have more, but may have less symmetry than the lattice itself.

2CB The wallpaper groups wiki has many online drawing tools.

3.2.2 C_{4v} factorization

If an N-disk arrangement has C_N symmetry, and the disk visitation sequence is given by disk labels $\{\epsilon_1\epsilon_2\epsilon_3\dots\}$, only the relative increments $\rho_i = \epsilon_{i+1} - \epsilon_i \mod N$ matter. Symmetries under reflections across axes increase the group to C_{Nv} and add relations between symbols: $\{\epsilon_i\}$ and $\{N-\epsilon_i\}$ differ only by a reflection. As a consequence of this reflection increments become decrements until the next reflection and vice versa. Consider four equal disks placed on the vertices of a square (figure 3.2). The symmetry group consists of the identity e, the two reflections σ_x, σ_y across x, y axes, the two diagonal reflections σ_{13}, σ_{24}, and the three rotations C_4, C_2 and C_4^3 by angles $\pi/2$, π and $3\pi/2$. We start by exploiting the C_4 subgroup symmetry in order to replace the absolute labels $\epsilon_i \in \{1,2,3,4\}$ by relative increments $\rho_i \in \{1,2,3\}$. By reflection across diagonals, an increment by 3 is equivalent to an increment by 1 and a reflection; this new symbol will be called $\underline{1}$. Our convention will be to first perform the increment and then to change the orientation due to the reflection. As an example, consider the fundamental domain cycle 112. Taking the disk $1 \to$ disk 2 segment as the starting segment, this symbol string is mapped into the disk visitation sequence $1_{+1}2_{+1}3_{+2}1\cdots = \overline{123}$, where the subscript indicates the increments (or decrements) between neighboring symbols; the period of the cycle $\overline{112}$ is thus 3 in both the fundamental domain and the full space. Similarly, the cycle $\overline{\underline{1}12}$ will be mapped into $1_{+1}2_{-1}1_{-2}3_{-1}2_{+1}3_{+2}1 = \overline{121323}$ (note that the fundamental domain symbol $\underline{1}$ corresponds to a flip in orientation after the second and fifth symbols); this time the period in the full space is twice

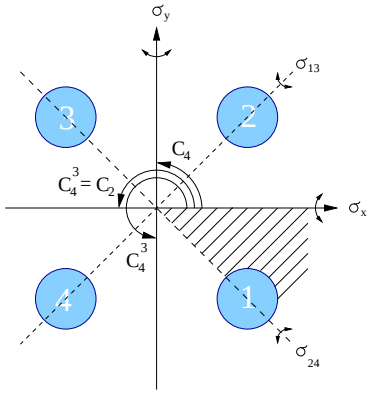

Figure 3.2: Symmetries of four disks on a square. A fundamental domain indicated by the shaded wedge.

that of the fundamental domain. In particular, the fundamental domain fixed points correspond to the following 4-disk cycles:

4-disk		reduced
12	$\leftrightarrow$	$\underline{1}$
1234	$\leftrightarrow$	1
13	$\leftrightarrow$	2

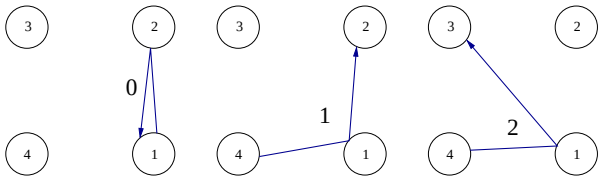

Figure 3.3: Reduced, fundamental domain symbolic dynamics for four disks on a square.

Conversions for all periodic orbits of reduced symbol period less than 5 are listed in table 3.1.

⇓PRIVATE

[1]

section ??

⇑PRIVATE

This symbolic dynamics is closely related to the group-theoretic structure of the dynamics: the global 4-disk trajectory can be generated by mapping the fundamental domain trajectories onto the full 4-disk space by the accumulated product of the C_{4v} group elements $g_{\underline{1}} = C$, $g_2 = C^2$, $g_{\underline{1}} = \sigma_{diag}C = \sigma_{axis}$, where C is a rotation by $\pi/2$. In the $\overline{\underline{1}12}$ example worked out above, this yields $g_{\underline{1}12} = g_2 g_1 g_{\underline{1}} = C^2 C \sigma_{axis} = \sigma_{diag}$, listed in the last column of table 3.1. Our convention is to multiply group elements in the reverse order with respect to the symbol sequence. We need these group elements for our next step, the dynamical zeta function factorizations.

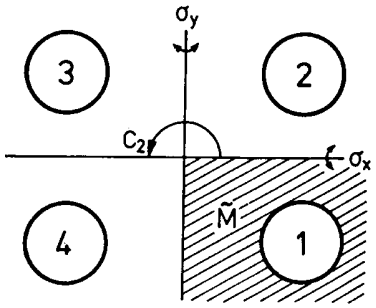

Figure 3.4: Symmetries of four disks on a rectangle. A fundamental domain indicated by the shaded wedge.

The C_{4v} group has four 1-dimensional representations, either symmetric (A_1) or antisymmetric (A_2) under both types of reflections, or symmetric under one and antisymmetric under the other (B_1, B_2), and a degenerate pair of 2-dimensional representations E. Substituting the C_{4v} characters

C_{4v}	A_1	A_2	B_1	B_2	E
e	1	1	1	1	2
C_2	1	1	1	1	-2
C_4, C_4^3	1	1	-1	-1	0
σ_{axes}	1	-1	1	-1	0
σ_{diag}	1	-1	-1	1	0

into (**??**) we obtain:

[1] Predrag 2009-01-18: redrew FigSrc/sune/xfig/ . dynamics.fig is now renamed c4vRelative.fig, see figure 3.3. Try to find fig2.eps?

Table 3.1: C_{4v} correspondence between the ternary fundamental domain prime cycles $\tilde{p}$ and the full 4-disk {1,2,3,4} labeled cycles p, together with the C_{4v} transformation that maps the end point of the $\tilde{p}$ cycle into an irreducible segment of the p cycle. For typographical convenience, the symbol $\underline{1}$ of sect. 3.2.2 has been replaced by 0, so that the ternary alphabet is $\{0, 1, 2\}$. The degeneracy of the p cycle is $m_p = 8|\tilde{p}|/|p|$. Orbit $\overline{2}$ is the sole boundary orbit, invariant both under a rotation by π and a reflection across a diagonal. The two pairs of cycles marked by (a) and (b) are related by time reversal, but cannot be mapped into each other by C_{4v} transformations.

$\tilde{p}$	p	$\mathbf{h}_{\tilde{p}}$
0	1 2	σ_x
1	1 2 3 4	C_4
2	1 3	C_2, σ_{13}
01	12 14	σ_{24}
02	12 43	σ_y
12	12 41 34 23	C_4^3
001	121 232 343 414	C_4
002	121 343	C_2
011	121 434	σ_y
012	121 323	σ_{13}
021	124 324	σ_{13}
022	124 213	σ_x
112	123	e
122	124 231 342 413	C_4
0001	1212 1414	σ_{24}
0002	1212 4343	σ_y
0011	1212 3434	C_2
0012	1212 4141 3434 2323	C_4^3
0021 (a)	1213 4142 3431 2324	C_4^3
0022	1213	e
0102 (a)	1214 2321 3432 4143	C_4
0111	1214 3234	σ_{13}
0112 (b)	1214 2123	σ_x
0121 (b)	1213 2124	σ_x
0122	1213 1413	σ_{24}
0211	1243 2134	σ_x
0212	1243 1423	σ_{24}
0221	1242 1424	σ_{24}
0222	1242 4313	σ_y
1112	1234 2341 3412 4123	C_4
1122	1231 3413	C_2
1222	1242 4131 3424 2313	C_4^3

$h_{\tilde{p}}$			A_1	A_2	B_1	B_2	E
e:	$(1-t_{\tilde{p}})^8$	=	$(1-t_{\tilde{p}})$	$(1-t_{\tilde{p}})$	$(1-t_{\tilde{p}})$	$(1-t_{\tilde{p}})$	$(1-t_{\tilde{p}})^4$
C_2:	$(1-t_{\tilde{p}}^2)^4$	=	$(1-t_{\tilde{p}})$	$(1-t_{\tilde{p}})$	$(1-t_{\tilde{p}})$	$(1-t_{\tilde{p}})$	$(1+t_{\tilde{p}})^4$
C_4, C_4^3:	$(1-t_{\tilde{p}}^4)^2$	=	$(1-t_{\tilde{p}})$	$(1-t_{\tilde{p}})$	$(1+t_{\tilde{p}})$	$(1+t_{\tilde{p}})$	$(1+t_{\tilde{p}}^2)^2$
σ_{axes}:	$(1-t_{\tilde{p}}^2)^4$	=	$(1-t_{\tilde{p}})$	$(1+t_{\tilde{p}})$	$(1-t_{\tilde{p}})$	$(1+t_{\tilde{p}})$	$(1-t_{\tilde{p}}^2)^2$
σ_{diag}:	$(1-t_{\tilde{p}}^2)^4$	=	$(1-t_{\tilde{p}})$	$(1+t_{\tilde{p}})$	$(1+t_{\tilde{p}})$	$(1-t_{\tilde{p}})$	$(1-t_{\tilde{p}}^2)^2$

The possible irreducible segment group elements $\mathbf{h}_{\tilde{p}}$ are listed in the first column; σ_{axes} denotes a reflection across either the x-axis or the y-axis, and σ_{diag} denotes a reflection across a diagonal (see figure 3.2).

In addition, degenerate pairs of boundary orbits can run along the symmetry lines in the full space, with the fundamental domain group theory weights $\mathbf{h}_p = (C_2 + \sigma_x)/2$ (axes) and $\mathbf{h}_p = (C_2 + \sigma_{13})/2$ (diagonals) respectively:

$$\begin{array}{rrcl} & & & A_1 \quad A_2 \quad B_1 \quad B_2 \quad E \\ \text{axes:} & (1-t_{\tilde{p}}^2)^2 & = & (1-t_{\tilde{p}})(1-0t_{\tilde{p}})(1-t_{\tilde{p}})(1-0t_{\tilde{p}})(1+t_{\tilde{p}})^2 \\ \text{diagonals:} & (1-t_{\tilde{p}}^2)^2 & = & (1-t_{\tilde{p}})(1-0t_{\tilde{p}})(1-0t_{\tilde{p}})(1-t_{\tilde{p}})(1+t_{\tilde{p}})^2 \end{array} \quad (3.8)$$

(we have assumed that $t_{\tilde{p}}$ does not change sign under reflections across symmetry axes). For the 4-disk arrangement considered here only the diagonal orbits $\overline{13}$, $\overline{24}$ occur; they correspond to the $\overline{2}$ fixed point in the fundamental domain.

The A_1 subspace in C_{4v} cycle expansion is given by

$$\begin{aligned} 1/\zeta_{A_1} &= (1-t_0)(1-t_1)(1-t_2)(1-t_{01})(1-t_{02})(1-t_{12}) \\ &\quad (1-t_{001})(1-t_{002})(1-t_{011})(1-t_{012})(1-t_{021})(1-t_{022})(1-t_{112}) \\ &\quad (1-t_{122})(1-t_{0001})(1-t_{0002})(1-t_{0011})(1-t_{0012})(1-t_{0021})\dots \\ &= 1-t_0-t_1-t_2-(t_{01}-t_0t_1)-(t_{02}-t_0t_2)-(t_{12}-t_1t_2) \\ &\quad -(t_{001}-t_0t_{01})-(t_{002}-t_0t_{02})-(t_{011}-t_1t_{01}) \\ &\quad -(t_{022}-t_2t_{02})-(t_{112}-t_1t_{12})-(t_{122}-t_2t_{12}) \\ &\quad -(t_{012}+t_{021}+t_0t_1t_2-t_0t_{12}-t_1t_{02}-t_2t_{01})\dots \end{aligned} \quad (3.9)$$

(for typographical convenience, $\underline{1}$ is replaced by 0 in the remainder of this section). For 1-dimensional representations, the characters can be read off the symbol strings: $\chi_{A_2}(\mathbf{h}_{\tilde{\mathbf{p}}}) = (-1)^{n_0}$, $\chi_{B_1}(\mathbf{h}_{\tilde{\mathbf{p}}}) = (-1)^{n_1}$, $\chi_{B_2}(\mathbf{h}_{\tilde{\mathbf{p}}}) = (-1)^{n_0+n_1}$, where n_0 and n_1 are the number of times symbols 0, 1 appear in the $\tilde{p}$ symbol string. For B_2 all t_p with an odd total number of 0's and 1's change sign:

$$\begin{aligned} 1/\zeta_{B_2} &= (1+t_0)(1+t_1)(1-t_2)(1-t_{01})(1+t_{02})(1+t_{12}) \\ &\quad (1+t_{001})(1-t_{002})(1+t_{011})(1-t_{012})(1-t_{021})(1+t_{022})(1-t_{112}) \\ &\quad (1+t_{122})(1-t_{0001})(1+t_{0002})(1-t_{0011})(1+t_{0012})(1+t_{0021})\dots \\ &= 1+t_0+t_1-t_2-(t_{01}-t_0t_1)+(t_{02}-t_0t_2)+(t_{12}-t_1t_2) \\ &\quad +(t_{001}-t_0t_{01})-(t_{002}-t_0t_{02})+(t_{011}-t_1t_{01}) \\ &\quad +(t_{022}-t_2t_{02})-(t_{112}-t_1t_{12})+(t_{122}-t_2t_{12}) \\ &\quad -(t_{012}+t_{021}+t_0t_1t_2-t_0t_{12}-t_1t_{02}-t_2t_{01})\dots \end{aligned} \quad (3.10)$$

The form of the remaining cycle expansions depends crucially on the special role played by the boundary orbits: by (3.8) the orbit t_2 does not contribute to A_2 and B_1,

$$\begin{aligned}
1/\zeta_{A_2} &= (1+t_0)(1-t_1)(1+t_{01})(1+t_{02})(1-t_{12}) \\
&\quad (1-t_{001})(1-t_{002})(1+t_{011})(1+t_{012})(1+t_{021})(1+t_{022})(1-t_{112}) \\
&\quad (1-t_{122})(1+t_{0001})(1+t_{0002})(1-t_{0011})(1-t_{0012})(1-t_{0021})\dots \\
&= 1+t_0-t_1+(t_{01}-t_0t_1)+t_{02}-t_{12} \\
&\quad -(t_{001}-t_0t_{01})-(t_{002}-t_0t_{02})+(t_{011}-t_1t_{01}) \\
&\quad +t_{022}-t_{122}-(t_{112}-t_1t_{12})+(t_{012}+t_{021}-t_0t_{12}-t_1t_{02})\dots
\end{aligned} \tag{3.11}$$

and

$$\begin{aligned}
1/\zeta_{B_1} &= (1-t_0)(1+t_1)(1+t_{01})(1-t_{02})(1+t_{12}) \\
&\quad (1+t_{001})(1-t_{002})(1-t_{011})(1+t_{012})(1+t_{021})(1-t_{022})(1-t_{112}) \\
&\quad (1+t_{122})(1+t_{0001})(1-t_{0002})(1-t_{0011})(1+t_{0012})(1+t_{0021})\dots \\
&= 1-t_0+t_1+(t_{01}-t_0t_1)-t_{02}+t_{12} \\
&\quad +(t_{001}-t_0t_{01})-(t_{002}-t_0t_{02})-(t_{011}-t_1t_{01}) \\
&\quad -t_{022}+t_{122}-(t_{112}-t_1t_{12})+(t_{012}+t_{021}-t_0t_{12}-t_1t_{02})\dots
\end{aligned} \tag{3.12}$$

In the above we have assumed that t_2 does not change sign under C_{4v} reflections. For the mixed-symmetry subspace E the curvature expansion is given by

$$\begin{aligned}
1/\zeta_E &= 1+t_2+(-{t_0}^2+{t_1}^2)+(2t_{002}-t_2{t_0}^2-2t_{112}+t_2{t_1}^2) \\
&\quad +(2t_{0011}-2t_{0022}+2t_2t_{002}-{t_{01}}^2-{t_{02}}^2+2t_{1122}-2t_2t_{112} \\
&\quad +{t_{12}}^2-{t_0}^2{t_1}^2)+(2t_{00002}-2t_{00112}+2t_2t_{0011}-2t_{00121}-2t_{00211} \\
&\quad +2t_{00222}-2t_2t_{0022}+2t_{01012}+2t_{01021}-2t_{01102}-t_2{t_{01}}^2+2t_{02022} \\
&\quad -t_2{t_{02}}^2+2t_{11112}-2t_{11222}+2t_2t_{1122}-2t_{12122}+t_2{t_{12}}^2-t_2{t_0}^2{t_1}^2 \\
&\quad +2t_{002}(-{t_0}^2+{t_1}^2)-2t_{112}(-{t_0}^2+{t_1}^2))
\end{aligned} \tag{3.13}$$

A quick test of the $\zeta = \zeta_{A_1}\zeta_{A_2}\zeta_{B_1}\zeta_{B_2}\zeta_E^2$ factorization is afforded by the topological polynomial; substituting $t_p = z^{|p|}$ into the expansion yields

$$1/\zeta_{A_1} = 1-3z\ , \quad 1/\zeta_{A_2} = 1/\zeta_{B_1} = 1\ , \quad 1/\zeta_{B_2} = 1/\zeta_E = 1+z\ ,$$

in agreement with (**??**).

exercise ??

3.2.3 C_{2v} factorization

An arrangement of four identical disks on the vertices of a rectangle has C_{2v} symmetry (figure 3.4 (b)). C_{2v} consists of $\{e, \sigma_x, \sigma_y, C_2\}$, i.e., the reflections across the symmetry axes and a rotation by π.

Table 3.2: C_{2v} correspondence between the ternary $\{0,1,2\}$ fundamental domain prime cycles $\tilde{p}$ and the full 4-disk {1,2,3,4} cycles p, together with the C_{2v} transformation that maps the end point of the $\tilde{p}$ cycle into an irreducible segment of the p cycle. The degeneracy of the p cycle is $m_p = 4|\tilde{p}|/|p|$. Note that the 012 and 021 cycles are related by time reversal, but cannot be mapped into each other by C_{2v} transformations. The full space orbit listed here is generated from the symmetry reduced code by the rules given in sect. 3.2.3, starting from disk 1.

$\tilde{p}$	p	g	$\tilde{p}$	p	g
0	1 4	σ_y	0001	1414 3232	C_2
1	1 2	σ_x	0002	1414 2323	σ_x
2	1 3	C_2	0011	1412	e
01	14 32	C_2	0012	1412 4143	σ_y
02	14 23	σ_x	0021	1413 4142	σ_y
12	12 43	σ_y	0022	1413	e
001	141 232	σ_x	0102	1432 4123	σ_y
002	141 323	C_2	0111	1434 3212	C_2
011	143 412	σ_y	0112	1434 2343	σ_x
012	143	e	0121	1431 2342	σ_x
021	142	e	0122	1431 3213	C_2
022	142 413	σ_y	0211	1421 2312	σ_x
112	121 343	C_2	0212	1421 3243	C_2
122	124 213	σ_x	0221	1424 3242	C_2
			0222	1424 2313	σ_x
			1112	1212 4343	σ_y
			1122	1213	e
			1222	1242 4313	σ_y

This system affords a rather easy visualization of the conversion of a 4-disk dynamics into a fundamental domain symbolic dynamics. An orbit leaving the fundamental domain through one of the axis may be folded back by a reflection on that axis; with these symmetry operations $g_0 = \sigma_x$ and $g_1 = \sigma_y$ we associate labels 1 and 0, respectively. Orbits going to the diagonally opposed disk cross the boundaries of the fundamental domain twice; the product of these two reflections is just $C_2 = \sigma_x\sigma_y$, to which we assign the label 2. For example, a ternary string $0\,0\,1\,0\,2\,0\,1\ldots$ is converted into 12143123..., and the associated group-theory weight is given by $\ldots g_1g_0g_2g_0g_1g_0g_0$.

Short ternary cycles and the corresponding 4-disk cycles are listed in table 3.2. Note that already at length three there is a pair of cycles (012 = 143 and 021 = 142) related by time reversal, but *not* by any C_{2v} symmetries.

The above is the complete description of the symbolic dynamics for 4 sufficiently separated equal disks placed at corners of a rectangle. However, if the fundamental domain requires further partitioning, the ternary description is insufficient. For example, in the stadium billiard fundamental domain one has to distinguish between bounces off the straight and the curved sections of the billiard wall; in that case five symbols suffice for constructing the covering

symbolic dynamics. [2]

The group C_{2v} has four 1-dimensional representations, distinguished by their behavior under axis reflections. The A_1 representation is symmetric with respect to both reflections; the A_2 representation is antisymmetric with respect to both. The B_1 and B_2 representations are symmetric under one and antisymmetric under the other reflection. The character table is

C_{2v}	A_1	A_2	B_1	B_2
e	1	1	1	1
C_2	1	1	-1	-1
σ_x	1	-1	1	-1
σ_y	1	-1	-1	1

Substituted into the factorized determinant (**??**), the contributions of periodic orbits split as follows

$g_{\tilde{p}}$			A_1	A_2	B_1	B_2
e:	$(1-t_{\tilde{p}})^4$	=	$(1-t_{\tilde{p}})$	$(1-t_{\tilde{p}})$	$(1-t_{\tilde{p}})$	$(1-t_{\tilde{p}})$
C_2:	$(1-t_{\tilde{p}}^2)^2$	=	$(1-t_{\tilde{p}})$	$(1-t_{\tilde{p}})$	$(1-t_{\tilde{p}})$	$(1-t_{\tilde{p}})$
σ_x:	$(1-t_{\tilde{p}}^2)^2$	=	$(1-t_{\tilde{p}})$	$(1+t_{\tilde{p}})$	$(1-t_{\tilde{p}})$	$(1+t_{\tilde{p}})$
σ_y:	$(1-t_{\tilde{p}}^2)^2$	=	$(1-t_{\tilde{p}})$	$(1+t_{\tilde{p}})$	$(1+t_{\tilde{p}})$	$(1-t_{\tilde{p}})$

Cycle expansions follow by substituting cycles and their group theory factors from table 3.2. For A_1 all characters are $+1$, and the corresponding cycle expansion is given in (3.9). Similarly, the totally antisymmetric subspace factorization A_2 is given by (3.10), the B_2 factorization of C_{4v}. For B_1 all t_p with an odd total number of 0's and 2's change sign:

$$\begin{aligned}
1/\zeta_{B_1} &= (1+t_0)(1-t_1)(1+t_2)(1+t_{01})(1-t_{02})(1+t_{12}) \\
&\quad (1-t_{001})(1+t_{002})(1+t_{011})(1-t_{012})(1-t_{021})(1+t_{022})(1+t_{112}) \\
&\quad (1-t_{122})(1+t_{0001})(1-t_{0002})(1-t_{0011})(1+t_{0012})(1+t_{0021})\dots \\
&= 1+t_0-t_1+t_2+(t_{01}-t_0t_1)-(t_{02}-t_0t_2)+(t_{12}-t_1t_2) \\
&\quad -(t_{001}-t_0t_{01})+(t_{002}-t_0t_{02})+(t_{011}-t_1t_{01}) \\
&\quad +(t_{022}-t_2t_{02})+(t_{112}-t_1t_{12})-(t_{122}-t_2t_{12}) \\
&\quad -(t_{012}+t_{021}+t_0t_1t_2-t_0t_{12}-t_1t_{02}-t_2t_{01})\dots
\end{aligned} \tag{3.14}$$

[2] Predrag : include paper with Kai?

For B_2 all t_p with an odd total number of 1's and 2's change sign:

$$\begin{aligned}
1/\zeta_{B_2} &= (1-t_0)(1+t_1)(1+t_2)(1+t_{01})(1+t_{02})(1-t_{12}) \\
&\quad (1+t_{001})(1+t_{002})(1-t_{011})(1-t_{012})(1-t_{021})(1-t_{022})(1+t_{112}) \\
&\quad (1+t_{122})(1+t_{0001})(1+t_{0002})(1-t_{0011})(1-t_{0012})(1-t_{0021})\dots \\
&= 1-t_0+t_1+t_2+(t_{01}-t_0t_1)+(t_{02}-t_0t_2)-(t_{12}-t_1t_2) \\
&\quad +(t_{001}-t_0t_{01})+(t_{002}-t_0t_{02})-(t_{011}-t_1t_{01}) \\
&\quad -(t_{022}-t_2t_{02})+(t_{112}-t_1t_{12})+(t_{122}-t_2t_{12}) \\
&\quad -(t_{012}+t_{021}+t_0t_1t_2-t_0t_{12}-t_1t_{02}-t_2t_{01})\dots
\end{aligned} \tag{3.15}$$

Note that all of the above cycle expansions group long orbits together with their pseudo-orbit shadows, so that the shadowing arguments for convergence still apply.

The topological polynomial factorizes as

$$\frac{1}{\zeta_{A_1}} = 1-3z \quad , \quad \frac{1}{\zeta_{A_2}} = \frac{1}{\zeta_{B_1}} = \frac{1}{\zeta_{B_2}} = 1+z,$$

consistent with the 4-disk factorization (**??**). [3]

3.2.4 Symmetries of the symbol square

Depending on the type of dynamical system, the symbol square might have a variety of symmetries. Under the time reversal

$$\cdots m_{-2}m_{-1}m_0.m_1m_2m_3\cdots \to \cdots m_3m_2m_1.m_0m_{-1}m_{-2}\cdots$$

the points in the symbol square for an orientation preserving map are symmetric across the diagonal $\gamma = \delta$, and for the orientation reversing case they are symmetric with respect to the $\gamma = 1-\delta$ diagonal. Consequently the periodic orbits appear either in dual pairs $p = m_1m_2m_3\dots m_n$, $\overline{p} = m_nm_{n-1}m_{n-2}\dots m_1$, or are self-dual under time reversal, $S_p = S_{\overline{p}}$. For the orientation preserving case a self-dual cycle of odd period has at least one point on the symmetry diagonal. In particular, all fixed points lie on the symmetry diagonal. Determination of such symmetry lines can be of considerable practical utility, as it reduces some of the periodic orbit searches to 1-dimensional searches.

3.3 Spatiotemporal cat map desymmetrization blog

2017-02-24 Predrag If we have serious intentions of computing the partition (or Zeta) function for spatiotemporal cat map, we need to reduce / factorize its discrete symmetries, first what is for Ising models called "time-reversal symmetry" (not a fortuitous name), and what Boris (and I think

[3] Predrag : add here Freddy p. 26; PER sect. 6.4.

only Boris - have not seen that anywhere in the literature) calls symmetry under "conjugation" [50].

For a two-letter alphabet this is worked out in ChaosBook sect. *C_2 factorization*. Should be similar for the C_2 reflection symmetries of cat map alphabets, and the $C_2 \times C_2$ symmetries of 2-dimensional spatiotemporal cat maps.

The true time-reversal symmetry (and, for spatiotemporal cat map, also space-reflection symmetry) might be harder. Basically, one should go to a fundamental domain which is a half-space in each translational direction. For a finite domain (no translation) this is worked out in ChaosBook Example 11.7 *Group D_1 and reduction to the fundamental domain*. For $O(2)$ this is worked out by Burak [24], and (with the slice rotated by $\pi/2$) by Xiong, in his thesis. In both cases, it is applied to a very specific problem, Kuramoto-Sivashinsky - the solution is not general. I believe that this is the symmetry that shapes the cat map topological zeta functions [65], and the Ising model Ihara zeta function, but that needs to be worked out.

2016-08-18 Predrag Refs. [21, 78, 79] are a few papers that discuss reversible systems.

2016-11-25 Predrag From scanning through Bosetti *et al.* [21] *Time-reversal symmetry and covariant Lyapunov vectors for simple particle models in and out of thermal equilibrium* I learned nothing earth-shaking:

"The system we consider here are invariant with respect to time reversal. This property leaves the equations of motion in phase and tangent space unchanged if the signs of all momentum like variables and of time are reversed, but leaving all position variables unchanged. This implies that there exists a smooth isometry σ of phase space, such that $f^t\sigma = \sigma f^{-t}$. Where necessary, we indicate the forward and backward directions of time by upper indexes (+) and (-), respectively. If this index is omitted, the forward direction is implied."

2CB

2016-11-25 Predrag Lamb and Roberts [78] *Time reversal symmetry in dynamical systems: A survey* fault me explicitly for ignoring time reversal symmetries (it is an omission that has always bugged me): " We note that, despite the success of group representation theory in quantum mechanics [114], the role of comparable symmetry methods in quantum chaology appears to be relatively unexplored. For a recent exception see Cvitanović and Eckhardt [35], who discuss the use of symmetries (but not time-reversal symmetries!) in the calculation of zeta-functions. "

3.4 Green's function counts all paths

This text is based on dasbuch/QMlectures/lectQM.tex. For reasons unbeknownst to me, it is below the dignity of any cat to work out any problem

in ChaosBook, or in the online course, no matter how often I point out that it is easier to understand what we do for spatiotemporal cat map if you first work it out for a standard 2-dimensional lattice.

We assume that the state of a particle is specified by its position, and that it has no further internal degrees of freedom, such as spin or color: $i = (x_1, x_2, \cdots, x_d)$. A particle either does nothing ($s =$ stopping probability) or steps into any of the $2d$ neighboring cells ($h =$ stepping probability). Counting paths on a lattice is a breeze. Let a particle start in the cell i and step along until it stops in the cell j. The probability of this process is $h^\ell s$, where ℓ is the number of steps in the corresponding path. The total probability that a particle wanders from the ith cell and stops in the jth cell is the sum of probabilities associated with all possible paths connecting the two cells:

$$\Delta_{ij} = s \sum_\ell h^\ell N_{ij}(\ell)\,, \tag{3.16}$$

where $N_{ij}(\ell)$ is the number of all paths of length ℓ connecting lattice sites i and j. In order to compute $N_{ij}(\ell)$, define a stepping operator

$$(\sigma^\mu)_{ij} = \delta_{i+n_\mu,j}\,, \tag{3.17}$$

where n_μ is a unit step in direction μ. If a particle is introduced into the ith cell by a source $J_k = \delta_{ik}$, the stepping operator moves it into a neighboring cell:

$$(\sigma^\mu J)_k = \delta_{i+n_\mu,k} \to \quad \overset{i}{\underset{i+n_\mu}{\overset{i}{\searrow}}} \; i + n_\mu$$

The operator

$$N_{ij} = \sum_{\mu=1}^{d} [(\sigma^\mu)_{ij} + (\sigma^\mu)_{ji}]\,, \tag{3.18}$$

generates all steps of length 1:

$$\mathbf{N}\,J = \quad \begin{matrix} 1 & & 1 \\ & \searrow\,\nearrow\;\searrow\,\nearrow & \\ 1 & & 1 \end{matrix}$$

(The examples are drawn in two dimensions). The paths of length 2 are counted by

$$\mathbf{N}^2 J = \quad \begin{matrix} 1 & & 2 & & 1 \\ & \searrow\,\nearrow\;\searrow\,\nearrow\;\searrow\,\nearrow & & & \\ 2 & & 4 & & 2 \\ & \searrow\,\nearrow\;\searrow\,\nearrow\;\searrow\,\nearrow & & & \\ 1 & & 2 & & 1 \end{matrix}$$

There are 4 ways of returning, 2 ways of reaching a diagonal corner, and so on. Note –and this is the key observation– that the kth component of the vector

$\mathbf{N}^\ell J$ counts the number of paths of length ℓ connecting the ith and the kth cells. The total probability that the particle stops in the kth cell is given by

$$\phi_k \;=\; s\sum_{\ell=0}^{\infty} h^\ell \mathbf{N}^\ell_{kj} J_j \,, \qquad \phi \;=\; \frac{s}{1-h\mathbf{N}} J \,. \tag{3.19}$$

The value of the field ϕ_k at a space point k measures the probability of observing the particle introduced into the system by the source J. The Euclidean free scalar particle propagator –or Green's function– (3.16) is given by

$$\Delta_{ij} = \left(\frac{s}{1-h\mathbf{N}}\right)_{ij} \,. \tag{3.20}$$

Consider a smooth function $\phi(x)$ evaluated on a d-dimensional lattice

$$\phi_\ell = \phi(x)\,, \qquad x = a\ell = \text{lattice point}\,, \quad \ell \in \mathbf{Z}^d\,, \tag{3.21}$$

where a is the lattice spacing. Each set of values of $\phi(x)$ (a vector ϕ_ℓ) is a possible lattice configuration. Assume the lattice is hyper-cubic, and let $\hat{n}_\mu \in \{\hat{n}_1, \hat{n}_2, \cdots, \hat{n}_d\}$ be the unit lattice cell vectors pointing along the d positive directions. The *lattice derivative* is then

$$(\partial_\mu \phi)_\ell = \frac{\phi(x+a\hat{n}_\mu) - \phi(x)}{a} = \frac{\phi_{\ell+\hat{n}_\mu} - \phi_\ell}{a} \,. \tag{3.22}$$

The lattice derivative as a linear operator, constructed from the *stepping operator* in the direction μ

$$(\sigma_\mu)_{\ell j} = \delta_{\ell+\hat{n}_\mu, j} \,. \tag{3.23}$$

In practice, the lattice will be a finite d-dimensional hyper-cubic lattice

$$\phi_\ell = \phi(x)\,, \qquad x = a\ell = \text{lattice point}\,, \quad \ell \in (\mathbf{Z}/N)^d \,, \tag{3.24}$$

where a is the lattice spacing and there are N^d points in all. For a hyper-cubic lattice the translations in different directions commute, $\sigma_\mu\sigma_\nu = \sigma_\nu\sigma_\mu$, so it is sufficient to understand the action of (3.23) on a 1-dimensional periodic lattice, on which the stepping operator is an $[N\times N]$ 'upper shift' cyclic permutation matrix

$$\sigma = \begin{bmatrix} 0 & 1 & & & & \\ & 0 & 1 & & & \\ & & 0 & 1 & & \\ & & & & \ddots & \\ & & & & 0 & 1 \\ 1 & & & & & 0 \end{bmatrix} \,, \tag{3.25}$$

with '1' in the lower left corner assuring periodicity. Applied to the lattice configuration $\phi = (\phi_1, \phi_2, \cdots, \phi_N)$, the stepping operator translates the configuration by one site, $\sigma\phi = (\phi_2, \phi_3, \cdots, \phi_N, \phi_1)$. Its transpose translates the

configuration the other way, so the transpose is also the inverse, $\sigma^{-1} = \sigma^T$. The partial lattice derivative (3.22) can now be written as a multiplication by a matrix:

$$\partial_\mu \phi_\ell = \frac{1}{a} \left(\sigma_\mu - \mathbf{1}\right)_{\ell j} \phi_j \,.$$

In the 1-dimensional case the $[N\times N]$ matrix representation of this lattice derivative is:

$$\partial = \frac{1}{a} \begin{bmatrix} -1 & 1 & & & & \\ & -1 & 1 & & & \\ & & -1 & 1 & & \\ & & & & \ddots & \\ & & & & & 1 \\ 1 & & & & & -1 \end{bmatrix} . \tag{3.26}$$

The symmetric (self-adjoint) combination $\Box = -\partial^T \partial$ [4]

$$\begin{aligned} \Box &= -\frac{1}{a^2} \sum_{\mu=1}^{d} \left(\sigma_\mu^{-1} - \mathbf{1}\right) \left(\sigma_\mu - \mathbf{1}\right) = -\frac{2}{a^2} \sum_{\mu=1}^{d} \left(\mathbf{1} - \frac{1}{2}(\sigma_\mu^{-1} + \sigma_\mu)\right) \\ &= \frac{1}{a^2} \left(\mathbf{N} - 2d\mathbf{1}\right) \end{aligned} \tag{3.27}$$

is the *lattice Laplacian*. In the 1-dimensional case the $[N\times N]$ matrix representation of the lattice Laplacian is:

$$\Box = \frac{1}{a^2} \begin{bmatrix} -2 & 1 & & & & 1 \\ 1 & -2 & 1 & & & \\ & 1 & -2 & 1 & & \\ & & & 1 & \ddots & \\ & & & & & 1 \\ 1 & & & & 1 & -2 \end{bmatrix} . \tag{3.28}$$

The lattice Laplacian measures the second variation of a field ϕ_ℓ across three neighboring sites: it is spatially *non-local*. The Euclidean "free scalar particle propagator" (3.20), or the "Green's function" can thus be written as

$$\Delta = \frac{1}{\mathbf{1} - \frac{a^2 h}{s} \Box} \,. \tag{3.29}$$

In spatiotemporal cat map we are not thinking of a continuum, so we set the lattice spacing to $a = 1$.

Now, were there even a single alert cat out there (and there should not be a dry eye in the feline audience at this moment), it would not escape her attention that (3.27) looks very much like the spatiotemporal cat map eq. (3.5):

$$(\Box_{zz'} + 2d\mathbf{1})_{zz'} x_{z'} = s x_z + m_z \,, \qquad x_z \in \mathbb{T}^1 \,, \quad m_z \in \mathcal{A} \,, \quad z \in \mathbb{Z}^d \,. \tag{3.30}$$

[4] Predrag : recheck the signs!

The operator $\mathbf{N} = s\mathbf{1}$ of (3.18) generates all steps of length 1. More precisely, all ways of staying at the site x_z. So now we know what s does in the spatiotemporal cat map equation (3.5): it counts in how many ways we can get from x_z to x_z, with some extra 'particles' subtracted by the source terms m_z. How "subtracted?" Well, Boris did not like Percival and Vivaldi [95] convention (too many "-"s!), so in (3.5) m_z shows up with the wrong sign.

3.5 Helmoltz and screened Poisson equations

The always trustworthy but so un-cited Soviet scientists (1781–1840) teach us that the inhomogeneous *Helmoltz equation* is an elliptical equation of form

$$(\Box + k^2)\, x(z) = -m(z)\,, \qquad z \in \mathbb{R}^d\,, \tag{3.31}$$

where $x(z)$ is a C^2 functions of coordinates, and $m(z)$ is a function with compact support. The Poisson equation is the $k \to 0$ limit of the Helmholtz equation, and for the $\lambda^2 = -k^2 > 0$ (imaginary k), the equation is known as the *screened Poisson equation* [40] (or Yukawa equation). The Green's function for Helmoltz equation satisfies

$$(\Box + k^2)\, g(z, z') = \delta(z - z')\,. \tag{3.32}$$

For example, in $d = 3$ several popular Green's functions are the stationary wave, the outgoing wave and the incoming wave:

$$\begin{aligned} g_0(z, z') &= -\frac{\cos(k|z - z'|)}{4\pi|z - z'|} \\ g_+(z, z') &= -\frac{e^{ik|z-z'|}}{4\pi|z - z'|} \\ g_-(z, z') &= -\frac{e^{-ik|z-z'|}}{4\pi|z - z'|}\,. \end{aligned} \tag{3.33}$$

Furthermore, to these any solution to the homogeneous Helmholtz equation

$$(\Box + k^2)\, f_0(z, z') = 0$$

can be added. On infinite space, the solution of (3.31) is of the form

$$x(z) = x_0(z) - \int_V d^d z'\, m(z')\, g(z, z')\,, \tag{3.34}$$

where $(\Box + k^2)\, x_0(z) = 0$.

The solutions of the screened Poisson equation $(\Box - \lambda^2)\, g(z, z') = \delta(z - z')$ are of the same form, but with the oscillatory $\sin, \cos$, and $\exp(i\cdots)$ solutions replaced by the hyperbolic $\sinh, \cosh$, and $\exp(-\cdots)$. In that case, (3.33) is known as the *Yukawa potential*

$$g(z, z') = -\frac{e^{-\lambda|z-z'|}}{4\pi|z - z'|}\,. \tag{3.35}$$

The d-dimensional spatiotemporal cat map

$$(\Box + (2d-s)\mathbf{1})_{zz'} x_{z'} = m_z \,, \qquad x_z \in \mathbb{T}^1 \,, \quad m_z \in \mathcal{A}^1 \,, \quad z \in \mathbb{Z}^d \tag{3.36}$$

is the discretization of the Helmholtz equation for $s < 2d$. The purely hyperbolic, $s > 2d$ spatiotemporal cat maps that we study are discretizations of the screened Poisson equation.

Let $g(z, z')$, with $z, z' \in \mathcal{R}$ be the corresponding Green's function on a bounded, simply connected domain $\mathcal{R} \subset \mathbb{R}^d$, satisfying some boundary condition (e.g., periodic, Dirichlet or Neumann) at $\partial\mathcal{R}$. The Green's function identity allows us to connect the values of x_z inside of $\mathcal{R}$ with the ones attained at the boundary (an arbitrary Soviet citation):

$$\begin{aligned} x(z) &= \int_{\mathcal{R}} g(z,z') m(z') dz' \\ &- \int_{\partial\mathcal{R}} \nabla_n \, g(z,z'') x(z'') \, dz'' + \int_{\partial\mathcal{R}} \nabla_n \, x(z'') g(z,z'') \, dz'' \,. \end{aligned} \tag{3.37}$$

wiki: In the homogeneous case, the screened Poisson equation is the same as the time-independent Klein–Gordon equation. In the inhomogeneous case, the screened Poisson equation is very similar to the inhomogeneous Helmholtz equation, the only difference being the sign within the brackets.

The Neumann boundary condition can be imposed by extending the original field symmetrically across its sides, so that the extended field, which is four times bigger, is symmetric and periodic.

At the risk of sounding repetitive: it's crazy to formulate this problem in terms of the symmetry-breaking domains with Dirichlet boundary conditions, when all that is needed are the trivial periodic solutions on 2-dimensional tori. To appreciate how difficult the Dirichlet problem is, you can at your leisure study the paper *On the solution of the Helmholtz equation on regions with corners* by Soviet mathematicians Serkh and Rokhlin [109] (one of them a Member of The National Academy of Sciences of The USA), who solve several boundary value problems for the Helmholtz equation on polygonal domains. In terms of the boundary integral equations of potential theory, the solutions are representable by series of appropriately chosen Bessel functions. Making the space discrete does not make these calculations any easier.

3.6 Green's function for 2-dimensional lattice

The Green's function $g(zz') = g(z - z', 0) =: \mathsf{g}_{n,t}$, $z - z' = (n, t) \in \mathbb{Z}^2$ solves the equation:

$$[(-\Box + s - 4)\mathsf{g}]_{n0,t0} = \delta_{n,0}\delta_{t,0} \,. \tag{3.38}$$

[5] The solution is given by the double integral:

$$\mathsf{g}_{n,t} = \frac{1}{\pi^2}\int_0^\pi\int_0^\pi \frac{\cos(nx)\cos(ty)}{s-2\cos x-2\cos y}dxdy\,, \tag{3.39}$$

an expression which can, in turn, be recast into single integral form,

$$\begin{aligned}\mathsf{g}_{n,t} &= \frac{1}{2\pi^3}\int_{-\infty}^{+\infty}d\eta\int_0^\pi\int_0^\pi \frac{\cos(nx)\cos(ty)}{(s/2-2\cos x-i\eta)(s/2-2\cos y+i\eta)}dxdy \\ &= \frac{1}{2\pi}\int_{-\infty}^{+\infty}d\eta\,\frac{\mathcal{L}(\eta)^{-n}\mathcal{L}^*(\eta)^{-t}}{|\mathcal{L}(\eta)-\mathcal{L}(\eta)^{-1}|^2}\,,\end{aligned} \tag{3.40}$$

where

$$\mathcal{L}(\eta)+\mathcal{L}(\eta)^{-1} = s/2+i\eta, \qquad |\mathcal{L}(\eta)|>1\,.$$

The above equation can be thought as the integral over a product of two $\mathbb{Z}^1$ functions:

$$\mathsf{g}_{n,t} = \frac{1}{2\pi}\int_{-\infty}^{+\infty}d\eta\,\mathsf{g}_n(s/2+i\eta)\mathsf{g}_t(s/2-i\eta)\,. \tag{3.41}$$

An alternative representation is given by modified Bessel functions $I_n(x)$ of the first kind [88]:

$$\mathsf{g}_{n,t} = \int_0^{+\infty}d\eta\,e^{-s\eta}I_n(\eta)I_t(\eta)\,, \tag{3.42}$$

which enables the evaluation of the diagonal elements explicitly, as a Legendre function,

$$\mathsf{g}_{n,n} = \frac{1}{2\pi i}Q_{n-1/2}(s^2/8-1), \qquad s^2/8-1>1\,.$$

The representation (3.41) demonstrates that $\mathsf{g}_{n,t}$ is positive for any n and t.

Dirichlet boundary conditions.

Consider next the Green's function $\mathsf{g}(z,z')$, $z=(n,t)\in\mathbb{Z}^2$, $z'=(n',t')\in\mathbb{Z}^2$ which satisfies (**??**) within the rectangular domain $\mathcal{R}=\{(n,t)\in\mathbb{Z}^2|0\le n\le \ell_1+1, 0\le t\le \ell_2+1\}$ and vanishes at its boundary $\partial\mathcal{R}$. By applying the same method as in the case of one-dimensional lattices we get

$$\begin{aligned}\mathsf{g}(z,z') &= \sum_{j_1,j_2=-\infty}^{+\infty} \mathsf{g}_{n-n'+2j_1(\ell_1+1),t-t'+2j_2(\ell_2+1)} + \mathsf{g}_{n+n'+2j_1(\ell_1+1),t+t'+2j_2(\ell_2+1)} \\ &- \mathsf{g}_{n-n'+2j_1(\ell_1+1),t+t'+2j_2(\ell_2+1)} - \mathsf{g}_{n+n'+2j_1(\ell_1+1),t-t'+2j_2(\ell_2+1)},\end{aligned}$$

where $\mathsf{g}_{n,t}$ is the free Green's function defined by (3.39). Substituting (3.41) yields

$$\mathsf{g}(z,z') = \frac{1}{2\pi}\int_{-\infty}^{+\infty}d\eta\,\mathsf{g}_{n,n'}(s/2+i\eta)\mathsf{g}_{t,t'}(s/2-i\eta)\,. \tag{3.43}$$

[5] Predrag 2017-08-03: please recheck: do you want to refer to (3.38) somewhere? Now that you have numbered it?

Exponential decay of Green's function.

We are now going to show that the Green's function $\mathrm{g}(z,z')$ decays exponentially as distance between points z and z' grows. The starting point is (3.43) by which

$$|\mathrm{g}(z,z')|^2 \leq \int_{-\infty}^{+\infty} \frac{d\eta}{2\pi} |\mathrm{g}_{n,n'}(s/2+i\eta)|^2 \int_{-\infty}^{+\infty} \frac{d\eta}{2\pi} |\mathrm{g}_{t,t'}(s/2-i\eta)|^2. \tag{3.44}$$

[6]

3.7 Toeplitz tensors

In sect. 3.4 we worked out the propagator in the only in $d=1$ configuration space, and stated the result for $d>1$ after the Fourier transform diagonalization. What are the generalizations of Topelitz matrices to $d>1$? They are called *Toeplitz tensors*.

2018-02-24 Predrag This one I think is not relevant to us: Lim [84] *Singular values and eigenvalues of tensors: A variational approach* - " A theory of eigenvalues, eigenvectors, singular values, and singular vectors for tensors based on a constrained variational approach much like the Rayleigh quotient for symmetric matrix eigenvalues. An illustration: a multilinear generalization of the Perron-Frobenius theorem. "

2018-02-24 Predrag Khoromskaia and Khoromskij [75] *Block circulant and Toeplitz structures in the linearized Hartree-Fock equation on finite lattices: Tensor approach* seems quite relevant to our project - they work out the $D=3$ lattice case: " grid-based tensor approach to solution of the elliptic eigenvalue problem for the 3D lattice-structured systems. We consider the linearized Hartree-Fock equation over a spatial $L_1 \times L_2 \times L_3$ lattice for both periodic and non-periodic case. In the periodic case the low-rank tensor structure in the diagonal blocks of the Fock matrix in the Fourier space reduces the conventional 3D FFT to the product of 1D FFTs. "

Xie, Jin and Wei [116] *A fast algorithm for solving circulant tensor systems*: " Circulant tensors is a generalization of the circulant matrix. We define the generalized circulant tensors which can be diagonalized by a Fourier matrix, and solve the circulant tensor system by a fast FFT algorithm. "

Cui *et al.* [32] *An eigenvalue problem for even order tensors with its applications*: " Using the matrix unfolding of even order tensors, we can establish the relationship between a tensor eigenvalue problem and a multilevel matrix eigenvalue problem. We show that higher order singular values are the square root of the eigenvalues of the product of the tensor and its conjugate transpose, as in the matrix case. Also we study

[6] Boris 2017-07-18: TO BE CONTINUED

an eigenvalue problem for Toeplitz/circulant tensors, and give the lower and upper bounds of eigenvalues of Toeplitz tensors. ”

Rezghi and Eldén [105] *Diagonalization of tensors with circulant structure*: “ A tensor of arbitrary order, which is circulant with respect to two modes, can be diagonalized in those modes by discrete Fourier transforms. This property can be used in the efficient solution of linear systems involving contractive products of tensors with circulant structure. Tensors with circulant structure occur in models with periodic boundary conditions. ”

2018-02-24 Predrag In 2007 the N-way Toolbox, Tensor Toolbox, and Multilinear Engine were software packages for working with tensors.

block-Toeplitz matrix

A tensor can be regarded as a multidimensional array of data. The order of a tensor is the number of dimensions. The dimensions of a tensor also are known as *ways* or *modes*.

Multilevel matrices arise in multidimensional applications.

3.8 Green's blog

2016-07-13 Predrag Cat map Green's functions are standard 'lattice propagators' for discrete lattices, obtained by discrete Fourier transform diagonalization of discrete Laplacian. Working through ChaosBook sections *D.3 Lattice derivatives* to *D.5.2 Lattice Laplacian diagonalized* might help you understand this material.

(All eq. numbers refer to svn ver. 5020 of 160521Gutkin.pdf and ChaosBook.org ver. 15.7. You can also use e-book but the chapter numbering is different.)

2017-02-17 Predrag For diffusion, a linear (symmetric, Vivaldi) code is needed.

For spatiotemporal cat map

1. linear code seems needed. Have not proven that.
2. its partition volumes have no relation to 2-tori weights
3. linear code pruning rules undercount 2-tori pruning rules
4. 2-tori are intrinsic to the flow, there might exist Markov partitions
   Boris 2017-02-17 Markov partitions for spatiotemporal cats exist, but their complexity grows exponentially with number of cats.
   Predrag 2017-03-04 That is what you keep saying, but if you mean *finite* Markov partitions for *the* spatiotemporal cat map, even on a finite spatially periodic domain, I have never seen it. It would require high-dimensional unstable/stable manifolds of the fixed point at the origin to map onto each other, in order to get a generating partition consisting of a finite number of volumes. Pretty amazing.

2017-08-25 Predrag I have not understood this before, but the $\mathcal{R} = [2\times 1]$ block

$$\mathsf{M} = \begin{bmatrix} m_{11}m_{21} \end{bmatrix}$$

is not just a 1D temporal cat map - the Dirichlet boundary conditions make this nasty as well,

$$\mathsf{M} \cup \partial\mathcal{R} = \begin{bmatrix} x_{12}x_{22} \\ x_{01}m_{11}m_{21}x_{31} \\ x_{10}x_{20} \end{bmatrix} .$$

2017-08-25 Predrag $\partial\mathcal{R} = \{x_1, x_2, \cdots x_8\}$ is not consistent with our notation: they live on sites, and should be labelled by index pairs $\partial\mathcal{R} = \{x_z\}$, in $\mathcal{R} = [2\times 1]$ example as $\partial\mathcal{R} = \{x_{01}, x_{02}, x_{13}, \cdots, x_{10}\}$. That is consistent with the cat map, where the corresponding block + boundary points is correctly labelled as $x_0 m_1 m_2 x_3$. The crazy thing is that even with the correct notation, there is no rhyme nor reason in the above 8 inequalities.

$$0 \le (x_{01} + x_{10} - m_{12})(s^2 - 2) + (x_{13} + x_{02} + x_{31} + x_{20} - m_{22} - m_{11})s + (x_{23} + x_{32} - m_{21})2 \le \nu_s$$
$$0 \le (x_{02} + x_{13} - m_{22})(s^2 - 2) + (x_{01} + x_{10} + x_{23} + x_{32} - m_{12} - m_{21})s + (x_{20} + x_{31} - m_{11})2 \le \nu_s$$
$$0 \le (x_{20} + x_{31} - m_{11})(s^2 - 2) + (x_{01} + x_{10} + x_{23} + x_{32} - m_{12} - m_{21})s + (x_{02} + x_{13} - m_{22})2 \le \nu_s$$
$$0 \le (x_{23} + x_{32} - m_{21})(s^2 - 2) + (x_{13} + x_{02} + x_{31} + x_{20} - m_{22} - m_{11})s + (x_{01} + x_{10} - m_{12})2 \le \nu_s$$

2017-08-30 Boris In principle you are right, but keeping 2 indices would only make things look terribly "heavy" (without a good justification, as anyway "there is no rhyme nor reason"). The single index notation for the boundary points seems to me the least evil.

2017-09-09 Predrag Dorr [36] *The direct solution of the discrete Poisson equation on a rectangle*

Hu, Ryu and O'Connell [62] *Analytical solution of the generalized discrete Poisson equation* " present an analytical solution to the generalized discrete Poisson equation (DPE), a matrix equation which has a tridiagonal matrix with fringes having an arbitrary value for the diagonal elements."

Many physical problems require the numerical solution of the Poisson equation on a rectangle. In general, one uses the finite-difference method [36], where the rectangle is replaced by an $N\times k$ grid, and the Poisson equation is solved in the finite-difference representation. In this way, the problem is reduced to the discrete Poisson equation (DPE) on an $[N\times k]$ grid, a matrix equation $\mathcal{D}x = m$ having a tridiagonal matrix $[k\times k]$ with fringes, of form

$$\mathcal{D} = \begin{pmatrix} M & 1 & 0 & 0 & \dots & 0 & 0 \\ 1 & M & 1 & 0 & \dots & 0 & 0 \\ 0 & 1 & M & 1 & \dots & 0 & 0 \\ \vdots & \vdots & \vdots & \vdots & \ddots & \vdots & \vdots \\ 0 & 0 & \dots & \dots & \dots & M & 1 \\ 0 & 0 & \dots & \dots & \dots & 1 & M \end{pmatrix} , \tag{3.45}$$

where M is a $[N \times N]$ symmetric tridiagonal matrix (1.56), with constant $-s$ along the diagonal, and the $[N \times N]$ identity matrix 1 as the off-diagonal elements. Thus, the matrix $\mathcal{D}$ consists of $[k \times k]$ submatrices of $[N \times N]$ elements. An important special case is $s = 4$, which is the matrix form for the Poisson equation on a rectangle arising from the difference method.

They invert $\mathcal{D}$ in three steps:

1. By applying the results of ref. [61], invert $\mathcal{D}$ into $\mathcal{D}^{-1}$. This generalizes (1.66) to a (sub)matrix formula, with g_{jk} replaced by submatrix Θ_{jk}, where Θ is an $[N \times N]$ matrix defined by
$$-2\cosh\Theta = M$$
2. The eigenvalues and eigenfunctions for the submatrices of the block matrix $g = \mathcal{D}^{-1}$ are given by (1.64).
3. Evaluate analytically each of the individual elements in the inverted matrix $\mathcal{D}^{-1}$ by the Schur decomposition scheme [49].

I find the procedure inelegant and cumbersome, as the two dimensions are treated in different ways. The result is, however, a bit more symmetric (but not written fully symmetric), written in terms of coefficients such as:

$$\alpha_{lm}(n) = \sqrt{\frac{2}{N+1}} \sinh\frac{ln\pi}{N+1} \sinh\frac{mn\pi}{N+1}\,.$$

In contrast, Boris formulation (3.39) is symmetric.

My intuition is explained in sect. 3.4 - the d translations commute, so should compute eigenvalues for each direction separately. Works out for periodic boundary conditions.

Also, in d-dimensional the Jacobian (1.58) for Dirchlet b.c. should generalized to the product of d Jacobians, one for each direction

$$\det\left(\mathcal{D}_{\ell_1\times\ell_2\times\cdots\ell_d}\right) = U_{\ell_1}(s/2)U_{\ell_2}(s/2)\cdots U_{\ell_d}(s/2)\,. \tag{3.46}$$

For example,

$$\det\left(\mathcal{D}_{1\times1}\right) = U_1(s/2)U_1(s/2) = s^2\,, \tag{3.47}$$

and

$$\det\left(\mathcal{D}_{2\times2}\right) = U_2(s/2)U_2(s/2) = (s^2-1)^2\,. \tag{3.48}$$

Unfortunately, these do not look like the factors in our paper...

How does one get cosh's and sinh's in the circulant matrix case?

2016-07-11 Predrag Boris cites P. A. Martin [88] *Discrete scattering theory: Green's function for a square lattice*

The *lattice Green's function* is the main subject of the paper.

We consider the simplest problem, with a two-dimensional, square lattice. Each lattice point can move out of the plane of the lattice, and that each point is connected to its neighbours by springs; only nearest-neighbour interactions are included. This leads to a system of partial difference equations. The same equations are obtained if the two-dimensional Helmholtz equation is discretized using the central-difference approximation (lattice d'Alembert operator) for the Laplacian.

2017-09-09 Predrag A few more links to digest:

Eigenvalues of periodic lattice Laplacian? uses the Kronecker product, and gives sensible, symmetric eigenvalues for a doubly-periodic torus, something like

$$\lambda_{jk} = 2s - 2\cos\frac{j\pi}{\ell_1} - 2\cos\frac{k\pi}{\ell_2}\,.$$

Statistical Approach to Quantum Field Theory: An Introduction By Andreas Wipf

arXiv:math/0010135 *Integrable Lattices: Random Matrices and Random Permutations*

arXiv:1702.00339 *Block circulant and Toeplitz structures in the linearized Hartree-Fock equation on finite lattices: tensor approach*

2017-09-08 Predrag NOTE: Chung and Yau [29] *Discrete Green's functions* gives explicitly in Theorem 6 an asymmetrical 2-dimensional lattice Green's function for $\mathcal{R}^{[\ell_1\times\ell_2]}$. This paper is cited over 100 times, maybe there is a better answer in that list.

Papathanasiou and Thorn [94] *Worldsheet propagator on the lightcone worldsheet lattice* give in Appendix B 2D lattice Neumann open string, Dirichlet open string, and closed string propagators.

Giles and Thorn [47] *Lattice approach to string theory*. The Giles-Thorn (GT) discretization of the worldsheet begins with a representation of the free closed or open string propagator as a lightcone worldsheet path integral defined on a lattice.

2017-09-11 Predrag Bhat and Osting [16] *Diffraction on the two-dimensional square lattice* write: The lattice Green's function is quite well known [39, 70].

Economou [39] *Green's Functions in Quantum Physics* contains a vast amount of useful information - GaTech does not have online access to it.

Katsura [72] *Lattice Green's function. Introduction*: The Helmholtz equation for the wavefunction $\psi(r)$ in the continuous space is given by

$$\left(\frac{1}{2}\Delta + E\right)\psi = 0$$

The Green's function $g(E, r)$ is the solution of

$$\left(\frac{1}{2}\Delta + E\right) g = \delta(r)$$

The real part of the square lattice Green's function (3.39) is odd or even function of s, and the imaginary part is even or odd function of s, if the sum of n and t is even or odd, respectively.

Morita and Horiguchi [92] *Calculation of the lattice Green's function for the bcc, fcc, and rectangular lattices*: see the appendix *The lattice Green's functions for the rectangular lattice* (includes the square lattice as a special case). They integrate (3.39) and express it as the complete elliptic integral of the first kind.

Katsura, Inawashiro and Abe [71] *Lattice Green's function for the simple cubic lattice in terms of a Mellin-Barnes type integral*

Katsura and Inawashiro [70] *Lattice Green's functions for the rectangular and the square lattices at arbitrary points*.

Morita [91] *Useful procedure for computing the lattice Green's function - square, tetragonal, and bcc lattices*: " A recurrence relation, which gives the values of the lattice Green's function along the diagonal direction from a couple of the elliptic integrals of the first and second kind, is derived for the square lattice by an elementary partial integration. The values of the square lattice Green's function at an arbitrary site are then calculated in a successive way with the aid of the difference equation defining the function. " The method yields a recursion formula for a peculiar lattice Green's function on a 2d lattice, but not the LGF itself.

Horiguchi [58] *Lattice Green's function for the simple cubic lattice* - GaTech does not have online access to it.

Horiguchi and Morita [59] *Note on the lattice Green's function for the simple cubic lattice*: " A simple recurrence relation connecting the lattice Green's function at (l,m n) and the first derivatives of the lattice Green's function at $(l \pm 1, m, n)$, is presented for the simple cubic lattice. By making use of that recurrence relation, the lattice Green's functions at (2,0,0) and (3,0,0) are obtained in closed forms, which contain a sum of products of the complete elliptic integrals of the first and the second kind. "

Cserti [31] *Application of the lattice Green's function for calculating the resistance of an infinite network of resistors*.

Asad [8] *Differential equation approach for one- and two-dimensional lattice Green's function* seems a continuation of ref. [59]: " A first-order differential equation of Green's function, at the origin G(0), for the one-dimensional lattice is derived by simple recurrence relation. Green's function at site (m) is then calculated in terms of G(0). A simple recurrence relation connecting the lattice Green's function at the site (m,n) and the first derivative of the lattice Green's function at the site $(m \pm 1, n)$ is presented for the

two-dimensional lattice, a differential equation of second order in G(0, 0) is obtained. By making use of the latter recurrence relation, lattice Green's function at an arbitrary site is obtained in closed form. "

2017-09-11 Boris Some caution on Green's functions: In 1D everything is explicit and simple. The real problem is $2D$. For the paper we need two facts – positivity of its elements, and exponential decay (both for Dirichlet boundary conditions). I was unable to extract them from the literature (which is bizarre), but checked numerically. Proofs are still lacking, but should be within reach.

2017-09-20 Predrag Continued feline misery. From the periodic orbit theory point of view, it is insane to work with finite lattice blocks with Dirichlet boundary conditions. The theory demands periodic boundary conditions. They preserve translational invariance which makes Green's matrices trivially diagonizable by discrete Fourier transforms. Now that Boris is such a mensch that he can do it, I am writing up a pedagogical Dirichlet/periodic b.c.'s Green's matrices appendix to ref. [50] (or per chance even a section of the paper proper, as this is no afterthought - this is the central point of the paper), an appendix whose ultimate goal is to show that the matrix elements are decaying exponentially as

$$\mathcal{D}_{zz'} \approx e^{-\lambda|z-z'|^d}\,, \tag{3.49}$$

i.e., in our humble $d = 2$ example as $\exp(-\lambda|z - z'|^2)$. If the coauthors were to understand or (gasp!) contribute to the write up, we would be in cat heaven.

So far, still writing up the $d = 1$ temporal cat example of sect. 1.7, but the determinant of the Helmholtz operator for any finite $d = 2$ rectangular lattice region of sect. 3.7 should play out the same way.

To Matt and Andy: This goes lock, stock and barrel into the continuum field theories, such as Kuramoto-Sivashinsky, with the Euclidian metric in (3.49) replaced by the (still to be thought through) correct Kuramoto-Sivashinsky spacetime metric.

2017-10-18 Predrag Glaser [48] *Numerical solution of waveguide scattering problems by finite-difference Green's functions* computes a 2-dimensional Green's function with boundary conditions on arbitrary shape approximated by a discrete boundary: "A finite-difference Green's function method for solving time-harmonic wave guide scattering problems involving metallic obstacles of finite size is applied to the two-dimensional problem of a TE10 mode impinging on cylindrical metallic posts of arbitrary shape in a rectangular waveguide."

2017-10-19 Predrag de la Llave [85] *Variational methods for quasiperiodic solutions of partial differential equations* has a pedagogical discussion of the discrete lattices gradient flows.

3.9 Spatiotemporal cat map literature

3.9.1 Hoover and Aoki / HooAok16

Predrag 2016-08-20 excerpts from or notes on several papers on coupled map lattices.

Hoover and Aoki [56] *Order and chaos in the one-dimensional ϕ^4 model : N-dependence and the second law of thermodynamics*. Will probably appear in *Intern. J. Bifurcation and Chaos*.

They study the one-discretized space dimension ϕ^4 time *flow* whose Hamiltonian is the sum of the kinetic, tethers, and pair-potential energies [3, 4, 60] (see also refs. [5, 6]):

$$\mathcal{H} = K + \Phi_{\rm tethers} + \Phi_{\rm pairs} = \sum_i^N [\ (p_i^2/2) + (q_i^4/4)\ ] + \sum_{i<j}^{\rm pairs} (q_i - q_j)^2/2\ .$$

Here the $\{\ q\ \}$ represent the displacements of the particles from their static lattice rest positions. The $\{\ p = \dot{q}\ \}$ are the corresponding momenta. The pair-potential part of the equations of motion:

$$\ddot{q}_i + q_i^3 = (i+1)d + q_{i+1} - 2(id + q_i) + (i-1)d + q_{i-1} \equiv q_{i+1} - 2q_i + q_{i-1}\ . \quad (3.50)$$

They study the periodic boundary case.

Note the discrete spatial Laplacian $q_{i+1} - 2q_i + q_{i-1}$. The time, however is still continuous, so no temporal discrete Laplacian in this model.

The model illustrates the state space dimensionality loss found in non-equilibrium steady states [55, 57, 90]. Unlike the harmonic chain, in which heat travels ballistically at the speed of sound, the one-dimensional ϕ^4 model exhibits Fourier heat conductivity with a finite large-system limit. One seeks for evidence that the fractal nonequilibrium state space distributions found for small systems persists in larger ones, as this then explains the Second Law of Thermodynamics. The fractals clarify the irreversible nature of the unidirectional repeller-to-attractor state space flow. This Second Law connection to fractal structures they established through studies of the Lyapunov spectra.

The Lyapunov spectrum $\{\ \lambda_i\ \}$ has a number of exponents equal to the dimensionality of the phase space, for which they use the symbol D . The exponents describe the growth and decay rates parallel to the orthogonal axes of a comoving and corotating state space hypersphere. As this fractal (or information) dimension D cannot be computed in practice, the use the Kaplan and Yorke D_{KY}.

Aoki and Kusnezov's ϕ^4 model provides many far-from-equilibrium examples of the relatively large dimensionality loss $\Delta D = D - D_I \simeq D - D_{KY}$. Present article seeks to characterize the Lyapunov instability of equilibrium loops and chains from the dynamical systems point of view, starting with the $N = 2$ pair of one-dimensional particles, the smallest system for which chaos is possible. They find periodic orbits and chaotic orbits, doing some suspect

numerical work and waffling about symmetric and antisymmetric periodic orbits. They find an infinite number of periodic orbits which are "computationally stable" while at the same time exhibiting positive Lyapunov exponents. BTW, even and odd N are different. Basically, it's not their shtick to think about detailed dynamics, so they do lots of ergodic simulations.

Based on many simulations with different initial conditions, they conjecture that the chaotic sea is likely unique. Given the number of particles and the energy it appears that there is only one chaotic sea, not two or three or an infinite number. They speculate on the uniqueness of the model's chaotic sea and on the connection of such collections of deterministic and time-reversible states to the Second Law of Thermodynamics.

Aoki [2] *Symmetry, chaos and temperature in the one-dimensional lattice ϕ^4 theory* writes: " The symmetries of the minimal ϕ^4 theory on the lattice, and trajectories which are chaotic, yet restricted to motions within subspaces due to symmetry reasons, are systematically analyzed. The chaotic dynamics of autonomous Hamiltonian systems are discussed, in relation to the thermodynamic laws. Possibilities of configurations with non-equal ideal gas temperatures in the steady state are investigated. The pairing of local (finite-time) Lyapunov exponents are analyzed, and their dependence on various factors, such as energy of the system, characteristics of the initial conditions are studied. "

He addresses question posed by Wm. G. Hoover and C. G. Hoover, CMST 23, 73 (2017), which does not seem to exist. The model has a discrete spatial reflection symmetry, and, for periodic boundary condition, the discrete translational symmetry, with finite number N of lattice sites. In addition, for N even, there is a parity symmetry. He shows how a symmetry of a model can restrict the trajectories to a subspace of a theory, while still being chaotic.

When the initial condition is invariant under translation by $m < N$, the solutions stay in the subspace.

A less obvious flow-invariant subspace exists for theory with anti-periodic boundary conditions, N/m even, and other examples can be found with twists added to boundary conditions.

A parity symmetry subspace is also flow-invariant.

He most have gotten a Grigoriev: "even in theories with chaos, there are non-chaotic orbits, such as periodic orbits[8, 10–14]." (All of references are news to me - have to check them)

Reading, to be continued....

3.9.2 Geist and Lauterborn / GeiLau88

Geist and Lauterborn [42] have a series of 3 papers on *The nonlinear dynamics of the damped and driven Toda chain*.

They study the dynamics of a periodically driven damped Toda $N = 15$ chain with periodic boundary conditions and show that periodic motions of different periodicity, quasiperiodic and aperiodic (chaotic) motions exist. Dissipative (or frictional) forces are introduced proportional to the particle veloci-

ties in the form

$$D_i = [v_{i+1} - 2v_i + v_{i-1}]\, d \tag{3.51}$$

with the damping coefficient d and $v_i = \dot{q}_i$. The damping coefficient is fixed to $d = 0.1$. They study bifurcations as they vary Toda parameters. They study the structure of the eigenvalue spectrum of the associated linearized flow map. They shown that quasiperiodic motions on torus of dimension $k = 3$ exist, and address the technical problems concerning the Fourier and Lyapunov analysis of the motions on tori T k ($k \geq 2$).

However, this model might be of limited use to us, as it is non-autonomous: one particle of the chain is driven by the single frequency external force.

3.9.3 Giacomelli, Lepri and Politi / GiLePo95

Predrag 2016-09-03 excerpts from or notes on
Giacomelli, Lepri and Politi [43].

All the systems are constructed in such a way that the corresponding two-dimensional (2D) representation is characterized by the same updating rule in the bulk. The main difference among them is the direction of the "time" axis in the plane. Despite the different causality relations among the various models, the resulting patterns are shown to be statistically equivalent. In particular, the *Kolmogorov-Sinai entropy density assumes always the same value*. Therefore, it can be considered as an absolute indicator, measuring the amount of disorder of a 2D pattern. The Kaplan-Yorke dimension density is instead rule dependent: this indicator alone cannot be used to quantify the degrees of freedom of a given pattern; one must further specify the direction of propagation in the plane.

3.9.4 Lepri, Politi and Torcini / LePoTo96

> In literary theory and philosophy of language, the chronotope is how configurations of time and space are represented in language and discourse.
>
> — Wikipedia : Chronotope

Predrag 2016-03-02, 2016-09-03 excerpts from or notes on
Lepri, Politi and Torcini [81] *Chronotopic Lyapunov analysis. I. A detailed characterization of 1D systems*

Linear stability analysis of chaotic dynamics is usually concerned with the problem of measuring the divergence of nearby trajectories. In extended systems, the full characterization of a generic perturbation involves both its temporal and spatial growth rates as complementary measures of its instability properties. Two classes of Lyapunov exponents have been separately introduced for this purpose: the former aims at describing the temporal evolution of disturbances with an exponential profile in space [102]; the latter deals with the spatial shape of a perturbation defined on a given site at all times [44]. The

most general perturbation is identified by two rates, the *temporal* exponent λ, and *spatial* exponent μ describing its growth in time and space, respectively.

Temporal Lyapunov exponents spectrum (TLS) is obtained by following the evolution of a perturbation in the tangent space, with spatial periodic boundary conditions.

Spatial Lyapunov exponents (SLS) have been introduced as a tool for investigating the structure of temporal Lyapunov vectors [44]. The main difficulty for them is that, in principle, it requires determine periodic orbits of discrete time period N. Instead, they assume a temporal exponential profile for the perturbation, and state the evolution equation in tangent space (PC: we do not need to do that). The spatial dynamics is "conservative." For a given time discretization T, there exist $2T$ spatial Lyapunov exponents μ_j. This doubling in the number of the degrees of freedom is related to the two-step spatial memory (PC: i.e., Laplacian in the temporal direction; in other words, 2D phase space). Moreover, the spatial Lyapunov spectrum (SLS) associated with any symmetric trajectory is invariant under "space" reversal.

The direct implementation of the above method faces the difficulty that iteration of the nonlinear equation in space usually does not converge onto the same attractor as obtained by iterating in time the original model. In fact, it turns out that the invariant spatiotemporal measure corresponds to a strange repeller in space [82]. Thus, one must first generate a 2D pattern of local multipliers and then use it in the computation of the spatial Lyapunov exponents.

The Lyapunov analysis of a given (1+1)D pattern can, in principle, be carried out along any direction. In fact, by performing a spatiotemporal rotation, i.e., by combining the role of space and time, it is possible to define still another class of "rotated" exponents [43].

Numerical simulations and approximate analytical results indicate that a well-defined thermodynamic limit for the set of Lyapunov exponents is reached for large enough system size, both in space and time. As a consequence, the Kaplan-Yorke dimension and the Kolmogorov-Sinai entropy are extensive quantities, so that the dynamics of a long chain can be roughly seen as that of many independent adjacent subchains. This fact allows us to define Lyapunov spectra independent of the system size.

They introduce the so-called (λ, μ) plane, which provides a compact graphical representation of Lyapunov spectra. It allows enlightening analogies and differences between spatial and temporal exponents, and reveals a sort of duality between the temporal and spatial representations.

They discuss two examples:

(a) A spatially homogeneous and stationary pattern, treated analytically.

(b) Spatiotemporal periodic orbits. Politi and Torcini [102] have noted that the standard TLS exhibits a band structure for for periodic (both in space and time) orbits, and that (λ, μ) plane has interesting structure.

The properties of these indicators are studied in several models of coupled map lattices (reaction-diffusion systems, many-degrees-of-freedom Hamilto-

nian dynamics, and systems with a conserved order parameter [22]), since we are confident that the tools and the results apply equally well to systems with continuous space and time variables.

Coupled maps are sometimes used also as test ground for extended Hamiltonian systems. The corresponding models are generally formulated in such a way that the evolution in tangent space is described by symplectic matrices. They study the coupled-standard-map lattice [69]

$$\begin{aligned} p_{n,t+1} &= p_{n,t} - k\left[\sin q_{n,t} + \frac{\epsilon}{2}\sin(q_{n+1,t} - q_{n,t}) + \frac{\epsilon}{2}\sin(q_{n-1,t} - q_{n,t})\right] \\ q_{n,t+1} &= q_{n,t} + p_{n,t+1} \pmod{2\pi}\,. \end{aligned} \tag{3.52}$$

Note the discrete spatial Laplacian,

$$\begin{aligned} p_{n,t+1} &= p_{n,t} - k\frac{\epsilon}{2}\partial_x^2 \sin q_{n,t} \\ q_{n,t+1} &= q_{n,t} + p_{n,t+1} \pmod{2\pi}\,. \end{aligned} \tag{3.53}$$

but temporal Hamiltonian dynamics; that needs to be recast in the Newtonian form to also have the temporal Laplacian. (Not really the discrete derivative ∂_q^2, and I'm being sloppy with its sign.)

... so-called two-ways communication (so-called Laplacian-type coupling), which is a restricted version of variable range coupling.

Symplectic maps: Both the symplectic structure and the time-reversal invariance induce a pairing in the Lyapunov spectrum which turns out to be invariant under the transformation $\lambda_j \to -\lambda_j$.

The spatial discrete Laplacian operator, introduced to describe diffusion, has the structure of a general tight-binding Hamiltonian.

In the stationary 2D Anderson model both dimensions are spatial directions and they can be exactly interchanged, leading to the exact invariance under the transformation $(\lambda, \mu) \to (\mu, \lambda)$.

While Giacomelli and Politi [44] note the formal analogy with the 2D Schrodinger problem, no purely exponential localization is observed in coupled maps.

But there is also "**entropy potential**" that might be relevant: Lepri, Politi and Torcini [83] *Entropy potential and Lyapunov exponents*: " According to a previous conjecture, spatial and temporal Lyapunov exponents of chaotic extended systems can be obtained from derivatives of a suitable function, the entropy potential. The numerical investigation of a continuous-time model provides a further confirmation to the existence of the entropy potential. Furthermore, it is shown that the knowledge of the entropy potential allows determining also Lyapunov spectra in general reference frames where the time-like and space-like axes point along generic directions in the space-time plane. Finally, the existence of an entropy potential implies that the integrated density of positive exponents (Kolmogorov-Sinai entropy) is independent of the chosen reference frame.

Conjecture: all the information on Lyapunov exponents can be obtained from a single observable: the entropy potential, a function of the temporal and

the spatial growth rates. The name "entropy potential" follows from the observation that for zero growth rates, this function coincides with the density of Kolmogorov-Sinai entropy.

We show a connection between spatial and temporal Lyapunov exponents by studying the evolution of perturbations along generic "world-lines" in the space-time, i.e. along directions other than the space and time axes. The extension of the usual definition of Lyapunov exponents to this more general class of frames, partially discussed in ref. [43], is appropriate for characterizing patterns with some anisotropy.

In the perspective of a complete characterization of spacetime chaos, one should consider the possibility of viewing a generic pattern as being generated along directions other than time and space axes. In fact, once a pattern is given, any direction can, a priori, be considered as an appropriate "time" axis.

In the case of patterns, the identification of the most appropriate spatial and temporal directions is a new and unavoidable element of the game. For this reason, we introduce the notion of *spatiotemporal exponents*. For the moment, we assume that the pattern is continuous both along space and time directions; we shall discuss later how the definitions can be extended to CML models.

When arbitrary directions are considered in the (x,t) plane, the coordinates must be properly scaled in order to force them to have the same dimension. We choose to multiply the time variable by c, where c is a suitable constant with the dimension of a velocity.

Although it is not obvious whether the invariant measure in the initial frame is still attracting in the new frame (see ref. [43] for a discussion of this point), one can anyhow study the stability properties by linearizing and defining the Lyapunov exponents in the usual way.

an exact implementation of the mapping rule requires acausal boundary conditions, since the knowledge of future (in the original frame) states is required [43] (this is a general problem occurring also in the continuous case). As we are interested in the thermodynamic limit, we bypass the problem by choosing periodic boundary conditions. Such a choice has been shown not to affect the bulk properties of the dynamical evolution [43].

Reaction-diffusion systems [30] are among the most relevant models for the study of spatiotemporal chaos.

A simplified class of models can be obtained by spatial discretization, i.e. by considering a 1D lattice of coupled oscillators [7]. (Ref. [7] seems to be about generalized Ginzburg-Landau equaton, nothing discrete).

A further simplification is achieved by discretizing also the time, i.e. by considering coupled map lattices (CML).

Consider a generic perturbation, assumed to possess an exponential profile both in space and time,

$$\delta = a(x,t)\exp(-\mu x + \lambda t) \tag{3.54}$$

Depending whether μ, or λ is considered as a free parameter, one can define either the temporal or the spatial Lyapunov spectrum.

...we have been able to substantiate the conjecture only in simple cases where the linear stability analysis reduces to the an eigenvalue equation for a fixed point or a periodic orbit. ... in ref. [82] a test on the existence of a potential has been performed by computing a certain circulation integral.

In order to test the general validity of our main ansatz, we consider now a continuous-time model. Since the generation mechanisms of the multipliers in tangent space are not important for our conclusions, we have assumed that they are the result of stochastic processes, thus escaping the need to integrate also some nonlinear equations in phase-space.

"

Kamizawa, Hara and Ohya [66] *On relations among the entropic chaos degree, the Kolmogorov-Sinai entropy and the Lyapunov exponent* seems a bit suspect. But they write: "

For properties of the Lyapunov exponents see ref. [97]

The Kolmogorov-Shinai entropy (KS entropy for brevity) is another important criterion to describe chaos. This criterion was introduced by Kolmogorov [76] to discuss the entropy in ergodic theory. The KS entropy measures the complexity of the system and the positivity of the KS entropy means the existence of chaos.

The KS entropy are extremely difficult to calculate in general. For the KS entropy, the map has to be measure-preserving; although this condition is not so strong, we have to know the invariant measure, which is difficult in general.

Ruelle [106] proved a relationship between the Lyapunov exponents and the KS entropy. The inequality, called Margulis-Ruelle inequality, states that the KS entropy is less than or equal to the sum of positive Lyapunov exponents. The opposite inequality was proved by Pesin under some restricted conditions. These two formulae indicate that, under some conditions, the two different criteria determine the same kind of chaotic behaviour. "

3.9.5 Lepri, Politi and Torcini / LePoTo97

Predrag 2016-03-02 excerpts from or notes on
Lepri, Politi and Torcini [82] *II. Towards a unified approach*.

From the analyticity properties of the equation governing infinitesimal perturbations, it is conjectured that all types of Lyapunov exponents introduced in spatially extended 1D systems can be derived from a single function that we call the entropy potential. The general consequences of its very existence on the Kolmogorov-Sinai entropy of generic spatiotemporal patterns are discussed.

3.9.6 Politi, Torcini and Lepri / PoToLe98

Predrag 2016-03-02 excerpts from or notes on
the follow-up, Politi, Torcini and Lepri [103] *Lyapunov exponents from node-counting arguments*.

Related to *Chronotopic analysis* is ref. [103] that I actually have not been able to find and read. The abstract: "A conjecture connecting Lyapunov exponents

of coupled map lattices and the node theorem is presented. It is based on the analogy between the linear stability analysis of extended chaotic states and the Schrödinger problem for a particle in a disordered potential. As a consequence, we propose an alternative method to compute the Lyapunov spectrum. The implications on the foundation of the recently proposed "chronotopic approach" are also discussed." Hopefully not relevant to us.

In summary, chromotopic approach looks very promising, but seems to led nowhere and had died a quiet death.

3.9.7 Pikovsky and Politi / PikPol98

MNG 2016-09-06 excerpts and basic idea of Pikovsky and Politi [101]. Includes results for coupled Logistic Maps, Coupled Symplectic maps, complex Ginzburg-Landau equation, Kuramoto-Sivashinsky equation, and a differential-delay equation.

Follows the treatment of the logarithm of "the" Lyapunov vector ("the" implying the vector associated with the maximal Lyapunov exponent) as a "profile/interface".

"In all cases, we look at the behaviour of the maximum Lyapunov exponent and of the corresponding Lyapunov vector for fixed size L, and increasing time T. We then study how the instability properties depend on L."

The "interface" is defined by

$$h(x,t) = \log|w(x,t)|$$

where h is the "interface" and w is the Lyapunov vector associated with the maximal Lyapunov exponent.

"The dynamics of the Lyapunov vector is characterized by two main features: an exponential growth and irregular fluctuations. The former corresponds to a linear movement of the profile, thus implying that the Lyapunov exponent is nothing but the interface velocity. The latter is a manifestation of the roughening process: if we start from a flat profile (meaning that the initial condition for the linearized equations is spatially uniform), the width of the interface grows in time, saturating to a value that diverges for increasing system size."

3.9.8 Szendro *et al.* / szendro-2007

Szendro *et al.* [112] *Spatiotemporal structure of Lyapunov vectors in chaotic coupled-map lattices* is focused on surface growth KPZ kinds of issues, using coupled logistic maps.

3.9.9 Bunimovich and Sinai / BunSin88

Bunimovich and Sinai [25] *Spacetime chaos in coupled map lattices*.

"One of the most appealing problems in the theory of nonlinear dynamical systems is an explanation of a widely observed phenomenon of the appearance of coherent structures (cs) from chaos. The first questions related to cs are met already in the first pages of the Bible. [...] The main thrust of this paper is that some cases of cs are connected with the theory of phase transitions and can be described in corresponding terms. [...] In the present paper we construct simple examples of infinite dimensional dynamical systems which are naturally described by two-dimensional lattice models of statistical mechanics. In these models one direction corresponds to the space translation while the other corresponds to the time direction generated by the dynamics. Our basic result is analogous to *high-temperature results in statistical mechanics*. Our result gives a more or less complete description of spacetime chaos. We believe that the low-temperature domain of parameters may lead to phase transitions where the emerging phases can be interpreted as coherent structures, "

"We consider simple examples of such systems generated by expanding maps of the unit interval (or circle) with some kind of diffusion coupling."

Model: They study finite spatial lattices with $-N_1 \leq n \leq N_2$. At each site $i \in \mathbb{Z}^1$ of the one-dimensional lattice we have a variable $x_i \in [0,1]$, and expanding (linear) map with expanding integer slope d, with site symbolic dynamics $\omega_n \in \{1, 2, \cdots, d\}$. I do not see any symbolic dynamics along the time direction, so *this is not 2D symbolic dynamics*.

$$x_{n,t+1} = f(x_{n,t}) + \frac{1}{2}\alpha(x_{n,t})\Box x_{n,t}\,. \tag{3.55}$$

3.9.10 Pesin and Sinai / PesSin88

Pesin and Sinai [98] *Space-time chaos in the system of weakly interacting hyperbolic systems*.

Coupled cat lattices were introduced by Pesin and Sinai [98] and extensively studied since, but always in the weak coupling, in order to prove the continuity of their SRB measure, with no detailed investigations of spatiotemporal symbolic dynamics. We do not have to cite any of that literature, beyond Pesin and Sinai [98].

" In this paper we consider those infinite-dimensional dynamical systems for which all degrees of freedom are in some sense equivalent. The direct consequence of this equivalence is the appearance of a new symmetry group acting on the degrees of freedom by shifts and commuting with the dynamics. Our main problem will be to study ergodic properties of the total group generated by the shifts and the dynamics, i.e. the group of space-time translations. If this group preserves some probability measure and is mixing with respect to it then we shall say that the space-time dynamics exhibits the space-time chaos.

The main result of ref. [25] was the construction of a natural invariant measure with respect to the group $\mathbb{Z}^2$ generated by the shift and the dynamics which was mixing, i. e. we had the space-time chaos. The goal of this paper is

to show a much more general result which states the space-time chaos when is an arbitrary hyperbolic transformation. "

Motivation: diffusion-reaction equation of the form

$$\frac{\partial u}{\partial t} = f(u) + \epsilon + \frac{\partial^2 u}{\partial x^2}\,. \tag{3.56}$$

$$u_{n,t+1} = f(u_{n,t}) + \epsilon(u_{n-1,t} + u_{n+1,t})\,. \tag{3.57}$$

Assume that f is a topologically transitive $\mathbb{C}^2$-Anosov diffeomorphism. The case of small ϵ corresponds to the high-temperature region in statistical mechanics where there are no phase transitions. [...] We shall study in this paper maps which can be called chains of interacting Anosov maps. For such maps we shall construct natural measures invariant under the action of the group $\mathbb{Z}^2$ generated by shift and the dynamics provided that couplings are sufficiently small. These measures are analogous of BRS-measures in the theory of finite dimensional hyperbolic systems.

2016-09-28 PC, 2016-10-04 .

All these papers, starting with Bunimovich and Sinai [25], and including de la Llave's (still to be identified) study weakly coupled cat maps (Predrag they are NOT mentioned in ref. [25]), and exploit the fact that weakly nonlinear Anosov maps retain the complete partition of the Arnol'd cat map, so symbolic dynamics is unchanged by the weak coupling. They focus on phase transitions - the weakly coupled cats maps case is the high-temperature phase.

Sinai [111] Some mathematical problems in the theory of quantum chaos

Ruelle and Ya. G. Sinai [108] From dynamical systems to statistical mechanics and back: " there is a class of nice systems (hyperbolic, or Axiom A systems) where one can define continuously an expanding and a contracting direction on A. For such systems one can almost replace the set A by the set of configurations of a 1-dimensional classical lattice spin system. For simplicity we describe this symbolic dynamics in the discrete time case, i.e., $t \in$ integers. "

Bonetto, Kupiainen and Lebowitz [20] *Absolute continuity of projected SRB measures of coupled Arnol'd cat map lattices*. Their lattice (they credit Pesin and Sinai [98] with introducing cat map lattices) is weakly coupled, and they prove that they can construct SRB measure continuous with respect to the Lebesgue measure (must satisfy a non-degeneracy condition, essentially that the maps are not free). The construct the systems via finite-dimensional approximations, with periodic lattices on $(\mathbb{Z}_N)^d$, where $\mathbb{Z}_N$ consists of integers of absolute value strictly less than N. Their Eq. (2.2) seems to apply that the dynamics is spatially asymmetric (not diffusive), and they assume coupling falling off exponentially with distance, not a next-neighbor coupling. The actual proofs are beyond my pay grade. The

paper seems to have 17 citations. All generic stat mech, only this one is of potential interest, in the sense that cat map is an idealization of a rotators:

Ruelle [107] *Nonequilibrium statistical mechanics and entropy production in a classical infinite system of rotators*. This is model is defined on an arbitrary (?) graph, with rotators at vertices and couplings on pairwise links between vertices. Gets more general from there, not relevant to us.

2016-11-20 Boris Single-alphabet symbolic dynamics overlaid on a $d = 2$ square lattice of coupled 1D maps was already in Bunimovich and Sinai [25]. Pesin and Sinai [98] was the same, but for weakly coupled $d = 2$ Anosov map lattices. The construction was always based on taking it from non-interacting case and use conjugation of two systems (which works only for weakly coupled systems). Pethel, Corron and Bollt [99, 100] used the same construction, just ignoring all surrounding math issues. It might be that we are the first who use $d = 2$ for strongly coupled maps. Strong coupled case was treated by math people but without symbolic dynamics.

2016-10-22 Predrag I've looked at these papers again. Bunimovich-Sinai is the first paper, on coupled 1D expanding maps. Pesin-Sinai is not an announcement of Bunimovich-Sinai, it is the second paper in the series, the one that introduces coupled 2D Anosov maps.

3.10 Cats' GHJSC16blog

Internal discussions of ref. [50] edits: Move good text not used in ref. [50] to this file, for possible reuse later.

2016-11-18 Predrag A theory of turbulence that has done away with *dynamics*? We rest our case.

2016-10-05 Predrag My approach is that this is written for field theorists, fluid dynamicists etc., who do not see any reason to look at cat maps, so I am trying to be pedagogical, motivate it as that chaotic counterpart of the harmonic oscillator, something that field theorists fell comfortable with (they should not, but they do).

2016-11-13 Predrag The next thing to rethink: Green's functions for periodic lattices are in ChaosBook sections D.3 Lattice derivatives and on, for the Hermitian Laplacian and $s = 2$. For real $s > 2$ cat map, the potential is inverted harmonic oscillator, the frequency is imaginary (Schrödinger in imaginary time), eigenvectors real - should be a straightforward generalization. Have done this already while studying Ornstein-Uhlenbeck with Lippolis and Henninger - the eigenfunctions are Hermite polynomials times Gaussians.

2016-11-13 Predrag The claim "the cat map $A = \begin{pmatrix} a & c \\ d & b \end{pmatrix}$ is assumed to be time-reversal invariant, i.e. $c = d$." seems to be in conflict with Boris choice $A = \begin{pmatrix} s-1 & 1 \\ s-2 & 1 \end{pmatrix}$

We write (1.90) as

$$(\Box + 2 - s)x_t = m_t \,, \tag{3.58}$$

Percival and Vivaldi [95] write their Eq. (3.6)

$$(\Box + 2 - s)x_t = -b_t \tag{3.59}$$

so their "stabilising impulses" b_t (defined on interval $x \in [-1/2, 1/2)$) have the opposite sign to our "winding numbers" m_t (defined on $x \in [0, 1)$).

Did not replace Arnol'd by PerViv choice.

$$A = \begin{pmatrix} 0 & 1 \\ -1 & s \end{pmatrix} , \tag{3.60}$$

$$\begin{aligned} x_{t+1} &= p_t \qquad \mod 1 \\ p_{t+1} &= -x_t + s\, p_t \qquad \mod 1 \end{aligned} \tag{3.61}$$

Predrag's formula, removed by Boris 2017-01-15:

$$\begin{array}{rcl} x_{t+1} &=& (s-1)\,x_t + p_t \\ p_{t+1} &=& (s-2)\,x_t + p_t \end{array} \qquad \mod 1\,, \tag{3.62}$$

Predrag's formula, removed by Boris 2017-01-15:
As the 3-point discretization of the second time derivative d^2/dt^2 (central difference operator) is $\Box\, x_t \equiv x_{t+1} - 2x_t + x_{t-1}$ (with the time step set to $\Delta t = 1$), the *temporal* cat map (**??**) can be rewritten as the discrete time Newton equation for inverted harmonic potential,

$$(\Box + 2 - s)\, x_t = m_t\,. \tag{3.63}$$

Predrag's formula, replaced by a more abstract form by Boris 2017-01-15:
a d-dimensional spatiotemporal pattern $\{x_z\} = \{x_{n_1 n_2 \cdots n_d}\}$ requires *d-dimensional* spatiotemporal block $\{m_z\} = \{m_{n_1 n_2 \cdots n_d}\}$,

for definiteness written as

$$A = \begin{pmatrix} 2 & 1 \\ 1 & 1 \end{pmatrix}\,, \tag{3.64}$$

2016-08-20 Predrag " The fact that even Dyson [38] counts cat map periods should give us pause - clearly, some nontrivial number theory is afoot. "

Not sure whether this is related to cat map symbolic dynamics that we use, dropped for now: " Problems with the discretization of Arnol'd cat map were pointed out in refs. [18, 19]. Ref. [19] discusses two partitions of the cat map unit square. "

" and resist the siren song of the Hecke operators [77, 89] "

While stability multipliers depend only on the trace s, the state space eigenvectors depend on the explicit matrix A, and so do "winding numbers" m_t (which also depend on the defining interval $x \in [-1/2, 1/2)$, Percival and Predrag choice, or Boris choice $x \in [0, 1)$. Time-reversed has different eigenvectors (orthogonal to the forward-time ones), so I am not even sure how time reversed m_t look.

2016-05-21 Predrag Behrends [14, 15] *The ghosts of the cat* is fun - he uncovers various regular patterns in the iterates of the cat map.

2016-09-27 Boris Cat maps and spatiotemporal cat maps

In the spatiotemporal cat map, "particles" (i.e., a cat map at each periodic lattice site) are coupled by the next-neighbor coupling rules:

$$q_{n,t+1} = p_{n,t} + (s-1)q_{n,t} - q_{n+1,t} - q_{n-1,t} - m^q_{n,t+1}$$
$$p_{n,t+1} = p_{n,t} + (s-2)q_{n,t} - q_{n+1,t} - q_{n-1,t} - m^p_{n,t+1}$$

The symbols of interest can be found by:

$$m_{n,t} = q_{n,t+1} + q_{n,t-1} + q_{n+1,t} + q_{n-1,t} - s\, q_{n,t}\,.$$

2016-10-27 Boris Gutkin and Osipov [53] write: "In general, calculating periodic orbits of a non-integrable system is a non-trivial task. To this end a number of methods have been developed," and then, for a mysterious reasons, they refer to ref. [13].

2016-10-27 Boris Added to sect. **??** the following references: M. Sieber and K. Richter [110], S. Müller, S. Heusler, P. Braun, F. Haake and A. Altland [93], B. Gutkin, V.Al. Osipov [52], B. Gutkin, V.Al. Osipov [51] (Predrag added ref. [53] as well).

2016-11-07 Predrag The dynamical systems literature tends to focus on *local* problems: bifurcations of a single time-invariant solution (equilibrium, relative equilibrium, periodic orbit or relative periodic orbit) in low-dimensional settings (3-5 coupled ODEs, 1-dimensional PDE). The problem that we face is *global*: organizing and relating *simultaneously* infinities of unstable relative periodic orbits in ∞-dimensional state spaces, orbits that are presumed to form the skeleton of turbulence (see ref. [45] for a gentle introduction) and are typically not solutions that possess the symmetries of the problem. In this quest we found the standard equivariant bifurcation theory literature not very helpful, as its general focus is on bifurcations of solutions, which admit all or some of the symmetries of the problem at hand.

2016-11-17 Predrag a simple generalization of a Bernoulli map to a Hamiltonian setting

finite grammars whenever all partition borders map onto partition borders.

If one neglects the width of the stretched-out area, get sawtooth maps, with infinity of finite grammars.

Adler and Weiss [1] discovered that certain mappings from the torus to itself, called hyperbolic toral automorphisms have Markov partitions, and in fact these partitions are parallelograms. One famous example is the Arnol'd Cat Map

(Axiom A; Anosov)

are a family of analytic hyperbolic automorphisms of the two-dimensional torus which

The "linear code" was introduced and worked out in detail in influential papers of Percival and Vivaldi [17, 95, 96].

For $d = 1$ lattice, $s = 5$ the spatial period 1 fixed point is equivalent to the usual $s = 3$ Arnol'd cat map.

The cat map partitions the state space into $|\mathcal{A}|$ regions, with borders defined by the condition that the two adjacent labels $k, k+1$ simultaneously

satisfy (1.90),

$$x_1 - sx_0 + x_{-1} - \epsilon = k\,, \tag{3.65}$$

$$x_1 - sx_0 + x_{-1} + \epsilon = k + 1\,, \tag{3.66}$$

$$x_2 - sx_1 + x_0 = m_1\,, \tag{3.67}$$

$$x_1 - sx_0 + x_{-1} = m_0\,, \tag{3.68}$$

$$(x_0, x_1) = (0,0) \to (0,0)\,, \quad (1,0) \to (0,-1)\,, \quad (0,1) \to (1,s)\,, \quad (1,1) \to (1,s-1)$$

2016-11-05 Predrag Dropped this:
Note the two symmetries of the dynamics [73]: The calculations generalize directly to any cat map invariant under time reversal [74].

2016-11-11 Boris "Deeper insight" into $d = 2$ symbolic dynamics Information comes locally (both in space and time). Allows to understand correlations between invariant 2-tori. Connection with field theories.

To Predrag: we have similar results on 2×1 blocks, but I think 1×1, 2×2 is enough. Agree?
2016-12-08 Predrag: I agree

2016-12-06 Boris Confused about Predrag's claim that refs. [28, 46] tile " spatially and temporally infinite domains"(?) In both papers the spatial extension of the system is finite, and the attractors have relatively small dimensions.
2016-12-08 Predrag: I rewrote that now, is it clearer?

2016-12-06 Boris Is this clai true: "Temporally chaotic systems are exponentially unstable with time: double the time, and roughly twice as many periodic orbits are required to describe it to the same accuracy. For large spatial extents, the complexity of the spatial shapes also needs to be taken into account. A spatiotemporally chaotic system is *extensive* in the sense that ..." Double the time and the number of periodic orbits is squared?
2016-12-08 Predrag: It is true only for discrete time, complete binary dynamics, but any other statement brings in more confusing words. I do not want to say "entropy" here. I rewrote it now.

2016-12-06 Boris Predrag's statement "Essentially, as the stretching is uniform, distinct admissible symbol patterns count all patterns of a given size, and that can be accomplished by construction the appropriate finite size transition matrices [33]." is true only for symbolic dynamics based on Markov partitions. Wrong e.g., for linear coding.
2016-12-08 Predrag: I rewrote that now, is it correct?

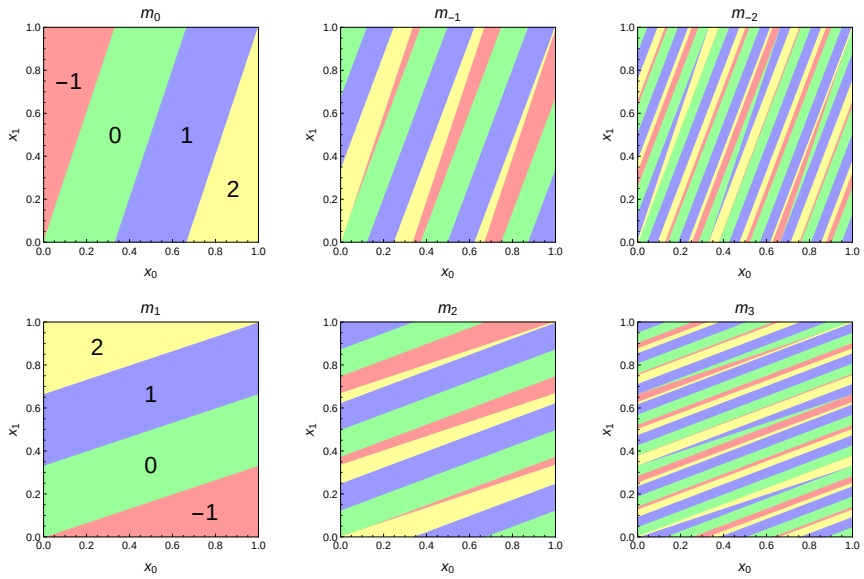

Figure 3.5: (Color online) Newtonian Arnol'd cat map (x_0, x_1) state space partition into (a) 4 regions labeled by m_0. , obtained from (x_{-1}, x_0) state space by one iteration (the same as figure 1.2). (b) 14 regions labeled by past block $m_{-1}m_0$. , obtained from (x_{-2}, x_{-1}) state space by two iterations. (c) 44 regions, past block $m_{-2}m_{-1}m_0$. (d) 4 regions labeled by $.m_1$, obtained from (x_2, x_1) state space by one backward iteration. (e) 14 regions labeled by future block $.m_1m_2$, obtained from (x_3, x_2) state space by two backward iterations. (f) 44 regions, future block $m_3m_2m_1$. Each color has the same total area ($1/6$ for $m_t = \underline{1}, 2$, and $1/3$ for $m_t = 0, 1$). All boundaries are straight lines with rational slopes.

2016-12-12 Predrag My claim (in a conversation with Boris) that spatiotemporal cat map symbolic dynamics is "d-dimensional" was nonsensical. I have now removed this from the draft: " The key innovation of ref. [53] is the realization (an insight that applies to all coupled-map lattices, and all PDEs modeled by them, not only the system considered here) that d-dimensional spatiotemporal orbit $\{x_z\}$ requires *d-dimensional* symbolic dynamics code $\{m_z\} = \{(m_1, m_2, \cdots, m_d)\}$, rather than a *single* temporal symbol sequence (as one is tempted to do when describing a finite coupled N^{d-1}-"particle" system)."

Li Han text: " To generate such state space partitions, we start with length $\ell = 1$. Consider first the symbol $m_0 = sx_0 - (x_1 + x_{-1}) = \lfloor sx_0 - x_1 \rfloor$, where $\lfloor \cdots \rfloor$ is the floor function. m_0 has symbol boundaries which are equally spaced parallel lines of slope s and passing through $(x_0, x_1) = (0, 0), (1, 1)$. We then look at the time-evolved images of these symbol regions under forward map (1.85). The transformed region there-

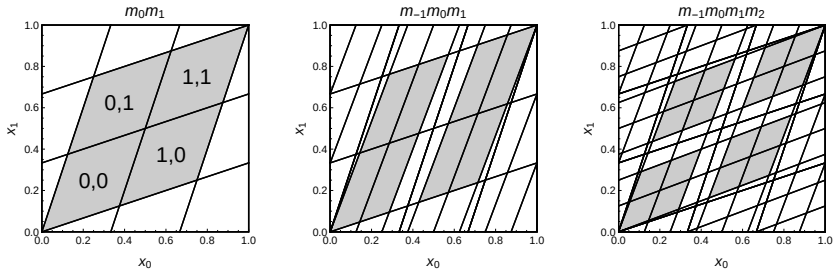

Figure 3.6: Newtonian Arnol'd cat map (x_0, x_1) state space partition into (a) 14 regions labeled by block $b = m_0.m_1$, the intersection of one past (figure 3.5 (a)) and one future iteration (figure 3.5 (d)). (b) block $b = m_{-1}m_0.m_1$, the intersection of two past (figure 3.5 (b)) and one future iteration (figure 3.5 (d)). (c) block $b = m_{-1}m_0.m_1m_2$, the intersection of two past (figure 3.5 (b)) and two future iterations (figure 3.5 (e)). Note that while some regions involving external alphabet (such as _22_ in (a)) are pruned, the interior alphabet labels a horseshoe, indicated by the shaded regions. Their total area is (a) $4 \times 1/8$, (b) $8 \times 1/21$, and (c) $16 \times 1/55$.

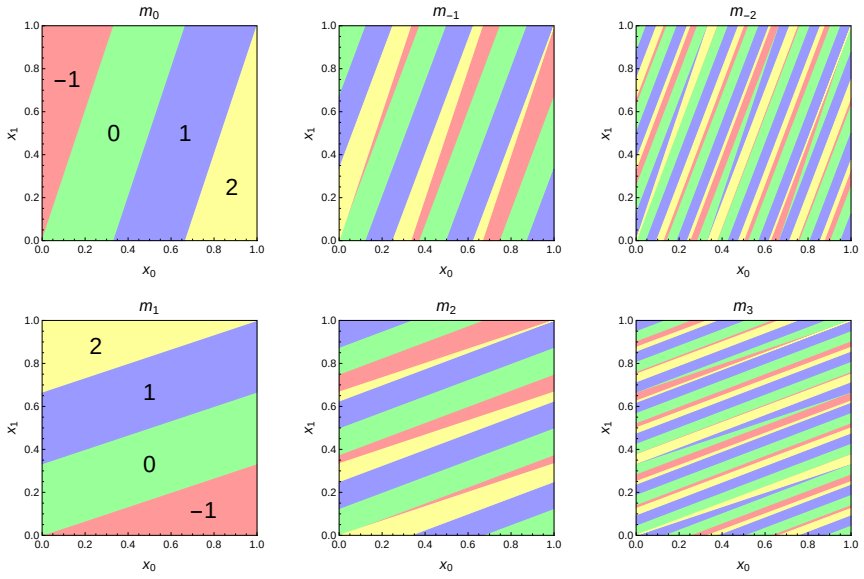

Figure 3.7: (Color online) $\ell = 1$ state spaces on (x_0, x_1) state space with respect to symbols m_t, $t = 0, -1, -2, 1, 2, 3$ for $s = 3$. In each block values of $m_t = -1, 0, 1, 2$ are shaded with light red, green, blue, and yellow, respectively, and each color has the same total area ($1/6$ for $m_t = -1, 2$, $1/3$ for $m_t = 0, 1$) in all blocks. All boundary lines are straight lines with rational slopes, while the slopes tend to irrational values set by stable/unstable directions of the cat map exponentially fast in the limit $t \to \pm\infty$.

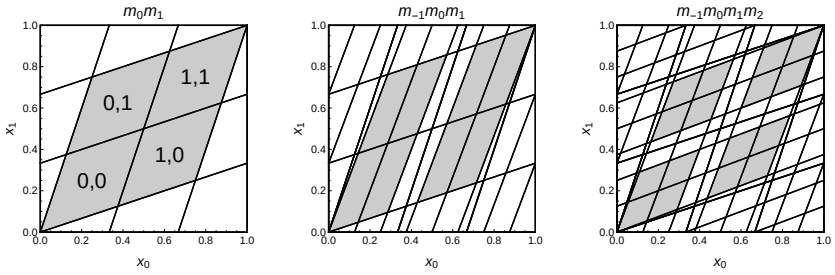

Figure 3.8: $\ell = 2, 3, 4$ state spaces on (x_0, x_1) state space for $s = 3$, using blocks m_0m_1, $m_{-1}m_0m_1$, and $m_{-1}m_0m_1m_2$ from the $\ell = 1$ diagrams. Shaded diamonds or rectangles correspond to sequences of all interior symbols $(0, 1)^{\otimes\ell}$, having a total area of $4 \times 1/8, 8 \times 1/21, 16 \times 1/55$ respectively from left to right.

fore means that at coordinate (x_{t+1}, Fx_{t+2}) the point has symbol m_t, which in turn implies that when interpreted back to (x_0, x_1) state space, a point is associated with symbol m_{-1}. As a result, we can generate all length-1 state spaces corresponding to symbols m_t, $t = 0, \pm1, \pm2, \cdots$ on the (x_0, x_1) state space simply by applying the forward map (1.85) or its inverse. We plot such length-1 diagrams in figure **??** for symbols m_0, m_{-1}, m_{-2} (top), and m_1, m_2, m_3 (bottom), and call them different blocks. Note that any of the blocks can be used to recover the 1-symbol measure $f_1(m)$ by calculating the total of respective region areas, while with blocks $m_0 = \lfloor sx_0 - x_1 \rfloor$ and $m_1 = \lfloor sx_1 - x_0 \rfloor$ the computations are the easiest, which have symbol boundaries of slopes s and $1/s$ respectively.

The fact that $\mu(m \in \mathcal{A}_0)$ are all equal and twice of $\mu(m \in \mathcal{A}_1)$ is also obvious from the m_0, m_1 blocks of length-1 state spaces.

A length-ℓ state space is then the superposition of any ℓ consecutive blocks of length-1 diagrams, while a choice that is symmetric about block m_0 or m_0 and m_1 will make the amount of calculations minimal. We have evaluated $\mu(m)$ up to $\ell = 12$ from both (**??**) and symbolic diagrams for $s = 3, 4, 5$, and they are consistent. In figure **??** we plot the symbolic diagrams for 2, 3, and 4 consecutive symbols using blocks $m_{0,1}$, $m_{-1,0,1}$, and $m_{-1,0,1,2}$ of figure **??**. Sequences of all interior symbols correspond to congruent parallelogram regions whose opposite sides are exactly parallel, and for even ℓ the regions are diamonds whose sides are of equal length. Sequences of symbols from both $\mathcal{A}_0$ and $\mathcal{A}_1$ are not all admissible, which is the topic of next section. Here we note that the corresponding regions of such sequences have general polygon shapes and are not parallelograms, no matter which consecutive set of blocks we use.

All boundary lines are straight lines with rational slopes, while the slopes tend to irrational values set by stable/unstable directions of the cat map

exponentially fast in the limit $t \to \pm\infty$.

From (**??**) the measure $\mu(b)$ for a block $b = m_1 m_2 \cdots m_\ell$ is proportional to the area of the polygon defined by inequalities (**??**).

The full list of measures $\mu(m_1 m_2 \cdots m_\ell)$ has a tensor structure of tensor rank ℓ with each index running over $\mathcal{A}$ and can be interpreted as a joint probability function. "

Boris results.tex text: " whose lower left corner is the (n, t) lattice site

$$\mathcal{R}_{n,t} = \{(n+i, t+j) | i = 0, \ldots, \ell_1 - 1, j = 0, \ldots, \ell_2 - 2\}\,,$$

It is straightforward to see that when M is such that all symbols m_z belong to $\mathcal{A}_0 = \{0, \ldots, s-4\}$ then M is always admissible. By positivity of Green's function (see appendix **??**) it follows immediately that $0 < x_z$ while the condition $\sum_{z' \in \mathbb{Z}} \mathsf{g}_{zz'} = s - 2$ implies that $x_z \leq 1$.
"

Predrag text, recycle: " Here the piecewise linearity of the spatiotemporal cat map enables us to go far analytically. Essentially, as the cat map stretching is uniform, distinct admissible symbol blocks count all blocks of a given shape (they all have the same stability, and thus the same dynamical weight), and that can be accomplished by linear, Green's function methods. "

Predrag removed Boris poetry: " The alphabet separation into interior and external parts nicely illustrates the transition of the model from the correlated regime to the uncorrelated Bernoulli process as parameter s in (5.29) tends to ∞. Indeed, the number of external symbols in $\mathcal{A}_1$ is fixed within a given differential operator $\Box$ structure, while the number of interior symbols in $\mathcal{A}_0$ grows linearly with the parameter s controlling the strength of chaos in a single map. For single cat map this transition can be achieved by merely increasing the time step of time evolution. Increasing the time step from 1 to 2 leaves the form of equation (1.90) intact, but renormalizes the constant $s \to s^2 - 1$. This reflects the fact that ϕ^2 is more "chaotic" than ϕ. With an increase of k the map ϕ^k resembles more and more uncorrelated Bernoulli process. Similar transition can be observed in the coupled $\mathbb{Z}$ map lattices, with a caveat that switch from Φ to Φ^k renormalizes not only the constant s, but $\Box$ itself. The resulting equation of motion will contain an elliptic operator $\Box^{(k)}$ of higher order. Still, it is straightforward to see that the number of external symbols is controlled by the order of the operator $\Box^{(k)}$ which grows linearly with k. On the other hand, the number of interior symbols grows in the same way as the constant s i.e., exponentially. "

Replaced N (for N "particles") by L (for spatial extent) throughout

2016-11-20 Boris The spatiotemporal symbols follow from the Newtonian equa-

tions in d spatiotemporal dimensions

$$\begin{aligned} m_{n,j} &= (q_{n,j+1} - 2q_{n,j} + q_{n,j-1}) + (q_{n+1,j} - 2q_{n,j} + q_{n-1,j}) - (s-4)q_{n,j} \\ m &= [\Box + 2d1 - s1]\, q\,. \end{aligned} \tag{3.69}$$

2017-01-03 Predrag I changed the sign of $m_{n,t}$ in (**??**), as in (5.29), do all cats approve?

2017-07-31 Boris Changed it back. Our present convention is the opposite one!

2017-02-16 Predrag To me, the Green's functions look strictly positive. Must harmonize definitions (**??**), (**??**), (3.38), (5.29) and (1.90), originating in Boris' flip-flop $m_t \to -m_t$

Is there a reference to Green's functions in terms of Chebyshevs?

2017-08-02 Boris Yes, and it is OK with our present convention - Green's functions must be positive.

2017-07-31 Boris "As every Anosov automorphism is topologically conjugate to a linear cat map ..." Is it really true ?

2017-08-11 Predrag That's what I read in some of the articles cited. But no need to say it here, so now this is removed from our article.

2016-11-13 Predrag to all cats - where we write (1.90), Percival and Vivaldi [95] write their Eq. (3.6) $(\Box + 2 - s)x_t = -b_t$ so their "stabilising impulses" b_t have the opposite sign to our "winding numbers" m_t (defined on $x \in [0,1)$).
To all cats: keep checking that after your flip of signs of m_t's Eqs. (5.29), (1.90), (**??**) and (3.69) are consistent.

2017-07-31 Boris Changed time ago. They should have the same sign as Percival and Vivaldi i.e., our m are positive!

2017-08-05 Predrag dropped this: " We illustrate this by first reviewing the $d = 1$ case (introduced in ref. [95]), but the focus of the paper is the $d = 2$ case (introduced in ref. [53]). "

2016-12-15 Predrag I worry a bit as whether it make sense. It works for a single letter, $\mathcal{R} = [1\times 1]$. Have to argue that for larger blocks $\mathcal{N}(\mathsf{M}_{\mathcal{R}}|\mathsf{M}_{[L\times T]})$ does not grow exponentially or as a power of LT? Perhaps obvious... Anyway, $\mathcal{N}$ is never mentioned again in the paper.

2017-07-29 Boris Looks like a misunderstanding here. I have tried to make the text more clear. We should distinguish between frequencies in (5.29) and measures $\mu(\mathsf{M}_{\mathcal{R}})$, at least on the level of definitions. They coincide for systems with unique ergodic measure. For me the normalization looks correct. Note that LT is just the total number of patterns within $\mathsf{M}_{[L\times T]}$ (minus boundary "effects"). $\mathcal{N}$ is never mentioned but we use it together with (**??**) to build histograms on fig. 5.

2017-08-11 Predrag I now get it. LT is the area of $\mathcal{R}$. The total number of blocks grows exponentially with the size of $\mathcal{R}$ and is bounded from above by $(LT)^{|\mathcal{A}|}$. You are saying that the number of times a *single* admissible block $\mathsf{M}_\mathcal{R}$ shows up over a region $[L\times T]$ grows linearly with the area LT, and so does the sum over frequencies of all distinct admissible blocks $\mathsf{M}'_\mathcal{R}$? These "frequencies" are *relative*, in the sense that correct normalization is not (**??**), but

$$\mu(\mathsf{M}_\mathcal{R}) = \frac{f(\mathsf{M}_\mathcal{R})}{\sum_{\mathsf{M}'_\mathcal{R}} f(\mathsf{M}'_\mathcal{R})}\,. \tag{3.70}$$

2017-08-05 Predrag Cylinder sets (**??**) are subtle: if we were counting only *admissible* X, the cylinder set would be much smaller. But we almost never know all inadmissible states.

2016-11-07 Predrag There is also a large literature on multi-dimensional shifts [9–12, 23, 26, 27, 41, 54, 63, 64, 86, 87, 104, 113] that does not seem to directly relevant to the 2-dimensional spatiotemporal symbolic dynamics studied here?

2017-08-02 Boris I have checked the consistency of the symbol definitions ($m \to -m$ issue). Double check might be needed in captions, but otherwise OK. Rule-of-thumb - internal symbols are non-negative, Green's functions are positive.

2017-07-31 Boris Li subsection *Blocks of length ℓ*, was siminos/cats/catGenerL.tex 2017-02-17, mostly contained repetitions of the previous stuff. Did not think we needed it. Few usable things could be brought to other places. Agree?

2017-08-23 Predrag Done.

2017-08-05 Boris We probably do not need to write again explicitely here the (5.29). Not sure about the above disassembling of map: $[\Box + 2d\,1]$ and $-s1$ is the on-site cat map dynamics. Sounds too mysterious.

2017-08-26 Predrag Removed: " The term $\Box + 2d\,1$ is the standard statistical mechanics diffusive inverse propagator that counts paths on a d-dimensional lattice [115], and $-s1$ is the on-site cat map dynamics (for the Hamiltonian formulation, see appendix **??**). 2CB

2017-08-05 Boris Something unclear here (at least for me). "The iteration of a map $g(x_t)$ generates a group of *time translations*". Why translations? g is a (time) map acting on all sites of lattice independently (no interaction). Note: I think the models in [98] and [25] are of the same type. Both can be thought of as products of two maps: " Interactions" · "Single particle propagations" (i.e., product of g's)
2017-09-04 Predrag: You are right, I have rewritten that text now.

2016-11-07 Predrag dropped " this is another path to a deeper understanding of foundations of statistical mechanics; ordered phases, chaotic phases, and the phase transitions that separate them. "

2017-08-28 Predrag For the Dirichlet (as opposed to periodic) boundary condition, which breaks the translational symmetry, we take the very unphysical b.c. $x_z = 0$ for $z \in \mathcal{R}$. Finite windows into turbulence that we describe by our symbol blocks never have such edges. Methinks...

2017-09-12 Boris This equation

$$\begin{aligned} x_{n,t+1} &= p_{n,t} + (s-3)x_{n,t} - (x_{n+1,t} - 2x_{n,t} + x_{n-1,t}) - m^x_{n,t+1} \\ p_{n,t+1} &= p_{n,t} + (s-4)x_{n,t} - (x_{n+1,t} - 2x_{n,t} + x_{n-1,t}) - m^p_{n,t+1} \end{aligned} \tag{3.71}$$

seems wrong. We use (**??**).

[7]

2017-09-04 Predrag "integer $s > 4$" is not the correct condition, for $d = 2$ $s = 4$ is already hyperbolic. For $d = 2$ $s = 4$ is presumably already hyperbolic. To add to the confusion, in his report Adrien computes for $s = 3$, the case with no interior alphabet symbols. So $s > 2$ is the correct hyperbolicity condition for all d? Give the correct condition on s, explain it.

2017-09-12 Boris Here are the answers to this and co. questions over the paper.

1. The system is uniformly (fully) hyperbolic for $s > 2d$. This means all eigenvalues of linearized map (see (**??**) for $d = 2$) are either $|\Lambda| < 1$ (stable subspaces) or $|\Lambda| > 1$ (unstable subspaces).
2. For $s = 2d$ the system is partially hyperbolic. This means everything as above except two Lyapunovs for which $\Lambda = 1$ (neutral subspaces).
3. For $|s| < 2d$ system is non-hyperbolic. Apparently for everything in this paper 1 & 2 is OK. But
4. drastically changes everything (suspect a phase transition in physics jargon i.e., non-unique SRB measure). So whatever we consider in the paper should be for $s \geq 2d$.

2017-09-26 Boris Dropped this: " with the corresponding probability of occurrence of a fixed symbol block $\mathsf{M}_\mathcal{R}$ given by

$$\mu(\mathsf{M}_\mathcal{R}|\mathsf{M}_{[L\times T]}) = \frac{f(\mathsf{M}_\mathcal{R}|\mathsf{M}_{[L\times T]})}{\sum_{\mathsf{M}'_\mathcal{R}} f(\mathsf{M}'_\mathcal{R}|\mathsf{M}_{[L\times T]})}\,, \qquad \sum_{\mathsf{M}_\mathcal{R}} \mu(\mathsf{M}_\mathcal{R}|\mathsf{M}_{[L\times T]}) = 1\,,$$

where the sum goes over all distinct admissible blocks $\mathsf{M}'_\mathcal{R}$."

[7] Boris 2017-09-14: Recall that (the Dirichlet) $\mathsf{g}_{zz''}$ is a function of both z and z'' and not just of the distance between them $|z - z''|$.

The point is that

$$\sum_{\mathsf{M}_{\mathcal{R}}} \mathcal{N}(\mathsf{M}_{\mathcal{R}}|\mathsf{M}_{[L\times T]}) = LT - \text{ "Terms linear in L and T".}$$

So no need in an artificial normalization - normalization in (**??**) would follow anyhow. Also I prefer not to use μ at this point, but rather leave it till (**??**). There it looks OK, since the explanation on μ follows immediately after.

2017-09-14 Boris A comment on $s = 2d$ case (do not know how much of it we need for the paper). Our results in this paper require in principle $s > 2d$ (all Lyapunovs are positive). However certain things still work (by whatever reason) for $s = 2d$ as two figs in sect. **??** show. In this case the total momentum $\sum_{n=1}^{L} p_{n,t}$ is preserved. This can be seen from the invariance of (5.29) under translation $x_{n,t} \to x_{n,t} + \alpha$. So the system is not ergodic and linear encoding is not one to one (different trajectories might have the same symbolic representation). However, it is (probably) ergodic on the shell $\sum_{n=1}^{L} p_{n,t} = const$. This is probably the reason why our formulas for frequencies of $\mathsf{M}_{\mathcal{R}}$ still work.

2017-09-14 Boris Replaced this eq.

$$\mathsf{M} \cup \partial\mathcal{R} = \begin{bmatrix} & x_{12} & \\ x_{01} & m_{11} & x_{21} \\ & x_{10} & \end{bmatrix} = \begin{bmatrix} & x_2 & \\ x_1 & m_{11} & x_3 \\ & x_4 & \end{bmatrix} \tag{3.72}$$

by the first plot in figure **??**.

2017-12-01 Predrag removed "X, being a solution, is by definition an admissible spatiotemporal block." from subsection*Statement of the problem.

2016-11-15, 2017-08-28 Predrag A side issue: When I look at the intersection of the diagonal with the partition strips in by inspecting figure **??**, I find that the Fibonacci numbers 1,2,3,5, ... give the numbers of periodic points, in agreement with the Adler–Weiss Markov partition. So the linear code is not a generating partition, but periodic orbits do the right thing anyway.

2018-04-05 to Adrien Predrag I think figure **??** is really hard to explain to a reader; why these axes, how did all points get mapped into the same unit square, why there are huge empty swaths - all stuff that distracts from the main point which is that x_z's within the center of the shared symbol block are exponentially close.

I think we can simplify this greatly, using the fact that the damped Poisson equation (**??**) is linear, so one can subtract patterns in order to visualize their distance.

In order to have a 2-dimensional visualisation for each block, color the symbol M_j $[\ell_1 \times \ell_2]$ block with discrete color alphabet $\mathcal{A}_0$, as in figure **??**,

and the corresponding state X_j $[\ell_1 \times \ell_2]$ block with colors chosen from a continuum color strip.

As this is a linear problem, you can also represent closeness of two $[\ell_1 \times \ell_2]$ blocks by using this coloring scheme for $\mathsf{M}_2 - \mathsf{M}_1$ and $\mathsf{X}_2 - \mathsf{X}_1$.

For pairs of distinct 2-tori which share the same region of m_z's, or a single 2-torus in which the same region of m_z's appears twice, the states x_z in the center of the region should be exponentially close, in order to demonstrate that they shadow each other.

So, replace figure **??** by (a) $\mathsf{M}_2 - \mathsf{M}_1$ from figure **??** (it will be all the same color in the shared region), and (b) plot $\mathsf{X}_2 - \mathsf{X}_1$. Mark the lattice point z with the minimal value of $|x_z^{(2)} - x_z^{(1)}|$ on this graph, and in the text state the minimal value of $|x_z^{(2)} - x_z^{(1)}|$. You can also state the mean Euclidean (or L2) distance between the two invariant 2-tori:

$$d_{\mathsf{X}_2-\mathsf{X}_1} = \left(\frac{1}{LT} \sum_z (x_z^{(2)} - x_z^{(1)})^2 \right)^{1/2} , \tag{3.73}$$

or distance averaged over the lattice points restricted a region $\mathcal{R}$.

Note to Predrag - send this paper to Vladimir Rosenhaus vladr@kitp.ucsb.edu

References

[1] R. L. Adler and B. Weiss, "Entropy, a complete metric invariant for automorphisms of the torus", Proc. Natl. Acad. Sci. USA **57**, 1573–1576 (1967).

[2] K. Aoki, Symmetry, chaos and temperature in the one-dimensional lattice ϕ^4 theory, 2018.

[3] K. Aoki and D. Kusnezov, "Bulk properties of anharmonic chains in strong thermal gradients: non-equilibrium ϕ^4 theory", Phys. Lett. A **265**, 250–256 (2000).

[4] K. Aoki and D. Kusnezov, "Non-equilibrium steady states and transport in the classical lattice ϕ^4 theory", Phys. Lett. B **477**, 348–354 (2000).

[5] K. Aoki and D. Kusnezov, "Nonequilibrium statistical mechanics of classical lattice ϕ^4 field theory", Ann. Phys. **295**, 50–80 (2002).

[6] K. Aoki and D. Kusnezov, "Violations of local equilibrium and linear response in classical lattice systems", Phys. Lett. A **309**, 377–381 (2003).

[7] I. S. Aranson, A. V. Gaponov-Grekhov, M. I. Rabinovich, and I. M. Starobinets, "Strange attractors and the spatial development of turbulence in flow systems", Sov. Phys. JETP **63**, 1000 (1986).

[8] J. H. Asad, "Differential equation approach for one- and two-dimensional lattice green's function", Mod. Phys. Lett. B **21**, 139–154 (2007).

[9] J.-C. Ban, W.-G. Hu, S.-S. Lin, and Y.-H. Lin, *Zeta functions for two-dimensional shifts of finite type*, Vol. 221, Memoirs Amer. Math. Soc. (Amer. Math. Soc., Providence RI, 2013).

[10] J.-C. Ban, W.-G. Hu, S.-S. Lin, and Y.-H. Lin, Verification of mixing properties in two-dimensional shifts of finite type, 2015.

[11] J.-C. Ban and S.-S. Lin, "Patterns generation and transition matrices in multi-dimensional lattice models", Discrete Continuous Dyn. Syst. Ser. A **13**, 637–658 (2005).

[12] J.-C. Ban, S.-S. Lin, and Y.-H. Lin, "Patterns generation and spatial entropy in two-dimensional lattice models", Asian J. Math. **11**, 497–534 (2007).

[13] M. Baranger, K. T. R. Davies, and J. H. Mahoney, "The calculation of periodic trajectories", Ann. Phys. **186**, 95–110 (1988).

[14] E. Behrends, "The ghosts of the cat", Ergod. Theor. Dynam. Syst. **18**, 321–330 (1998).

[15] E. Behrends and B. Fielder, "Periods of discretized linear Anosov maps", Ergod. Theor. Dynam. Syst. **18**, 331–341 (1998).

[16] H. S. Bhat and B. Osting, "Diffraction on the two-dimensional square lattice", SIAM J. Appl. Math. **70**, 1389–1406 (2010).

[17] N. Bird and F. Vivaldi, "Periodic orbits of the sawtooth maps", Physica D **30**, 164–176 (1988).

[18] M. . Blank, *Discreteness and Continuity in Problems of Chaotic Dynamics* (Amer. Math. Soc., Providence RI, 1997).

[19] M. Blank and G. Keller, "Random perturbations of chaotic dynamical systems: stability of the spectrum", Nonlinearity **11**, 1351–1364 (1998).

[20] F. Bonetto, A. Kupiainen, and J. L. Lebowitz, "Absolute continuity of projected SRB measures of coupled Arnold cat map lattices", Ergod. Theor. Dynam. Syst. **25**, 59–88 (2005).

[21] H. Bosetti, H. A. Posch, C. Dellago, and W. G. Hoover, "Time-reversal symmetry and covariant Lyapunov vectors for simple particle models in and out of thermal equilibrium", Phys. Rev. E **82**, 1–10 (2010).

[22] M. S. Bourzutschky and M. C. Cross, "Coupled map models for chaos in extended systems", Chaos **2**, 173–181 (1992).

[23] M. Boyle, R. Pavlov, and M. Schraudner, "Multidimensional sofic shifts without separation and their factors", Trans. Amer. Math. Soc. **362**, 4617–4653 (2010).

[24] N. B. Budanur and P. Cvitanović, "Unstable manifolds of relative periodic orbits in the symmetry-reduced state space of the Kuramoto-Sivashinsky system", J. Stat. Phys. **167**, 636–655 (2015).

[25] L. A. Bunimovich and Y. G. Sinai, "Spacetime chaos in coupled map lattices", Nonlinearity **1**, 491 (1988).

[26] S.-N. Chow, J. Mallet-Paret, and W. Shen, "Traveling waves in lattice dynamical systems", J. Diff. Equ. **149**, 248–291 (1998).

[27] S.-N. Chow, J. Mallet-Paret, and E. S. Van Vleck, "Pattern formation and spatial chaos in spatially discrete evolution equations", Random Comput. Dynam. **4**, 109–178 (1996).

[28] F. Christiansen, P. Cvitanović, and V. Putkaradze, "Spatiotemporal chaos in terms of unstable recurrent patterns", Nonlinearity **10**, 55–70 (1997).

[29] F. Chung and S.-T. Yau, "Discrete Green's functions", J. Combin. Theory A **91**, 19–214 (2000).

[30] M. C. Cross and P. C. Hohenberg, "Pattern formation outside of equilibrium", Rev. Mod. Phys. **65**, 851–1112 (1993).

[31] J. Cserti, "Application of the lattice Green's function for calculating the resistance of an infinite network of resistors", Amer. J. Physics **68**, 896–906 (2000).

[32] L.-B. Cui, C. Chen, W. Li, and M. K. Ng, "An eigenvalue problem for even order tensors with its applications", Linear and Multilinear Algebra **64**, 602–621 (2015).

[33] P. Cvitanović, "Counting", in *Chaos: Classical and Quantum* (Niels Bohr Inst., Copenhagen, 2016).

[34] P. Cvitanović, R. Artuso, R. Mainieri, G. Tanner, and G. Vattay, *Chaos: Classical and Quantum* (Niels Bohr Inst., Copenhagen, 2017).

[35] P. Cvitanović and B. Eckhardt, "Symmetry decomposition of chaotic dynamics", Nonlinearity **6**, 277–311 (1993).

[36] F. W. Dorr, "The direct solution of the discrete Poisson equation on a rectangle", SIAM Rev. **12**, 248–263 (1970).

[37] M. S. Dresselhaus, G. Dresselhaus, and A. Jorio, *Group Theory: Application to the Physics of Condensed Matter* (Springer, New York, 2007).

[38] F. J. Dyson and H. Falk, "Period of a discrete cat mapping", Amer. Math. Monthly **99**, 603–614 (1992).

[39] E. N. Economou, *Green's Functions in Quantum Physics* (Springer, Berlin, 1979).

[40] A. L. Fetter and J. D. Walecka, *Theoretical Mechanics of Particles and Continua* (Dover, New York, 2003).

[41] S. Friedland, "On the entropy of Z^d subshifts of finite type", Linear Algebra Appl. **252**, 199–220 (1997).

[42] K. Geist and W. Lauterborn, "The nonlinear dynamics of the damped and driven Toda chain: I. Energy bifurcation diagrams", Physica D **31**, 103–116 (1988).

[43] G. Giacomelli, S. Lepri, and A. Politi, "Statistical properties of bidimensional patterns generated from delayed and extended maps", Phys. Rev. E **51**, 3939–3944 (1995).

[44] G. Giacomelli and A. Politi, "Spatio-temporal chaos and localization", Europhys. Lett. **15**, 387–392 (1991).

[45] J. F. Gibson and P. Cvitanović, Movies of plane Couette, tech. rep. (Georgia Inst. of Technology, 2015).

[46] J. F. Gibson, J. Halcrow, and P. Cvitanović, "Visualizing the geometry of state-space in plane Couette flow", J. Fluid Mech. **611**, 107–130 (2008).

[47] R. Giles and C. B. Thorn, "Lattice approach to string theory", Phys. Rev. D **16**, 366–386 (1977).

[48] J. I. Glaser, "Numerical solution of waveguide scattering problems by finite-difference Green's functions", IEEE Trans. Microwave Theory Tech. **18**, 436–443 (1970).

[49] G. H. Golub and C. F. Van Loan, *Matrix computations* (J. Hopkins Univ. Press, Baltimore, MD, 1996).

[50] B. Gutkin, L. Han, R. Jafari, A. K. Saremi, and P. Cvitanović, Linear encoding of the spatiotemporal cat map, In preparation, 2018.

[51] B. Gutkin and V. Osipov, "Clustering of periodic orbits and ensembles of truncated unitary matrices", J. Stat. Phys. **153**, 1049–1064 (2013).

[52] B. Gutkin and V. Osipov, "Clustering of periodic orbits in chaotic systems", Nonlinearity **26**, 177 (2013).

[53] B. Gutkin and V. Osipov, "Classical foundations of many-particle quantum chaos", Nonlinearity **29**, 325–356 (2016).

[54] M. Hochman and T. Meyerovitch, "A characterization of the entropies of multidimensional shifts of finite type", Ann. Math. **171**, 2011–2038 (2010).

[55] B. L. Holian, W. G. Hoover, and H. A. Posch, "Resolution of Loschmidt's paradox: the origin of irreversible behavior in reversible atomistic dynamics", Phys. Rev. Lett. **59**, 10–13 (1987).

[56] W. G. Hoover and K. Aoki, "Order and chaos in the one-dimensional ϕ^4 model : N-dependence and the Second Law of Thermodynamics", Commun. Nonlinear Sci. Numer. Simul. **49**, 192–201 (2017).

[57] W. G. Hoover, H. A. Posch, K. Aoki, and D. Kusnezov, "Remarks on non-Hamiltonian statistical mechanics: Lyapunov exponents and phase-space dimensionality loss", Europhys. Lett. **60**, 337 (2002).

[58] T. Horiguchi, "Lattice Green's function for the simple cubic lattice", J. Phys. Soc. Jpn. **30**, 1261–1272 (1971).

[59] T. Horiguchi and T. Morita, "Note on the lattice Green's function for the simple cubic lattice", J. Phys. C **8**, L232 (1975).

[60] B. Hu, B. Li, and H. Zhao, "Heat conduction in one-dimensional nonintegrable systems", Phys. Rev. E **61**, 3828–3831 (2000).

[61] G. Y. Hu and R. F. O'Connell, "Analytical inversion of symmetric tridiagonal matrices", J. Phys. A **29**, 1511 (1996).

[62] G. Y. Hu, J. Y. Ryu, and R. F. O'Connell, "Analytical solution of the generalized discrete Poisson equation", J. Phys. A **31**, 9279 (1998).

[63] W.-G. Hu and S.-S. Lin, "Nonemptiness problems of plane square tiling with two colors", Proc. Amer. Math. Soc. **139**, 1045–1059 (2011).

[64] W.-G. Hu and S.-S. Lin, "On spatial entropy of multi-dimensional symbolic dynamical systems", Discrete Continuous Dyn. Syst. Ser. A **36**, 3705–3717 (2016).

[65] S. Isola, "ζ-functions and distribution of periodic orbits of toral automorphisms", Europhys. Lett. **11**, 517–522 (1990).

[66] T. Kamizawa, T. Hara, and M. Ohya, "On relations among the entropic chaos degree, the Kolmogorov-Sinai entropy and the Lyapunov exponent", J. Math. Phys. **55** (2014) 10.1063/1.4868217.

[67] K. Kaneko, "Transition from torus to chaos accompanied by frequency lockings with symmetry breaking: In connection with the coupled-logistic map", Prog. Theor. Phys. **69**, 1427–1442 (1983).

[68] K. Kaneko, "Period-doubling of kink-antikink patterns, quasiperiodicity in antiferro-like structures and spatial intermittency in coupled logistic lattice: Towards a prelude of a "field theory of chaos"", Prog. Theor. Phys. **72**, 480–486 (1984).

[69] H. Kantz and P. Grassberger, "Chaos in low-dimensional Hamiltonian maps", Phys. Let. A **123**, 437–443 (1987).

[70] S. Katsura and S. Inawashiro, "Lattice Green's functions for the rectangular and the square lattices at arbitrary points", J. Math. Phys. **12**, 1622–1630 (1971).

[71] S. Katsura, S. Inawashiro, and Y. Abe, "Lattice Green's function for the simple cubic lattice in terms of a Mellin-Barnes type integral", J. Math. Phys. **12**, 895–899 (1971).

[72] S. Katsura, T. Morita, S. Inawashiro, T. Horiguchi, and Y. Abe, "Lattice Green's function. Introduction", J. Math. Phys. **12**, 892–895 (1971).

[73] J. P. Keating, "Asymptotic properties of the periodic orbits of the cat maps", Nonlinearity **4**, 277 (1991).

[74] J. P. Keating and F. Mezzadri, "Pseudo-symmetries of Anosov maps and spectral statistics", Nonlinearity **13**, 747–775 (2000).

[75] V. Khoromskaia and B. N. Khoromskij, "Block circulant and Toeplitz structures in the linearized Hartree-Fock equation on finite lattices: Tensor approach", Comput. Methods Appl. Math. **17**, 43–455 (2017).

[76] A. N. Kolmogorov, "A new metric invariant of transient dynamical systems and automorphisms in Lebesgue spaces", Dokl. Akad. Nauk SSSR **119** (1958).

[77] P. Kurlberg and Z. Rudnick, "Hecke theory and equidistribution for the quantization of linear maps of the torus", Duke Math. J. **103**, 47–77 (2000).

[78] J. S. W. Lamb and J. A. G. Roberts, "Time reversal symmetry in dynamical systems: A survey", Physica D **112**, 1–39 (1998).

[79] J. S. W. Lamb and C. Wulff, "Reversible relative periodic orbits", J. Diff. Eqn. **178**, 60–100 (2002).

[80] L. D. Landau and E. M. Lifshitz, *Theory of Elasticity*, 3rd ed. (Pergamon Press, Oxford, 1970).

[81] S. Lepri, A. Politi, and A. Torcini, "Chronotopic Lyapunov analysis. I. A detailed characterization of 1D systems", J. Stat. Phys. **82**, 1429–1452 (1996).

[82] S. Lepri, A. Politi, and A. Torcini, "Chronotopic Lyapunov analysis. II. Towards a unified approach", J. Stat. Phys. **88**, 31–45 (1997).

[83] S. Lepri, A. Politi, and A. Torcini, "Entropy potential and Lyapunov exponents", Chaos **7**, 701–709 (1997).

[84] L.-H. Lim, Singular values and eigenvalues of tensors: A variational approach, in 1st IEEE International Workshop on Computational Advances in Multi-Sensor Adaptive Processing (2005).

[85] R. de la Llave, Variational methods for quasiperiodic solutions of partial differential equations, in Hamiltonian Systems and Celestial Mechanics (HAMSYS–98), edited by J. Delgado, E. A. Lacomba, E. Pérez-Chavela, and J. Llibre (2000).

[86] J. Mallet-Paret and S. N. Chow, "Pattern formation and spatial chaos in lattice dynamical systems. I", IEEE Trans. Circuits Systems I Fund. Theory Appl. **42**, 746–751 (1995).

[87] J. Mallet-Paret and S. N. Chow, "Pattern formation and spatial chaos in lattice dynamical systems. II", IEEE Trans. Circuits Systems I Fund. Theory Appl. **42**, 752–756 (1995).

[88] P. A. Martin, "Discrete scattering theory: Green's function for a square lattice", Wave Motion **43**, 619–629 (2006).

[89] F. Mezzadri, "On the multiplicativity of quantum cat maps", Nonlinearity **15**, 905–922 (2002).

[90] B. Moran, W. G. Hoover, and S. Bestiale, "Diffusion in a periodic Lorentz gas", J. Stat. Phys. **48**, 709–726 (1987).

[91] T. Morita, "Useful procedure for computing the lattice Green's function - square, tetragonal, and bcc lattices", J. Math. Phys. **12**, 1744–1747 (1971).

[92] T. Morita and T. Horiguchi, "Calculation of the lattice Green's function for the bcc, fcc, and rectangular lattices", J. Math. Phys. **12**, 986–992 (1971).

[93] S. Müller, S. Heusler, P. Braun, F. Haake, and A. Altland, "Semiclassical foundation of universality in quantum chaos", Phys. Rev. Lett. **93**, 014103 (2004).

[94] G. Papathanasiou and C. B. Thorn, "Worldsheet propagator on the light-cone worldsheet lattice", Phys. Rev. D **87**, 066005 (2013).

[95] I. Percival and F. Vivaldi, "A linear code for the sawtooth and cat maps", Physica D **27**, 373–386 (1987).

[96] I. Percival and F. Vivaldi, "Arithmetical properties of strongly chaotic motions", Physica D **25**, 105–130 (1987).

[97] Y. B. Pesin, "Characteristic Lyapunov exponents and smooth ergodic theory", Russian Math. Surveys **32**, 55–114 (1977).

[98] Y. B. Pesin and Y. G. Sinai, "Space-time chaos in the system of weakly interacting hyperbolic systems", J. Geom. Phys. **5**, 483–492 (1988).

[99] S. D. Pethel, N. J. Corron, and E. Bollt, "Symbolic dynamics of coupled map lattices", Phys. Rev. Lett. **96**, 034105 (2006).

[100] S. D. Pethel, N. J. Corron, and E. Bollt, "Deconstructing spatiotemporal chaos using local symbolic dynamics", Phys. Rev. Lett. **99**, 214101 (2007).

[101] A. Pikovsky and A. Politi, "Dynamic localization of Lyapunov vectors in spacetime chaos", Nonlinearity **11**, 1049–1062 (1998).

[102] A. Politi and A. Torcini, "Periodic orbits in coupled Hénon maps: Lyapunov and multifractal analysis", Chaos **2**, 293–300 (1992).

[103] A. Politi, A. Torcini, and S. Lepri, "Lyapunov exponents from node-counting arguments", J. Phys. IV **8**, 263 (1998).

[104] A. N. Quas and P. B. Trow, "Subshifts of multi-dimensional shifts of finite type", Ergod. Theor. Dynam. Syst. **20**, 859–874 (2000).

[105] M. Rezghi and L. Eldén, "Diagonalization of tensors with circulant structure", Linear Algebra Appl. **435**, 422–447 (2011).

[106] D. Ruelle, "An inequality for the entropy of differentiable maps", Bol. Soc. Bras. Mat. **9**, 83–87 (1978).

[107] D. Ruelle, "Nonequilibrium statistical mechanics and entropy production in a classical infinite system of rotators", Commun. Math. Phys. **270**, 233–265 (2007).

[108] D. Ruelle and Y. G. Sinai, "From dynamical systems to statistical mechanics and back", Physica A **140**, 1–8 (1986).

[109] K. Serkh and V. Rokhlin, "On the solution of the Helmholtz equation on regions with corners", Proc. Natl. Acad. Sci. USA **113**, 9171–9176 (2016).

[110] M. Sieber and K. Richter, "Correlations between periodic orbits and their rôle in spectral statistics", Phys. Scr. **2001**, 128 (2001).

[111] Y. G. Sinai, "Some mathematical problems in the theory of quantum chaos", Physica A **163**, 197–204 (1990).

[112] I. G. Szendro, D. Pazó, M. A. Rodríguez, and J. M. López, "Spatiotemporal structure of Lyapunov vectors in chaotic coupled-map lattices", Phys. Rev. E **76**, 025202 (2007).

[113] T. Ward, "Automorphisms of Z^d-subshifts of finite type", Indag. Math. **5**, 495–504 (1994).

[114] E. P. Wigner, *Group Theory and Its Application to the Quantum Mechanics of Atomic Spectra* (Academic, New York, 1959).

[115] A. Wirzba and P. Cvitanović, "Appendix: Discrete symmetries of dynamics", in *Chaos: Classical and Quantum* (Niels Bohr Inst., Copenhagen, 2016).

[116] Z.-J. Xie, X.-Q. Jin, and Y.-M. Wei, "A fast algorithm for solving circulant tensor systems", Linear and Multilinear Algebra **65**, 1894–1904 (2016).

Chapter 4

Ising model in 2D

Exercise 14.1 Time reversibility. Hamiltonian flows are time reversible. Does that mean that their transition graphs are symmetric in all node $\to$ node links, their transition matrices are adjacency matrices, symmetric and diagonalizable, and that they have only real eigenvalues?

— An open exercise from ChaosBook.org

2CB

2016-02-19 Predrag A wild idea, to keep in mind, if we get to the point where QFT is within reach. 'Fundamental domain' appears in an interesting stat mech context in Wipf *et al.* [70, 71] *Generalized Potts-models and their relevance for gauge theories*. They study the 3-state Potts model, a natural extension of the Ising model with 3 vectors at each site, whose global symmetries are point group C_3, and the 1d lattice of discrete translations. The domain of the traced Polyakov loop variable (?) for SU(3) is a triangle, with a C_3 fundamental domain. Then they compute leading terms in the strong coupling limit using characters χ_{pq} for the SU(3) representation (p, q). These characters transform under C_3, so they restrict calculations to the fundamental domain inside the above triangle. Or perhaps D_3, could not tell in my first, very superficial reading. These articles were immediately followed up by a bunch of other articles - there are too many quantum field theorists out there:)

In other words, Potts model could provide a bridge from Boris' cat maps to QFT on lattices.

There is also a continuation with G_2 Yang-Mills by the same authors, but that's for another, more ambitious time...

2016-06-02 Predrag From my notes on S. Isola [41] *ζ-functions and distribution of periodic orbits of toral automorphisms*, see sect. 1.6.3: [...] The topological

ζ-function for cat-map class of models is

$$1/\zeta(z) = \frac{(1-\Lambda z)(1-\Lambda^{-1}z)}{(1-z)^2} = \frac{1-sz+z^2}{(1-z)^2}\,. \tag{4.1}$$

I believe $(1-z)^2$ should be interpreted as taking care of the over-counting of the fixed point at the origin due to the 2-periodicity on the torus.

I wonder whether the fact that this is quadratic in z has something to do with the time-reversibility, and the unsigned graph's Ihara zeta functions?

2016-10-03 Predrag Not quick or easy to explain, but I have a hunch that the spatiotemporal zeta function should be something like the 2D Ising model zeta function described by Aizenman (click here). It should assign a weight for every spatiotemporal domain, described by its 2D symbolic dynamics.

I cannot, at the moment, tell the difference between Ihara and what I call the "topological" zeta function in ChaosBook.org (section 18.4; the chapter alone is here). I find Aizenman's derivation of 2D Onsager solution beautiful - will have to chew on it.

2016-10-08 Predrag qmath16 Aizenman talk notes (mostly gbberish - my fault):

It is known (?) that QM is emergent from the *classical* stat mech of Ising models. Key tools: Pfaffians. Random current representation of Ising.

Groenevald-Boel-Kasteleyn'78: describe correlations in the planar Ising model, by boundary segments, ordered cyclically. Pfaffian refers to spin-spin correlations along the boundary. There is a parity sign that makes it a non-interacting fermion model.

Aizenman et al. extend it to nonplanar modles, where planarity *emerges* at the critical point. ADTW'16 proof utilizes the *random current representation*. Starts with high temperature expansion. Partition function is a sum over loops. In a correlation, sources are connected pairwise by lines, ie, Gaussian limit. Above critical dimension - four - the theory is free (sum of products over pairs). In 2D, fermionic case, you get Pfaffian. Leads to the integrability of the model. (Read Chelkak-Cimasoni-Kassel '15.)

"Almost planar"

Order-disorder variables.

Aizenman: Two implications of planarity

1) For any planar graph, and a symmetric edge function

$$\mathcal{F}(\{K_\theta\}) = \det(1-K\mathcal{W})$$

is the *square of a multilinear function* of the parameters $\{K_\theta\}_{\theta\in\epsilon_0}$. This is proven through a reduction to an antisymmetric matrix A, and (Kasteleyn matrix '63):

$$\det(A) = \mathrm{Pf}[A]^2.$$

For planar models, done by Kac-Ward. Works for any planar graph ("amorphous graphs"), not only on a regular lattice.

2) For any planar loop of oriented non-backtracking edges $\{e_1, e_2, \cdots\}$

$$\prod_{j=1}^{n} \mathcal{W}_{e_{j+1},e_j} = (-1)^{w(\rho^*)} = (-1)^{n(\rho^*)} .$$

with $w(\rho^*)$ = winding number, and $n(\rho^*)$ = # of self crossings [Whitney's Thm].

This is then combined with the *Ihara relation*, for matrices indexed by oriented edges:

$$\det (1 - KW)_{\epsilon_0 \times \epsilon_0} = \prod_{\ell} \left[1 + (-1)^{n(\ell)} \chi_{-K}(\ell)\right]^2 .$$

the product being over unoriented loops on $\mathbb{G}$ (hence the power 2).

2016-10-05 Predrag Aizenman, Laínz Valcázar and Warzel [2] *Pfaffian correlation functions of planar dimer covers* does not seem to be what we need (no word 'zeta' in this paper). They refer to 2016 preprint of

M. Aizenman H. Duminil-Copin, V. Tassion, S. Warzel, *Fermionic correlation functions and emergent planarity in 2D Ising models*. (that paper does not seem to be available anywhere, as yet)

The structure of the solution of Kac and Ward has been explained in unpublished lectures by Feynman (Aizenman referred to Feynman's stat mech book).

Sherman [62] *Combinatorial aspects of the Ising model for ferromagnetism. I. A conjecture of Feynman on paths and graphs*

Hurst and Green [39] *New solution of the Ising problem for a rectangular lattice*

Burgoyne [14] *Remarks on the combinatorial approach to the Ising problem*

Vdovichenko [66] *A calculation of the partition function for a plane dipole lattice*. The steps: a) the sum over polygons is reduced to a sum over closed loops without intersections; b) the sum over closed loops without intersections is transformed into a sum over all loops; c) the sum over all loops is reduced to a random-walk problem and is calculated easily.

Cimasoni [19] *A generalized Kac-Ward formula*: " As a consequence of our second proof, we also obtain the following fact: the Kac–Ward and the Fisher–Kasteleyn methods for solving the Ising model are one and the same. "

Cimasoni [20] *The critical Ising model via Kac-Ward matrices*: The Kac-Ward formula [42] allows to compute the Ising partition function on any finite graph G from a determinant with quite remarkable properties. First of

all, they satisfy some generalized Kramers-Wannier duality: there is an explicit equality relating the determinants associated to a graph and to its dual graph. Also, they are proportional to the determinants of the discrete critical Laplacians on the graph G.

Fisher [27] *On the dimer solution of planar Ising models*

Kasteleyn [44] *The statistics of dimers on a lattice: I. The number of dimer arrangements on a quadratic lattice*

Kasteleyn [45] *Dimer statistics and phase transitions*

H. Au-Yang, J. H. H. Perk. Ising correlations at the critical temperature. Physics Letters A 104, 131–134 (1984).

Kager, Lis and Meester [43] *The signed loop approach to the Ising model: Foundations and critical point*

Lis [49] *A short proof of the Kac-Ward formula*:

$$\det\left(Id - \Lambda\right) = \mathbb{Z}^2 \tag{4.2}$$

The original proof of Kac and Ward [42] famously contained an error. We refer the reader to ref. [43] for a longer discussion on the history of this theorem. The main improvement here, in comparison with ref. [43], is that there is no need for expanding the generating functions into generating functions of collections of loops. The combinatorial mechanism of the Kac-Ward formula is here as transparent as the one of the loop-erased walks.

Chertkov, Chernyak and Teodorescu [16] *Belief propagation and loop series on planar graphs*, write: " We discuss a generic model of Bayesian inference with binary variables defined on edges of a planar graph. The Loop Calculus approach of Chertkov and Chernyak [15] is used to evaluate the resulting series expansion for the partition function. We show that, for planar graphs, truncating the series at single-connected loops reduces, via a map reminiscent of the Fisher transformation [26], to evaluating the partition function of the dimer-matching model on an auxiliary planar graph. Thus, the truncated series can be easily re-summed, using the Pfaffian formula of Kasteleyn [44]. This allows us to identify a big class of computationally tractable planar models reducible to a dimer model via the Belief Propagation (gauge) transformation. The Pfaffian representation can also be extended to the full Loop Series, in which case the expansion becomes a sum of Pfaffian contributions, each associated with dimer matchings on an extension to a subgraph of the original graph. Algorithmic consequences of the Pfaffian representation, as well as relations to quantum and non-planar models, are discussed. "

" As the seminal work of Onsager [55] on the two-dimensional Ising model and its combinatorial interpretation by Kac and Ward [42] have shown, the planarity constraint dramatically simplifies statistical calculations. "

Onsager [55] computed the free energy, and Yang [72] obtained a formula for the magnetization. In particular, this formula implies that the magnetization is zero at criticality. These results have been reproved in a number of papers since then. See Werner [69] for a recent proof.

Onsager's computation of the free energy is based on the study of the eigenvalues of the so-called transfer matrices. The original strategy used by Onsager is based on the fact that the transfer matrix is the product of two matrices whose commutation relations generate a finite dimensional Lie algebra. Later on, Kaufman [46] gave a simpler solution using Clifford algebra and anti-commuting spinor (free-fermion) operators.

The most famous expansions of the partition function are called the low and high temperature expansions. An expansion in terms of subgraphs of the original graph, called the random-cluster model, was found by Fortuin and Kasteleyn [28]. The strength of all these expansions is that they work for all graphs. They do not lead to an explicit computation of the partition function or the free energy, but they provide new insight and often highlight specific properties of the model.

4.1 Ihara zeta functions

Wiki

4.1.1 Clair / Clair14

Clair [21] *The Ihara zeta function of the infinite grid*

Bryan Clair is a great fan of Ihara zeta functions.

Zeta functions of infinite graphs are discussed, for example, by Bryan Clair and Shahriar Mokhtari-Sharghi [31] [22], Rostislav Grigorchuk and Andrzej Zuk [46], and Daniele Guido, Tommaso Isola, and Michel Lapidus [31]. Shahriar Mokhtari-Sharghi [22, 23] have shown that Ihara's construction can be extended to infinite graphs on which a discrete group acts isomorphically and with finite quotient. Their works seems to deal with trees, not lattices, though Clair [21] does discuss infinite square lattice, see (4.6). Grigorchuk and Zuk is about Cayley trees.

Read Guido, Isola, and Lapidus [31] *Ihara zeta functions for periodic simple graphs*.

The Ihara zeta function may be considered as a modification of the Selberg zeta function [11], and was originally written in terms of the variable s, where $z = q^{-s}$. One of main properties of the Ihara zeta function is the *determinant formula*, i.e., that its inverse is the determinant of a matrix-valued polynomial. A consequence of the determinant formula is that the Ihara zeta function meromorphically extends to the whole complex plane, and its completions satisfy a functional equation.

The main formula in all these papers gives a connection between the zeta function, originally defined as an infinite product, and the Laplacian of the graph.

Pollicott [56] explains in *Dynamical zeta functions* Sect. 3.3 what the Laplacian for a undirected graph is, relates it to the adjacency matrix in a somewhat obvious way, as we are used to on a lattice. He defines Ihara for undirected graph

1. the graph G has valency $q+1$ with $q \geq 2$ (i.e., every vertex has $q+1$ edges attached)
2. there is at most one edge between any two vertices
3. there are no edges starting and finishing at the same vertex

He outlines a proof of the determinant formula (originally due to Bass) using depends the Bowen-Lanford zeta function. 2CB

Loop: A closed path in G, up to cyclic equivalence, without backtracking.

Prime: A loop p which is not a power (a repeat) of another loop.

Back-track: A path has a back-tracking if a subsequence of the form $\cdots, x, y, x, \cdots$ appears.

The Ihara zeta function of a finite graph G

$$\zeta(z) = \prod_p \frac{1}{1 - z^{|p|}} \tag{4.3}$$

It is instructive to have a look at the octahedral graph in Clair's talk above. There is no self-crossing condition, so $\zeta(z)$ always has an infinity of prime cycles, of arbitrary length (as does any topological $\zeta(z)$).

As a power series in z, the Ihara zeta has non-negative coefficients, and thus a finite radius of convergence. However, the inverse of the Ihara zeta is a polynomial.

Ihara considered the special case of regular graphs (those all of whose vertices have the same degree; i.e., the same number of oriented edges coming out of the vertex). A graph is k-regular if every vertex has degree k.

Terras [65] defines the $m \times m$ *adjacency* matrix as,

$$A_{ij} \quad = \quad \begin{cases} k & \text{if a transition } \mathcal{M}_j \to \mathcal{M}_i \text{ is possible in } k \text{ ways} \\ 2\,\ell_j & \text{if } i = j \\ 0 & \text{otherwise}\,, \end{cases} \tag{4.4}$$

where ℓ_j is the number of loops at vertex j. She then assigns to every of the e unoriented edges a pair of oriented edges. Her graphs are finite, connected and undirected, without "backtracks" and "tails". It will usually be assumed that they contain no degree 1 vertices (called "leaves" or "hair" or "danglers").

We will also usually assume the graphs are not cycles or cycles with hair. A cycle graph is obtained by arranging the vertices in a circle and connecting each vertex to the 2 vertices next to it on the circle. We will allow our graphs to have loops and multiple edges. For any closed loop, the equivalence class is the set of all its cyclic permutations. Two loops are equivalent if they differ only by the starting vertex.

Terras: We do not consider zeta functions of infinite graphs here. Nor do we consider directed graphs. Zeta functions for such graphs are discussed, for example, by Matthew Horton [36].

There is no unique factorization into primes. The only nonprimes are powers of primes. We distinguish prime p from p^{-1} which is the loop traversed in the opposite direction. All graphs have infinity of primes, with exception of the cycle graph that has only 2 primes p, p^{-1}, traversing the vertices in the opposite directions.

Theorem [11, 40]: Consider a finite connected graph G (without degree 1 vertices) with m vertices, e unoriented (or undirected) edges, deg m_i the number of (undirected) edges going into vertex i. Let A be the adjacency matrix, Q be the $m \times m$ diagonal matrix with $Q_{ii} = \deg m_i - 1$, and $\Delta_z = I - zA + z^2 Q$. The (vertex) adjacency matrix A of G is a $m \times m$ matrix whose i,j entry is the number of directed edges from vertex i to vertex j. The matrix Q is a diagonal matrix whose j-th diagonal entry is 1 less than the degree of the j-th vertex. If there is a loop at a vertex, it contributes 2 to the degree.

$$1/\zeta(z) = (1-z^2)^{e-m} \det \Delta_z \tag{4.5}$$

(then comes Riemann Hypothesis for the spectrum of a regular graph G, and Ramanujan graphs).

Next, consider the 'grid' zeta function for G the infinite grid, i.e., a square 2D lattice. Let $\pi = \mathbb{Z} \times \mathbb{Z}$ be a translation acting on G. The zeta function is still

$$\zeta(z) = \prod_{[p]} \frac{1}{1 - z^{|p|}} \tag{4.6}$$

where $[p]$ is an equivalence class of loops under translation by π:

$$1/\zeta(z) = (1-z^4)^2 (1-z^6)^4 (1-z^8)^{26} (1-z^1 0)^{152} \cdots \tag{4.7}$$

(look at the 8-loops in Clair's talk - there seems to be an extra factor 2 in loop counting. I only see two 6-loops, not four).

On infinite graphs, the adjacency matrix becomes an $\ell^2(\mathbb{Z} \times \mathbb{Z}) \to \ell^2(\mathbb{Z} \times \mathbb{Z})$ adjacency operator. For the infinite grid,

$$\Delta_z = I - zA + z^3 \tag{4.8}$$

There is still a determinant formula for the zeta function:

$$1/\zeta_\pi(z) = (1-z^2) \det{}_\pi \Delta_z \,. \tag{4.9}$$

With $\pi = \mathbb{Z} \times \mathbb{Z}$, $\det_\pi$ is an operator determinant:

$$\det{}_\pi \Delta_z = \exp \operatorname{tr}_\pi \log \Delta_z \,, \tag{4.10}$$

where tr_π is the trace on the group von Neumann algebra $\mathcal{N}(\pi)$.

The adjacency operator on a square lattice is essentially the 2D Laplacian. Clair throws in the 2D Ising, then Kasteleyn [45] and ends up with

$$1/\zeta_\pi(z) = (1 - z^2)(1 + 3z^2) \exp \mathbf{I}(k) \,, \tag{4.11}$$

with a simple set of singularities, and $\mathbf{I}(k)$ is related to an elliptic integral of the first kind, expressed in terms of theta functions (whose squares are modular forms of weight 1).

2016-10-05 Predrag Unlike in dynamical systems, Ihara zeta functions are defined on graphs with unoriented (or undirected) edges.

Hashimoto [33] *Zeta functions of finite graphs and representations of p-adic groups*

Bass [11] *The Ihara-Selberg zeta function of a tree lattice*. It seems that Ihara zeta function walks carry signs - investigate.

In *A Window Into Zeta and Modular Physics* [47] (that should warm Li Han's heart) Audrey Terras discusses Ihara zeta function. She says: "the Ruelle zeta function of a dynamical system, will be shown to be a generalization of the Ihara zeta." Things are looking deep. "It turns out (using the Ihara determinant formula again) that the Riemann hypothesis means that the graph is Ramanujan", etc. She also discusses it in ref. [65] *Zeta Functions of Graphs: A Stroll through the Garden*.

To swoon over the multitude of zetas, read Bartholdi [10] *Zeta functions of graphs: a stroll through the garden, by Audrey Terras [65]. Book review*.

Teimoori Faal and M. Loebl [64] Bass' identity and a coin arrangements lemma

Like my topological zeta functions, Loebl's Ihara-Selberg function of G is the infinite product is over the set of the prime reduced cycles of G.

Loebland and Somberg [50] *Discrete Dirac operators, critical embeddings and Ihara-Selberg functions*

da Costa [24] *The Feynman identity for planar graphs*: " The Feynman identity (FI) of a planar graph relates the Euler polynomial of the graph to an infinite product over the equivalence classes of closed nonperiodic signed cycles in the graph. The main objectives of this paper are to compute the number of equivalence classes of nonperiodic cycles of given length and sign in a planar graph and to interpret the data encoded by the FI in the context of free Lie superalgebras. This solves in the case of planar graphs a problem first raised by Sherman and sets the FI as the denominator identity of a free Lie superalgebra generated from a graph. Other results are obtained on the zeta functions of graphs. "

Mizuno and Sato [54] *Zeta functions of digraphs* define a zeta function of a digraph and an L-function of a symmetric digraph.

Sato [60] *Bartholdi zeta functions of group coverings of digraphs*

Horton [36] *Ihara zeta functions of digraphs* considers digraphs whose adjacency matrices are directed edge matrices.

Tarfulea and R. Perlis [63] An Ihara formula for partially directed graphs: " In 2001 Mizuno and Sato showed that the Ihara zeta function of a fully directed graph has a similar expression, and in 2005, Sato [60] generalized Ihara's formula to connected, simple, partially directed graphs. (Sato proved his formula for the more-general two-variable Bartholdi zeta function.) This paper provides a new proof of Ihara's formula for the Ihara zeta function of any finite graph, not necessarily connected or simple, no matter whether it is undirected, fully directed, or partially directed. "

2017-03-08 Predrag Reading Band, Harrison and Joyner [9] *Finite pseudo orbit expansions for spectral quantities of quantum graphs* one expects to run into another rediscovery of Ihara zeta functions, as the links are not directed:

" The *quantum graphs* we consider are metric graphs equipped with a self-adjoint differential operator $\mathcal{H}$, the Hamiltonian. Here we are particularly interested in the negative Laplace operator,

$$\mathcal{H} \ : \ f(x) \mapsto -\frac{d^2 f}{dx^2} \ , \tag{4.12}$$

or the more general Schrödinger operator,

$$\mathcal{H} \ : \ f(x) \mapsto -\frac{d^2 f}{dx^2} + V(x) f(x) \ , \tag{4.13}$$

where $V(x)$ is a *potential*, which we assume to be bounded and piecewise continuous. Note that the value of a function or the second derivative of a function at a point on the bond is well-defined, thus it is not important which coordinate, x_b or $x_{\hat{b}}$ is used. This is in contrast to the first derivative which changes sign according to the direction of the chosen coordinate. "

Indeed, they go through the usual steps of defining oriented graphs and then putting pairs of oriented bonds on each link, etc. This is explored further in

Guido, Isola and Lapidus [32] *A trace on fractal graphs and the Ihara zeta function*

Ren, Aleksić, Emms, Wilson and Hancock [58] *Quantum walks, Ihara zeta functions and cospectrality in regular graphs*

Setyadi and Stor [61] *Enumeration of graphs with the same Ihara zeta function*

Higuchi, Konno, Sato and Segawa [34] *A remark on zeta functions of finite graphs via quantum walks*

4.1.2 Maillard

Another scary line of literature. Connecting Baxter to dynamical zetas functions. Maillardinians have a burst at the end of 20th century. Very easy to collect the literature, as only they cite their own articles, and nobody else cites them.

A cute cat map exercise - but I have to bike home, will continue later...

2016-11-16 Predrag Anglès d'Auriac, J. -Ch. and Boukraa, S. and Maillard [3] *Functional relations in lattice statistical mechanics, enumerative combinatorics, and discrete dynamical systems* write " ... non-linear functional relations appearing in [...] lattice statistical mechanics [...] We then consider discrete dynamical systems corresponding to birational transformations. The rational expressions for dynamical zeta functions obtained for a particular two-dimensional birational mapping, depending on two parameters [...] compatible with a chaotic dynamical system.

They obsess about the Arnol'd complexity, which counts the number of intersections between a fixed line and its nth iterate. I do not see why we should care.

I like Bedford and Diller [12] *Real and complex dynamics of a family of birational maps of the plane: The golden mean subshift* better, so follow their notation here. It's a rather impressive paper.

For reasons known to some people (symmetries of Baxter models?) they study a birational transformation and its inverse,

$$\begin{array}{rclcrcl} x_{n+1} &=& y_n \frac{x_n+a}{x_n-1} & & x_{n-1} &=& y_n+1-a \\ y_{n+1} &=& x_n+a-1 & & y_{n-1} &=& x_n \frac{y_n-aa}{y_n+1} \end{array} \quad , \qquad a \in \mathbb{R} \,. \tag{4.14}$$

The map is area-preserving in the sense that it preserves a meromorphic 2-form

$$\frac{dx \wedge dy}{y-x+1}$$

and is reversible, which means that the map is conjugate to its inverse via involution $(x, y) \to (-y, -x)$. The inverse transformation amounts to $y_n \leftrightarrow -z_n$, i.e., the time reversal symmetry, and the $x - y = 0$ line is the *time-reversal invariant line*. The topological ζ-function for (4.14) is

$$1/\zeta(z) = \frac{1-z-z^2}{1-z^2} \,. \tag{4.15}$$

It counts all periodic orbits, real and complex. Interestingly, this zeta satisfies a very elegant functional relation relating $\zeta(z)$ and $\zeta(1/z)$.

The zeta function for real roots is complicated and depends on the parameter a. 2CB

Bedford and Diller [12] construct a generating partition and the Markov diagram (they call that Graph of Filtration), including the transient nodes.

The recurrent part of this graph is just the golden mean graph, with 11 repeats forbidden. They obsess much about their "rectangles." Show that all periodic orbits are hyperbolic. Discuss pre-periodic orbits. Zeta functions are never mentioned, though topological entropy is computed.

Abarenkova*et al.* [1] *Rational dynamical zeta functions for birational transformations* is not worth reading - the material is better explained in their other papers.

If the dynamical zeta function can be interpreted as the ratio of two characteristic polynomials of two linear operators A and B, namely $\zeta(z) = \det(1 - zB) = \det(1 - zA)$, then the number of fixed points can be expressed from $\mathrm{tr}\,(A^n) - \mathrm{tr}\,(B^n)$. In this linear operators framework, the rationality of the ζ function [30, 53], and therefore the algebraicity of the exponential of the topological entropy, amounts to having a finite dimensional representation of the linear operators A and B.

Their only explicit example of a rational zeta dynamical function is the case of the Arnol'd cat map on torus $\mathbb{T}^2 = \mathbb{R}^2/\mathbb{Z}^2$,

$$A = \begin{pmatrix} 2 & 1 \\ 1 & 1 \end{pmatrix}, \qquad B = \begin{pmatrix} 1 & 0 \\ 0 & 1 \end{pmatrix} \tag{4.16}$$

The topological ζ-function [41] for Arnol'd cat map is

$$1/\zeta(z) = \frac{\det(1 - zA)}{\det(1 - zB)} = \frac{1 - 3z + z^2}{(1 - z)^2}\,. \tag{4.17}$$

Note that

$$A = \begin{pmatrix} 2 & 1 \\ 1 & 1 \end{pmatrix} = \begin{pmatrix} 1 & 1 \\ 1 & 0 \end{pmatrix}^2 \tag{4.18}$$

which leads to factorization

$$\frac{1}{\zeta(z)} = \frac{1}{\zeta'(t)\zeta'(-t)} = \frac{1 - t - t^2}{1 - t} \cdot \frac{1 + t - t^2}{1 - t} = \frac{1 - 3z + z^2}{(1 - z)^2}\,, \quad z = t^2\,. \tag{4.19}$$

This agrees with

$$\det(1 - tC)\det(1 + tC) = \det(1 - zC^2)\,. \tag{4.20}$$

This all has to do with time reversibility - we should exploit time and space reversal symmetries in this way, and - who knows - understand Ihara zeta functions better. It also reminds me of the discrete symmetry factorizations of zeta's in ChaosBook.org.

4.2 Zeta functions in d=2

2CB "symbols" are sometimes called "colors".

[1] Let $\mathbb{Z}^2$ be a two-dimensional planar lattice. For any $m, n \geq 1$ and $(i, j) \in \mathbb{Z}^2$, the $m \times n$ rectangular lattice with the left-bottom vertex (i, j) is denoted by

$$\mathbb{Z}_{m\times n}((i, j)) = \{(i + m', j + n') \mid 0 \leq m' \leq m - 1, 0 \leq n' \leq n - 1\} .$$

and $\mathbb{Z}_{m\times n} = \mathbb{Z}_{m\times n}((0, 0))$. Let $\mathcal{S}_p$ be an alphabet of p (≥ 2) symbols. For $m, n \geq 1$, $\Sigma_{m\times n}(p) = \mathcal{S}_p^{\mathbb{Z}_{m\times n}}$ is the set of all $m \times n$ local patterns or rectangular blocks, and $\Sigma_{m\times n}(\mathcal{B})$ is the set of admissible $m \times n$ patterns. $\Sigma(\mathcal{B})$ is the set of all admissible patterns in $\mathcal{B}$.

2016-05-04 Predrag There is much literature on multi-dimensional shifts that we have to understand (or at least understand whether it is relevant to our 2-dimensional symbolic dynamics):

Ward [68] *An algebraic obstruction to isomorphism of Markov shifts with group alphabets* introduced Z^2-subshift, or the space of doubly indexed sequences over a finite abelian compact group G.

Ward [67] *Automorphisms of $\mathbb{Z}^d$-subshifts of finite type*

Al Refaei 2011 "The group Z^2 acts natural on the space ?? via left and upward shifts" is gibberish, ignore it.

Roettger [59], *Periodic points classify a family of Markov shifts*, writes:

Ledrappier introduced the following type of space of doubly indexed sequences over a finite abelian group G,

$$X_G = \{(x_{s,t}) \in G^{\mathbb{Z}^2} | x_{s,t+1} = x_{s,t} + x_{s+1,t} \quad \text{for all } s, t \in \mathbb{Z}\}.$$

The group $\mathbb{Z}^2$ acts naturally on the space X_G via left and upward shifts.

Chow, Mallet-Paret and Van Vleck [17, 18, 51, 52] *Pattern formation and spatial chaos in spatially discrete evolution equations*

(Actually, Bunimovich might have worked on this)

Friedland [29] *On the entropy of $\mathbb{Z}^d$ subshifts of finite type*

Quas and Trow [57] *Subshifts of multi-dimensional shifts of finite type*

Desai [25] *Subsystem entropy for $\mathbb{Z}^d$ sofic shifts*

Ban and Lin [7, 8] *Patterns generation and transition matrices in multi-dimensional lattice models*

Boyle, Pavlov and Schraudner [13] *Multidimensional sofic shifts without separation and their factors*

Hochman and Meyerovitch [35] *A characterization of the entropies of multi-dimensional shifts of finite type*

Ban, Hu, Lin, and Lin [6], *Verification of mixing properties in two-dimensional shifts of finite type*

[1] Predrag 2016-10-11: From Ban *et al.* [6], on two-dimensional $\mathbb{Z}^2$-shifts of finite type

Hu and Lin [37] *Nonemptiness problems of plane square tiling with two colors*

Hu and Lin [38], *On spatial entropy of multi-dimensional symbolic dynamical systems*, discuss multi-dimensional shift space for a rectangular spatial entropy which is the limit of growth rate of admissible local patterns on finite rectangular sublattices.

2016-05-04 Predrag Ban, Hu, Lin, and Lin [5], *Zeta functions for two-dimensional shifts of finite type* seems to be a must read, with exhaustive references. The zeta functions of two-dimensional shifts of finite type which generalizes the Artin-Mazur [4] zeta function was given by Lind [48] for $\mathbb{Z}^2$-action. The rotationally symmetric trace operator is the transition matrix for x-periodic patterns with period n and height 2. The rotational symmetry induces the reduced trace operator, and the zeta function in the x-direction is now a reciprocal of an infinite product of polynomials. The zeta function can be presented in the y-direction and in the coordinates of any unimodular transformation in $GL_2(\mathbb{Z})$. Therefore, there exists a family of zeta functions that are meromorphic extensions of the same analytic function. The Taylor series for these zeta functions at the origin are equal with integer coefficients, yielding a family of identities, which are of interest in number theory.

Predrag 2016-10-11 Boris has explained the strategy of Ban *et al.* [5], approach that he himself has used: one constructs ζ functions for finite periodic domain in one direction, i.e., infinite strip $\mathbb{Z}_{\infty\times n}$ or $\mathbb{Z}_{m\times\infty}$. with a transfer operator generating the other, infinite direction (see figure **??**). Those zeta functions are multiplied. The infinite products, a different formula for each direction, describe the same set of admissible patterns, resulting in some unexpected identities.

I find this very unnatural - intelligent zeta should account for all commuting directions democratically.

References

[1] N. Abarenkova, J.-C. Anglès d'Auriac, S. Boukraa, S. Hassani, and J.-M. Maillard, "Rational dynamical zeta functions for birational transformations", Physica A **264**, 264–293 (1999).

[2] M. Aizenman, M. Laínz Valcázar, and S. Warzel, "Pfaffian correlation functions of planar dimer covers", J. Stat. Phys. **166**, 1078–1091 (2017).

[3] J.-C. Anglès d'Auriac, S. Boukraa, and J.-M. Maillard, "Functional relations in lattice statistical mechanics, enumerative combinatorics, and discrete dynamical systems", Ann. Comb. **3**, 131–158 (1999).

[4] M. Artin and B. Mazur, "On periodic points", Ann. Math. **81**, 82–99 (1965).

[5] J.-C. Ban, W.-G. Hu, S.-S. Lin, and Y.-H. Lin, *Zeta functions for two-dimensional shifts of finite type*, Vol. 221, Memoirs Amer. Math. Soc. (Amer. Math. Soc., Providence RI, 2013).

[6] J.-C. Ban, W.-G. Hu, S.-S. Lin, and Y.-H. Lin, Verification of mixing properties in two-dimensional shifts of finite type, 2015.

[7] J.-C. Ban and S.-S. Lin, "Patterns generation and transition matrices in multi-dimensional lattice models", Discrete Continuous Dyn. Syst. Ser. A **13**, 637–658 (2005).

[8] J.-C. Ban, S.-S. Lin, and Y.-H. Lin, "Patterns generation and spatial entropy in two-dimensional lattice models", Asian J. Math. **11**, 497–534 (2007).

[9] R. Band, J. M. Harrison, and C. H. Joyner, "Finite pseudo orbit expansions for spectral quantities of quantum graphs", J. Phys. A **45**, 325204 (2012).

[10] L. Bartholdi, "Zeta functions of graphs: a stroll through the garden, by Audrey Terras. book review", Bull. Amer. Math. Soc. **51**, 177–185 (2014).

[11] H. Bass, "The Ihara-Selberg zeta function of a tree lattice", Int. J. Math. **3**, 717–797 (1992).

[12] E. Bedford and J. Diller, "Real and complex dynamics of a family of birational maps of the plane: The golden mean subshift", Amer. J. Math. **127**, 595–646 (2005).

[13] M. Boyle, R. Pavlov, and M. Schraudner, "Multidimensional sofic shifts without separation and their factors", Trans. Amer. Math. Soc. **362**, 4617–4653 (2010).

[14] P. N. Burgoyne, "Remarks on the combinatorial approach to the Ising problem", J. Math. Phys. **4**, 1320–1326 (1963).

[15] M. Chertkov and V. Y. Chernyak, "Loop calculus in statistical physics and information science", Phys. Rev. E **73**, 065102 (2006).

[16] M. Chertkov, V. Y. Chernyak, and R. Teodorescu, "Belief propagation and loop series on planar graphs", J. Stat. Mech. **2008**, P05003 (2008).

[17] S.-N. Chow, J. Mallet-Paret, and W. Shen, "Traveling waves in lattice dynamical systems", J. Diff. Equ. **149**, 248–291 (1998).

[18] S.-N. Chow, J. Mallet-Paret, and E. S. Van Vleck, "Pattern formation and spatial chaos in spatially discrete evolution equations", Random Comput. Dynam. **4**, 109–178 (1996).

[19] D. Cimasoni, "A generalized Kac-Ward formula", J. Stat. Mech. **2010**, P07023 (2010).

[20] D. Cimasoni, "The critical Ising model via Kac-Ward matrices", Commun. Math. Phys. **316**, 99–126 (2012).

[21] B. Clair, "The Ihara zeta function of the infinite grid", Electron. J. Combin. **21**, P2–16 (2014).

[22] B. Clair and S. Mokhtari-Sharghi, "Zeta functions of discrete groupsacting on trees", J. Algebra **237**, 591–620 (2001).

[23] B. Clair and S. Mokhtari-Sharghi, "Convergence of zeta functions of graphs", Proc. Amer. Math. Soc. **130**, 1881–1887 (2002).

[24] G. A. T. F. da Costa, "The Feynman identity for planar graphs", Lett. Math. Phys. **106**, 1089–1107 (2016).

[25] A. Desai, "Subsystem entropy for Z^d sofic shifts", Indag. Math. **17**, 353–359 (2006).

[26] M. E. Fisher, "Statistical mechanics of dimers on a plane lattice", Phys. Rev. **124**, 1664–1672 (1961).

[27] M. E. Fisher, "On the dimer solution of planar Ising models", J. Math. Phys. **7**, 1776–1781 (1966).

[28] C. Fortuin and P. Kasteleyn, "On the random-cluster model: I. Introduction and relation to other models", Physica **57**, 536–564 (1972).

[29] S. Friedland, "On the entropy of Z^d subshifts of finite type", Linear Algebra Appl. **252**, 199–220 (1997).

[30] J. Guckenheimer, "Axiom A + no cycles $\Rightarrow \zeta_f(t)$ rational", Bull. Amer. Math. Soc. **76**, 592–594 (1970).

[31] D. Guido, T. Isola, and M. L. Lapidus, "Ihara zeta functions for periodic simple graphs", in *C*-algebras and Elliptic Theory II*, edited by D. Burghelea, R. Melrose, A. S. Mishchenko, and E. V. Troitsky (Birkhäuser, Basel, 2008), pp. 103–121.

[32] D. Guido, T. Isola, and M. L. Lapidus, "A trace on fractal graphs and the Ihara zeta function", Transactions of the American Mathematical Society **361**, 3041–3041 (2009).

[33] K. Hashimoto, "Zeta functions of finite graphs and representations of p-adic groups", Adv. Stud. Pure Math. **15**, 211–280 (1989).

[34] Y. Higuchi, N. Konno, I. Sato, and E. Segawa, "A remark on zeta functions of finite graphs via quantum walks", Pacific J. Math. Industry **6**, 1–8 (2014).

[35] M. Hochman and T. Meyerovitch, "A characterization of the entropies of multidimensional shifts of finite type", Ann. Math. **171**, 2011–2038 (2010).

[36] M. D. Horton, "Ihara zeta functions of digraphs", Linear Algebra Appl. **425**, 130–142 (2007).

[37] W.-G. Hu and S.-S. Lin, "Nonemptiness problems of plane square tiling with two colors", Proc. Amer. Math. Soc. **139**, 1045–1059 (2011).

[38] W.-G. Hu and S.-S. Lin, "On spatial entropy of multi-dimensional symbolic dynamical systems", Discrete Continuous Dyn. Syst. Ser. A **36**, 3705–3717 (2016).

[39] C. A. Hurst and H. S. Green, "New solution of the Ising problem for a rectangular lattice", J. Chem. Phys. **33**, 1059–1062 (1960).

[40] Y. Ihara, "On discrete subgroups of the two by two projective linear group over p-adic fields", J. Math. Society of Japan **18**, 219–235 (1966).

[41] S. Isola, "ζ-functions and distribution of periodic orbits of toral automorphisms", Europhys. Lett. **11**, 517–522 (1990).

[42] M. Kac and J. C. Ward, "A combinatorial solution of the two-dimensional Ising model", Phys. Rev. **88**, 1332–1337 (1952).

[43] W. Kager, M. Lis, and R. Meester, "The signed loop approach to the Ising model: Foundations and critical point", J. Stat. Phys. **152**, 353–387 (2013).

[44] P. W. Kasteleyn, "The statistics of dimers on a lattice: I. The number of dimer arrangements on a quadratic lattice", Physica **27**, 1209–1225 (1961).

[45] P. W. Kasteleyn, "Dimer statistics and phase transitions", J. Math. Phys. **4**, 287–293 (1963).

[46] B. Kaufman, "Crystal statistics. II. Partition function evaluated by spinor analysis", Phys. Rev. **76**, 1232–1243 (1949).

[47] K. Kirsten and F. L. Williams, *A Window Into Zeta and Modular Physics* (Cambridge Univ. Press, 2010).

[48] D. A. Lind, "A zeta function for Z^d-actions", in *Ergodic theory of Z^d actions*, edited by M. Pollicott and K. Schmidt (Cambridge Univ. Press, 1996), pp. 433–450.

[49] M. Lis, "A short proof of the Kac-Ward formula", Annales de l'Institut Henri Poincaré D **3**, 45–53 (2016).

[50] M. Loebl and P. Somberg, "Discrete Dirac operators, critical embeddings and Ihara-Selberg functions", Electron. J. Combin. **22**, P1–10 (2015).

[51] J. Mallet-Paret and S. N. Chow, "Pattern formation and spatial chaos in lattice dynamical systems. I", IEEE Trans. Circuits Systems I Fund. Theory Appl. **42**, 746–751 (1995).

[52] J. Mallet-Paret and S. N. Chow, "Pattern formation and spatial chaos in lattice dynamical systems. II", IEEE Trans. Circuits Systems I Fund. Theory Appl. **42**, 752–756 (1995).

[53] A. Manning, "Axiom A diffeomorphisms have rational zeta function", Bull. London Math. Soc. **3**, 215–220 (1971).

[54] H. Mizuno and I. Sato, "Zeta functions of digraphs", Linear Algebra Appl. **336**, 181–190 (2001).

[55] L. Onsager, "Crystal statistics. I. A Two-dimensional model with an order-disorder transition", Phys. Rev. **65**, 117–149 (1944).

[56] M. Pollicott, Dynamical zeta functions, in Smooth Ergodic Theory and Its Applications, Vol. 69, edited by A. Katok, R. de la Llave, Y. Pesin, and H. Weiss (2001), pp. 409–428.

[57] A. N. Quas and P. B. Trow, "Subshifts of multi-dimensional shifts of finite type", Ergod. Theor. Dynam. Syst. **20**, 859–874 (2000).

[58] P. Ren, T. Aleksić, D. Emms, R. C. Wilson, and E. R. Hancock, "Quantum walks, Ihara zeta functions and cospectrality in regular graphs", Quantum Inf. Process. **10**, 405–417 (2010).

[59] C. G. J. Roettger, "Periodic points classify a family of markov shifts", J. Number Theory **113**, 69–83 (2005).

[60] I. Sato, "Bartholdi zeta functions of group coverings of digraphs", Far East J. Math. Sci. **18**, 321–339 (2005).

[61] A. Setyadi and C. K. Storm, "Enumeration of graphs with the same Ihara zeta function", Linear Algebra Appl. **438**, 564–572 (2013).

[62] S. Sherman, "Combinatorial aspects of the Ising model for ferromagnetism. I. A conjecture of Feynman on paths and graphs", J. Math. Phys. **1**, 202–217 (1960).

[63] A. Tarfulea and R. Perlis, "An Ihara formula for partially directed graphs", Linear Algebra Appl. **431**, 73–85 (2009).

[64] H. Teimoori Faal and M. Loebl, "Bass' identity and a coin arrangements lemma", Eur. J. Combinatorics **33**, 736–742 (2012).

[65] A. Terras, *Zeta functions of graphs: a stroll through the garden* (Cambridge Univ. Press, 2010).

[66] N. V. Vdovichenko, "A calculation of the partition function for a plane dipole lattice", Sov. Phys. JETP **20**, 477–479 (1965).

[67] T. Ward, "Automorphisms of Z^d-subshifts of finite type", Indag. Math. **5**, 495–504 (1994).

[68] T. B. Ward, "An algebraic obstruction to isomorphism of Markov shifts with group alphabets", Bull. London Math. Soc. **25**, 240–246 (1993).

[69] W. Werner, *Percolation et modèle d'Ising* (Société mathématique de France, 2009).

[70] A. Wipf, T. Heinzl, T. Kaestner, and C. Wozar, "Generalized Potts-models and their relevance for gauge theories", SIGMA **3**, 6–14 (2007).

[71] C. Wozar, T. Kaestner, A. Wipf, T. Heinzl, and B. Pozsgay, "Phase structure of $\mathbb{Z}(3)$-Polyakov-loop models", Phys. Rev. D **74**, 114501 (2006).

[72] C. N. Yang, "The spontaneous magnetization of a two-dimensional Ising model", Phys. Rev. **85**, 808–816 (1952).

Chapter 5

Han's blog

Han Liang <han_liang@gatech.edu> work blog
The latest entry at the bottom for this blog

2018-03-18 Predrag Our blog posts are divided into sect. 5.1 *Rhomboid corner partition*, sect. 5.2 *Rhomboid center partition*, sect. 5.3 *Reduction to the fundamental domain*, and sect. 5.4 *Spatiotemporal cat map partition*

2018-01-19 Han Here is an example of text edit by me, and here one of a footnote by me[1].

2018-01-19 Han (Discussion with Predrag, cat maps project Spring 2018:

- blog the project progress here
- blog whatever I'm reading and learning about dynamical systems here

2018-06-05 to 06-11 Predrag Read chapter ?, part of ?, and ? of Chaosbook. Do homework of online Course 1, Weeks ? and ?.

2018-01-19 to 02-11 Han Read Chapters ?, ?, part of ?, and ? of Chaosbook. Did homework of Weeks ? and ?.

2018-01-11 Predrag to Han: Caution - my posts can be erased your edits, if you omit to *svn up* before starting your edit.

Regarding new figures: always save *HL*.png* (or *HL*.pdf*) in *siminos/figs/*, then *svn add HL*.png* (where * is a name of the figure.

Remember, always, before starting your work session with *svn up* and colcluding it with

[1] Han 2018-01-19: Han test footnote

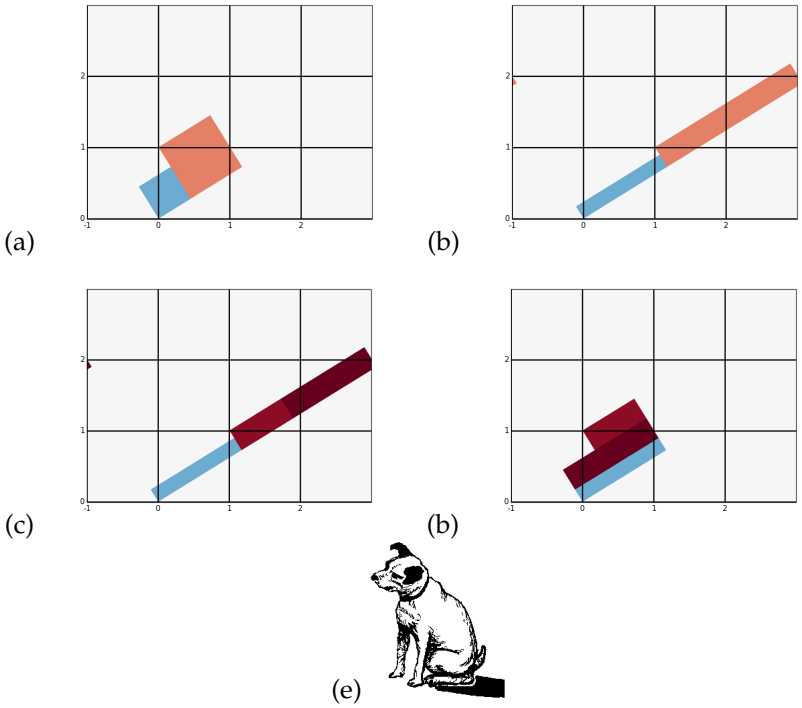

Figure 5.1: Figure 1.1 recomputed with my python code. (a) Two-squares Adler-Weiss generating partition for the canonical Thom-Arnol'd cat map (1.1), with borders given by stable-unstable manifolds of the unfolded cat map lattice points near to the origin. (b) The first iterate of the partition. (c) The first iterate of the partition intersections, (d) The iterate pulled back into the generating partition, and (e) the corresponding 5-letter transition graph. In (b) and (c) we still have to relabel Crutchfield's arbitrary partition labels with our shift code. This is a "linear code," in the sense that for each square on can count how many side-lengths are needed to pull the overhanging part of (c) back into the two defining squares.

svn ci-m"added entropy figures" you have to go to the root directory, *cd [...]/siminos*. Otherwise you are not refreshing all bibtex, figures and other files in the repository.

2018-01-12 Predrag to Han

On *zero.physics.gatech.edu*, or Matt's *light.physics.gatech.edu*, or your and Andy's *hard.physics.gatech.edu*, or visitor office *love.physics.gatech.edu*, or any other CNS linux workstation your userid is

XXXX? (the same passwd as for svn - please change it once you log in)

Do not do calculations on the server *zero.physics.gatech.edu* - from any CNS machine

ssh *XXXX?@hard.physics.gatech.edu*

save all data on the local hard disk */usr/local/home/han/*. I should make a link in your CNS home directory:

cd homeHard

Help for CNS system, and all our documentation is on www.cns.gatech.edu/CNS-only cnsuser cnsweb

but current crop of grad students, as a matter of principle, never look at any info, or add to these homepages.

Good luck - Matt knows `linux` best, also Simon Berman, Xiong Ding and Burak Budanur (via Skype) know a lot.

5.1 Rhomboid corner partition

2018-01-18 Han `figSrc/han/python/HLcatmapArnold.py` reproduces the standard Arnol'd map partition, figure 5.1. The plots are in `siminos/figs/`.

`figSrc/han/python/HLcatmapPV.py` reproduces Predrag's hand-sketch of the Percival-Vivaldi [14] "two-configuration representation" cat map partition, figure 5.2.

2018-01-19 Predrag In the Percival-Vivaldi partition, (1.5) there is only one partition, the $[x_0, x_1]$ unit square. In the Adler-Weiss partition of figure 5.2 (a) there are two rhomboid partitions, each with its own coordinates, lets say the big rhomboid $[x_0^A, x_1^A]$ and the small rhomboid $[x_0^B, x_1^B]$ (and perhaps also its time-reversal partner $[x_0^{B'}, x_1^{B'}]$), each bounded not by a unit square, but by the vectors (S^A, U^A), (S^B, U^B) of the stable/unstable manifold segments that border the rhomboids. As this is a symplectic mapping, the important property of these rhomboids is their (oriented) area, for $1D$ dof given by the wedge or skew-symmetric product

$$A^\alpha = U^\alpha \wedge S^\alpha = U_i^\alpha \epsilon^{ij} S_j^\alpha \,, \qquad \alpha \in \{A, B\} \,. \tag{5.1}$$

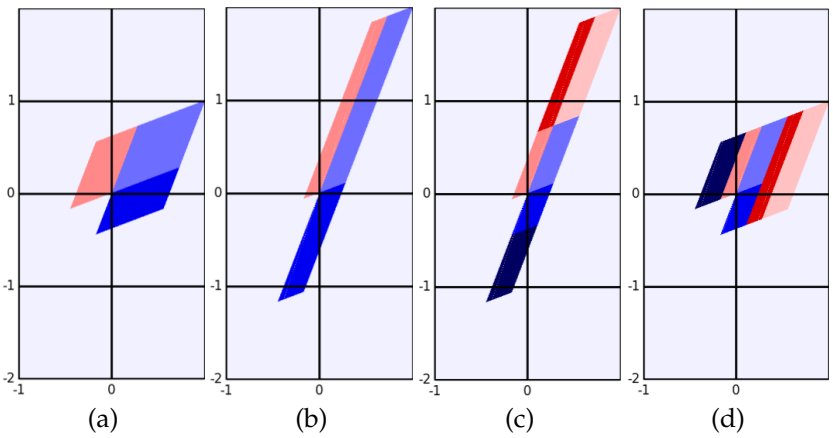

Figure 5.2: Figure 1.6 recomputed with my python code. (a) 3-rectangle, time-reversaal symmetric Percival-Vivaldi cat map (1.5) partition. (b) The first forward iterate of the partition. (c) The first forward iterate of the partition, with the stable manifold intersections dividing it into 6 regions. (d) The 6 rhomboids (5 when the two blue regions are treated as one) are translated back into the generating partition, with the subscript label indicating the square-lattice vertical translation group elements: $\{T_{AA} = g_0^{A\to A}, T_{BB} = g_0^{B\to B}, T_{BA} = g_{-1}^{A\to B}, T'_{AA} = g_1^{A\to A}, T_{AB} = g_1^{B\to A}\}$. If the two blue regions are considered as a single partition, one obtains the standard Adler-Weiss 2-partition, with 5 distinct return maps one step forward in time, and the corresponding 5-letter transition graph of figure 5.1 (e). Together, these transitions make up the transition graph of figure 1.1 (c). The partition is generating, in the sense that the walks on this transition graph generate all admissible sequences.

The figure 5.1 and figure 5.2 partitions are related by canonical (in $1D$ dof area-preserving) transformations, so for given stretching s, the small and the large rectangle/rhomboid areas are the same in any partition. Likewise, topologically the dynamics should be the same, i.e., have the same transition graph figure 1.1 (c).

That should naturally follow from the generator (Lagrangian) formulation sect. 1.4 in any choice of symplectically-paired coordinates.

Having several coordinate systems, one for each partition, is standard; a typical example are the three Poincaré sections of the 3-disk pinball, Fig. 15.15: *Poincaré section coordinates for the 3-disk game of pinball*, ChaosBook chapter *Charting the state space* [6].

2018-01-25 Predrag Figure out Toeplitz matrix for the simplest cycle(s) of length two (for Toeplitz matrices, see the post of **2017-09-09** on page 106, and the posts in sect. 1.8).

Hopefully only a [2×2] matrix. Understand its stability multipliers, eigenvectors.

2018-01-19 Han I've been working on reading the ChaosBook materials and doing the online Course 1.

2018-01-26 Predrag to Han: Can you compute analytically areas of partitions in figure 5.2, show that they are the same as those in figure 1.1 and figure 5.1? I expect them to be simple formulas in terms of stability multipliers (1.6).

2018-01-27 Han I have computed the area of the small partition B in figure 5.2 and figure 5.1. The areas of the small partitions are the same, for $s = 3$ they are $A_B = \frac{1}{2}(1 - \frac{1}{\sqrt{5}})$. If the stability multipliers are $(\Lambda, 1/\Lambda)$, where $\Lambda > 1$, as in (1.6), the area of the small partition B in figure 5.1 is given by

$$A_B = \frac{1 - 1/\Lambda}{\sqrt{D}} = \frac{1}{\Lambda + 1}\,. \tag{5.2}$$

The area of figure 5.2 is $A_B = \frac{(\Lambda-1)/\Lambda}{\sqrt{D}}$, i.e., the same.

2018-02-16 Predrag Is $|\mathcal{M}_B| = (\Lambda - 2)/\sqrt{D}$ in (1.93), for $s = 3$, the same as $|\mathcal{M}_B| = \frac{1-1/\Lambda}{\sqrt{D}} = \frac{1}{\Lambda+1}$ of (5.2)? Indeed, that follows from (1.83) by inspection.

2018-01-27 Predrag Thanks! Did you use (5.1) to compute them? I think we need that formalism to harmonize the discussion with sect. 1.4 generating functions.

Did you also check that the area of the big partition is $A_A = (1+1/\Lambda)/\sqrt{D}$?

We might want to state the similarity transformation that maps (1.1) into (1.5), and also maps the associated eigenvectors. Also there should be a

canonical (symplectic) transformation that does that - presumably in this simple 2-dimensional case they are the same transformation, but I do not remember... In any case, matrices (1.7), up to normalization, probably already do the job.

2018-01-27 Predrag Maybe you do not see what has happened in the blog - I always use `svn diff` (it works nicely in the Windows GUI) to see what has changed.

Anyway, I stared the explicit construction of the Perron-Frobenius operator in example 1.5, so we also need the sub-partitions areas to check that.

2018-01-31 Han to Predrag: I have checked the area of the big partition. Adding the areas of each partition together we will get 1, so it should be correct. I didn't use (5.1) to compute the area. I found the coordinates of all the vertices on the edges of the parallelograms and got the vectors that border the partition then did the cross product (kind of tedious...). Using (5.1) to compute the areas should be very easy.
2018-02-10 Predrag computed them in (1.93).

I also tried to find the similarity transformation that maps (1.1) into (1.5).

$$\mathbf{A} = \begin{bmatrix} 2 & 1 \\ 1 & 1 \end{bmatrix} \tag{5.3}$$

$$\mathbf{B} = \begin{bmatrix} 0 & 1 \\ -1 & 3 \end{bmatrix} \tag{5.4}$$

I get

$$\mathbf{B} = \mathbf{C}^{-1}\mathbf{A}\mathbf{C} \tag{5.5}$$

where $\mathbf{C} = \begin{bmatrix} -1 & 2 \\ 0 & 1 \end{bmatrix}$. Matrices (1.7) can diagonalize (1.5) (I may be wrong).

2018-01-19 Predrag Read chapter *Walkabout: Transition graphs* [7]. Always try to work through examples. Eventually we want to try to solve Exercise 17.1 *Time reversibility*. The solution might be someplace here, in sect. 4.1 *Ihara zeta functions*.

2018-01-31 Han I have read chapter *Walkabout: Transition graphs*.

2018-02-01 Predrag I think a good partition is given in figure 5.3. The symbolic dynamics notation should probably be a 7-letter alphabet, something like

$$\begin{array}{rcl@{\qquad}rcl@{\qquad}rcl} A & \to & A_{(0,0)}\,, & B_2 & \to & B_{(0,0)}\,, & B'_2 & \to & B'_{(0,0)} \\ B_1 & \to & B_{(-1,0)}\,, & B'_1 & \to & B_{(0,-1)} & & & \\ B_3 & \to & B_{(-1,-1)}\,, & B'_3 & \to & B'_{(-1,-1)}\,. & & & \end{array} \tag{5.6}$$

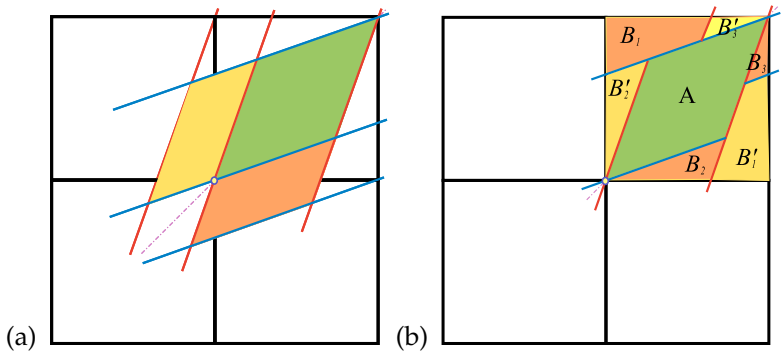

Figure 5.3: Abandoned attempt: (a) The three-rectangle, time reversal symmetric generating partition for the Percival-Vivaldi cat map (1.5), with borders given by cat map stable-unstable manifolds. (b) The three-rectangle partition of the unit square. In this partition A, B_2, B_2' already lie within the unit square, while B_1 is shifted by $(-1, 0)$, B_3 is shifted by $(-1, -1)$, and B_1' is shifted by $(0, -1)$, B_3' is shifted by $(-1, -1)$. It is more partitions than going forward in time, but I feel it will be the right thing for the Lagrangian formulation.

2018-02-01 Predrag [2018-02-11 accomplished for the two-rectangle partition**]** Next we need to write down the transition graph for admissible itineraries, and the circulant matrices (periodic boundary condition Green's functions) that convert any admissible itinerary into periodic orbit points $\{x_n\}$. These should be rational numbers.

Han points out that the unit square borders, have no physical meaning, and that the partition still has only three regions A, B, B', as in figure 1.8. The time forward partition is given in figure 1.7 (b).

2018-02-11 Han I have verified some admissible and inadmissible orbits by the Green's function. The Percival-Vivaldi cat map matrix with $s = 3$ is:

$$\mathbf{A} = \begin{bmatrix} 0 & 1 \\ -1 & 3 \end{bmatrix} \tag{5.7}$$

For the finite time $T = 4$ we can represent $\mathcal{D}$ with periodic boundary conditions by a 4×4 circulant matrix [2]

$$\mathcal{D} = \begin{bmatrix} 3 & -1 & 0 & -1 \\ -1 & 3 & -1 & 0 \\ 0 & -1 & 3 & -1 \\ -1 & 0 & -1 & 3 \end{bmatrix} \tag{5.8}$$

[2] Predrag 2018-02-11: Before your notation diverges from the one we use in papers - I think you have an overall "-" sign compared to sect. 1.7 *Green's function for 1-dimensional lattice*. Fix it now, so it does not plague you later.

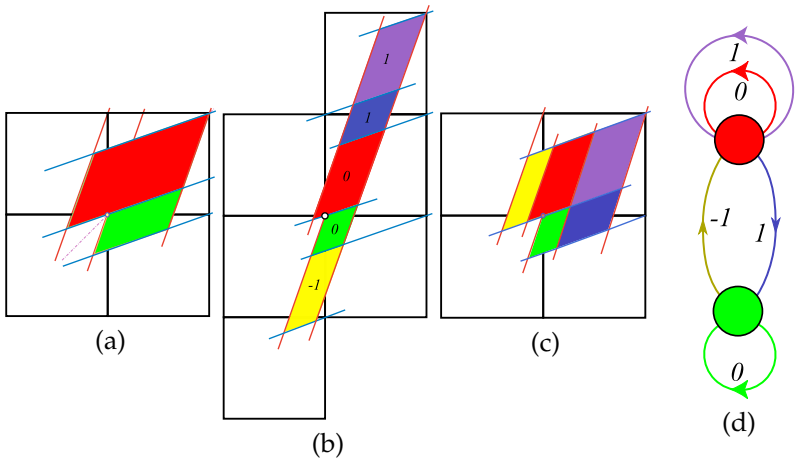

Figure 5.4: (Color online) (a) An Adler-Weiss generating partition of the unit torus into rectangles $\mathcal{M}_A$ (red) and $\mathcal{M}_B$ (green) for the Percival-Vivaldi cat map (1.5), with borders given by the cat map stable (blue) and unstable (red) manifolds. (b) Mapped one step forward in time, the rectangles are stretched along the unstable direction and shrunk along the stable direction. Sub-rectangles $\mathcal{M}_j$ that have to be translated back into the partition are indicated by color and labeled by their lattice translation $m_j \in \{\underline{1}, 0, 1\}$. (c) The sub-rectangles $\mathcal{M}_j$ translated back into the unit square yield a generating partition labelled by the 5-letter alphabet (5.13), with (d) the finite grammar given by the transition graph for this partition. The nodes refer to the rectangles A and B, and the five links correspond to the five sub-rectangles induced by one step forward-time dynamics. (Compare with figure 1.2. For details, see ChaosBook [8]).

The corresponding Green's function is the inverse matrix of $\mathcal{D}$

$$\mathbf{g} = \begin{bmatrix} \frac{7}{15} & \frac{1}{5} & \frac{2}{15} & \frac{1}{5} \\ \frac{1}{5} & \frac{7}{15} & \frac{1}{5} & \frac{2}{15} \\ \frac{2}{15} & \frac{1}{5} & \frac{7}{15} & \frac{1}{5} \\ \frac{1}{5} & \frac{2}{15} & \frac{1}{5} & \frac{7}{15} \end{bmatrix} \tag{5.9}$$

Then given block $p = m_0 m_1 m_2 m_3$ of 'sources', we can calculate the corresponding orbit $\mathcal{M}_p = (x_1, x_2, x_3, x_4)$. For example, if

$$\mathbf{m} = \begin{bmatrix} 0 \\ 2 \\ 2 \\ 0 \end{bmatrix} \quad \Rightarrow \quad \mathbf{x} = \frac{1}{3} \begin{bmatrix} 2 \\ 4 \\ 4 \\ 2 \end{bmatrix} . \tag{5.10}$$

This orbit should be inadmissible since it contains the pruned block 22, and indeed the corresponding periodic points fall outside the unit interval, $\{x_1, x_2\} > 1$. Two admissible 4-cycles:

$$\begin{bmatrix} 0 \\ 2 \\ 0 \\ 0 \end{bmatrix} \Rightarrow \quad \mathbf{x} = \frac{1}{15} \begin{bmatrix} 6 \\ 14 \\ 6 \\ 4 \end{bmatrix} ; \qquad \begin{bmatrix} 0 \\ 1 \\ 1 \\ 0 \end{bmatrix} \Rightarrow \quad \mathbf{x} = \frac{1}{3} \begin{bmatrix} 1 \\ 2 \\ 2 \\ 1 \end{bmatrix}$$

We can verify that these are periodic orbits by explicitly iterating

$$\mathbf{A} \begin{bmatrix} x_{t-1} \\ x_t \end{bmatrix} = \begin{bmatrix} x_t \\ x_{t+1} \end{bmatrix} + \begin{bmatrix} 0 \\ m_t \end{bmatrix} . \tag{5.11}$$

2018-02-11 Predrag Very nice! Let's take your Green's function (5.9) for 4-cycles

$$\mathbf{g} = \frac{1}{15} \begin{bmatrix} 7 & 3 & 2 & 3 \\ 3 & 7 & 3 & 2 \\ 2 & 3 & 7 & 3 \\ 3 & 2 & 3 & 7 \end{bmatrix} \tag{5.12}$$

but now test whether all length 4 closed walks on the transition graph of figure 5.7 (d) yield admissible 4-cycles.

The partition figure 5.4 (c) is labeled / colored by a 5-symbol alphabet (1.9):

$$\mathcal{A} = \{1, 2, 3, 4, 5\} = \{A^0A, B^1A, A^1A, B^0B, A^1B\} , \tag{5.13}$$

that labels the five sub-rectangles $\mathcal{M}_{m_j}$ of the cat map state space, $\mathcal{M} = \cup \mathcal{M}_{m_j}$, by the links of the transition graph of figure **??** (d), with all admissible itineraries generated by all walks on the transition graph. Rational values correspond to periodic orbits, with the state space periodic points uniquely labeled by the admissible itineraries of symbols from $\mathcal{A}$.

Bird and Vivaldi [4] tabulate the numbers of prime cycles (they call that $N_T(\lambda)$ in their Table 1, with $s = K = 3$ and 4),

$$\sum_{T=1}^{\infty} z^T N_T = z + 2\,z^2 + 5\,z^3 + 10\,z^4 + 24\,z^5 \cdots \tag{5.14}$$

They say that there are $N_4(\lambda) = 10$ admissible prime 4-cycles. They can be read off as walks on figure 5.4 (d):

$$\begin{array}{ccccc} \overline{1113} & \overline{1125} & \overline{1245} & \overline{1253} & \overline{1325} \\ 0001 & 001\underline{1} & 010\underline{1} & 01\underline{1}1 & 011\underline{1} \\ \overline{1133} & \overline{3325} & \overline{3331} & \overline{3245} & \overline{4452} \\ 0011 & 111\underline{1} & 1110 & 110\underline{1} & 00\underline{1}1 \end{array} \tag{5.15}$$

prime4cycles with the corresponding translations read off the superscripts in (5.13). My sub-rectangles alphabet (5.13) is superfluous; the translations

$$m_t \in \{\underline{1}, 0, 1\} \tag{5.16}$$

from (5.13) alone label uniquely the admissible orbits, as they should, as the relation is linear. We have to figure out how to argue that reading $\{m_t\}$ off the graph alone suffices to label the orbit. Not obvious, as links 0 and 1 occur twice. Green 0 has to be followed by $\underline{1}$, the red 0 has to be followed by 3 or 2, so they are distinct. The blue 1 must eventually be followed by $\underline{1}$, but how is that different from the purple 1?

Some clever recoding idea is called for.

To Han: please plot these cycles in the partition of figure 5.4 (c), verify that each cycle point x_t lands into the correct $\mathcal{M}_{m_t}$.

2018-02-11 Han I have computed all ten 4-cycles using Green's function (5.12) and plotted all their periodic points in figures 5.5 and 5.6.

$$\mathsf{M} = \begin{bmatrix} 0 \\ 0 \\ 0 \\ 1 \end{bmatrix} \Rightarrow \quad \mathsf{X}_{0001} = \frac{1}{15} \begin{bmatrix} 3 \\ 2 \\ 3 \\ 7 \end{bmatrix} .$$

Likewise,

$$\begin{aligned} \mathsf{X}_{001\underline{1}} &= \frac{1}{15}\begin{bmatrix} -1 & 1 & 4 & -4 \end{bmatrix}, \qquad \mathsf{X}_{010\underline{1}} = \frac{1}{15}\begin{bmatrix} 0 & 5 & 0 & -5 \end{bmatrix} \\ \mathsf{X}_{01\underline{1}1} &= \frac{1}{15}\begin{bmatrix} 4 & 6 & -1 & 6 \end{bmatrix}, \qquad \mathsf{X}_{011\underline{1}} = \frac{1}{15}\begin{bmatrix} 2 & 8 & 7 & -2 \end{bmatrix} \\ \mathsf{X}_{0011} &= \frac{1}{15}\begin{bmatrix} 5 & 5 & 10 & 10 \end{bmatrix}, \qquad \mathsf{X}_{111\underline{1}} = \frac{1}{15}\begin{bmatrix} 9 & 11 & 9 & 1 \end{bmatrix} \\ \mathsf{X}_{1110} &= \frac{1}{15}\begin{bmatrix} 12 & 13 & 12 & 8 \end{bmatrix}, \qquad \mathsf{X}_{110\underline{1}} = \frac{1}{15}\begin{bmatrix} 7 & 8 & 2 & -2 \end{bmatrix} \\ \mathsf{X}_{00\underline{1}1} &= \frac{1}{15}\begin{bmatrix} 1 & -1 & -4 & 4 \end{bmatrix} \end{aligned} \tag{5.17}$$

I verified these orbits by finding the position of each point (x_t, x_{t+1}) on the partition $\mathcal{M}_A$ or $\mathcal{M}_B$. They are all admissible.

2018-02-11 Predrag It feels like magic; we know that what the 2-rectangle partition is, and we have derived the transition graph of figure 5.4 (d), and that by similarity transformation this is the same for any $s = 3$ cat map, but it is still not obvious that the 3-letter alphabet (5.16) does the job. I do not know if you have checked any of the original literature, but I do not recall seeing such alphabet...

In (the current draft of) Gutkin *et al.* [12] I wrote "The Adler–Weiss Markov partition for the Arnol'd cat map [1–3] utilizes the stable / unstable manifold of the fixed point at the origin to partition the torus into a 3-rectangles generating partition (see, for example, Devaney [5, 10]). It is a subshift of finite type (3 symbols alphabet $\bar{\mathcal{A}}$, with a finite grammar), or a 5 symbols full shift."

That I learned from Creagh, who explains both the 3-letter and the 5-letter alphabet in ref. [5] Sect. III. A. *The classical map*. On **2016-06-02** I had written this down in sect. 1.6.4. The 3-rectangles generating partition is constructed for the anti-symplectic map (1.2), with only even length cycles retained. I do not see how to take a square root of Percival-Vivaldi (5.7) (your similarity transformation (5.5) should do the job), and how this would result in our pretty shifts 3-letter alphabet (5.16).

2018-02-11 Predrag Next: I have mostly solved and moved example 1.5 *Perron-Frobenius operator for the Arnol'd cat map* to section sect. 1.13 *Examples*. It would be good if you worked through it and understood the transfer matrix L (1.94), which I am reading off figure 5.7, in particular computed it eigenvalues (interpret the $\lambda = 1$ eigenvalue) and eigenvectors (the leading one should be the natural measure). Here $s = 3$, so $\Lambda = \frac{3+\sqrt{5}}{2} = 2.6180$ and $D = 5$.

2018-02-12 Predrag Can you plot the stretched domains corresponding to figure 5.4 (b) for one step back in time (inverse map)? Should look something like figure 5.8. The intersections of the past and future might help you intuition, in the way staring at the figure following figure 1.2 in Gutkin *et al.* [12] reveals the Smale-horseshoe structure.

Remember, our goal is to reformulate the problem in a global, Lagrangian way that is explicitly invariant under time reversal.

2018-03-01 Han I have calculated the stretched domains corresponding to figure 5.4 (b) for one step back in time. The result is in figure 5.9 (c) which is not same as figure 5.8 (b). I guess this is because I start from partition in figure 5.9 (a). If I start from the partition flipped from figure 5.9 (a) across the $x_1 = x_0$ I will get figure 5.8 (b). The overlap 2 partition is also different from figure 5.8 (c). I'm not sure...

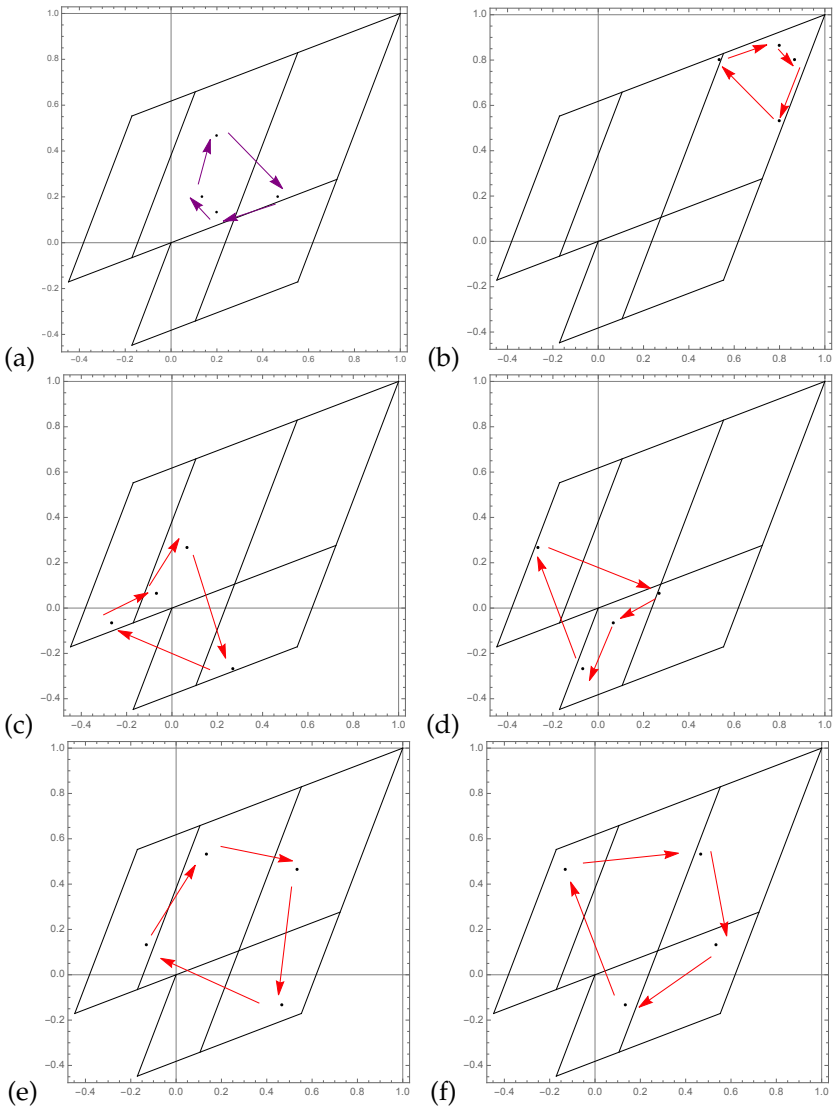

Figure 5.5: Abandoned attempt: All 4-cycles from (5.17): (a) $X_{0001} = X_{1113}$, (b) X_{1110}, (c) X_{0011}, (d) X_{0011}, (e) X_{0111}, (f) X_{1101}, (g) to (j) continued in figure 5.6.

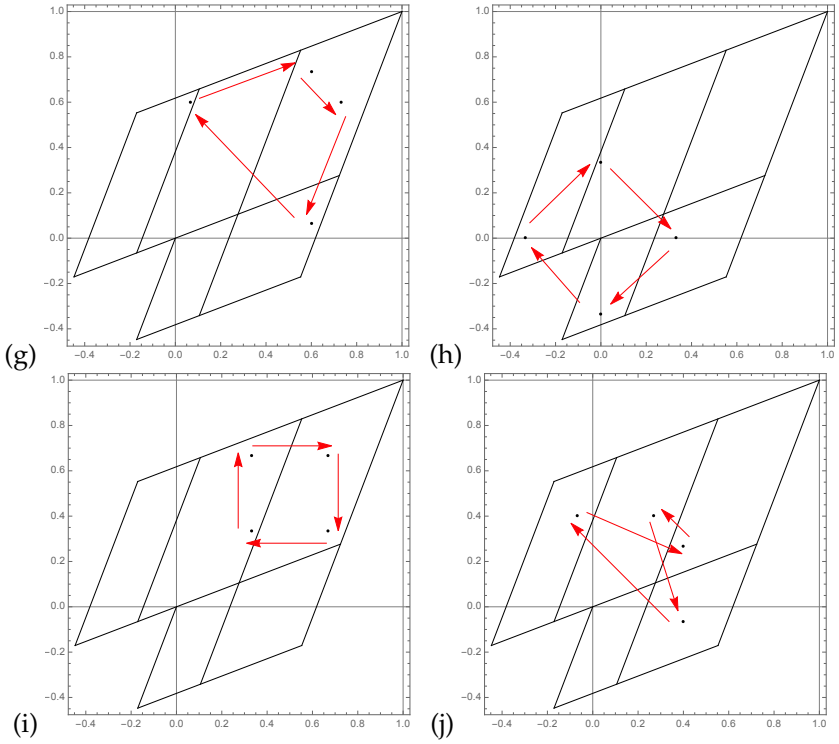

Figure 5.6: Continuation of figure 5.5: (g) X_{1111}, (h) X_{0011}, (i) X_{0011}, and (j) X_{0111},

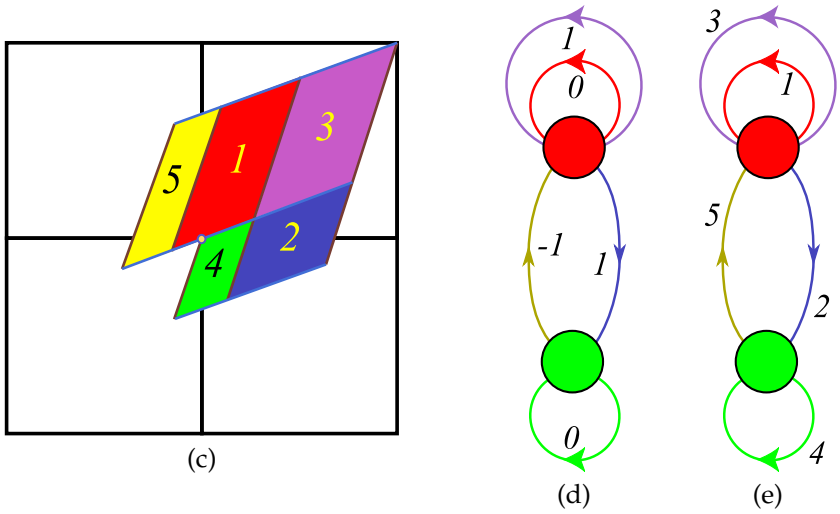

Figure 5.7: (Figure 5.4 continued) (c) The sub-rectangles $\mathcal{M}_j$, indicated by the compact 5-letter alphabet (5.13). (d) Admissible orbits correspond to walks on the transition graph for this partition. The nodes refer to the rectangles A and B, and the five colored links, labeled by their lattice translation $m_j \in \{1, 0, 1\}$, correspond to the five sub-rectangles reached in one step forward-time dynamics. (e) Compact labeling, see (5.13).

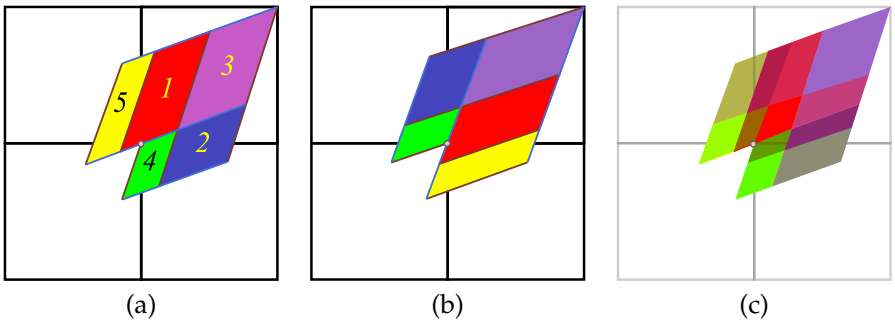

Figure 5.8: (From figure 5.4) (a) The forward in time sub-rectangles $\mathcal{M}_j$, indicated by color / 5-letter alphabet (5.13). (b) The corresponding partition defined for one step backward in time (not the partition (a) iterated back). (c) The overlap 2-step partition. Not sure this is right.

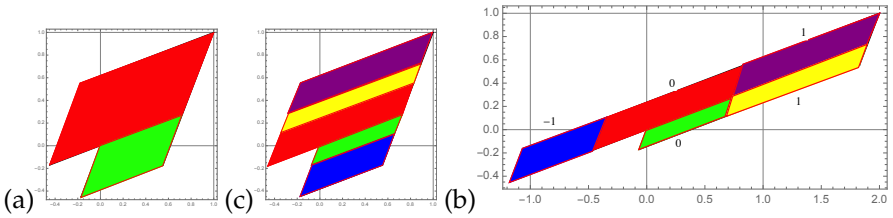

Figure 5.9: (a) The two rectangles partition of the Percival-Vivaldi cat map. (b) Mapped one step backward in time. (c) The stretched partition has been translated back to the original shape.

2018-03-01 Predrag My figure 5.8 was just a quick sloppy sketch. I'm confident that your figure 5.9 is right.

2018-02-13 Predrag Your Green's function is symmetric. Diagonalize?

2018-02-13 Han The eigenvalues of this Green's function are 1, 1/3, 1/3, 1/5. These are also the diagonal elements of the diagonalized matrix.

2018-02-13 Predrag Mhm - you sure? I was expecting $\sqrt{5}$'s. What about eigenvectors? Try 5-cycles. 5 is a prime.

2018-02-13 Han When the circulant matrix and the Green's function are $[5\times5]$ matrices, the eigenvalues of the Green's function are

$$1, (7+\sqrt{5})/2, (7+\sqrt{5})/2, (7-\sqrt{5})/2, (7-\sqrt{5})/2, \tag{5.18}$$

corresponding to eigenvectors:
$(1,1,1,1,1)$,
$((-1+\sqrt{5})/2, (1-\sqrt{5})/2, -1, 0, 1)$,
$(-1, (1-\sqrt{5})/2, (-1+\sqrt{5})/2, 1, 0)$,
$((-1-\sqrt{5})/2, (1+\sqrt{5})/2, -1, 0, 1)$,
$(-1, (1+\sqrt{5})/2, (-1-\sqrt{5})/2, 1, 0)$.

2018-02-13 Predrag Mhm - surprised again. I was motivated by (1.112) and (1.75), and expected you to (re)discover sort of a discrete Fourier transform, but with hyperbolic functions. Back to drawing board.

2018-02-15 Han I have read the section *Markov Partitions for Hyperbolic Toral Automorphisms* of Robinson's book. I'm currently working on example 1.5. The (1.94) seems not correct. I'm working on it.

2018-02-16 Predrag I'm complicating this unnecessarily - it would be nice to get the correct 5-rectangles transfer matrix (1.94), but it is unnecessary for our purposes: the two-rectangle partition $[2\times2]$ Markov matrix, where one sums over all admissible transitions, should suffice (for notation, see

(5.13) and ref. [9]):

$$\begin{bmatrix} \phi'_A \\ \phi'_B \end{bmatrix} = L\phi = \begin{bmatrix} L_{A^0A} + L_{A^1A} & L_{A^1\underline{1}B} \\ L_{B^1A} & L_{B^0B} \end{bmatrix} \begin{bmatrix} \phi_A \\ \phi_B \end{bmatrix} \tag{5.19}$$

$$\begin{aligned} L &= \begin{bmatrix} L_{A^0A} + L_{A^1A} & L_{A^1\underline{1}B} \\ L_{B^1A} & L_{B^0B} \end{bmatrix} = \begin{bmatrix} \frac{|\mathcal{M}_1|+|\mathcal{M}_3|}{|\mathcal{M}_A|} & \frac{|\mathcal{M}_5|}{|\mathcal{M}_A|} \\ \frac{|\mathcal{M}_2|}{|\mathcal{M}_B|} & \frac{|\mathcal{M}_4|}{|\mathcal{M}_B|} \end{bmatrix} \\ &= \frac{1}{\Lambda} \begin{bmatrix} 2 & \Lambda - 2 \\ \Lambda - 1 & 1 \end{bmatrix} . \end{aligned} \tag{5.20}$$

in compact notation $\{A^0A, B^1A, A^1A, B^0B, A^1\underline{1}B\} = \{1, 2, 3, 4, 5\}$. Then

$$\begin{aligned} \det(1 - zL) &= \begin{vmatrix} 1 - 2z/\Lambda & -z(\Lambda - 2)/\Lambda \\ -z(\Lambda - 1)/\Lambda & 1 - z/\Lambda \end{vmatrix} \\ &= 1 - 3\frac{z}{\Lambda} + 2\frac{z^2}{\Lambda^2} - \frac{z^2}{\Lambda^2}(\Lambda - 1)(\Lambda - 2) \\ &= 1 - 3\frac{z}{\Lambda} - \frac{z^2}{\Lambda}(\Lambda - 3) , \end{aligned} \tag{5.21}$$

in agreement with the loop expansion (1.96).

2018-02-16 Predrag For $s \geq 3$, the 3-letter alphabet (1.9) generalizes to

$$\mathcal{A} = \{\underline{1}, 0, 1, \cdots, s - 2\} . \tag{5.22}$$

What keeps the forward iterates of the small rectangle in check is the way this area shrinks with large Λ in (1.93).

2018-02-18 Han For $s \geq 3$ the alphabet for the 2- (and 3-) rectangle partition is (5.22): see the 3-rectangle stable and unstable manifolds borders partition for $s = 5$ in figure 5.10.

2018-02-18 Predrag Great. It should led to more sensible labelling of figure 5.7 (e) transition graph, for arbitrary s. You can see that, much like in the Percival-Vivaldi figure 1.2, there is an *interior* $(s-1)$-letter alphabet $\mathcal{A}_0$ which is a full shift ($(s-1)$ loops attached to node A), and some kind of 2-letter *exterior* alphabet $\mathcal{A}_1$ that has to do with node B.

A well-understood alphabet can help us with solving the 2-dimensional spatiotemporal cat map - there the interior alphabet $\mathcal{A}_0$ is still a full shift, while the exterior alphabet $\mathcal{A}_1$ is a bit bigger.

2018-02-19 Predrag The alphabet (5.16), $m_t \in \{\underline{1}, 0, 1\}$ is not good, as it seems not to encode any of the symmetries of orbits in figures 5.5 and 5.6.

2018-02-19 Predrag The flip across the $x_1 = x_0$ diagonal together with the reversal of the direction of evolution is the C_2 symmetry that corresponds to the invariance of cat map under time reversal. There are at least two kinds of orbits:

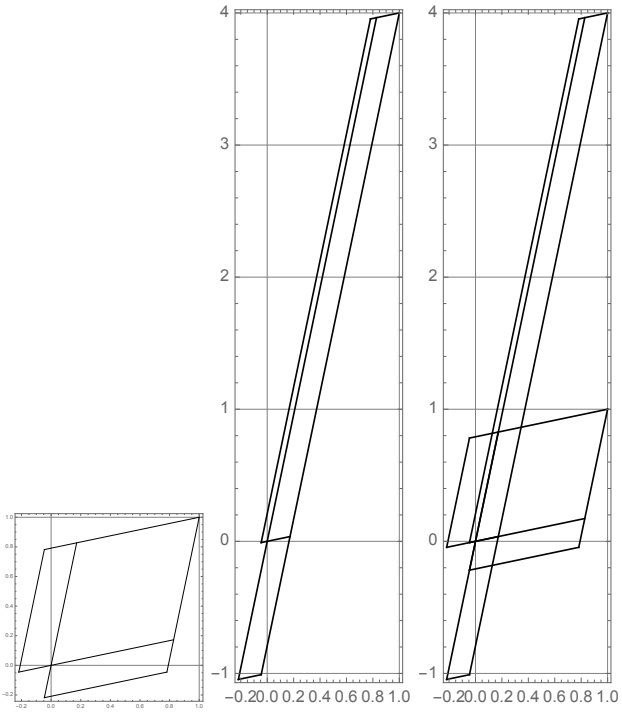

Figure 5.10: (a) The 3-rectangle partition for $s = 5$. (b) The first forward iterate of the partition. (c) I put (a) and (b) together so it obvious that the alphabet is from -1 to 4.

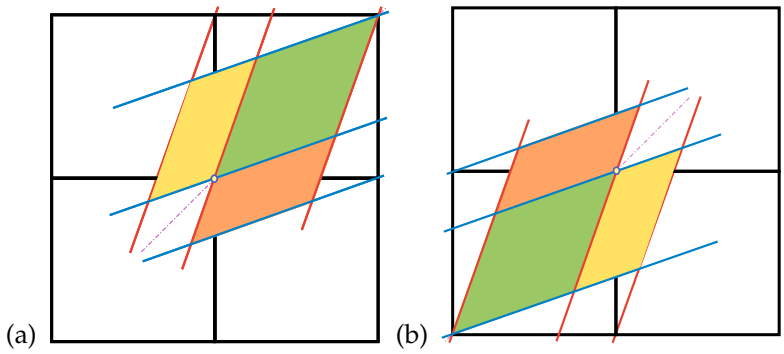

Figure 5.11: Abandoned attempt: (a) The three-rectangle, time reversal symmetric generating partition for the Percival-Vivaldi cat map (1.5), with borders given by cat map stable-unstable manifolds. (b) The three-rectangle partition obtained by space reversal (reflection across the anti-diagonal) is also a valid generating partition, but the distinct from (a). Thus this partition does not exhibit in a simple way the space reflection symmetry that is evident in figure 1.2.

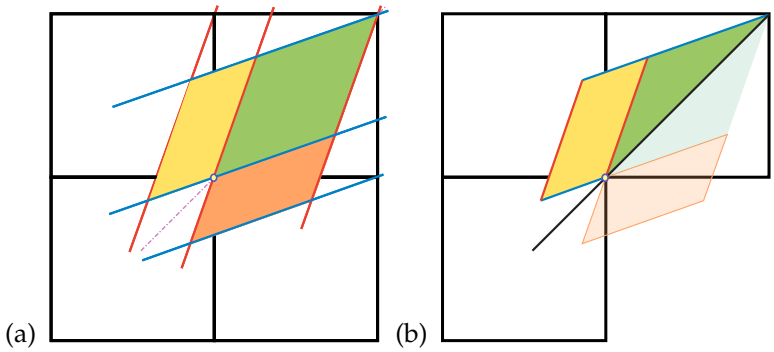

Figure 5.12: Abandoned attempt: (a) The three-rectangle, time reversal symmetric generating partition for the Percival-Vivaldi cat map (1.5), with borders given by cat map stable-unstable manifolds. Large rectangle is self-dual under time reversal (reflection across the diagonal), while the two small rectangles are mapped into each other. This implies that we should go to a fundamental domain (positive time only), and recode the dynamics according to sect. 1.9 $C_2 = D_1$ *factorization*: (b) The three-rectangle partition time reversal fundamental domain (the half of the full partition, cut in two by the time reflection diagonal). Need to check whether we can handle the reflection of m_n as well.

1. self-dual, here figure 5.5 (a) and (b), figure 5.6 (g), (h), (i) and (j)
   - even period cycles have $0, 2, 4, \cdots$ points on the diagonal
   - odd period cycles have $1, 3, 5, \cdots$ points on the diagonal (need to plot odd length cycles to see that they always have at least one point on the diagonal)
2. orbits that come in pairs, here figure 5.5 (c) $\leftrightarrow$ (d), (e) $\leftrightarrow$ (f)
3. There is also invariance of the cat map dynamics (1.8) spatial reflection flip across the $x_1 = -x_0$ anti-diagonal, together with $m_n \to -m_n$ so the full symmetry is in some sense $C_2 \times C_2$.
   - 1 copy, self-dual under both symmetries: figure 5.6 (h)
   - Figure 5.5 (a) $\leftrightarrow$ (b), self-dual under time reversal
   - Figure 5.5 (c) $\leftrightarrow$ (d) is self-dual under the second reflection
   - 4 copies (need to get longer cycles to see examples)
4. However, as figure 5.11 illustrates, the partition is only in part invariant under the spatial reflection, resulting in some cycles missing their spatial-reflection sisters:
   - Figure 5.5 (e) and (f)
   - Figure 5.6 (g) and (j)

2018-02-19 Predrag I wonder why all cycles (except for a small kink in $X_{01\underline{1}1}$) turn clockwise? Reminds me of harmonic oscillator, that also has a unique rotation direction - might be a consequence of symplectic dynamics.

2018-02-21 Predrag The time reversal symmetry fundamental domain is given in figure 5.12 (b). One needs to describe the symmetry reduced dynamics on the fundamental domain, as in ChaosBook.org *Figure 11.7*: "The bimodal Ulam sawtooth map restricted to the fundamental domain."

2018-02-21 Predrag The Green's function (5.12) and eigenvalues and eigenvectors (5.18) all have Toeplitz matrix structure. In case like this, when the problem has been around for centuries, reading literature is a great time saver, especially if someone has already done the dive into literature for you. You can understand your Mathematica results by the analytic solution for any cycle lengts and any s, for example (1.64) and (1.67). Here you learn, explicitly, that for $s > 2$, the lattice should not be expanded in Fourier modes, but in $\sinh$ and $\cosh$'s. There ae some other cute formulas in literatures, for example (1.75) and (1.124).

2018-02-27 Han I have read the Chapter 15 *Counting* of Chaosbook. It's not easy. Finally have some general ideas about the topological zeta function.

2018-02-18 Predrag Percival-Vivaldi alphabet can be made symmetric under spatial reflection by picking the origin in the middle of the unit interval, see sect. 1.2.1. The tiling figure 1.4 (b) and the partition figure 5.3 (b) suggests that partition should be centered differently to fully exploit the symmetries of the tiling - perhaps with the fixed point in the center of the square, rather with the fixed point in the corner.

5.2 Rhomboid center partition

Partitions, alphabets. A division of state space $\mathcal{M}$ into a disjoint union of distinct regions $\mathcal{M}_A, \mathcal{M}_B, \ldots, \mathcal{M}_Z$ constitutes a *partition*. Label each region by a symbol m from an N-letter *alphabet* $\mathcal{A} = \{A, B, C, \cdots, Z\}$, where $N = |\mathcal{A}|$ is the number of such regions. Alternatively, one can distinguish different regions by coloring them, with colors serving as the "letters" of the alphabet. For notational convenience, in alphabets we sometimes denote negative integer m by underlining them, as in $\mathcal{A} = \{-2, -1, 0, 1, 2\} = \{\underline{2}, \underline{1}, 0, 1, 2\}$.

A generating partition must map borders onto borders under dynamics (Adler-Weiss), but a really nice partition should also embody all symmetries of the dynamics; invariance under spatial reflections and the time reversal.

For the Percival-Vivaldi cat map the dynamics commutes with the spatial reflection σ (across anti-diagonal), while time reversal will require extra thinking.

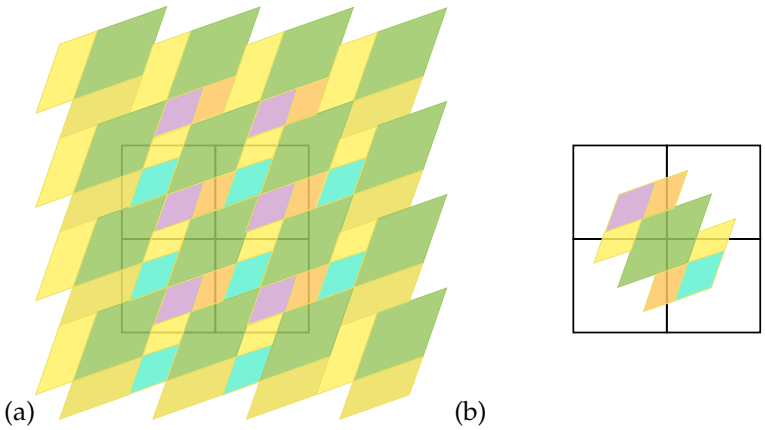

Figure 5.13: Abandoned attempt: (a) Tiling of the square lattice by a five-rectangle, time reversal and space reflection symmetric partition. Note that we have used the continuous translation invariance to place the center of the large tile A at the origin. (b) An almost a generating five-rectangle, time reversal and space reflection symmetric partition, except that the yellow / orange rectangles appear twice, so the area this covers exceeds the unit area.

For the Percival-Vivaldi cat map the flip across the $x_1 = x_0$ diagonal together with the reversal of the direction of evolution is the C_2 symmetry that corresponds to the invariance of cat map under time reversal.

2018-02-28 Predrag A proposal for a space and time symmetric partition in figure 5.13. Do you see how to fix it?

2018-02-28, 018-03-18 Han Yes! A space reflection symmetric partition in figure 5.13 is obtained by cutting the yellow and orange rectangles into halves, as shown in figure 5.14. That is natural in the centered unit square tiling of the plane, i.e., the grid going through multiples of $(1/2, 1/2)$. Figure 5.14 (c) shows that this partition tiles the whole space. The forward image of the partition of figure 5.14 (b) figure 5.15. Figure **??** is the labeled 7-rectangle partition, together with the transition graph. The alphabet is

$$m_t \in \{\underline{2}, \underline{1}, 0, 1, 2\}\,. \tag{5.23}$$

2018-03-05 Han All prime 4-cycles in the symmetric partition figure 5.14 (b)

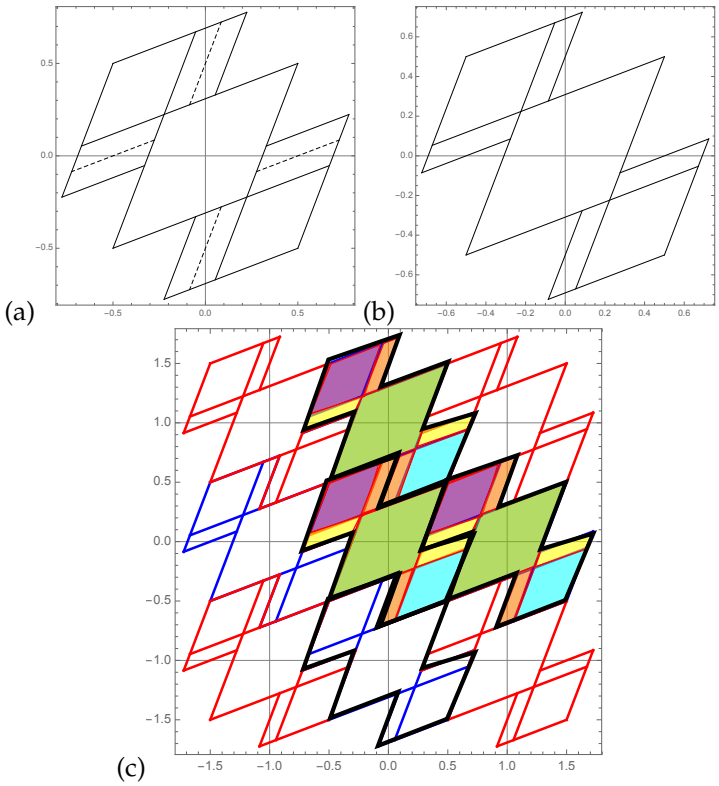

Figure 5.14: (a) Start with the partition of figure 5.13 (b). The dashed lines in the directions of stable and unstable manifolds cut the yellow and orange rectangles into halves. (b) The symmetric partition obtained by removing halves of yellow and orange rectangles has area 1. (c) The partition tiles the square lattice.

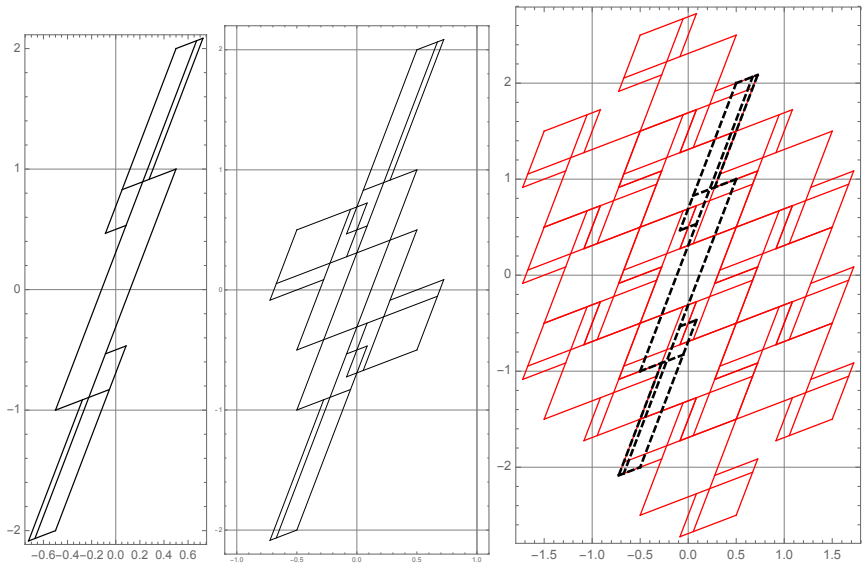

(a) (b) (c)

Figure 5.15: (a) The forward image of the 7-rectangle partition figure 5.14 (b). (b) The stretched partition overlaid over the original partition. (c) The stretched partition overlaid over the tiled lattice. The x and y axes are not plotted to the same scale.

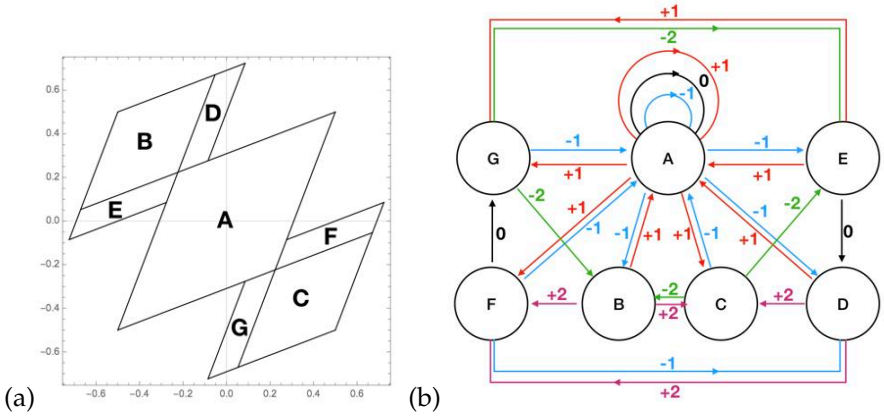

(a) (b)

Figure 5.16: (a) The labeled 7-rectangle partition, and (b) the corresponding 7-node transition graph.

are

$$
\begin{aligned}
\mathsf{X}_{11\underline{11}} &= \frac{1}{15}\begin{bmatrix} 5 & 5 & -5 & -5 \end{bmatrix}, & \mathsf{X}_{0\underline{2}02} &= \frac{1}{15}\begin{bmatrix} 0 & -10 & 0 & 10 \end{bmatrix} \\
\mathsf{X}_{001\underline{1}} &= \frac{1}{15}\begin{bmatrix} -1 & 1 & 4 & -4 \end{bmatrix}, & \mathsf{X}_{00\underline{1}1} &= \frac{1}{15}\begin{bmatrix} 1 & -1 & -4 & 4 \end{bmatrix} \\
\mathsf{X}_{1\underline{2}2\underline{1}} &= \frac{1}{15}\begin{bmatrix} 2 & -7 & 7 & -2 \end{bmatrix}, & \mathsf{X}_{2\underline{2}1\underline{1}} &= \frac{1}{15}\begin{bmatrix} 7 & -7 & 2 & -2 \end{bmatrix} \\
\mathsf{X}_{01\underline{1}1} &= \frac{1}{15}\begin{bmatrix} 4 & 6 & -1 & 6 \end{bmatrix}, & \mathsf{X}_{\underline{1}01\underline{1}} &= \frac{1}{15}\begin{bmatrix} -6 & -4 & -6 & 1 \end{bmatrix} \\
\mathsf{X}_{101\underline{2}} &= \frac{1}{15}\begin{bmatrix} 3 & 2 & 3 & -8 \end{bmatrix}, & \mathsf{X}_{\underline{1}01\underline{2}} &= \frac{1}{15}\begin{bmatrix} -3 & -2 & -3 & 8 \end{bmatrix}
\end{aligned}
\tag{5.24}
$$

The orbits are in figures 5.17 and 5.19. All orbits are symmetric about both $x_1 = x_0$ and $x_1 = -x_0$, either self-dual or come in pairs.

2018-03-05 Predrag Beautiful! We have the doubly symmetric partition nailed. I do not think this is anywhere in the literature. Can you connect to symmetries to cycle itineraries?

2018-04-08 Han I have recomputed the 4-cycles of (5.24) in the face-centered Percival-Vivaldi unit square non-partition. That screws up the above $\mathsf{X}_{101\underline{2}}$, $\mathsf{X}_{0\underline{2}02}$, and $\mathsf{X}_{\underline{1}01\underline{2}}$:

$$
\begin{aligned}
\mathsf{X}_{\underline{11}11} &= \frac{1}{15}\begin{bmatrix} -5 & -5 & 5 & 5 \end{bmatrix}, & \mathsf{X}_{\underline{1}010} &= \frac{1}{15}\begin{bmatrix} -5 & 0 & 5 & 0 \end{bmatrix} \\
\mathsf{X}_{001\underline{1}} &= \frac{1}{15}\begin{bmatrix} -1 & 1 & 4 & -4 \end{bmatrix}, & \mathsf{X}_{00\underline{1}1} &= \frac{1}{15}\begin{bmatrix} 1 & -1 & -4 & 4 \end{bmatrix} \\
\mathsf{X}_{1\underline{2}2\underline{1}} &= \frac{1}{15}\begin{bmatrix} 2 & -7 & 7 & -2 \end{bmatrix}, & \mathsf{X}_{2\underline{2}1\underline{1}} &= \frac{1}{15}\begin{bmatrix} 7 & -7 & 2 & -2 \end{bmatrix} \\
\mathsf{X}_{01\underline{1}1} &= \frac{1}{15}\begin{bmatrix} 4 & 6 & -1 & 6 \end{bmatrix}, & \mathsf{X}_{\underline{1}01\underline{1}} &= \frac{1}{15}\begin{bmatrix} -6 & -4 & -6 & 1 \end{bmatrix} \\
\mathsf{X}_{0001} &= \frac{1}{15}\begin{bmatrix} 3 & 2 & 3 & 7 \end{bmatrix}, & \mathsf{X}_{\underline{1}000} &= \frac{1}{15}\begin{bmatrix} -7 & -3 & -2 & -3 \end{bmatrix}
\end{aligned}
\tag{5.25}
$$

2018-03-05 Predrag I still think that if one day you plot all cycle *points* (no lines connecting them) on a single copy of the generating partition, you'll find the resulting picture very cute:)

A hint from literature: Percival and Vivaldi [14] write: "For the cat maps the periodic orbits lie on a rational lattice, so all surds cancel, as shown in the companion paper [15] on the number theory of the periodic orbits of the automorphisms of the torus."

Sect. 6.2 *Numbers of periodic orbits* and sect. 7.2.1 *Periodic orbits - first approach* might also help with developing some intuition about figure 5.21.

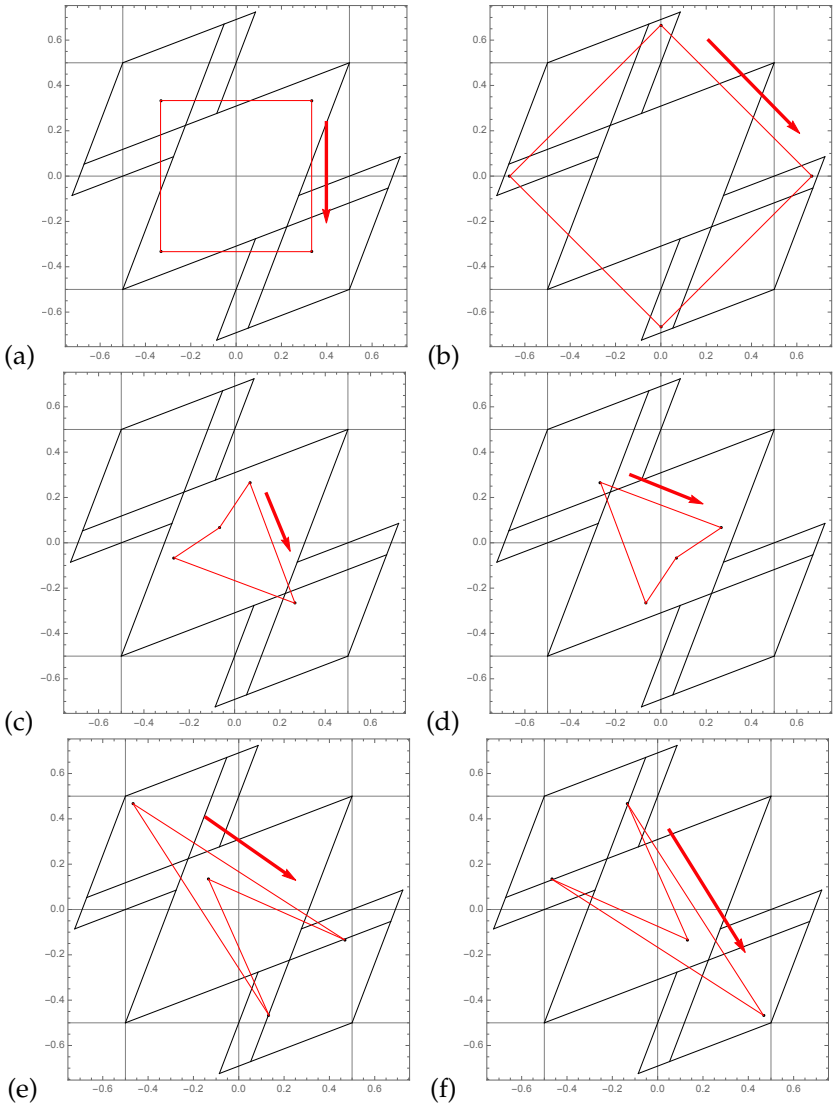

Figure 5.17: All 4-cycles from (5.24): (a) $X_{1\underline{111}}$ (b) $X_{0\underline{2}02}$, (c) $X_{001\underline{1}}$, (d) $X_{00\underline{11}}$, (e) $X_{\underline{1}1\underline{2}2}$, (f) $X_{2\underline{2}1\underline{1}}$, (g) to (j) continued in figure 5.19.

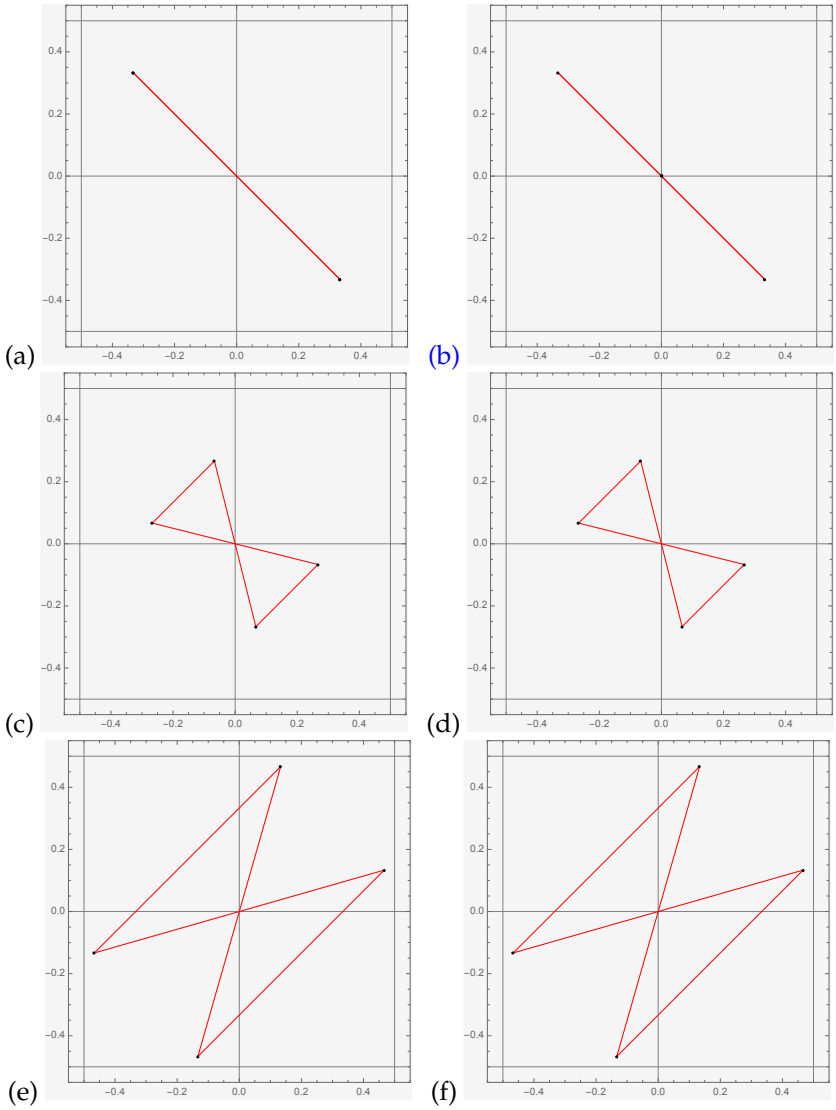

Figure 5.18: All 4-cycles from (5.25) plotted in "Lagrangian" coordinates $\{x_{t-1},\, x_{t+1}\}$, in the order of figure 5.17: (a) $X_{\underline{1}\underline{1}\underline{1}\underline{1}}$ is a "Laplacian" self-retracing 2-cycle (5.65). So is (b) $X_{\underline{1}010}$, once replotted as (5.66), the symmetric partition cycle $X_{0\underline{2}0\underline{2}}$; (c) $X_{0011\underline{1}}$, (d) $X_{00\underline{1}\underline{1}}$ and its time reversal (e) $X_{1\underline{2}\underline{2}\underline{1}}$ map into one cycle; and its time reversal (f) $X_{\underline{2}\underline{2}\underline{1}\underline{1}}$ map into one cycle; (g) to (j) continued in figure 5.20.

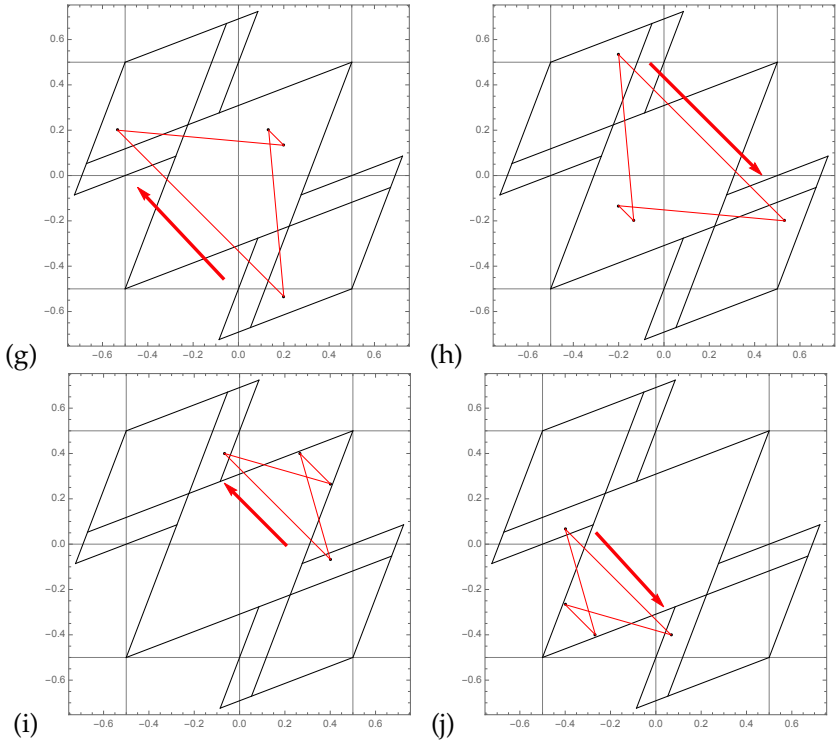

Figure 5.19: Continuation of figure 5.17: (g) X_{1012}, (h) X_{1012} (i) X_{0111}, and (j) X_{0111},

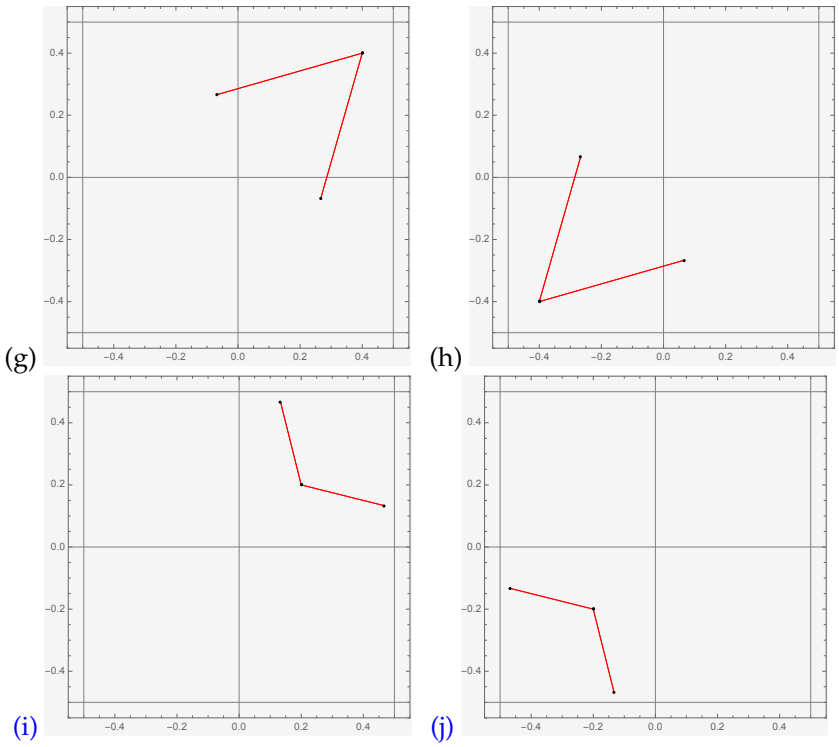

Figure 5.20: Continuation of figure 5.18 - the space reflection dual pairs: (g) $X_{01\underline{1}1}$ and its time reversal (h) $X_{\underline{1}01\underline{1}}$ map into space-reflection dual cycles; (i) X_{0001} (should be replotted as the symmetric partition $X_{101\underline{2}}$), and (j) $X_{\underline{1}000}$ (should be replotted as the symmetric partition $X_{\underline{1}01\underline{2}}$).

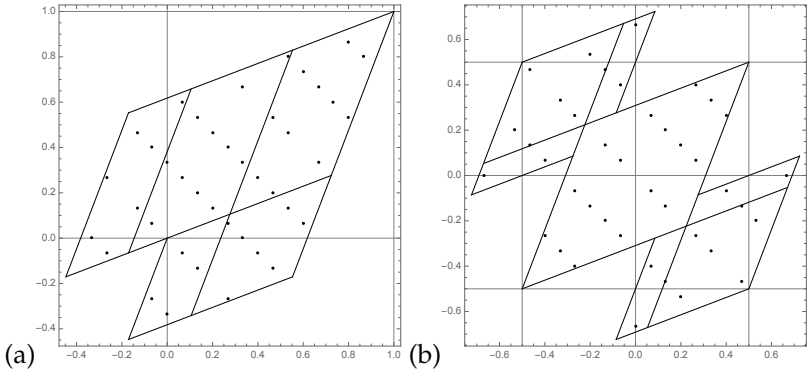

Figure 5.21: All prime 4-cycles periodic points in the partition of (a) figure 5.4, and (b) figure 5.14. The holes correspond to missing cycle-1 and cycle-2 points.

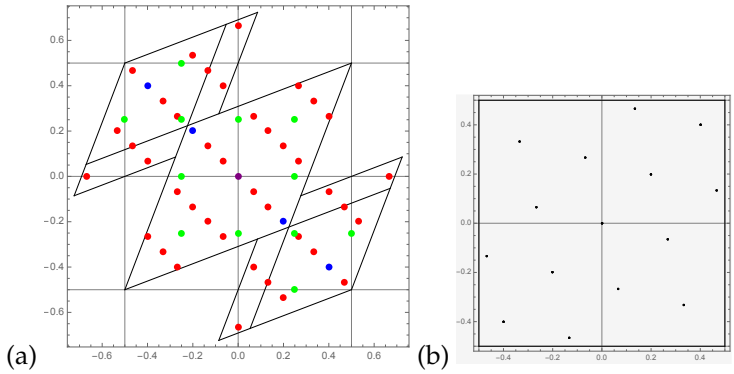

Figure 5.22: (a) All periodic points that belong to the 1 (purple), 2 (blue) and 4 (red) prime cycles, plotted in "Hamiltonian" coordinates $\{x_t,\ x_{t+1}\}$. The prime 1- and 2-cycles fill the holes between 4-cycles in the figure 5.21 (b). The 3 (green) cycles start a new grid, to be filled out by the prime 6, 9, etc cycles. (b) All periodic points that belong to the 4 prime cycles of figure 5.22 plotted in in "Lagrangian" coordinates $\{x_{t-1},\ x_{t+1}\}$, but modulo face centered unit square, rather than the "symmetric" partition indicated in (a). The numbers of prime cycles are listed in (5.14).

2018-03-15 Han In figure 5.21 I plotted all the cycle points on a single copy of the partition for both partitions of figures 5.4 and 5.14.

2018-03-22 Han I have added the 1, 2 and 3 cycles to figure 5.22. The 1 and 2 cycles fill the holes of figure 5.21 (b). Each of the 3-cycles has only one symmetry, and they have the other symmetry in pairs.

2018-03-13 Predrag An aside, not important, and in retrospect, not even right: going from the partition of figure 5.4 to the partition of figure 5.14 we have translated the origin to $\tilde{x}_t = x_t - 1/2$, so the map (1.5) is now

$$\begin{bmatrix} \tilde{x}'_{t+1} \\ \tilde{x}'_t \end{bmatrix} = \mathbf{A} \begin{bmatrix} \tilde{x}_t \\ \tilde{x}_{t-1} \end{bmatrix} - \frac{1}{2} \begin{bmatrix} 0 \\ s-2 \end{bmatrix} . \tag{5.26}$$

I'm not sure why we would be allowed to drop such translational terms. A cute fact is that Percival and Vivaldi [14] actually define the map (1.5) on $x_t \in [-1/2, 1/2]$ interval, i.e., without the translation term in (5.26). Such translations should not affect the map (it's the same automorphism of the torus, just in different coordinates) but I do not have a clean argument that they do not matter.

2018-03-15 Han We didn't change the origin when the partition changed from figure 5.4 to figure 5.14. The map is also not changed. What we did is changing the boundary of the partition. So the map is still:

$$\begin{bmatrix} x_{t+1} \\ x_t \end{bmatrix} = \mathbf{A} \begin{bmatrix} x_t \\ x_{t-1} \end{bmatrix} . \tag{5.27}$$

2018-04-08 Han I have plotted in figures 5.18 and 5.20. all 4-cycles in 'Lagrangian' coordinates $\{x_{t-1},\, x_{t+1}\}$, in the unit-square face centered partition of figure 5.16. The periodic orbits in this partition are given by (5.25) (which seems to be (5.24) modulo some cyclic permutations). Note that sometimes different solutions appear to have the same orbit, and that sometimes points belonging to different solutions appear in the same position. The reason is that given the field values x_{t-1} and x_{t+1} we cannot decide x_t without knowing the m_t. For example, the points $\{x_1,\, x_3\}$ for the first two solutions $\mathsf{X}_{\underline{1}\underline{1}11}$ and $\mathsf{X}_{\underline{1}010}$ are the same.

I also plotted all of the solutions in figure 5.22 (b). There are fewer points than figure 5.22 (a), because some of the points coincide. The 2-cycle and the fixed point solutions

$$\begin{aligned} \mathsf{X}_{\underline{1}1} &= \frac{1}{15}\begin{bmatrix} -3 & 3 \end{bmatrix}, \qquad \mathsf{X}_{\underline{2}2} = \frac{1}{15}\begin{bmatrix} -6 & 6 \end{bmatrix} \\ \mathsf{X}_0 &= \begin{bmatrix} 0 \end{bmatrix} \end{aligned} \tag{5.28}$$

also coincide with points of the 4-cycle solutions.

2018-04-05 Predrag Everything works like charm in the "Lagrangian" coordinates $\{x_{t-1},\, x_{t+1}\}$ formulation, also for 2-cycles: they are self-dual, as in (5.65), and the fixed point is very special, as it sits in the maximally invariant subspace.

5.3 Reduction to the fundamental domain

2018-03-07 Predrag While the original cell has edges of length 1, the quarter cells with edges of length $1/2$ are already set up for a reduction to $1/4$ fundamental domain, whose sides are the diagonal and the anti-diagonal. That might be the justification for halving the side-strips as you have done: the cutting line goes through the length $1/2$ lattice.

2018-03-11 Predrag Figure 5.23 (b) is cute. To me it suggests a 3-node (A, B, C) transition graph, with alphabet to be figured out.
(a) $\overline{1\underline{1}1\underline{1}} \to \overline{A}$? (on both space and time symmetry lines) and
(b) $\overline{0\underline{2}0\underline{2}} \to \overline{C}$ (space, time flip symmetric) are now fixed points.
(c) $\overline{00\underline{1}1}$ and (d) $\overline{0\underline{0}1\underline{1}}$ (2 points on space symmetry line) are now one 2-cycle $\to \overline{AB}$,
(e) $\overline{\underline{1}1\underline{2}2}$ and (f) $\overline{\underline{2}2\underline{1}1}$ (on space symmetry line) are now one 2-cycle $\to \overline{A?B?}$,
(g) $\overline{101\underline{2}}$ and (h) $\overline{\underline{1}0\underline{1}2}$ (time flip symmetric) are now one 2-cycle $\to \overline{A?B?}$,
(i) $\overline{0\underline{1}1\underline{1}}$, and (j) $\overline{0\underline{1}1\underline{1}}$ (time flip symmetric) are now one 2-cycle $\to \overline{AC}$.
This 3-partitions alphabet is not the right alphabet - still need to work out the the corresponding 5-letter transition graph links alphabet.

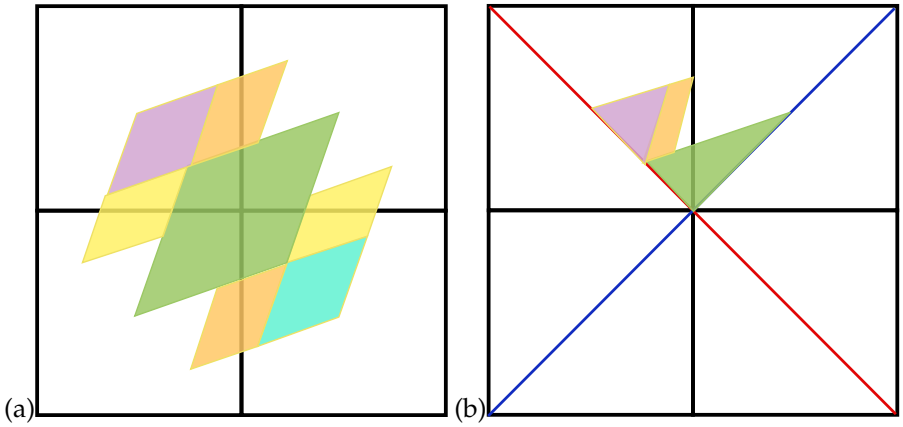

(a) (b)

Figure 5.23: Figure 5.13 (b) continued. (a) Almost correct time reversal and space reflection symmetric partition - the correct one is figure 5.14 (b). (b) Three triangles/rectangles fundamental domain partition. Could it be cuter?

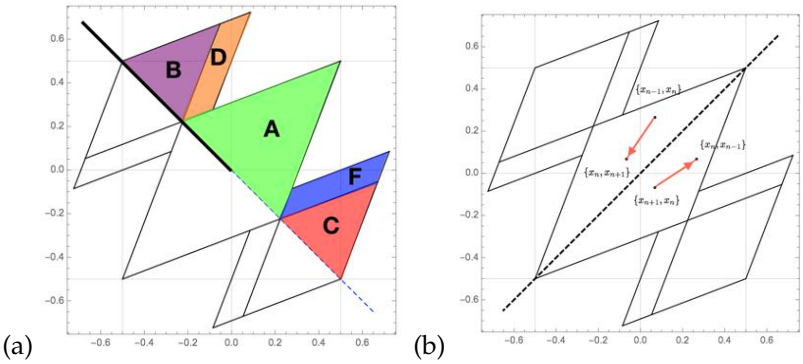

(a) (b)

Figure 5.24: (a) The labeled space inversion fundamental domain partition. (b) The 1-step orbit after *time reversal*.

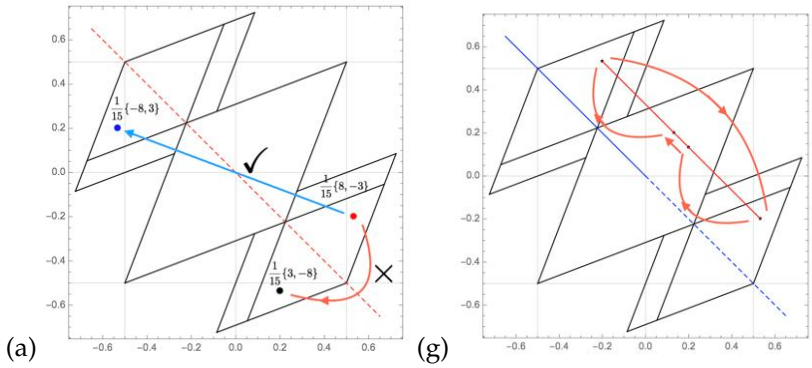

Figure 5.25: (a) The *space inversion* operation. Point $(-8/15, 3/15)$ happens to be a periodic point of period 4, cycle $\overline{1012} \to \overline{CAAB}$, see (5.17) (g,h). Actually, any fractional coordinate belongs to a periodic orbit. The orange line is here just to confuse you; under inversion $(3/15, -8/15)$ maps into $(-3/15, 8/15)$ (not drawn). (g) The two corresponding 4-cycles reduced to a single 4-cycle in the space inversion fundamental domain, $\overline{1012}$ and $\overline{1012} \to \overline{CAAB}$.

2018-03-15 Han The fundamental domain figure 5.23 (b) symbolic dynamics
(a) $\overline{1111} \to \overline{AB}$ (on both space and time symmetry lines, see figure 5.26 (a)) and
(b) $\overline{0202} \to \overline{C}$ (space, time flip symmetric) are now fixed points.
(c) $\overline{0011}$ and (d) $\overline{0011} \to \overline{AAAB}$,
(e) $\overline{1122}$ and (f) $\overline{2211} \to \overline{ABBB}$,
(g) $\overline{1012}$ and (h) $\overline{1012}$ (time flip symmetric) $\to \overline{AABB}$,
(i) $\overline{0111}$, and (j) $\overline{0111}$ (time flip symmetric) $\to \overline{AACC}$.

2018-03-22 Han If we reduce the partition by the spatial inversion symmetry, the fundamental domain is shown in figure 5.24 (a). Note that the boundary $\{0, 0\} \to \{\infty, -\infty\}$ goes to $\{0, 0\} \to \{-\infty, \infty\}$ after inversion. So for the boundary I only keep the points on $(\{0, 0\}, \{-\infty, \infty\})$ half-diagonal (the thick black line in figure **??** (a)). For example, consider the orbit of $\overline{1111}$. This orbit is shown in figure 5.26 (a). The inversion will move the point $\frac{1}{3}\{1, -1\}$ to $\frac{1}{3}\{-1, 1\}$, so I only keep the $\frac{1}{3}\{1, -1\}$ and discard $\frac{1}{3}\{-1, 1\}$ which is on the dashed line. Then this orbit become a 2-cycle $\overline{AB}$.

From figure 5.26 we can see that the rest of the cycles in figures 5.17 and 5.19 are:

(a) $\overline{1111} \to \overline{AB}$
(b) $\overline{0202} \to \overline{DF}$,
(c) $\overline{0011}$ and (d) $\overline{0011} \to \overline{AAAB}$,
(e) $\overline{1122}$ and (f) $\overline{2211} \to \overline{BBCA}$,
(g) $\overline{1012}$ and (h) $\overline{1012} \to \overline{CAAB}$,

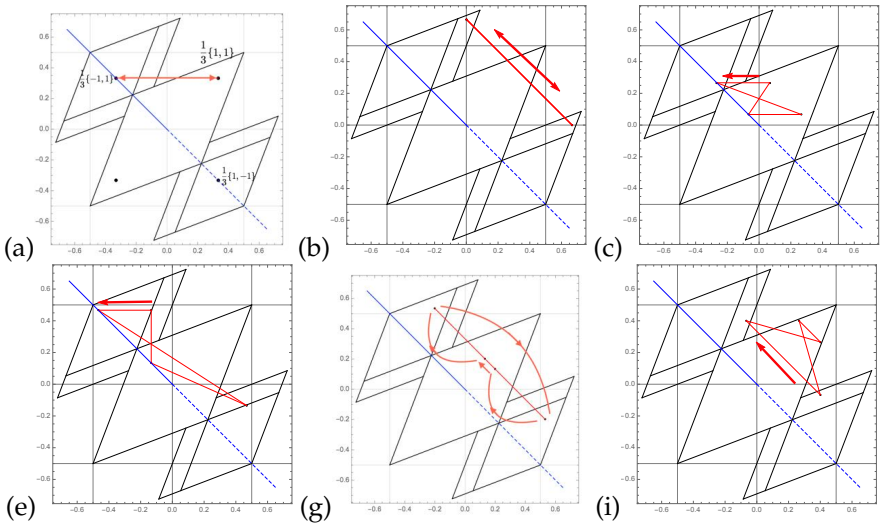

Figure 5.26: The orbits in the fundamental domain of 4-cycles (a) $\overline{11\underline{1}\underline{1}} \to \overline{AB}$ in the fundamental domain. (b) $\overline{0\underline{2}02} \to \overline{DF}$, (c) $\overline{001\underline{1}}$ and $\overline{00\underline{1}1} \to \overline{AAAB}$, (e) $\overline{\underline{1}1\underline{2}2}$ and $\overline{2\underline{2}1\underline{1}} \to \overline{BBCA}$, (g) $\overline{101\underline{2}}$ and $\overline{\underline{1}01\underline{2}} \to \overline{CAAB}$, (i) $\overline{01\underline{1}1}$, and $\overline{0\underline{1}1\underline{1}} \to \overline{AAFD}$. Compare with figures 5.17 and 5.19.

(i) $\overline{01\underline{1}\underline{1}}$, and (j) $\overline{0\underline{1}1\underline{1}} \to \overline{AAFD}$.
Now we have two 2-cycles but the rest of the 4-cycles are still 4-cycles. The two 2-cycles (blue points in figure 5.22) in the full domain are now fixed points.

2018-03-22 Han If we have a orbit $\{x_{n-1}, x_n\} \to \{x_n, x_{n+1}\}$, the time reversal will change this orbit to $\{x_{n+1}, x_n\} \to \{x_n, x_{n-1}\}$. Do a flip across the diagonal we will get the orbit after time reversal but the direction of the orbit also changed, as shown in figure 5.24 (b). I guess this is why the time reversal is more tricky...

5.4 Spatiotemporal cat map partition

Consider a d-dimensional hypercubic lattice, infinite in extent, with each site labeled by d integers $z \in \mathbb{Z}^d$. The d-dimensional *spatiotemporal cat map* is defined by the discrete screened Poisson equation equation

$$\begin{aligned}(-\Box + s - 2d)\, x_z &= m_z\,, \qquad m_z \in \mathcal{A}\,, \\ &\mathcal{A} = \{-(s+1)/2, \cdots, -1, 0, 1, 2, \cdots, (s+1)/2\}\,,\end{aligned} \tag{5.29}$$

where $x_z \in \mathbb{T}^1$. The map is smooth and fully hyperbolic for integer $s > 2d$.

For a discrete d-dimensional Euclidean space-time the Laplacian is given

by

$$\begin{aligned} \Box\, x_n &\equiv x_{n+1} - 2\, x_n + x_{n-1} && (5.30)\\ \Box\, x_{n_1 n_2} &\equiv (\Box_1 + \Box_2)\; x_{n_1 n_2} && (5.31)\\ \Box_1\, x_{n_1 n_2} &= x_{n_1+1, n_2} - 2\, x_{n_1 n_2} + x_{n_1-1, n_2} \\ \Box_2\, x_{n_1 n_2} &= x_{n_1, n_2+1} - 2\, x_{n_1 n_2} + x_{n_1, n_2-1} \end{aligned}$$

in $d = 1, 2, \cdots$ dimensions.

What role do the spatiotemporal neighbors play? The local strength of "turbulence" at each site is parameterized by the stretching parameter s. The effect of neighbors is to "calm down" the local turbulence by distributing the stretching parameter $s-2$ along the d directions in (5.29), effectively decreasing it as $s-2 \to s/d-2$,

$$\sum_{j=1}^{d} (-\Box_j + s/d - 2)\, x_z \;=\; m_z\,. \tag{5.32}$$

Assign to each site z a letter m_z from the alphabet $\mathcal{A}$. A particular fixed set of letters m_z corresponds to a particular lattice state $\mathsf{M} = \{m_z\} = \{m_{n_1 n_2 \cdots n_d}\}$, which yields a complete specification of the corresponding state X. In the lattice case, the *full shift* is the set of all d-dimensional symbol arrays that can be formed from the letters of the alphabet $\mathcal{A}$

$$\hat{\Sigma} = \{\{m_z\} : m_z \in \mathcal{A} \quad \text{for all} \quad z \in \mathbb{Z}^d\}\,. \tag{5.33}$$

A d-dimensional spatiotemporal field $\{x_z\}$ is determined by the corresponding *d-dimensional* spatiotemporal symbol array $\{m_z\}$. Consider next a finite block of symbols $\mathsf{M}_{\mathcal{R}} \subset \mathsf{M}$, over a finite rectangular $[\ell_1 \times \ell_2 \cdots \times \ell_d]$ lattice region $\mathcal{R} \subset \mathbb{Z}^d$. In particular, let M_p over a finite rectangular $[\ell_1 \times \ell_2 \cdots \times \ell_d]$ lattice region. be the $[\ell_1 \times \ell_2 \cdots \times \ell_d]$ d-periodic block of M whose repeats tile $\mathbb{Z}^d$.

Commuting discrete translations. For an autonomous dynamical system, the evolution law f is of the same form for all times. If f is also of the same form at every lattice site, the group of lattice translations, acting along jth lattice direction by shift d_j, is a spatial symmetry that commutes with the temporal evolution. A temporal mapping f that satisfies $f \circ d_j = d_j \circ f$ along the $d-1$ spatial lattice directions is said to be *shift invariant*, with the associated symmetry of dynamics given by the d-dimensional group of discrete spatiotemporal translations.

Periodic points, invariant d-tori. A state space point x_z is spatiotemporally *periodic* $x_z = x_{z+\ell_p}$ if its spacetime orbit returns to it after a finite lattice shift $\ell_p = (\ell_1, \ell_2, \cdots, \ell_d)$; the infinity of repeats of block M_p^∞ tiles the lattice is often denoted by a bar over the finite 'prime' block (the smallest such block) of symbols.

A *prime* cycle p is a single traversal of the orbit; its label is a block of $|p|$ symbols that cannot be written as a repeat of a shorter block. Each *periodic point* $x_{m_1 m_2 \cdots m_{|p|}}$ is labeled by the starting symbol m_1, followed by the next

$(|p|-1)$ steps of its future itinerary. The set of periodic points $\mathcal{M}_p$ that belong to a given periodic orbit form a *cycle*

$$p = \overline{m_1 m_2 \cdots m_{|p|}} = \{x_{m_1 m_2 \cdots m_{|p|}}, x_{m_2 \cdots m_{|p|} m_1}, \cdots, x_{m_{|p|} m_1 \cdots m_{|p|-1}}\}\,. \quad (5.34)$$

More generally, a state space point is *spatiotemporally periodic* if it belongs to an invariant d-torus, i.e., its symbolic representation is a block over region $\mathcal{R}$ defined by

$$\mathsf{M}_p = \mathsf{M}_{\mathcal{R}}\,, \qquad \mathcal{R} = \mathcal{R}^{[\ell_1 \times \ell_2 \times \cdots \ell_d]}\,, \quad (5.35)$$

that tiles the lattice state M periodically, with period ℓ_j in the jth lattice direction.

An $[\ell \times \ell]$ circulant matrix

$$C = \begin{bmatrix} c_0 & c_{\ell-1} & \dots & c_2 & c_1 \\ c_1 & c_0 & c_{\ell-1} & & c_2 \\ \vdots & c_1 & c_0 & \ddots & \vdots \\ c_{\ell-2} & & \ddots & \ddots & c_{\ell-1} \\ c_{\ell-1} & c_{\ell-2} & \dots & c_1 & c_0 \end{bmatrix}\,,$$

has eigenvectors (discrete Fourier modes) and eigenvalues $Cv_k = \lambda_k v_k$

$$\begin{aligned} v_k &= \frac{1}{\sqrt{\ell}}(1, \epsilon^k, \epsilon^{2k}, \dots, \epsilon^{k(\ell-1)})^{\mathrm{T}}\,, \qquad k = 0, 1, \dots, \ell-1 \\ \lambda_k &= c_0 + c_{\ell-1}\epsilon^k + c_{\ell-2}\epsilon^{2k} + \dots + c_1 \epsilon^{k(\ell-1)}\,, \end{aligned} \quad (5.36)$$

where

$$\epsilon = \mathrm{e}^{2\pi \mathrm{i}/\ell} \quad (5.37)$$

is a root of unity.

For example, the eigenvalues of the damped Poisson matrix (5.32) in $d = 1$ are

$$\lambda_k = s - \epsilon^k - \epsilon^{-k} = s - 2\cos(2k\pi k/\ell)\,. \quad (5.38)$$

The unitary matrix U obtained by stacking eigenvectors (5.36) into a Vandermonde matrix is the discrete Fourier transform S

$$U_{kj} = \frac{1}{\sqrt{\ell}} \mathrm{e}^{2\pi \mathrm{i} kj/\ell}\,, \quad (5.39)$$

which diagonalizes any circulant matrix C,

$$U^\dagger C U = \mathrm{diag}(\lambda)\,.$$

In d dimensions the discrete Fourier transform is no longer a 2-index matrix, but it acts tensorially,

$$U_{kz} = U_{k_1 k_2 \cdots k_d, n_d \cdots n_2 n_1} = \frac{1}{\sqrt{\ell_1 \cdots \ell_d}} \mathrm{e}^{2\pi \mathrm{i} \sum_{j=1}^d k'_j n_j/\ell_j}\,. \quad (5.40)$$

As the d translations commute, U diagonalizes the d-dimensional damped Poisson equation (5.32) yielding the Fourier-transformed field for each discrete d-dimensional Fourier component

$$\tilde{x}_k = \frac{1}{2d - s + 2\sum_{j=1}^{d} \cos(2\pi k_j/\ell_j)}\, \tilde{m}_k \,, \tag{5.41}$$

where $k = (k_1, k_2)\,, \tilde{x} = Ux\,, \tilde{m} = Um$, and U is the discrete Fourier transformation (5.40).

2018-03-05 Predrag Not sure you have ever worked through these formulas, so here they are as exercise 1.1 and exercise 1.2. Can you go through them, and fix both the formulation of the problems, and current sketches of the solutions?

2018-03-08 Han Wrote up solution 1.1 and solution 1.2. I have compared (1.119) with the Green's function of 4-cycles (5.12) for $s = 3$, but prefer to keep the actual calculations secret. Trust me: each cycle point matches.

Disposed of Predrag's wild guess (1.109) for the $d = 2$ Green's function. Wrote up solution 1.3.

2018-03-11 Predrag In $d = 2$ dimensions any solution X uniquely recovered from its symbolic representation M,

$$x_z = \sum_{z' \in \mathbb{Z}^2} g_{zz'} m_{z'}, \qquad g_{zz'} = \left(\frac{1}{-\Box + s - 4} \right)_{zz'} , \tag{5.42}$$

where $g_{zz'} = g_{nt,n't'}$, $z = (nt), z' = (n't') \in T^2_{[\ell_1 \times \ell_2]}$, is the Green's function for the 2-dimensional damped Poisson equation. A lattice state M is admissible if and only if all x_z given by (5.42) fall into the generating partition.

Take $\mathcal{R} = \mathcal{R}^{[\ell_1 \times \ell_2]}$ to be a rectangular region. Any $L \times T$ block of interior symbols $\mathsf{M} = \{m_z \in \mathcal{A}_0 | z \in \mathbb{Z}^2_{\rm LT}\}$,

$$\mathbb{Z}^2_{\rm LT} = \{z = (n,t) | n = 1, \ldots, L, t = 1, \ldots T\}\,,$$

is admissible and generates a invariant 2-torus solution. Its coordinate representation $\Gamma = \{x_z, z \in \mathbb{Z}^2_{\rm LT}\}$, is obtained by taking inverse of (5.29):

$$x_z = \sum_{z' \in \mathbb{Z}^2_{\rm LT}} \mathsf{g}^0_{zz'} m_{z'}, \qquad m_{z'} \in \mathcal{A}_0, \tag{5.43}$$

where $\mathsf{g}^0_{zz'}$ is the corresponding Green's function with periodic boundary conditions. The block $\mathsf{M} = \{m_{nt} \in \mathcal{A}\,,\ (n,t) \in \mathbb{Z}^2\}$ can be used as a 2-dimensional symbolic representation of the lattice system state.

2018-03-15 Han I have found a solution of the Green's function in 2-dimensional lattice in Morita [13] *Useful procedure for computing the lattice Green's function - square, tetragonal, and bcc lattices*. Our Green's function should be:

$$\mathsf{g}_{l't',lt} = \frac{1}{\pi^2}\int_0^\pi dy \int_0^\pi dz \frac{\cos[(l-l')y]\cos[(t-t')z]}{s-\cos y-\cos z}\,. \tag{5.44}$$

I threw this to Mathematica and it told me it's a hypergeometric function. Maybe it can be written in a easier form... I'm still trying.

2018-03-15 Predrag I had read Morita [13], and a number of similar papers, see sect. 3.8 Green's blog. We had used (5.44) in our paper [12], see (3.39). I would be very impressed if Mathematica fetched this bone you threw at it, and brought back anything intelligent. When you read this literature, be alert for what boundary conditions they use. We only need the periodic bc. Any other bc, such as Dirichlet, breaks translation invariance, and makes evaluation of Green's functions a very difficult problem.

I'm hoping we can simply verify a simple guess (the wrong guess (1.109) was not it), for any d, that would be so much simpler to write up.

2018-03-16 Predrag The bold and reckless proposal of **2018-03-05, 2018-03-11 Predrag** continued: I believe we have the lattice Green's functions in d dimensions nailed.

- consider a d-dimensional discretized torus, with $(n_1, n_2, ..., n_d)$ points along each direction
- for each lattice site z pick admissible block $\{m_z\}$ allowed by our generating partition for given s
- Do the d-dimensional discrete Fourier transform of our damped Poisson equation. This yields the Fourier-transformed field for each discrete d-dimensional Fourier component, where $\tilde{x} = Ux\,, \tilde{m} = Um$, and U is the discrete Fourier transformation (a stack of Fourier eigenfunctions).
- Then get the field in the original configuration space by the inverse Fourier transform (relax - it is just a matrix multiplication)

$$x = U^\dagger \tilde{x}\,. \tag{5.45}$$

I've been always asking myself what would a Fourier transform of a periodic orbit orbit look like, and what it would mean. Well, now we can plot $(\tilde{x}_k, \tilde{x}_{k+1})$ for each periodic orbit p, and ponder it.

(Han, continue at your leisure:)

2018-03-05 Predrag With 5-cycles I expect that you will find orbits that have only one or no symmetries.

2018-03-18 Predrag Staring at the partition of figure **??**: no wander I failed to draw it by hand. In figure **??** (b) there are little holes next to D and G and the weird overlaps $\mathcal{M}_D \cap f(\mathcal{M}_E)$, $\mathcal{M}_G \cap f(\mathcal{M}_F)$, it's a miracle that the partition works. You might want to check it for longer period orbits in $\mathcal{M}_D$.

2018-03-07 Predrag The alphabet (5.23) seems to make sense. Space reflection acts as

$$j \leftrightarrow \underline{j}\,. \tag{5.46}$$

The total translation (the sum of symbols) is zero (the orbit is periodic, standing) for all, except for figure 5.19 (i) and (j) which translate by ± 1 (the orbit is relative periodic, running).

The time reversal should reverse the order of symbols, which it seems to do, at least for figures 5.17 and 5.19:

$$(c,d)\ 001\underline{1} \leftrightarrow 00\underline{1}1\,, \quad (e,f)\ \underline{1}1\underline{2}2 \leftrightarrow 2\underline{2}1\underline{1}\,, \tag{5.47}$$

rest self-dual.

2018-03-18 Predrag As illustrated in figure **??** (a), dynamics commutes with the spatial reflection σ (across anti-diagonal), while time reversal will require extra thinking. Why don't you first implement symmetry reduction for the spatial reflection σ, with the fundamental domain the partition being half above the anti-diagonal in figure 5.23 (a), and we postpone figure 5.23 (b) for later?

2018-03-05,2018-03-18 Predrag I have flashed out in the above the bold and reckless proposal for symbolic dynamics in d dimensions. We probably do not need the $d = 2$ Green's function in configurations space, as all periodic orbits can be computed directly in the momentum space, then Fourier transformed.

2018-03-18 Predrag Check in $d = 1$ whether (5.41) together with the inverse Fourier transform (5.45) recovers any of your periodic orbits?

Does the circulant eigenvalue formula (5.36) explain your (5.18)?

2018-03-19 Predrag Does the inverse Fourier transform of the propagator in (5.41) reproduce the usual $d = 1$ configuration Green's function (1.106)?

2018-03-22 Han I think the operation corresponding to the spatial reflection $\{x_{n-1}, x_n\} \to \{-x_{n-1}, -x_n\}$ is not the reflection σ across the anti-diagonal but the rotation of π about the origin as shown in figure 5.25 (a).

2018-03-22 Predrag I might be wrong, but I would not go for a rotation interpretation - I think it is identical to the parity operation in case at hand. $x_t \in T^1$ is the only state space coordinate at lattice site t. Parity sends

$x_t \to -x_t$, $m_t \to -m_t$. It is a symmetry of the equations of motion, see (5.11) for the time-forward 2D version, or (5.29) for the $d = 1$ lattice formulation. To be able to rotate, you need to think of $x_t \in (-\infty, \infty)$ as embedded in 2 or 3 dimensions. That is motivated by our 2D plots, but not necessary.

I replaced "rotation" by "inversion" in your notes - if I am wrong, we can easily revert the commented-out parts.

2018-03-22 Predrag I think you have the spatial inversion fundamental nailed. What about the transition graph?

2018-03-22 Han In $d = 1$, (5.41) can recover the periodic orbits. (5.41) can be written as:

$$\tilde{\mathbf{x}} = \mathrm{diag}(\lambda)^{-1}\, \tilde{m}\,, \tag{5.48}$$

where λ is the eigenvalue of the damped Poisson matrix (5.32). Then we have:

$$\mathbf{x} = U^\dagger\, \mathrm{diag}(\lambda)^{-1} U\, m\,, \tag{5.49}$$

When $d = 1$, $s = 3$ and $n = 4$ (4-cycles),

$$\mathrm{diag}(\lambda)^{-1} = \begin{pmatrix} 1 & 0 & 0 & 0 \\ 0 & 3 & 0 & 0 \\ 0 & 0 & 5 & 0 \\ 0 & 0 & 0 & 3 \end{pmatrix} \tag{5.50}$$

Then the Green's function for 4-cycle is:

$$\mathsf{g} = U^\dagger\, \mathrm{diag}(\lambda)^{-1} U = \frac{1}{15} \begin{pmatrix} 7 & 3 & 2 & 3 \\ 3 & 7 & 3 & 2 \\ 2 & 3 & 7 & 3 \\ 3 & 2 & 3 & 7 \end{pmatrix} \tag{5.51}$$

which is same as (5.12).

Using (5.36) we can also get the result of (5.18).

2018-03-22 Predrag Trying to incorporate dynamics into a generalized, time-reversal invariant Laplacian by replacing a time forward cat map A by something like a time reversal invariant combination $AA^\top$:

Incidence matrix B entries are $b_{ij} = \pm 1$, depending on whether v_i is a *target* or a *source*.

For the finite transition graph figure 5.4 (d) and (5.19) the incidence matrix is (PC - looks wrong, literature discusses 'simple' graphs, i.e., graphs without 1-loops)

$$\begin{bmatrix} \phi'_A \\ \phi'_B \end{bmatrix} = B\phi = \begin{bmatrix} 2 & 1 \\ -1 & 1 \end{bmatrix} \begin{bmatrix} \phi_A \\ \phi_B \end{bmatrix} \tag{5.52}$$

and

$$BB^\top = \begin{bmatrix} 2 & 1 \\ -1 & 1 \end{bmatrix} \begin{bmatrix} 2 & -1 \\ 1 & 1 \end{bmatrix} = \begin{bmatrix} 5 & -1 \\ -1 & 2 \end{bmatrix} . \tag{5.53}$$

Actually, we need something that acts on the whole chain, some Toeplitz matrix like

$$BB^\top \text{“}=\text{”} - \begin{bmatrix} -2 & 1 & & & & & 1 \\ 1 & -2 & 1 & & & & \\ & 1 & -2 & 1 & & & \\ & & & 1 & & \ddots & \\ & & & & & & 1 \\ 1 & & & & & 1 & -2 \end{bmatrix} , \tag{5.54}$$

but with 2 fields $[\phi_{A,t}, \phi_{B,t}]^\top$ at each site t.

Proposition 17.2. [Godsil and Royle [11]] Given any directed graph G if B is the incidence matrix of G, A is the adjacency matrix of G, and D is the degree matrix such that $D_{ii} = d(v_i)$, then

$$BB^\top = D - A . \tag{5.55}$$

The matrix $L = D - A$ is called the (unnormalized) graph Laplacian of the graph G. $BB^\top$ is independent of the orientation of G and D-A is symmetric, positive, semidefinite; that is, the eigenvalues of D.

Each row of L sums to zero (because $B^\top \mathbf{1} = 0$). Consequently, the vector $\mathbf{1}$ is in the nullspace of L.

2018-03-26 Predrag I have a hunch that the partition can be related to the Lagrangian (the generating function).

Area-preserving maps that describe kicked rotors subject to a discrete time sequence of angle-dependent impulses $P(x_n)$ of form (1.77), (1.78) have a *generating function* (1.79)

$$F(q_n, q_{n+1}) = \frac{1}{2}(q_n - q_{n+1})^2 - V(q_n)^2 , \qquad P(q) = -\frac{dV(q)}{dq} . \tag{5.56}$$

This generating function is the discrete time Lagrangian for a particle moving in potential $V(x)$. Eq. (1.77) says that in one time step Δt the configuration trajectory starting at x_n reaches $x_{n+1} = x_n + p_{n+1}\Delta t$, and (1.78) says that at each kick the angular momentum p_n is accelerated to p_{n+1} by the force pulse $P(x_n)\Delta t$.

2018-03-05 Predrag In $d = 2$ case compute the eigenvalues, eigenvectors for $s = 5$ and the transition graph (I think you already have them). Then you can test it by generating a bunch of admissible [2×2] or [3×2] or [4×2] blocks. The number of distinct ones can be reduced by reflection symmetries. It is not clear to me which ones are admissible, as yet, so you

can generate all, solve by inverting corresponding the doubly-periodic 2-tori Toeplitz (tensor) matrix → Green's function which gives you doubly-periodic lattice states. Then you can check which ones are within your Adler-Weiss partition.

2018-03-29 Han In $d = 2$ dimensions the Green's function $\mathsf{g}_{zz'} = g_{\ell t,\ell' t'}$, $z = (\ell t), z' = (\ell' t') \in T^2_{(n_1,n_2)}$ is a $[3 \times 3] \times [3 \times 3]$ tensor. Using the tensor Fourier transform (5.40), I calculated several periodic $[3 \times 3]$ blocks, with $z = (\ell t), z' = (\ell' t') \in T^2_{(3,3)}$. For example, the symbol blocks and the corresponding 9 field values of two admissible 2-torus states are, in the notation of (5.35),

$$\mathsf{M}_1 = \begin{pmatrix} 1 & 0 & 0 \\ 0 & 1 & 0 \\ 0 & 0 & 1 \end{pmatrix} \Rightarrow \quad \mathsf{X}_1 = \frac{1}{14} \begin{pmatrix} 6 & 4 & 4 \\ 4 & 6 & 4 \\ 4 & 4 & 6 \end{pmatrix} \tag{5.57}$$

$$\mathsf{M}_2 = \begin{pmatrix} 1 & 0 & 0 \\ 0 & 1 & 2 \\ 0 & 0 & 1 \end{pmatrix} \Rightarrow \quad \mathsf{X}_2 = \frac{1}{14} \begin{pmatrix} 8 & 6 & 7 \\ 7 & 9 & 12 \\ 6 & 6 & 9 \end{pmatrix} \tag{5.58}$$

In this calculation I used the Percival-Vivaldi partition of figure 1.2, with $0 \leq x < 1$, and $s = 5$.

As the blocks are doubly periodic, a single prime 2-torus p represents all vertical and horizontal cyclic permutations of the corresponding symbol block M_p. Furthermore, by lattice symmetries, M_p related by reflection and axes interchange symmetries are equivalent, (and -not sure of this- by the site symmetries, also internally space and time reversed) states are equivalent.

In $d = 1$ dimension, the Percival-Vivaldi partition alphabet is an $s = (s-2)+2$ letter alphabet (5.22). It has been shown in Gutkin *et al.* [12] that in $d = 2$ dimensions the Percival-Vivaldi partition $s+3 = (s-4)+7$ letter alphabet $\mathcal{A} = \mathcal{A}_0 \cup \mathcal{A}_1$ can be split into into the interior $\mathcal{A}_0$ and exterior $\mathcal{A}_1$ alphabets

$$\mathcal{A}_0 = \{0, \ldots, s-4\}, \quad \mathcal{A}_1 = \{\underline{3}, \underline{2}, \underline{1}\} \cup \{s-3, s-2, s-1\}\,. \tag{5.59}$$

For example, for $s = 5$ the interior, respectively exterior alphabets are

$$\mathcal{A}_0 = \{0, 1\}, \quad \mathcal{A}_1 = \{\underline{3}, \underline{2}, \underline{1}\} \cup \{2, 3, 4\}\,. \tag{5.60}$$

If all m_z belong to $\mathcal{A}_0$ then $\mathsf{M} = \{m_z | z \in \mathbb{Z}^2\}$ is a full shift (5.33). In particular, the above M_1 is admissible, while M_2 could have been pruned (in this case the explicit calculation shows it is admissible).

2018-03-29 Predrag Make sure you understand the alphabet (5.60). My alphabet (5.29) might be wrong; for s large the number of letters does grow as s, but I do not quite see what corresponds to the $\mathcal{A}_1$ letters. It has something to do with distributing s between d dimensions, as in (5.32).

2018-03-29 Predrag We'll have to think of how to visualize the states X, something analogous to figure 5.17. There is no preferred time evolution direction, so it does not make sense to connect them by lines. But the states will align on lattices, as in figure 5.22.

2018-03-29 Predrag Keeping in mind where we want to go with this, might be better to use spatially-symmetric, unit-square face centered partition (5.29), rather than the unit-square corner (vertex?) partition of figure 1.2.

2018-03-30 Predrag regarding your Tuesday, April 3 **Diffusion confusion** presentation: use it as a motivation for learning some theory applicable to your spatiotemporal cat map project. Do not do too much in the class, just work out a few things in full detail (otherwise nobody learns anything).

Read ChaosBook.org Chapter 24 *Deterministic diffusion*. You also might find my online lectures, Week 13 helpful. Maybe also have a glance at ChaosBook.org Appendix A24 *Deterministic diffusion*. As Dan has already covered everything, you can pick and chose: maybe redo the 1-dimensional example sect. 24.2 *Diffusion induced by chains of 1-dimensional maps* using the discrete Fourier that you are using for cat maps? Doing some nontrivial partitions, as in figure 24.4 of example 24.4?

My Group Theory course birdtracks.eu/courses/PHYS-7143-17 might be of interest. Cyclic group C_n shows up in week 2 Examples 2.3 and 2.4.

Because of the reflection symmetries, the cat map and spatiotemporal cat map symmetry is actually not C_n, but the dihedral group D_n, whose irreducible representations are not the complex 1-dimensional $\exp(2\pi \mathrm{i} kj/\ell)$, but the real 2-dimensional $(\cos(2\pi \mathrm{i} kj/\ell), \sin(2\pi \mathrm{i} kj/\ell)$, see week 4 Exercises 4.3 and 4.4.

The most important for you is week 8 *Space groups*. The symmetries of our spatiotemporal cat map are summarized by figure 8.1 and in the exercise 8.1. *Band structure of a square lattice*. The elastic (not chaotic) cousin of spatiotemporal cat map is described in sect. 8.2 *Elastodynamic equilibria of 2D solids*.

The whole course is a subversion repository that I can give you access to, if you want to reuse any of the LaTeX, or see the solution sets.

2018-04-05 Han I have calculated all admissible [2×2] periodic blocks in the unit-square face centered partition, $-\frac{1}{2} \le x_{n_1 n_2} < \frac{1}{2}$, for $s = 5$. The alphabet is:

$$\mathcal{A} = \{-4, -3, -2, -1, 0, 1, 2, 3, 4\} \tag{5.61}$$

Using the coordinates $\{x_{l-1,t}, x_{l,t-1}, x_{l,t}\}$ to represent a point in the block, I plot all periodic points of the admissible blocks in a 3-dimensional unit cube, as shown in figure 5.27.

2018-04-05 Predrag Were there any inadmissible blocks in the unit-square face centered partition? Or are you using the transition graph for $s = 5$ to generate only admissible blocks?

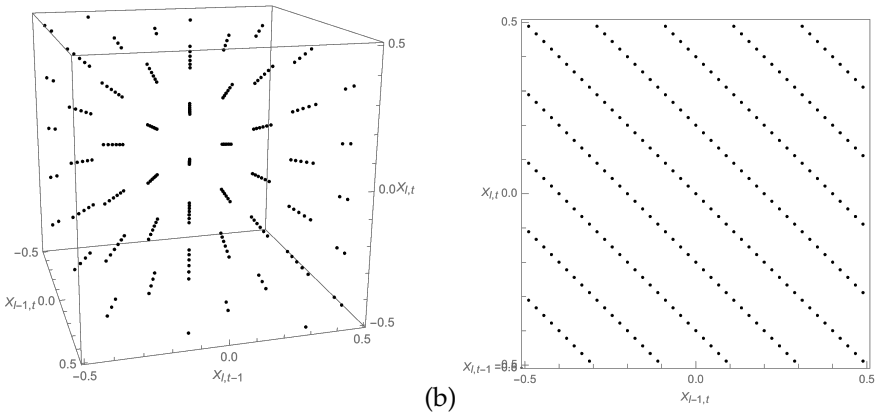

Figure 5.27: (a) All of the points in the periodic [2×2] blocks. The coordinates of each points are $x_{l-1,t}$, $x_{l,t-1}$ and x_{lt}. (b) The front view of (a). Clearly these points are arranged in lines.

2018-04-05 Predrag The visualization of figure 5.27 is quite interesting. All periodic points $x_{n_1 n_2}$ have the same denominator?

2018-04-05 Predrag If you want to have a 2-dimensional visualisation for each block analogous to (5.57), color the symbol M_j $[\ell_1 \times \ell_2]$ block with 9 discrete color alphabet $\mathcal{A}$ from (5.61), and the corresponding state X_j $[\ell_1 \times \ell_2]$ block with colors chosen from a continuum color strip.

2018-04-05 Predrag As this is a linear problem, you can also represent closeness of two $[\ell_1 \times \ell_2]$ blocks by using this coloring scheme for $\mathsf{M}_2 - \mathsf{M}_1$ and $\mathsf{X}_2 - \mathsf{X}_1$. To find the closest "distance" between 2-tori, you will have to go through all cyclic permutations of the second one to align it optimally (or, if you understand ChaosBook course, you'll have to 'slice').

For pairs of distinct 2-tori which share the same region of m_z's, or a single 2-torus in which the same region of m_z's appears twice, the states x_z in the center of the region should be exponentially close, in order to argue that they shadow each other.

This is illustrated in ref. [12], but there we do not use the linearity to actually subtract $\mathsf{X}_2 - \mathsf{X}_1$.

2018-04-05 Predrag Mark the lattice point z with the minimal value of $|x_z^{(2)} - x_z^{(1)}|$ on above graphs, and in the text state the minimal value of $|x_z^{(2)} - x_z^{(1)}|$.

You can also state the mean Euclidean (or L2) distance between the two

invariant 2-tori:

$$d_{\mathsf{X}_2-\mathsf{X}_1} = \left(\frac{1}{LT} \sum_z (x_z^{(2)} - x_z^{(1)})^2 \right)^{1/2} , \tag{5.62}$$

or distance averaged over the lattice points restricted a region $\mathcal{R}$.

An aside: not sure that the Euclidean distance is the correct one. A better one might be the overlap, with the Green's function sandwiched something like

$$\frac{\mathsf{X}_2{}^\top \mathsf{g} \mathsf{X}_1}{\mathsf{X}_2{}^\top \mathsf{X}_1} \tag{5.63}$$

correctly normalized (as it stands, it is dimensionally wrong - is this "fidelity"?), and maximized by going through all cyclic permutations of X_2 (to align it optimally, or by 'slicing'). The overlap is maximal for $\mathsf{X}_2 = \mathsf{X}_1$, and falls off exponentially, depending on how much of the two invariant 2-tori differ.

The correct distance really should be the difference between two actions - that is symplectically invariant.

2018-04-05 Han This problem probably is not important. And I might be wrong. In the [2×2] blocks if we use the unit-square corner partition, we have the symbol block and the corresponding 4 field values:

$$\mathsf{M} = \begin{pmatrix} 1 & 1 \\ 1 & 1 \end{pmatrix} \Rightarrow \quad \mathsf{X} = \begin{pmatrix} 1 & 1 \\ 1 & 1 \end{pmatrix} \tag{5.64}$$

which is not admissible, since for the unit-square corner partition the range of the field values is $0 \leq x_{lt} < 1$. But if all m_z belong to $\mathcal{A}_0 = \{0, 1\}$ then $\mathsf{M} = \{m_z | z \in \mathbb{Z}^2\}$ should be a full shift (according to (5.60)).

2018-04-05 Predrag This, I think, is important (search for 'Manning' in this blog), and we have to understand it. I think you have to define *all* partition regions *including* the borders, in this example as $0 \leq x_{lt} \leq 1$, and then take care of over-counting the border points, such as (5.64) by quotienting the zeta function as in (1.46).

2018-04-05 Predrag Everything works like charm in the "Lagrangian" coordinates $\{x_{t-1},\, x_{t+1}\}$ formulation, except that you should fix a few cycles in figure 5.22 (b), figures 5.18 and 5.20: so far you are plotting periodic points in Percival-Vivaldi face centered unit square non-partition, rather than our 7-region partition. Please replace all plots by plots with the 7-rectangle partition of figure 5.14 (b) indicated, as in figure 5.17.

If

$$\mathsf{X}_{11\underline{11}} = \frac{1}{15} \begin{bmatrix} 5 & 5 & -5 & -5 \end{bmatrix}$$

then points on the orbit are (ignoring the 1/15 factor) a self-retracing 2-cycle

$$(x_{t-1}, x_{t+1}) = \{(-5,5),(5,-5),(5,-5),(-5,5),\} = \mathsf{X}_{1\underline{1}} + \mathsf{X}_{1\underline{1}}{}^{\top} . \quad (5.65)$$

If

$$\mathsf{X}_{0\underline{2}02} = \frac{1}{15}\begin{bmatrix} 0 & -10 & 0 & 10 \end{bmatrix}$$

then points on the orbit are (ignoring the 1/15 factor) a self-retracing 2-cycle

$$(x_{t-1}, x_{t+1}) = \{(10,-10),(0,0),(-10,10),(0,0)\} = \mathsf{X}_{0\underline{2}} + \mathsf{X}_{0\underline{2}}{}^{\top} , \quad (5.66)$$

where '+' stands for string concatenation.

All this is very instructive about how "Laplacian" graphs implement time-reversal invariance. My hunch is that the correct formulation is a "Laplacian" representation such as (5.55). Briefly, B is the (directed) incidence matrix of our directed graph G transition graph, giving us our 7-rectangles partition, and A is the adjacency matrix of (undirected) G.

(Read also sect. 4.1.1.)

That gives us a reformulation of directed graphs as undirected graphs, and maybe we will know how to do it directly, rather than via (to me unappealing) Ihara zeta functions route.

We still have to take care of space-reversal invariance. I think we need to go to the fundamental domain figure 5.24 (a).

No one ever promised us A Rose Garden :)

References

[1] R. L. Adler and B. Weiss, "Entropy, a complete metric invariant for automorphisms of the torus", Proc. Natl. Acad. Sci. USA **57**, 1573–1576 (1967).

[2] R. L. Adler and B. Weiss, *Similarity of automorphisms of the torus*, Vol. 98, Memoirs Amer. Math. Soc. (Amer. Math. Soc., Providence RI, 1970).

[3] V. I. Arnol'd and A. Avez, *Ergodic Problems of Classical Mechanics* (Addison-Wesley, Redwood City, 1989).

[4] N. Bird and F. Vivaldi, "Periodic orbits of the sawtooth maps", Physica D **30**, 164–176 (1988).

[5] S. C. Creagh, "Quantum zeta function for perturbed cat maps", Chaos **5**, 477–493 (1995).

[6] P. Cvitanović, "Charting the state space", in *Chaos: Classical and Quantum*, edited by P. Cvitanović, R. Artuso, R. Mainieri, G. Tanner, and G. Vattay (Niels Bohr Inst., Copenhagen, 2018).

[7] P. Cvitanović, "Walkabout: Transition graphs", in *Chaos: Classical and Quantum*, edited by P. Cvitanović, R. Artuso, R. Mainieri, G. Tanner, and G. Vattay (Niels Bohr Inst., Copenhagen, 2018).

[8] P. Cvitanović, R. Artuso, R. Mainieri, G. Tanner, and G. Vattay, *Chaos: Classical and Quantum* (Niels Bohr Inst., Copenhagen, 2017).

[9] P. Cvitanović, R. Artuso, L. Rondoni, and E. A. Spiegel, "Transporting densities", in *Chaos: Classical and Quantum*, edited by P. Cvitanović, R. Artuso, R. Mainieri, G. Tanner, and G. Vattay (Niels Bohr Inst., Copenhagen, 2017).

[10] R. L. Devaney, *An Introduction to Chaotic Dynamical systems*, 2nd ed. (Westview Press, 2008).

[11] C. Godsil and G. . Royle, *Algebraic Graph Theory* (Springer, New York, 2013).

[12] B. Gutkin, L. Han, R. Jafari, A. K. Saremi, and P. Cvitanović, Linear encoding of the spatiotemporal cat map, In preparation, 2018.

[13] T. Morita, "Useful procedure for computing the lattice Green's function - square, tetragonal, and bcc lattices", J. Math. Phys. **12**, 1744–1747 (1971).

[14] I. Percival and F. Vivaldi, "A linear code for the sawtooth and cat maps", Physica D **27**, 373–386 (1987).

[15] I. Percival and F. Vivaldi, "Arithmetical properties of strongly chaotic motions", Physica D **25**, 105–130 (1987).

Chapter 6

Frequencies of Cat Map Winding Numbers

Rana Jafari Summer 2016 Report

6.1 Introduction

The linear mapping A on unit 2-torus is defined as follows:

$$A = \begin{pmatrix} a & 1 \\ ab-1 & b \end{pmatrix}$$

$$\begin{pmatrix} q_{t+1} \\ p_{t+1} \end{pmatrix} = A \begin{pmatrix} q_t \\ p_t \end{pmatrix} \qquad \mathrm{mod}\ 1 \tag{6.1}$$

Such 'toral automorphisms' provide very simple examples of chaotic Hamiltonian dynamical system. The unit determinant results in measure preservation, and $|\mathrm{tr}\,(A)| > 2$ in hyperbolicity. We shall refer to the $s = 3$ case as the 'Arnol'd cat map' (also known as the Arnol'd-Sinai cat map [1, 3]), and to cases where integer $s > 3$ as 'cat maps'. The integers obtained by taking modulo 1 can be interpreted as winding numbers [6]. Rational and irrational initial coordinates generate periodic and ergodic orbits, respectively. The properties of periodic orbits are studied in detail by Percival and Vivaldi [7]. The initial part of this report focuses on finding the frequencies of winding numbers generated by the iterations of map (6.1) for different integer values of $s = \mathrm{tr}\, A$. These frequencies enable us to find the areas of partitions in phase space corresponding to words of symbolic dynamics of Arnol'd cat map. In sect. 6.4 we apply these methods to computation of the frequencies of symbol patterns for spatiotemporal cat maps.

6.2 Numbers of periodic orbits

The number of period-n periodic points of the $[2\times 2]$ matrix transformation $\mathbf{A}$ on a unit torus $[0,1)\times[0,1)$, is equal to number of fixed points of transformation $\mathbf{A}^n$. [1] We can find this number by solving:

$$\mathbf{A}^n\mathbf{x}_0 = \mathbf{x}_0 \qquad \mod 1 \tag{6.2}$$

$$\Rightarrow (\mathbf{A}^n - \mathbf{I})\,\mathbf{x}_0 = \mathbf{v}$$

where $\mathbf{v}$ is an integer valued column vector. The number of solutions to (6.2) is equal to $|\det(\mathbf{A}^n - \mathbf{I})|$. Since the $(\mathbf{A}^n - \mathbf{I})\mathbf{x}_0$ transforms unit square to parallelogram with area $|\det(\mathbf{A}^n - \mathbf{I})|$, the parallelogram covers the unit square $|\det(\mathbf{A}^n - \mathbf{I})|$ times. By direct calculation, or by the $[2\times 2]$ matrix identity

$$\det(\mathbf{A}+\mathbf{B}) = \det(\mathbf{A}) + \det(\mathbf{B}) + \mathrm{tr}\,(\mathbf{A})\,\mathrm{tr}\,(\mathbf{B}) - \mathrm{tr}\,(\mathbf{AB}),$$

together with $\det(\mathbf{A}^n) = (\det(\mathbf{A}))^n = 1$:

$$\det(\mathbf{A}^n - \mathbf{I}) = \det(\mathbf{A}^n) + 1 + (-2)\,\mathrm{tr}\,(\mathbf{A}^n) - \mathrm{tr}\,(-\mathbf{A}^n)$$

Hence the number of periodic points is

$$N_n = |\mathrm{tr}\,(\mathbf{A}^n) - 2\,| = |\Lambda^n + \Lambda^{-n} - 2\,|\,. \tag{6.3}$$

where Λ is the larger eigenvalue of $\mathbf{A}$.

For the Arnol'd cat map

$$\mathbf{A} = \begin{pmatrix} 1 & 1 \\ 1 & 2 \end{pmatrix},$$

the powers of $\mathbf{A}$ are given by the Fibonacci numbers [2]

$$\mathbf{A}^n = \begin{pmatrix} F_{2n-1} & F_{2n} \\ F_{2n} & F_{2n+1} \end{pmatrix}$$

with seed values $F_1 = 1,\ F_2 = 1$. Therefore,

$$N_n = F_{2n-1} + F_{2n+1} - 2$$

For example

$$\begin{aligned} N_1 &= F_1 + F_3 - 2 = 1 + 2 - 2 = 1 \\ N_2 &= F_3 + F_5 - 2 = 2 + 5 - 2 = 5\,, \qquad \cdots \end{aligned} \tag{6.4}$$

[1] Predrag 2016-08-03: refer to where this is proven, or derive this statement here?

[2] Predrag 2016-05-21: to RS and AKS make this into an exercise, write up the solution

6.2.1 Keating's counting of periodic points

Keating [5] derives the number of periodic points of the cat map as follows:

The (q_j, p_j) periodic point of period n satisfy

$$\begin{pmatrix} q_{fixed} \\ p_{fixed} \end{pmatrix} = (A^n - I)^{-1} \begin{pmatrix} m \\ n \end{pmatrix} \tag{6.5}$$

"where m and n are integers which correspond to the winding numbers of the associated point $(q_{fixed},\ p_{fixed})$ around the torus under the action of the map A. For this point to have coordinates between 0 and 1, m and n must lie within the parallelogram formed by the action of the matrix $(A^n - I)^{-1}$ on the unit square. We call this the fundamental parallelogram associated with A^n. It tessellates the plane in which the (integer) lattice of winding numbers $(m,\ n)$ lies. Hence the number of fixed points of A^n is given by its area, which is $\det(A^n - I) = \mathrm{tr}\,(A^n) - 2$. It may be seen from (6.5) that these fixed points form a lattice in phase space."

6.3 Relative frequencies of cat map words

In this section we evaluate the number of times that a symbol appears in the symbolic sequence of an ergodic orbit of a cat map. The Arnol'd cat map alphabet consists of 4 letters $\mathcal{A} = \{\underline{2}, \underline{1}, 0, 1\}$. $\mathcal{A}$ is obtained from the equation of motion:

$$q_{n-1} - 3q_n + q_{n+1} = m_n, \quad m_n \in \mathcal{A} \tag{6.6}$$

For notational convenience, in alphabets we shall denote negative m by underlining them, i.e., $\{\underline{2}, \underline{1}, 0, 1\} = \{-2, -1, 0, 1\}$. To find $p(m)$, the relative frequency of symbol m, a Python program was written in which 100 arbitrary initial points are iterated for $n = 500000$ times. After each iteration, the obtained symbols are stored in an array of length n, and four counter variables are used to find how many times a symbol appears in the sequence. Finally, the average of number of repetitions for each symbol is found. Dividing these averages by n gives the frequency of each symbol. The final result is

$$p(\underline{2}) = 0.16670,\ p(\underline{1}) = 0.33328,\ p(0) = 0.33333,\ p(1) = 0.16669$$

Next, we look for the relative frequency of $-m_i m_{i+1}-$, $p(m_i\ m_{i+1})$. To find $p(m_i\ m_{i+1})$, a function is added to the previous program which checks the next symbol of each item of array, and then, increments the corresponding counter. The relative frequencies of the four symbols with 4^2 combinations (for $\_s_i s_{i+1}\_$) are listed in Table 6.1. Table 6.2 lists N_n, the total number of pruned blocks of length $n = n_a$, and $\tilde{N}_n$, the number of new pruned blocks of length n_a, with all length n_a blocks that contain shorter pruned blocks already eliminated.

The relative frequencies can be obtained analytically by eliminating two coordinates corresponding to 2-symbol from the equations of motion. Excluding two coordinates from the equations of motion and applying boundary

	$\underline{2}$	$\underline{1}$	0	1
$\underline{2}$	0	0.0208	0.0625	0.0833
$\underline{1}$	0.0209	0.125	0.125	0.0625
0	0.0625	0.125	0.125	0.0209
1	0.0833	0.0625	0.0209	0

$=$

	$\underline{2}$	$\underline{1}$	0	1
$\underline{2}$	0	1/48	1/16	1/12
$\underline{1}$	1/48	1/8	1/8	1/16
0	1/16	1/8	1/8	1/48
1	1 /12	1/16	1/48	0

Table 6.1: The relative frequencies of 2-symbol words $\_m_i m_{i+1}\_$ for the Arnol'd cat map, obtained (left) from a long-time numerical simulation, (right) analytically. Column: m_i. Row: m_{i+1}. There is only one pruning rule: $\_\underline{1}1\_$ is pruned. By the reflection symmetry, also $\_2\underline{2}\_$ is pruned. As defined by (6.7), these frequencies are rational numbers, and their sum is 1.

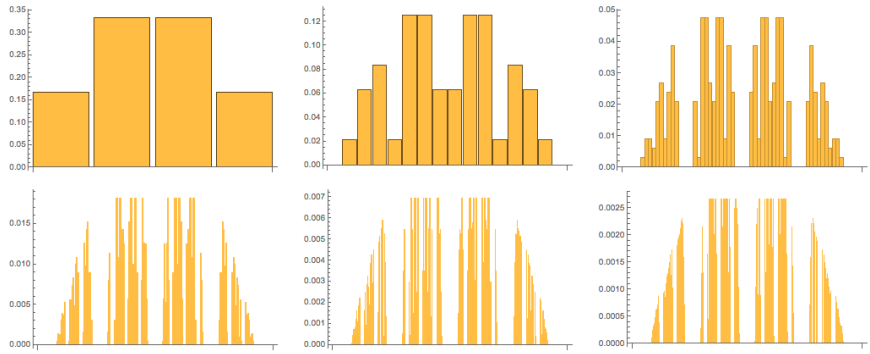

Figure 6.1: Frequencies of words of symbols. (Left to right: sub sequences of length 1, 2, 3, ..., 6.)

conditions ($0 \le q < 1$) gives the following inequalities for 2-symbol words $-m_i m_{i+1}-$:

$$\begin{aligned} 0 &\le \frac{1}{8}(-3m_i - m_{i+1} + 3x_1 + x_2) < 1, \\ 0 &\le \frac{1}{8}(-m_i - 3m_{i+1} + x_1 + 3x_2) < 1. \end{aligned} \tag{6.7}$$

The areas of regions confined by these inequalities represents the relative frequencies corresponding to each 2-symbol word (Table 6.1). Figure 6.1 shows the analytically found frequencies of words with lengths 1 to 6.

6.3.1 Numerical computations

To find all the possible periodic lengths of initial sets, $\{q_1, q_2\} = \{\frac{P_1}{N}, \frac{P_2}{N}\}$, we can consider the initial points to be (P_1, P_2) on $[0,\ N)^2$, and, following ref. [2], after each iteration we take $\mod N$. In this way, we use only s integers, and, after each iteration the output is exact, with no floating point round-off errors. The periods that we obtain for the lowest values of N are as follows:

n_a	N_n	$\tilde{N}_n$
2	2	2
3	22	8
4	132	2
5	684	30
6	3164	2
7	13882	

(a)

n_a	N_n	$\tilde{N}_{n-1}$
2	2	0
3	22	2
4	132	8
5	684	2
6	3164	30
7	13894	2
8	58912	70
9	244678	16
10	1002558	198
11	4073528	2
12	16460290	528
13		2

(b)

Table 6.2: N_n is the total number of pruned blocks of length $n = n_a$ for the Arnol'd cat map, $s = \mathrm{tr}\,[A] = 3$. $\tilde{N}_n$ is the number of new pruned blocks of length n_a, with all length n_a blocks that contain shorter pruned blocks already accounted for. (a) Computation carried in this report. (b) Numbers obtained by Li Han (unpublished). Note that (empirically) there is a single new pruning rule for each prime-number period (it is listed as 2 rules, but by the reflection symmetry there is only one).

for $\{q_1, q_2\} = \{\frac{P_1}{10}, \frac{P_2}{10}\}$: $T \in \{1,\ 2,\ 3,\ 6,\ 10,\ 30\}$,
for $\{q_1, q_2\} = \{\frac{P_1}{100}, \frac{P_2}{100}\}$: $T \in \{1,\ 2,\ 3,\ 6,\ 10,\ 30,\ 50,\ 150\}$
for $\{q_1, q_2\} = \{\frac{P_1}{8}, \frac{P_2}{8}\} : T \in \{1,\ 3,\ 6\}$
for $\{q_1, q_2\} = \{\frac{P_1}{17}, \frac{P_2}{17}\} : T \in \{1, 18\}$

6.3.2 Entropy

Given the frequencies $p(a)$ with which a blocks $a = a_1 a_2 ... a_{n_a}$ occur, the sum

$$\lim_{n_a \to \infty} -\frac{1}{n_a} \sum_a p(a) \log p(a) \ = -\log \Lambda \,, \tag{6.8}$$

where $\Lambda = \frac{3-\sqrt{5}}{2}$ is the eigenvalue of $\mathbf{A} = \begin{pmatrix} 1 & 1 \\ 1 & 2 \end{pmatrix}$.

Evaluating

$$\mathcal{S} = -\frac{1}{n_a} \sum_a p(a) \log p(a) \tag{6.9}$$

for $n_a = 1$ to 10 gives the values listed in table 6.3. Excluding all sequences that contain the external symbols and evaluating $\mathcal{S}$ for the remaining pure $\{\underline{1}, 0\}$ sequences gives the exact, complete symbolic dynamics expression (B. Gutkin,

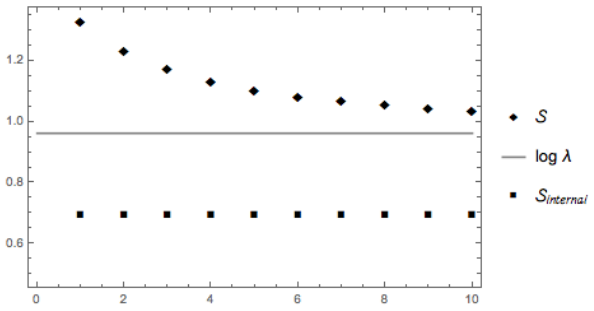

Figure 6.2: Entropies $\mathcal{S}$ and $\mathcal{S}_{internal}$ vs. the length n_a of periodic orbits used to estimate them.

n_a	$\mathcal{S}$	$\frac{\mathcal{S}-\log\Lambda}{\log\Lambda}$
1	1.3297	%38.1
2	1.2348	%28.3
3	1.1731	% 21.9
4	1.1337	%17.8
5	1.1051	%14.8
6	1.0843	%12.7
7	1.0682	%11.0
8	1.0558	%9.71
9	1.0458	%8.67
10	1.0378	%7.83

Table 6.3: Entropies (6.9) for strings of lengths $n_a = 1$ to 10, $s = 3$ Arnol'd cat map.

unpublished)

$$\mathcal{S}_{internal} = -\frac{1}{n_a}\log\frac{1}{2^{n_a}} = \log 2\,,$$

which we verify numerically in figure 6.2.

6.4 Spatiotemporal cat map

In the spatiotemporal cat map, "particles" (i.e., a cat map at each lattice site) are coupled together by the next-neighbor coupling rules:

$$q_{n,t+1} = p_{n,t} + (s-1)q_{n,t} - q_{n+1,t} - q_{n-1,t} - m^q_{n,t+1}$$

$$p_{n,t+1} = p_{n,t} + (s-2)q_{n,t} - q_{n+1,t} - q_{n-1,t} - m^p_{n,t+1}$$

n	$\underline{3}$	$\underline{2}$	$\underline{1}$	0	1	2	3	N
3	0.04169	0.49896	0.96169	1	0.97298	0.49965	0.04116	4.016
7	0.04062	0.50008	0.95917	1	0.95131	0.50284	0.04054	3.995
10	0.04127	0.50135	0.96255	1	0.96019	0.50066	0.04178	4.007
20	0.04120	0.50256	0.95779	1	0.95871	0.50171	0.04087	4.003

Table 6.4: $s = 4$. Numerically, the relative frequencies of symbols $\underline{1}, 0$ and 1 are close to 1.

The symbols of interest can be found by:

$$m_{n,t} = q_{n,t+1} + q_{n,t-1} + q_{n+1,t} + q_{n-1,t} - s\, q_{n,t}\,.$$

The results presented in this section are obtained by simulations. In order to make the computation exact, the denominators and numerators of the coordinates are stored as integers, i.e., only integers are used in all calculations presented here.

6.4.1 Frequencies of symbols

The obtained relative frequencies for different values of parameter b in [3]

$$A = -\frac{1}{c}\begin{pmatrix} a & 1 \\ ab - c^2 & b \end{pmatrix}$$

(where $s = \mathrm{tr}\, A = a + b$) shows the existence of 6 external and $s - 3$ internal symbols from the alphabet $\mathcal{A} = \{-s+1, -s, ..., 2, 3\}$. The numerical results were close to the expected values, which are $p(3) = p(-s+1) = \frac{1}{4!}$, $p(2) = p(-s+2) = \frac{1}{2}$, and $p(1) = p(-s+3) = 1 - \frac{1}{4!}$ (the relative frequency of an internal symbols is 1).

The results of Table 6.4 and Table 6.5, suggest that the frequencies are independent of n, the number of particles. Also, the values in Table 6.6 suggest that the normalization factor N is expected to be $1/s$. These values agree with the analytical values derived for the internal and external sequences:

$$\frac{1}{N}\left[6\left(\frac{1}{4!} + (1 - \frac{1}{4!}) + \frac{1}{2}\right) + (s-3)(1)\right] = 1$$

$$\Rightarrow N = s$$

[4]

[3] Predrag 2016-11-03: Where did the c come from? Shouldn't it be $c = -1$ by area preservation? Oh, I see - it has to do with coupling between sites [4].

[4] Predrag 2016-12-20: I do not get $N = s$ from this formula...

n	$\underline{7}$	$\underline{6}$	$\underline{5}$	$\underline{4}$	$\underline{3}$	$\underline{2}$	$\underline{1}$	0	1	2	3	N
3	0.0417	0.4996	0.9560	1.	0.9961	0.9993	0.9980	0.9974	0.9535	0.4982	0.0414	7.981
10	0.0414	0.4994	0.9535	0.9942	0.9978	0.9902	0.9938	1.	0.9551	0.49881	0.0411	7.965
20	0.0410	0.5017	0.9442	0.9839	0.9916	0.9837	1	0.9795	0.9576	0.4887	0.0419	7.980

Table 6.5: $s = 8$. Numerically, the relative frequencies of symbols $\underline{4}$, $\underline{3}$, $\underline{2}, \underline{1}, 0$ and 1 are close to 1.

s	N
5	5.0004
6	5.9988
7	7.0101
8	8.0014
9	8.9946

Table 6.6: N, he normalization factor of relative frequencies.

6.4.2 Frequency of blocks of length two

Next, we look for frequencies of blocks of length 2. These blocks can be formed by two consecutive symbols of one particle (e.g. $m_{n,t}m_{n,t+1}$) or symbols corresponding to two different particles at time t (e.g $m_{n,t}m_{n+1,t}$). Based on the results, there is a symmetry between symbols for a particle (Figure 6.3), and symbols at time t for two different particles (Figure 6.4) (with the same normalization factor, $N \approx 15$).

The only pruned blocks for both cases are $\underline{33}$ and 33, which is in agreement with the analytical results obtained by simplifying the inequalities of both cases in Mathematica (which implies that the confined area between the hyper planes is zero):

$$0 \leq \frac{1}{15}\left(-4a_1 - a_2 + 4x_1 + x_2 + x_3 + x_4 + 4x_5 + 4x_6\right) < 1,$$

$$0 \leq \frac{1}{15}\left(-a_1 - 4a_2 + x_1 + 4x_2 + 4x_3 + 4x_4 + x_5 + x_6\right) < 1.$$

According to the simulations, the sum of volumes confined between these planes should be 15.

The normalization factors, N, for different values of s are shown in Table 6.7. By comparing these values with inequalities obtained by excluding 2 coordinates corresponding to 2 symbols, it is observed that the normalization factors appear in equalities as the biggest common denominator. For example, for $s = 5$ we have the following inequality:

$$0 \leq \frac{1}{35}\left(-6a_1 - a_2 + 6x_1 + 6x_2 + x_3 + x_4 + x_5 + 6x_6\right) < 1,$$

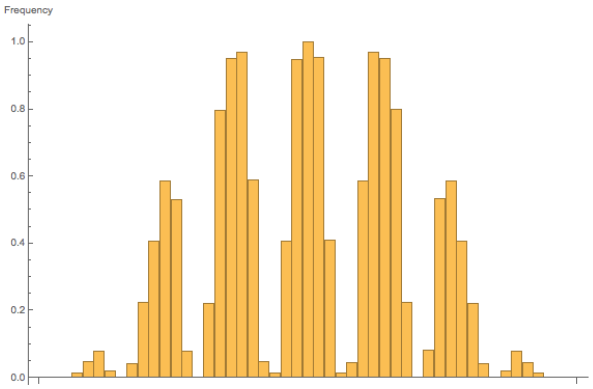

Figure 6.3: Relative frequencies of two symbols for a particle $(m_{n,t}m_{n,t+1})$. $s = 4$.

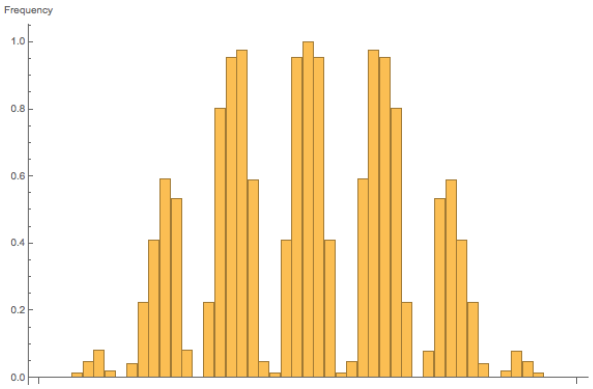

Figure 6.4: Relative frequencies of two symbols at time t for two different particles $(m_{n,t}m_{n+1,t})$. $s = 4$.

s	N
4	14.9168
5	23.8374
6	34.8851
7	48.1024

Table 6.7: Normalization factor, N, for different values of$s$.

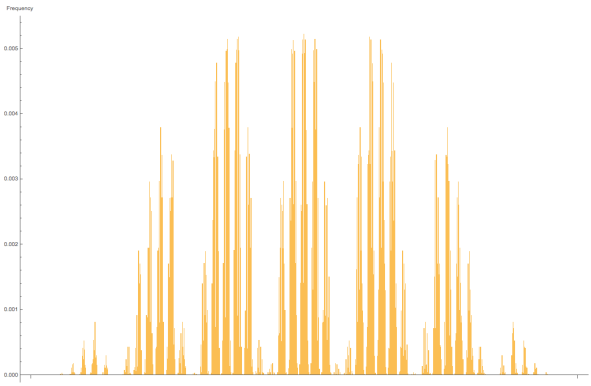

Figure 6.5: $s = 4$. Frequencies of $[2\times 2]$ spatiotemporal domains.

$$0 \leq \frac{1}{35}\left(-a_1 - 6a_2 + x_1 + x_2 + 6x_3 + 6x_4 + 6x_5 + x_6\right) < 1$$

The normalization factor obtained from simulations is approximately 35.

6.4.3 Frequencies of $[2\times 2]$ spatiotemporal domains

Frequencies of $[2\times 2]$ spatiotemporal domains of 20 coupled particles for two values of $s = 4$ and $s = 8$ are estimated. The results are presented in Figure 6.5 and Figure 6.6, respectively. The horizontal axes of graph, represents points starting from $\begin{matrix} -s+1 & -s+1 \\ -s+1 & -s+1 \end{matrix}$ to $\begin{matrix} 3 & 3 \\ 3 & 3 \end{matrix}$.

By arranging elements of the block (square) on a line (due to symmetry, the vertical or horizontal order of arrangement does not matter) as $-s+1\ -s+1\ -s+1\ -s+1$ to 3 3 3 3 and shifting each element of sequence $m_1m_2m_3m_4$ by $(s-1)$, we can reproduce the symbols as numbers in base $s+3$, and increment them from 0 to $(s+2\ s+2\ s+2\ s+2)_{s+3}$ on the horizontal axes.

By looking at data, the $[2\times 2]$ spatiotemporal domains with relative frequencies close to 1 do not only consist of internal symbols. For example, for $s = 8$, $\begin{matrix} 5 & 3 \\ 1 & 0 \end{matrix}$ has a relative frequency equal to 0.995755. The results suggest that if a column or row of symbols consist of internal symbols, the relative frequency is going to be close to 1. [5]

6.5 Summary

The results obtained by simulations for the frequencies of words are consistent with the unpublished B. Gutkin analytical results. By evaluating analytical

[5] Predrag 2016-08-07: Can you describe Boris' result more precisely? is it 'close to' or 'exactly' 1?

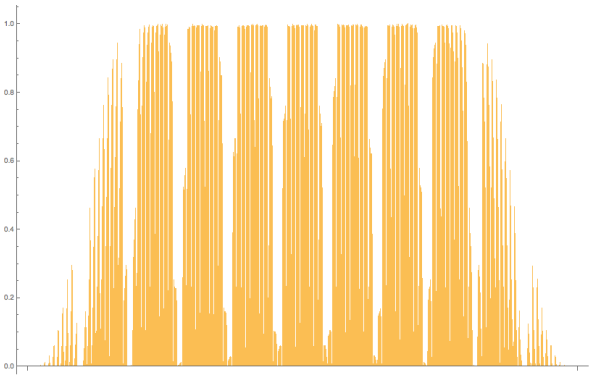

Figure 6.6: $s = 8$. Frequencies of $[2\times 2]$ spatiotemporal domains.

inequalities and finding the areas corresponding to the frequencies of words of single cat map, we are able to find the inadmissible sequences for words of up to length 6.

While for the spatiotemporal cat maps the general inequalities can be stated for any rectangular spatiotemporal domain, determining the volumes confined by these inequalities remains an open problem.

References

[1] V. I. Arnol'd and A. Avez, *Ergodic Problems of Classical Mechanics* (Addison-Wesley, Redwood City, 1989).

[2] J. Bao and Q. Yang, "Period of the discrete Arnold cat map and general cat map", Nonlinear Dyn. **70**, 1365–1375 (2012).

[3] R. L. Devaney, *An Introduction to Chaotic Dynamical systems*, 2nd ed. (Westview Press, 2008).

[4] B. Gutkin and V. Osipov, "Classical foundations of many-particle quantum chaos", Nonlinearity **29**, 325–356 (2016).

[5] J. P. Keating, "Asymptotic properties of the periodic orbits of the cat maps", Nonlinearity **4**, 277 (1991).

[6] J. P. Keating, "The cat maps: quantum mechanics and classical motion", Nonlinearity **4**, 309–341 (1991).

[7] I. Percival and F. Vivaldi, "Arithmetical properties of strongly chaotic motions", Physica D **25**, 105–130 (1987).

Chapter 7

Symbolic Dynamics for Coupled Cat Maps

Adrien K. Saremi Summer 2016 Report

Abstract
Classical particles are governed by Hamiltonian equations of motion. Instead of continuous function of time, we break down our system's evolution through a series of discrete instants; the generalized coordinates $\{q_{n,t}, p_{n,t}\}$ are then solutions to a system of coupled linear equations, written down in matrix form. Our research consists in studying symbolical dynamics in relation with our N-particle system, through a time evolution of length T by obtaining the nature of our alphabet, by computing the frequencies of appearance of our symbols and by deriving the inadmissible symbolic spatiotemporal domains, through analytic studies and computational models.

7.1 Introduction

Let a system of N particle, evolving through time, over a time lapse of value T. We assume that our system lies in one dimension of space, therefore our generalized coordinates, position and momentum are described as follows:

$$\{q_{n,t}, p_{n,t}\} \text{ where } n \in \{1, \dots, N\} \text{ and } t \in \{1, \dots, T\}$$

Obviously, n is the particle variable and t the time variable. We also refer to n as our space variable. At an instant t, we define our generalized coordinate vector $\mathcal{Z}_t$:

$$\mathcal{Z}_t = \left\{ \begin{array}{c} q_{n,t} \\ p_{n,t} \end{array} \right\}_{1\leqslant n\leqslant N} = \left\{ \begin{array}{c} q_{1,t} \\ p_{1,t} \\ q_{2,t} \\ p_{2,t} \\ ... \\ p_{N,t} \\ q_{N,t} \end{array} \right\}$$

Following Gutkin and Osipov [2] *Classical foundations of many-particle quantum chaos*, we write Hamilton's equations for our generalized coordinate vector $\mathcal{Z}_t$ described in this paper's sect. *3.1 Dynamics*:

$$\mathcal{Z}_{t+1} = \mathcal{B}_N \mathcal{Z}_t$$

with

$$\begin{aligned} \mathcal{B}_N &= \begin{pmatrix} A & B & 0 & \dots & 0 & B \\ B & A & B & \dots & 0 & 0 \\ 0 & B & A & \dots & 0 & 0 \\ \vdots & \vdots & \vdots & \ddots & \vdots & \vdots \\ 0 & 0 & 0 & \dots & A & B \\ B & 0 & 0 & \dots & B & A \end{pmatrix} \\ A &= \frac{1}{c}\begin{pmatrix} a & 1 \\ ab-c^2 & b \end{pmatrix}, \quad B = -\frac{1}{c}\begin{pmatrix} d & 0 \\ db & 0 \end{pmatrix} \end{aligned} \tag{7.1}$$

We start with a system of just $N = 1$ particle. This is usually referred as *Arnol'd cat map*.

7.2 Arnol'd Cat Map

In this section, we introduce the concept of iterative process and compute the time evolution of our system. We fix the parameters of our $\mathcal{B}_N$ matrix:

$$\mathcal{B}_N = \mathcal{B}_1 = A = \begin{pmatrix} 1 & 1 \\ 1 & 2 \end{pmatrix}, \qquad \det A = 1\,.$$

Here we picked the values $a = 1$, $b = 2$ and $c = -1$. The system of equations can be rewritten:

$$\begin{pmatrix} q_{t+1} \\ p_{t+1} \end{pmatrix} = A \begin{pmatrix} q_t \\ p_t \end{pmatrix} \mod 1 \tag{7.2}$$

For the sake of phase space volume conservation, we set the matrix A to have a determinant equal to 1. The underlying difficulty of this problem is that our coordinates must also remain within an interval of length 1. At first we pick this interval to be $[0, 1)$. We will see later that we change this interval

to $[-\frac{1}{2}, \frac{1}{2})$ in order to preserve the symmetry of our coordinates and of our symbolic dynamics with respect to 0.

Our goal is now to find prime periodic orbits p of period T_p and initial points $\{q_{p,1}, p_{p,1}\}$ such that:

$$\begin{pmatrix} q_{p,T_p} \\ p_{p,T_p} \end{pmatrix} = \begin{pmatrix} q_{p,1} \\ p_{p,1} \end{pmatrix} \mod 1$$

In what follows, we explain the two approaches in order to reach this goal. For the sake of notational simplicity, we denote our initial set as $\{q_1, p_1\}$,and the final set as $\{q_{T_p}, p_{T_p}\}$. It is understood that we deal with the prime periodic orbit p.

7.2.1 Periodic orbits - first approach

Consider

$$\begin{pmatrix} q_{T_p} \\ p_{T_p} \end{pmatrix} = A^{T_p} \begin{pmatrix} q_1 \\ p_1 \end{pmatrix} \mod 1$$

We demand that $\{q_1, p_1\}$ is a periodic point in a prime periodic orbit p on a two–dimensional torus $\mathbf{T}^2$, i.e., a relative periodic orbit on $\mathbb{Z}^2$, periodic up to a shift by integers $\{m_q, m_p\}$:

$$\begin{pmatrix} q_1 \\ p_1 \end{pmatrix} = A^{T_p} \begin{pmatrix} q_1 \\ p_1 \end{pmatrix} + \begin{pmatrix} m_q \\ m_p \end{pmatrix}$$

Therefore:

$$\begin{pmatrix} q_1 \\ p_1 \end{pmatrix} = (\mathbb{1} - A^{T_p}) \begin{pmatrix} m_q \\ m_p \end{pmatrix}$$

The number of periodic orbits (AKA the number of sets of $\{q_1$,$p_1\}0$ would be then given by:

$$|\det(\mathbb{1} - A^{T_p})| = |(1 - \lambda^{T_p})(1 - \frac{1}{\lambda^{T_p}})|$$

where λ is the largest eigenvalue of A: $\lambda = \frac{3+\sqrt{5}}{2} = 2.6180$ also known as *Floquet multiplier*

Instead of dealing with multiples of the A matrix, and the large number of coordinate vectors $\mathcal{Z}_t$, the second approach includes a larger matrix computation, but allows us to store all coordinates in one single vector.

7.2.2 Periodic orbits - second approach

Here we eliminate $\{p_t\}$ in favor of a 2-step recurrence equation on the position coordinate $\{q_t\}$:

$$p_t = \frac{q_t - q_{t-1}}{\Delta t} = q_t - q_{t-1}$$

Combined with:

$$q_{t+1} = q_t + p_t$$

We obtain:

$$\begin{aligned} q_3 - 3q_2 + q_1 &= m_2 \\ q_4 - 3q_3 + q_2 &= m_3 \\ &\vdots \\ q_{T_p+1} - 3q_{T_p} + q_{T_p-1} &= m_{T_p} \\ q_{T_p+2} - 3q_{T_p+1} + q_{T_p} &= m_{T_p+1} \end{aligned} \tag{7.3}$$

Since we look for periodic orbits, $q_{T_p+1} = q_1$ and $q_{T_p+2} = q_2$. Therefore the last equation reduces to:

$$q_2 - 3q_1 + q_{T_p} = m_1 \,,$$

and the system of equations into the matrix form:

$$\mathcal{D}\, Q_{T_p} = m_{T_p}$$

with

$$\begin{aligned} Q_{T_p} &= \begin{pmatrix} q_1 \\ q_2 \\ \vdots \\ q_{T_p} \end{pmatrix}, \qquad m_{T_p} = \begin{pmatrix} m_1 \\ m_2 \\ \vdots \\ m_{T_p} \end{pmatrix} \\ \mathcal{D} &= \begin{pmatrix} -3 & 1 & 0 & 0 & 0 & \dots & 1 \\ 1 & -3 & 1 & 0 & 0 & \dots & 0 \\ \vdots & & & & & & \\ 1 & 0 & 0 & 0 & \dots & 1 & -3 \end{pmatrix} \end{aligned} \tag{7.4}$$

It then comes down to the nature of our initial set: if the starting set is rational, we will necessarily obtain a periodic system. Indeed, if we assume that the initial momentum and position are rational numbers with some common denominator N, and since the cat map is composed of integers, after t steps, momentum and coordinate have the form $q_t = a_t/N$, $p_t = b_t/N$. And if we travel on the lattice of the size $N \times N$, it will take us a maximum step N to close the loop. Usually, the periodicity is smaller than N, and this is what our MATLAB code computes.

Program evaluation

Using the 2^{nd} approach, sect. 7.2.2, our program computes the position coordinates of our particle for a given initial condition $\{q_1, q_2\}$. The numbers $\{q_t\}$'s and the integers $\{m_t\}$'s are then stored in the matrices Q and m. The program stops if for some iteration t we obtain the same starting set $\{q_{t+1}, q_{t+2}\} = \{q_1, q_2\}$, in which case the period is $T_p = t$.

If it doesn't stop, and it completes all the iteration that the user required, the program then looks for periodic behavior in the m matrix. In other words: does an integer T_p exist such that for all t, $m_{t+T_p} = m_t$. If it's the case, the orbit in question is also periodic, and the program wasn't accurate enough to observe periodicity among the position coordinates (a point that we will discuss later this section).

Results for periodic orbits

We now understand that the rational nature of our initial set $\{q_1, q_2\}$ is determinant for the periodic behavior of our system. We try several sets $\{q_1, q_2\}$ of the form $\{q_1, q_2\} = \{\frac{i}{N}, \frac{j}{N}\}$ where $i, j \in \{0, \ldots, N-1\}$.

- For $\{q_1, q_2\} = \{\frac{i}{10}, \frac{j}{10}\}$, the periodicities found were: $T_p = 1, 2, 3, 6, 10, 30$
- For $\{q_1, q_2\} = \{\frac{i}{100}, \frac{j}{100}\}$, they were: $T_p = 1, 2, 3, 6, 10, 30, 50, 150$
- For $\{q_1, q_2\} = \{\frac{i}{8}, \frac{j}{8}\}$, $T_p = 1, 3, 6$
- And for $\{q_1, q_2\} = \{\frac{i}{17}, \frac{j}{17}\}$ $T_p = 1, 18$
- Nevertheless, for an irrational starting set such as $\{q_1, q_2\} = \{\frac{\pi}{6}, \frac{\pi}{8}\}$ we do not obtain any periodic behaviors, despite running $20\,000$ iterations.

Before moving to the next part, we briefly discuss the accuracy of our computations, and the limits of our program when it comes to find periodic orbits.

Round-off errors

Our MATLAB calculations often gave us unexpected results, where we could not find periodic orbits through our position coordinates. The advantage of looking at the m sequence instead is that it is made of integers, while the q's are decimal numbers, and it is possible that after many iteration, the round-off error in computation becomes quite large.

In fact, such errors are directly related to the nature of our system, more precisely the matrix A. The Floquet multiplier λ has an impact on the calculation of the computed value after t iterations, compared to the real value $q_{real,t}$:

$$q_{computed,t} = q_{real,t} + \epsilon\, \lambda^t, \text{ where } \lambda = \frac{3+\sqrt{5}}{2} = \text{multiplier}$$

and where ϵ is the round off error of the system. For a 64-bit operating system, $\epsilon = 2^{-53} \approx 10^{-16}$. Now, if we look for a computed value of q within 10^{-4} of its real value, then the maximum number of iteration t_{max} is technically:

$$|\epsilon\, \lambda^{t_{max}}| \leq 10^{-4}$$

$$\Rightarrow t_{max} \approx \ln(\lambda)\ \ln(\frac{10^{-4}}{\epsilon})$$

$$\Rightarrow t_{max} = 26$$

The exponential growth in error imposes the use of different computation techniques, or to application of the command **digits(n)** which forces n significant digits to any computations.

Through our MATLAB program, we now focus on the nature of the alphabet (m matrix), as well as the frequency of appearance of our symbols. The big stuff....

7.2.3 Symbolic dynamics for 1 particle

Nature of our alphabet

We recall that given our matrix A:

$$q_{i-1} + q_{i+1} = 3q_i + m_i \quad \forall i$$

In fact for a random matrix A (as long as $det(A) = 1$), if we denote the trace of A by s =trace(A), then this equation is rewritten as:

$$q_{i-1} + q_{i+1} = s\, q_i + m_i \quad \forall i$$

Since the nature of m_i only depends on q_{i-1}, q_{i+1} and q_i, consider a sequence of length 3: $\{q_1, q_2, q_3\}$ with the constraint conditions on q_i's:

$$q_1 + q_3 = s\, q_2 + m$$
$$q_i \in [0, 1) \ \forall i$$

Then:

$$0 \leqslant q_1 < 1$$
$$0 \leqslant q_3 < 1$$
$$m \leqslant q_1 + q_3 < m + s$$

The value of s then becomes determinant to why only few symbols are admissible. For example, for $s = 3$ we find that $m_t \in \{-2, -1, 0, 1\}$.

Frequencies of symbols

Using our program, we then compute the frequencies of each symbol for the case $s = 3$. By performing 1 iteration in time to obtain q_3 from q_1 and q_2 and by repeating with several different starting set, we obtain a good probability distribution of symbolic dynamics. We pick starting sets of the form $\{q_1, q_2\} = \{\frac{i}{200}, \frac{j}{200}\}$ where $i, j \in \{0, \ldots, 199\}$ and obtain a distribution over $40\,000$ points:

$$p_{-2} = 0.16583, p_{-1} = 0.33335, p_0 = 0.33310, p_1 = 0.16773$$

In fact, if we plug the different values of m in the system of equation above for $s = 3$, we obtain inequalities on q_1 and q_3. The admissible area in our

lattice defined by (q_1, q_3) is then the probability of obtaining the symbol p_m. For example for $m = -1$:

$$\begin{aligned} 0 \leqslant q_1 < 1 \\ 0 \leqslant q_3 < 1 \\ -1 \leqslant q_1 + q_3 < 2 \end{aligned}$$

The admissible area is then $\mathcal{A} = 1$, but for $m = -2$:

$$\begin{aligned} 0 \leqslant q_1 < 1 \\ 0 \leqslant q_3 < 1 \\ -2 \leqslant q_1 + q_3 < 1 \end{aligned}$$

And here the admissible area is $\mathcal{A} = \frac{1}{2}$. For $m = 0$ and $m = 1$, we respectively find $\mathcal{A} = 1$ and $\mathcal{A} = \frac{1}{2}$. Therefore our probability distribution matches our numerical calculations and:

$$p_{-2} = \frac{1}{6}, p_{-1} = \frac{1}{3}, p_0 = \frac{1}{3}, p_1 = \frac{1}{6}$$

We observe that the inner symbols -1 and 0 have a higher frequency than the outer ones, a point that will have a major importance when we study many symbols frequencies.

Frequency of sequences of symbols

Another approach to the computation of one or more-than-two sequence of symbols is to analyze the symbolic distribution over an **ergodic** orbit, i.e., a non-periodic orbit. If the sequence of symbols is long enough, one sequence is sufficient to observe a frequency distribution that matches with the theory. This also works for a given sequence of length p, such as $\{m_1 m_2 \dots m_p\}$. We define $N_n(m_1 m_2, \dots m_p)$ as the number of periodic orbits of length n that generate the given sequence. The probability of obtaining the sequence $\{m_1, m_2, \dots, m_p\}$ is then:

$$p(m_1 m_2 \dots m_p) = \lim_{n \to \infty} \frac{N_n(m_1 m_2 \dots m_p)}{N_n}$$

Figuring out the probability distribution by mathematical analysis (as we did for 1 symbol) can become quite hard as the length of the given sequence increases. We will cover in this section the case of many particles. However, what we can observe is the correlation between disjoint sequence of symbols.

Given a sequence $A = [a_1, \dots, a_u]$ of length u, and a sequence $B = [a_1, \dots, a_v]$ of length v, we now examine the frequency of seeing one repeated a length *space* after the other. Comparing with the product of their distinct frequencies, we then increase the *spacing* and observe how the correlation factor

$$Correl = p(A, space, B) - p(A)\, p(B) \text{ behaves}$$

We obviously limit our study to admissible sequences. For the ergodic orbit $\{q_1, q_2\} = \{\frac{\sqrt{5}}{4}, \frac{\sqrt{2}}{2}\}$ of length $N = 1,000\,000$, and the sequences $A = [-1, 1]$ and $B = [-2, 0]$

$$p(A) = 0.1249 \qquad p(B) = 0.0623$$

$Spacing$	$P(A, space, B)$	$Correl$
1	0.0085	$7.3567\ 10^{-4}$
2	0.0066	-0.0011
3	0.0073	$-4.6733\ 10^{-4}$
4	0.0080	$1.8867\ 10^{-4}$
5	0.0079	$6.8666\ 10^{-5}$
6	0.0078	$4.6655\ 10^{-6}$

For longer sets $A = [-1, -1, -1, -1]$ and $B = [-2, 1, -1, 0]$, and the same orbit, the probabilities are as follow:

$$p(A) = 0.0178 \qquad p(B) = 0.0151$$

$Spacing$	$P(A, space, B)$	$Correl$
1	$2.9400\ 10^{-4}$	$2.4439\ 10^{-5}$
2	$2.2400\ 10^{-4}$	$-4.5561\ 10^{-5}$
3	$2.4900\ 10^{-4}$	$-2.0561\ 10^{-5}$
4	$2.5100\ 10^{-4}$	$-1.8561\ 10^{-5}$
5	$2.7300\ 10^{-4}$	$3.4392\ 10^{-6}$
6	$2.6900\ 10^{-4}$	$-5.6081\ 10^{-7}$

In both scenarios, the correlation factor diminishes as the separation between the two blocs increases. We notice that for longer sets A and B, the correlation is small enough (but not zero) even for small spacing. It is quite interesting how this correlation, which translates the dependence between future and past symbolic dynamics, vanishes exponentially...

7.3 Coupled Cat Maps

We now extend our study to a many particle system, where N is the number of particles. T will be now known as the period of the orbit, and if it doesn't exist, T will just refer to our ultimate time iteration in the computation of the symbols m's. Among the objectives of this section, we will explain the impact of the trace of the A matrix (s =trace(A)) on the nature of our alphabet, the length of the periodic orbits, and the admissibility of sequences of symbols.

We will first look at the computation of our periodic orbits, then the nature of our alphabet, and finally the rules that determine whether a sequence of symbols is inadmissible, and if not, what is its frequency of recurrence.

7.3.1 Computation of symbols

As we saw in sect. 7.2, there are two approaches to compute our symbolic dynamics. Here the 1st method that we described in sect. 7.2.1 presents more advantage in the computation of another symbolic dynamics.

Computing the coordinates

Our interval of study is $[-\frac{1}{2}, \frac{1}{2})$, the equation $\mathcal{Z}_{t+1} = \mathcal{B}_N \, \mathcal{Z}_t \mod 1$ involves the introduction of *generalized* symbolics $m^{q,p}$ such that:

$$\mathcal{Z}_{t+1} = \mathcal{B}_N \, \mathcal{Z}_t + m^{q,p}_{t+1}$$

$$\text{where } m^{q,p}_t = \{m^q_t, m^p_t\} = \{m^q_{1,t}, m^p_{1,t}, m^q_{2,t}, m^p_{2,t}, \ldots, m^q_{N,t}, m^p_{N,t}\}$$

In fact the MATLAB can now store all the entries of the $\mathcal{Z}_t$ vectors in a larger matrix, where T is the number of columns, and $2N$, which refers to the 2 coordinates or each particle, is the number of rows.

In a effort to keep the time evolution row-wise, and the space evolution column-wise, only the momentum coordinates $\{q_{n,t}\}^{1 \leqslant n \leqslant N}_{1 \leqslant t \leqslant T}$ are then stored in the Q matrix:

$$Q = \begin{pmatrix} q_{n,1} \\ q_{n,2} \\ \vdots \\ q_{n,T} \end{pmatrix} = \begin{pmatrix} q_{1,t} & q_{2,t} & \cdots & q_{N,t} \end{pmatrix} = \begin{pmatrix} q_{1,1} & q_{2,1} & \cdots & q_{N,1} \\ q_{1,2} & q_{2,2} & \cdots & q_{N,1} \\ \vdots & \vdots & & \vdots \\ q_{1,T} & q_{2,T} & \cdots & q_{N,T} \end{pmatrix}$$

Note that in the label $Q = \{q_{n,t}\}$, the column index is n and the row index is t.

Computing the alphabet

What we actually focus on is the symbolic dynamics. The $m^{q,p}$ matrix mentioned above is the *generalized* dynamics, while the one we studied for $N = 1$ was the *Newtonian* dynamics m. There are two ways to compute the later:

- Use our generalized symbolics:

$$m_{n,t} = -b \, m^q_{n,t} - c \, m^q_{n,t+1} + m^p_{n,t}$$

- Use the Q coordinates:

$$c \, (q_{n,t+1} + q_{n,t-1}) + d \, (q_{n+1,t} + q_{n-1,t}) = -s \, q_{n,t} + m_{n,t}$$

For computations of admissible sequences, the later method is preferred. And even if our dynamics is not defined at the boundaries, for either $n \in \{1, N\}$ or $t =\in \{1, T\}$, the choice of ergodic orbits that run for very large N and T makes irrelevant that a few number of symbols can no longer be computed. For the case of periodic orbits, where T is usually a small number, we will only focus on the generalized coordinates $m^{q,p}$ instead.

Periodic orbits

The absolute criteria to obtain periodic orbits is to start with a rational set $\mathcal{Z}_1$, and use integers for the parameters a, b, c and d. Unless specified, we use the following values throughout the rest of our study:

- $c = -1$ such that $det(A) = 1$
- $d = c$ in order to preserve the symmetry between space and time evolutions
- $b = 1$ and $a = 2$ in order to obtain $s = a + b =$trace$(A) = 3$. To observe a hyperbolic evolution, a must remain greater than 2; which is why we will only increase the value of a, and leave b as a fixed parameter, to study the influence of s on our system.

Few periodic orbits were computed, for different number of particles:

- for $N = 3$ and $\mathcal{Z}_1 = \left\{ \begin{array}{cccccc} \frac{31}{100} & \frac{29}{100} & \frac{7}{50} & -\frac{13}{100} & \frac{31}{100} & \frac{3}{100} \end{array} \right\}$

  the periodicity is $T = 60$, and the symbolic dynamics is:

$$\begin{aligned} m^{q,p} &= -2, p_{-2} = 0.011111 \\ m^{q,p} &= -1, p_{-1} = 0.222222 \\ m^{q,p} &= 0, p_0 = 0.536111 \\ m^{q,p} &= 1, p_1 = 0.227778 \\ m^{q,p} &= 2, p_2 = 0.002778 \end{aligned}$$

- for $N = 7$ and

$$\mathcal{Z}_1 = \left\{ \begin{array}{cccccccccccccc} \frac{-19}{100} & \frac{21}{50} & \frac{-7}{100} & \frac{-8}{25} & \frac{2}{5} & \frac{47}{100} & \frac{-7}{100} & \frac{-39}{100} & -\frac{1}{4} & -\frac{1}{10} & \frac{9}{100} & \frac{-6}{25} & \frac{1}{10} & \frac{21}{100} \end{array} \right\}$$

  the periodicity is $T = 2790$, and the symbolic dynamics is:

$$\begin{aligned} m^{q,p} &= -2, p_{-2} = 0.012110 \\ m^{q,p} &= -1, p_{-1} = 0.226472 \\ m^{q,p} &= 0, p_0 = 0.526882 \\ m^{q,p} &= 1, p_1 = 0.224014 \\ m^{q,p} &= 2, p_2 = 0.010522 \end{aligned}$$

By always finding periodicity, the program confirms that it evaluates the right coordinates. It also validate that neither the number of particle N, nor the periodicity T have an influence on the nature of our alphabet.

7.3.2 Nature of our alphabet

Through an analytic study, and by confirm with our simulations, we now focus on the impact of the trace of A

Analytically

Given equation ???? and with $c = d = -1$:

$$s\, q_{n,t} = q_{n,t+1} + q_{n,t-1} + q_{n+1,t} + q_{n-1,t} + m_{n,t}$$

Since we study the nature of 1 symbol at the time, let's pick the following notations

$$n = 1 \text{ and } t = 1$$

$$q_{1,1} = q_1 \qquad m_{1,1} = m_1 \qquad q_{1,0} = x_1 \qquad q_{2,1} = x_2 \qquad q_{1,2} = x_3 \qquad q_{0,1} = x_4$$

A system is relabelled as (we will see that this notation is useful for sequence of many symbols)

$$\begin{array}{ccccccccc} & & q_{1,0} & & & & x_1 & & \\ q_{0,1} & & \boldsymbol{q_{1,1}} & q_{2,1} & = & x_4 & \boldsymbol{q_1} & x_2 & . \\ & & q_{1,2} & & & & x_3 & & \end{array}$$

This system we can rewrite as:

$$q_1 = \frac{1}{s}(m_1 + \sum_{i=1}^{4} x_i)$$

with the constraints on q_1 and x_i:

$$\begin{cases} -\frac{s}{2} \leqslant m_1 + \sum\limits_{i=1}^{4} x_i < \frac{s}{2} \\ -\frac{1}{2} \leqslant x_i < \frac{1}{2}\,, \qquad \text{for } i = 1, \ldots, 4 \end{cases}$$

For the Arnol'd cat map case $s = 3$, this reduces to

$$\begin{cases} -\frac{3}{2} - m_1 \leqslant \sum\limits_{i=1}^{4} x_i \leqslant \frac{3}{2} - m_1 \\ -2 \leqslant \sum\limits_{i=1}^{4} x_i \leqslant 2 \end{cases}$$

This system of inequalities allows us to derive which symbols are admissible. For a given m_1, the system doesn't admit real solutions for x_i's (or if the solution is empty), then the symbol is forbidden. For the case $s = 3$, we confirm what we obtained for $N = 1$ and $m \in \{-3, -2, \ldots, 2, 3\}$.

Program

Here ergodic orbits run for a large number of particles and over many time iterations T. To speed up the computing process, the program stops looking

for periodic orbits and only focus on the symbolic dynamics, as well as it probability distribution. The simulations are for different values of s, with $N = 5$, $T = 80\,000$, and a random irrational starting set:

$s=3$		$s=4$		$s=5$	
				$m=-4$	$p_{-4}=0.000592$
$m=-3$	$p_{-3}=0.000850$	$m=-3$	$p_{-3}=0.010696$	$m=-3$	$p_{-3}=0.040080$
$m=-2$	$p_{-2}=0.067293$	$m=-2$	$p_{-2}=0.126391$	$m=-2$	$p_{-2}=0.159941$
$m=-1$	$p_{-1}=0.264819$	$m=-1$	$p_{-1}=0.236452$	$m=-1$	$p_{-1}=0.198742$
$m=0$	$p_0=0.332571$	$m=0$	$p_0=0.250635$	$m=0$	$p_0=0.199551$
$m=1$	$p_1=0.267269$	$m=1$	$p_1=0.239835$	$m=1$	$p_1=0.201197$
$m=2$	$p_2=0.066364$	$m=2$	$p_2=0.125378$	$m=2$	$p_2=0.159721$
$m=3$	$p_3=0.000833$	$m=3$	$p_3=0.010613$	$m=3$	$p_3=0.039697$
				$m=4$	$p_4=0.000479$

$s=6$		$s=7$	
		$m=-5$	$p_{-5}=0.000363$
$m=-4$	$p_{-4}=0.006921$	$m=-4$	$p_{-4}=0.028955$
$m=-3$	$p_{-3}=0.083823$	$m=-3$	$p_{-3}=0.113895$
$m=-2$	$p_{-2}=0.159604$	$m=-2$	$p_{-2}=0.141662$
$m=-1$	$p_{-1}=0.167262$	$m=-1$	$p_{-1}=0.142537$
$m=0$	$p_0=0.165642$	$m=0$	$p_0=0.144154$
$m=1$	$p_1=0.166942$	$m=1$	$p_1=0.142207$
$m=2$	$p_2=0.159625$	$m=2$	$p_2=0.142849$
$m=3$	$p_3=0.083206$	$m=3$	$p_3=0.114120$
$m=4$	$p_4=0.006975$	$m=4$	$p_4=0.028863$
		$m=5$	$p_5=0.000396$

The resulting alphabet increases in size for larger s. And the more "centered" a symbol is, the more frequently it appears.

For $s \geqslant 3$, the number of different admissible symbols L is always greater than 7. We define the *external* symbols as the 6 outer symbols in our alphabet (3 on each side) and the *internal* symbols as the remaining ones. Then, for a given s, the probabilities of the internal symbols tend to be the same, an observation we will extend for sequences of many symbols.

7.3.3 Admissibility of sequences of more than 2 symbols

Knowing which symbols are admissible allows us to expand our study to sequences of many symbols, spread over both space and time dimensions. Consider sequence m:

$$\begin{bmatrix} m_{1,1} & \dots & m_{j,1} \\ \vdots & & \vdots \\ m_{1,i} & \dots & m_{j,i} \end{bmatrix} \text{ with } i \text{ and } j \geqslant 2$$

$[2\times2]$ spatiotemporal domains

For aesthetic reasons, we redefine our symbols and our coordinates:

$$\begin{array}{ccccc} & & q_{1,0}=x_1 & q_{2,0}=x_2 & \\ q_{0,1}=x_8 & & \boldsymbol{q_{1,1}=q_1} & \boldsymbol{q_{2,1}=q_2} & q_{3,1}=x_3 \\ q_{0,2}=x_7 & & \boldsymbol{q_{1,2}=q_3} & \boldsymbol{q_{2,2}=q_4} & q_{3,2}=x_4 \\ & & q_{1,3}=x_6 & q_{2,3}=x_5 & \end{array}$$

as well as $m_{1,1}=a_1$, $m_{2,1}=a_1$, $m_{1,2}=a_3$ and $m_{2,2}=a_4$. And using the Newtonian equation ????, the system of inequalities then becomes:

$$\begin{array}{l} q_1=\frac{1}{s}(a_1+q_2+q_3+x_1+x_8) \\ q_2=\frac{1}{s}(a_2+q_1+q_4+x_2+x_3) \\ q_3=\frac{1}{s}(a_3+q_1+q_4+x_6+x_7) \\ q_4=\frac{1}{s}(a_4+q_2+q_3+x_4+x_5) \end{array} ,$$

with conditions

$$\begin{array}{ll} \forall i\in\{1,\ldots,4\}\,, & -\frac{1}{2}\leqslant q_i<\frac{1}{2} \\ \forall j\in\{1,\ldots,8\}\,, & -\frac{1}{2}\leqslant x_j<\frac{1}{2} \\ \forall k\in\{1,\ldots,4\}\,, & m_k\in\{\text{alphabet}\} \end{array}$$

For $s=3$:

$$\begin{array}{l} -\frac{3}{2}-a_1\leqslant q_2+q_3+x_1+x_8<\frac{3}{2}-a_1 \\ -\frac{3}{2}-a_2\leqslant q_1+q_4+x_2+x_3<\frac{3}{2}-a_2 \\ -\frac{3}{2}-a_3\leqslant q_1+q_4+x_6+x_7<\frac{3}{2}-a_3 \\ -\frac{3}{2}-a_4\leqslant q_2+q_3+x_4+x_5<\frac{3}{2}-a_4 \end{array} \quad \text{with} \quad \left\{ \begin{array}{l} -\frac{1}{2}\leqslant q_i<\frac{1}{2} \\ -\frac{1}{2}\leqslant x_j<\frac{1}{2} \\ m_k\in\{-3,-2,\ldots,2,3\} \end{array} \right.$$

For the Arnol'd cat map case $s=3$, there are a total of $7^4=2\,401$ possible $[2\times2]$ spatiotemporal blocks. [1]unning on Mupad, we solve this system of inequalities for different a's. The number of empty solutions we obtain is 552 which represents a total of 23% inadmissible spatiotemporal domains, which seems too small...

Running many sequences on MATLAB

We now try to confirm this percentage using our MATLAB program. The probabilistic distribution of every [2×2] spatiotemporal domain has the shape shown in figure 7.1.

The difference in results from our analytical study is quite significant since the number of inadmissible sequences is 1,665 out of 2,401 (69.3%). A number that could be blamed on the size of our sample being not large enough.

[1]Predrag 2017-09-08 In ref. [1] I wrote that the $d=1$ Arnol'd cat map $s=3$ alphabet has 5 letters $\mathcal{A}=\{\underline{2},\underline{1},0,1,2\}$. Am I wrong? You mean $d=2$ spatiotemporal cat map $s=3$ alphabet on $[-\frac{1}{2},\frac{1}{2})\times[-\frac{1}{2},\frac{1}{2})$ phase space has $s+4=7$ letters? : R

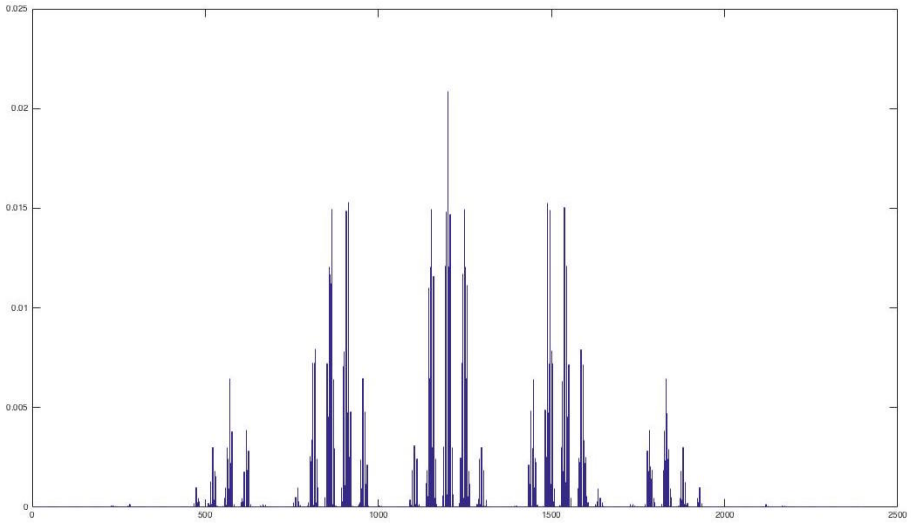

Figure 7.1: Probability distribution for *all* $[2\times2]$ spatiotemporal domains. $N = 100 \quad T = 20\,000 \quad s = 3$.

Nevertheless, if our statistical analysis is improved, few other analysis can be accomplished:

- Try spatiotemporal domains of size $[3\times3]$. But because the total number $7^9 = 40\,353\,607$, an even larger sample would then be required to appropriately study the probability distribution of those blocks, at least of order of 10^9.

- Next, look for probing rules for spatiotemporal domains of size $[3\times3]$, that are NOT probing rules for $[2\times2]$ spatiotemporal domains...

Internal symbols

We close our discussion by focusing on the significance or internal symbols. The frequencies of appearance of all [2×2] and [3×3] internal blocks are analyzed for the case $s = 5$. The internal symbols are then $\{-1, 0, 1\}$ and the simulations are for $N = 30$ and $T = 50\,000$. For this sample, the 81 $[2\times2]$ blocks of internal symbols are spread evenly (figure 6.2 a), which confirms that for a given trace s, the internal symbols have a uniform distribution. For the 19683 $[3\times3]$ blocks, the same behavior tends to be observed but the ratio *number of sequences* to *size of the sample* seems once again to "deform" such distribution.

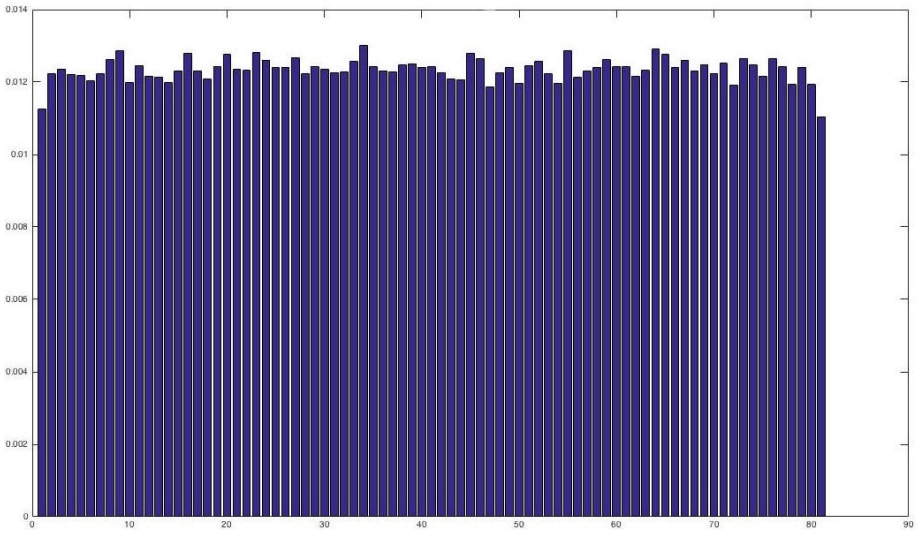

Figure 7.2: (a) $[2\times 2]$ spatiotemporal domains.

7.4 Future work...

A lot still remains to be done in order to get a complete understanding of Coupled Cat Maps. Among other things, one important factor is the fact that this symbolic dynamics present a symmetry between space and time. In figure 7.3 the probability distribution for spatiotemporal domains of shape $[2\times 1]$ (evolution in time) and $[1\times 2]$ (evolution in space) are both drawn. A total of 81 spatiotemporal domains in each case is obtained, and present very similar distributions. [2]

Other future work also involve the reconstruction of orbits in the phase space based on symbolic sequences. A significant step in the understanding of semi-classical particles in a chaotic regimes...

References

[1] B. Gutkin, L. Han, R. Jafari, A. K. Saremi, and P. Cvitanović, Linear encoding of the spatiotemporal cat map, In preparation, 2018.

[2] B. Gutkin and V. Osipov, "Classical foundations of many-particle quantum chaos", Nonlinearity **29**, 325–356 (2016).

[2] Predrag 2016-08-02 Rather than 'similar', aren't they supposed to be identically the same? Are there some numerical differences in the columns of the two figures (they cannot be seen in the plots)?:

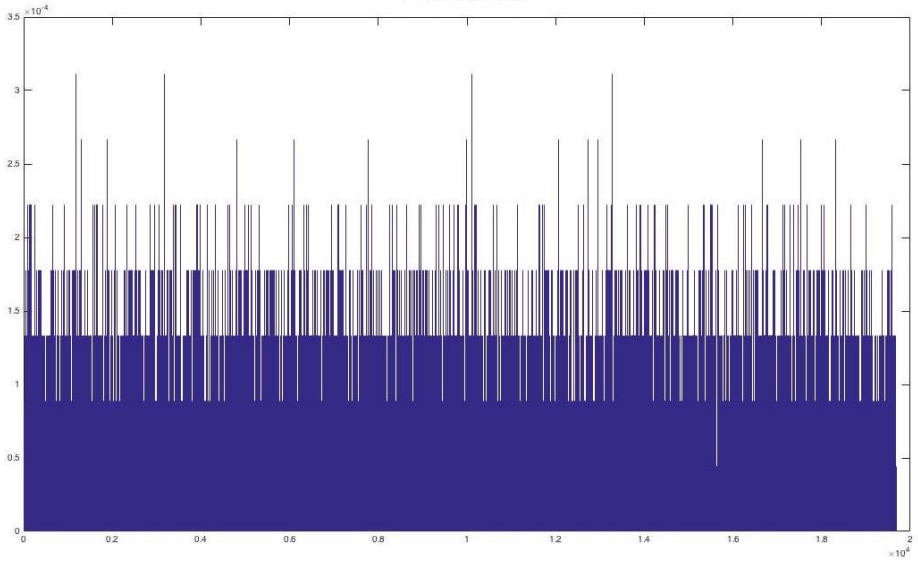

Figure 7.2: (b) $[3\times 3]$ spatiotemporal domains.
Probability distribution for sequences of internal symbols.
$N = 30 \quad T = 50\,000 \quad s = 5$.

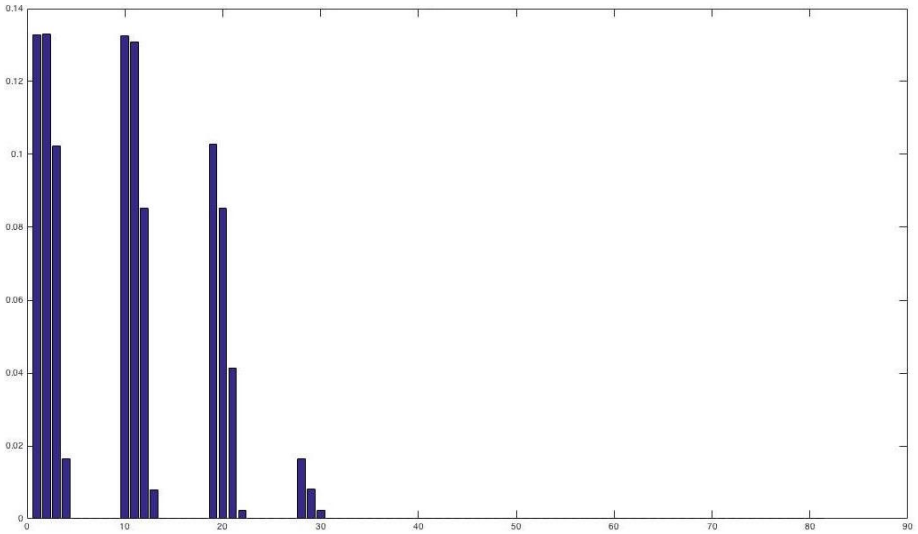

Figure 7.3: (a) $[2\times 1]$ spatiotemporal domains.

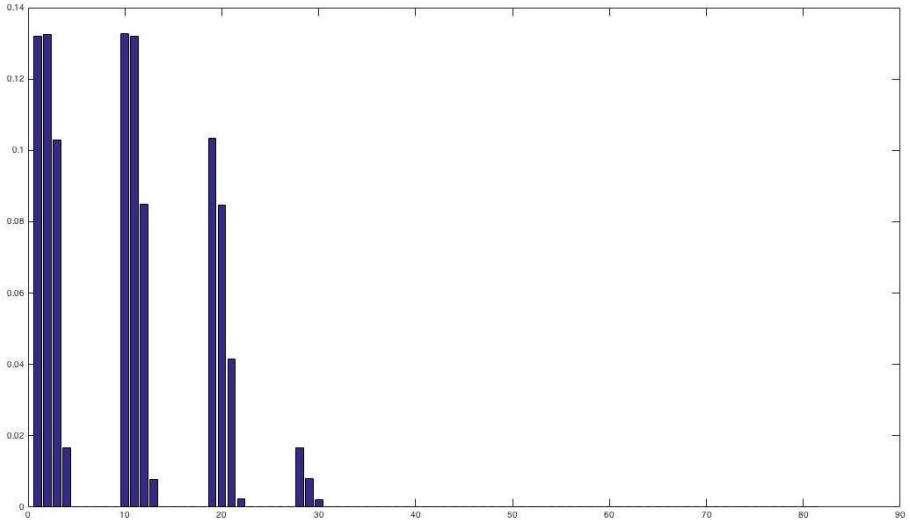

Figure 7.3: (b) $[1\times 2]$ spatiotemporal domains.
Probability distribution of *all* $[2\times 1]$ and $[1\times 2]$ spatiotemporal domains.
$N = 30 \quad T = 50\,000 \quad s = 5$.

Chapter 8

Rana's blog

Rana Jafari <jafari.rana@gmail.com> work blog
The latest entry at the bottom for this blog

2016-01-19 Rana Here is an example of text edit by me, and here one of a footnote by me[1].

2015-11-20 Rana (Discussion with Predrag, Kuramoto-Sivashinsky equilibria and relative equilibria project Spring 2016:

- blog the project progress here
- blog whatever I'm reading and learning about dynamical systems here

2016-01-19 Rana I've been working on reading the ChaosBook materials and doing the online Course 1.

2016-06-05 to 06-11 Rana Read Chapters 14, 17, part of 18, and 19 of Chaosbook. Did homework of Weeks 9 and 10. Read 1st chapter of Hao and Zheng [1] *Applied Symbolic Dynamics and Chaos*, and started reading 2nd chapter.

2016-06-13 Predrag Try not to get further into Hao and Zheng [1] than necessary. You want to return to symbolic dynamics for cat map as fast as possible, and then understand Gutkin and Osipov coupled lattice generalization.

2016-07-08 Predrag to Rana: Do you agree with Li Han table 1.1 on the numbers of pruned blocks?

2016-07-10 Rana Li's and my results are in agreement.

[1] Rana 2016-01-19: Rana test footnote

2016-07-11 Predrag to Rana: Can you complete table 1.1? Li Han did not write what the numbers of new pruned blocks are.

2016-07-11 Predrag to Rana: I can already see that several of my posts has not been recovered after you erased my edits (by mitting to *svn up* before starting your edits). For example, all my instructions about how to add figures are gone (but there is a copy at the end of Adrien's blog. You have to add *RJfrequencies.png* (or *RJfrequencies.pdf*) to *siminos/figs/*, then *svn add Jfrequencies.png*.

Can you quickly recheck your blog, make sure I have not introduced new errors while trying to recover my edits?

2016-07-12 Rana Li and I checked our the results at the meeting, and we had the same results for $|a|$ up to 5 . I saw table 1.1 today, the number of inadmissible sequences that I found for $|a| = 7$ differs from Li's. I wrote my results in table 6.2.

2016-07-12 Predrag You might have *svn add RJfrequencies.png* (or *RJfrequencies.pdf*) to *siminos/figs/*, but it has not been added to the repository yet (you can see that from the commit emails). Wonder why? Perhaps this:

Remember, always, before *svn up* and *svn ci-m"added entropy figures"* you have to go to the root directory, *cd [...]/siminos*. Otherwise you are not refreshing bibtex, figures and other files in the repository.

2016-07-12 Predrag to Rana:

On *zero.physics.gatech.edu*, or Matt's *light.physics.gatech.edu*, or Xiong's *hard.physics.gatech.edu*, or Boris' *love.physics.gatech.edu*, or any other CNS linux workstation your userid is

rjafari7 (the same passwd as for svn - please change it once you log in)

Do not do calculations on the server *zero.physics.gatech.edu* - from any machine (including your laptop)

ssh *rjafari7@light.physics.gatech.edu*

save all data on the local hard disk */usr/local/home/rjafari7/*. I have made a link in your CNS home directory:

cd homeLight

Help for CNS system is on

www.cns.gatech.edu/CNS-only cnsuser cnsweb

but current crop of grad students, as a matter of principle, never look at any info, or add to these homepages.

Good luck - Xiong knows `linux` best, also Chris Marcotte and Burak Budanur (via Skype) know a lot. All our documentation is on

References

[1] B.-L. Hao and W.-M. Zheng, *Applied Symbolic Dynamics and Chaos* (World Scientific, Singapore, 1998).

Chapter 9

Adrien's blog

Adrien K. Saremi <adriensaremi@gmail.com> work blog
The latest entry at the bottom for this blog

9.1 Introduction

Following Gutkin and Osipov [3] *Classical foundations of many-particle quantum chaos*, we write Hamilton's equations for a set of N particles with generalized coordinates $\{q_n, p_n\}$ described in the section *3.1 Dynamics*. Let

$$\mathcal{Z}_t = \left\{ \begin{array}{c} q_t \\ p_t \end{array} \right\} = \left\{ \begin{array}{c} q_{1,t} \\ p_{1,t} \\ ... \\ p_{N,t} \\ q_{N,t} \end{array} \right\} .$$

The equations of motion are represented in the matrix form:

$$\mathcal{Z}_{t+1} = \mathcal{B}_N \mathcal{Z}_t$$

with

$$\begin{aligned} \mathcal{B}_N &= \begin{pmatrix} A & B & 0 & \dots & 0 & B \\ B & A & B & \dots & 0 & 0 \\ 0 & B & A & \dots & 0 & 0 \\ \vdots & \vdots & \vdots & \ddots & \vdots & \vdots \\ 0 & 0 & 0 & \dots & A & B \\ B & 0 & 0 & \dots & B & A \end{pmatrix} \\ A &= \frac{1}{c} \begin{pmatrix} a & 1 \\ ab - c^2 & b \end{pmatrix}, \qquad B = -\frac{1}{c} \begin{pmatrix} d & 0 \\ db & 0 \end{pmatrix} \end{aligned} \tag{9.1}$$

9.2 Arnol'd cat map

To start our project, Boris advised us to start with just one particle $N = 1$ and pick the values $a = 1$, $b = 2$ and $c = -1$ (Arnol'd cat map) such that

$$\mathcal{B}_N = \mathcal{B}_1 = A = \begin{pmatrix} 1 & 1 \\ 1 & 2 \end{pmatrix}, \qquad \det A = 1\,.$$

This system can be written as:

$$\begin{pmatrix} q_{t+1} \\ p_{t+1} \end{pmatrix} = A \begin{pmatrix} q_t \\ p_t \end{pmatrix} \mod 1 \tag{9.2}$$

The goal is now to find prime periodic orbits p of period T_p and initial points $(q_{p,1}, p_{p,1})$ such that:

$$\begin{pmatrix} q_{p,T_p} \\ p_{p,T_p} \end{pmatrix} = \begin{pmatrix} q_{p,1} \\ p_{p,1} \end{pmatrix} \mod 1$$

9.2.1 First approach

Consider

$$\begin{pmatrix} q_{||} \\ p_{||} \end{pmatrix} = A^{||} \begin{pmatrix} q_0 \\ p_0 \end{pmatrix} \mod 1$$

Now demand that (q_0, p_0) is periodic point in a prime periodic orbit p on $\mathbf{T}^2$ (two–dimensional torus), i.e., a relative periodic orbit on $\mathbb{Z}^2$, periodic up to a shift by integers (m_q, m_p):

$$\begin{pmatrix} q_0 \\ p_0 \end{pmatrix} = A^{||} \begin{pmatrix} q_0 \\ p_0 \end{pmatrix} + \begin{pmatrix} m_q \\ m_p \end{pmatrix}$$

Therefore:

$$\begin{pmatrix} q_0 \\ p_0 \end{pmatrix} = (\mathbb{1} - A^{||})^{-1} \begin{pmatrix} m_q \\ m_p \end{pmatrix}$$

Boris suggested that we take two random points (M_q, M_p) apply the inverse of $\mathbb{1} - A^{||}$, and remove the integer part (modulo 1) to find (q_0, p_0). Unfortunately it is hard to find the number $||$... The number of periodic orbits (AKA the number of sets of (q_0,p_0) would be then given by:

$$|\det(\mathbb{1} - A^{||})| = |(1 - \lambda^{||})(1 - \frac{1}{\lambda^{||}})|$$

where λ is the largest eigenvalue of A: $\lambda = \frac{3+\sqrt{5}}{2} = 2.6180\cdots$.

We also tried two random initial points $q_0 = 0.5$ and $p_0 = 0.4$, and applied the A matrix several times in hope that the iteration would return to the initial points, but this was unsuccessful (as expected)

9.2.2 2nd approach

Here we eliminate $\{p_t\}$ in favor of a 2-step recurrence equation for $\{q_t\}$ only. Boris gave us a different set of equations of motion, but I believe that we can obtain equations only on $\{q_t\}$ the following way:

$$p_t = \frac{q_t - q_{t-1}}{\Delta t} = q_t - q_{t-1}$$

Combined with:

$$q_{t+1} = q_t + p_t$$

We obtain:

$$\begin{aligned} q_3 - 3q_2 + q_1 &= m_2 \\ q_4 - 3q_3 + q_2 &= m_3 \\ &\vdots \\ q_{||+1} - 3q_{||} + q_{||-1} &= m_{||} \\ q_{||+2} - 3q_{||+1} + q_{||} &= m_{||+1} \end{aligned} \tag{9.3}$$

Given that we are looking for periodic orbits, and that $q_{||+1} = q_1$ and $q_{||+2} = q_2$, the last equation reduces to:

$$q_2 - 3q_1 + q_{||} = m_1$$

This set of equations reduces to the following matrix form:

$$\mathcal{D}Q = m$$

With $Q = \begin{pmatrix} q_1 \\ q_2 \\ \vdots \\ q_{||} \end{pmatrix}$, $m = \begin{pmatrix} m_1 \\ m_2 \\ \vdots \\ m_{||} \end{pmatrix}$, and $\mathcal{D} = \begin{pmatrix} -3 & 1 & 0 & 0 & 0 & \dots & 1 \\ 1 & -3 & 1 & 0 & 0 & \dots & 0 \\ \vdots & & & & & & \\ 1 & 0 & 0 & 0 & \dots & 1 & -3 \end{pmatrix}$

Boris suggested to pick a random set of integers $\begin{pmatrix} M_1, M_2, \cdots, M_{||-1} \end{pmatrix}^T$ apply the $\mathcal{B}$ matrix, and take the modulo.

BUT AGAIN: how are we supposed to get the size of the matrix?!?!

9.2.3 Computing periodic orbits

2016-06-01 Adrien Since our web meeting of Friday, May 27th, Boris suggested to run simulations on Matlab as follows:

1. use the 2nd approach, sect. 9.2.2, and start with random q_1 and q_2
2. compute q_3 and m_1 using (9.3)
3. q_3 is the decimal part of the equation, while m_1 is the integer part
4. repeat for a large number of iterations

5. if we come back on our feet, AKA $q_{n+1} = q_1$ and $q_{n+2} = q_2$, we have a periodic orbit of period n

I did those simulations, and obtain, as Li Han, values of $m_j \in \{-1, 0, 1, 2\}$. What I also found was that, depending on the few starting point of form $\{q_1, q_2\} = \{\frac{P_1}{10}, \frac{P_2}{10}\}$ that I tried, the period n is either $1, 6, 7, 10, 30$ or does not converge to a periodic orbit, computing in Matlab, double precision.

2016-06-17 Predrag You are sure the periods were " $1, 6, 7, 10, 30$", or is there a typo in this list? [1]

2016-06-09 Adrien Explaining the results:

This program allows us to start with many different sets of points q_1, q_2. For example, the program will first run the set of points $\{q_1, q_2\} = \{0.0, 0.0\}$, do the computations of $N = 100$ points, and "pray" to find periodicity. What I observed so far was that the largest periodicity for a given starting set would be $n = 30$, otherwise, the orbit would not be periodic.

The next part of the program is to do the same computations for a different starting set, following this method:

$$q_1 = q_1 + \Delta_1 \quad q_2 = q_2 + \Delta_2$$

such that the starting points remain in the unit interval $[0, 1]$.

For $\Delta_1 = \Delta_2 = 0.1$, we obtain orbits for 100 starting sets:

$$\{q_1, q_2\} \in \big\{\{0.0, 0.0\}, \{0.0, 0.1\} \dots \{0.0, 0.9\}, \{1.0, 0.0\}, \{1.0, 0.1\} \dots \{0.9, 0.9\}\big\}$$

These starting sets are rational numbers P/Q, $1 \leq P < Q$ of form $P/10$. I have observed that for several different starting sets, the frequency of repetition of symbols $\{-1, 0, 1, 2\}$ has some similarities. For example:

- For $\{q_1, q_2\} = \{0.2, 0.0\}$ the probabilities I obtain are:

$$p_{-1} = 0.204, p_0 = 0.398, p_1 = 0.194, p_2 = 0.204$$

- For $\{q_1, q_2\} = \{0.3, 0.6\}$ we get:

$$p_{-1} = 0.204, p_0 = 327, p_1 = 0.265, p_2 = 0.204$$

- And for $\{q_1, q_2\} = \{0.8, 0.3\}$ we get:

$$p_{-1} = 0.204, p_0 = 0.337, p_1 = 0.255, p_2 = 0.204$$

Observations:

[1] Predrag : the correct list is (9.4)

1. For those sets, the outer symbols repeat with the same frequency, the inner ones change. Something to look into...
2. There are many frequencies that keep reappearing over for different starting sets. Some even have the same p_{-1}, p_0, p_1, p_2 but different m_j sequences...
3. I still happen to find that some orbits, even though all starting sets are rationals, are not periodic. Pretty sure I still have to work on precision and removing error, because I should obtain periodic orbits, or should I??

2016-06-12 Predrag Don't you think that if you get more statistics (you put no error brackets on your numbers) $p_2 = 0.204$ will become $p_2 = 1/5$, for example?

2016-06-13 Boris If your starting points q_1, q_2 are rational, the resulting orbit is always periodic by the following reason. Assume the initial momentum and coordinate are rational numbers with some common denominator N. Since cat map is composed of integers, after n steps momentum and coordinate have the form $q_n = a_n/N$, $p_n = b_n/N$ i.e., have the same denominator N. So you travel on the lattice of the size $N \times N$ and sooner or later must close the loop. The reason why sometimes you do not find periodic orbits is due to round-off errors. Another point - the frequency of a symbol appearances in periodic orbits (generated by picking "random" rational initial conditions) might be quit different from one for a generic non-periodic orbit.

2016-06-15 Adrien Explaining results, follow up...:

If I run the program for $N = 1000$, I find the following probabilities:

- For $\{q_1, q_2\} = \{0.2, 0.0\}$:

$$p_{-1} = \frac{1}{5}, p_0 = \frac{2}{5}, p_1 = \frac{1}{5}, p_2 = \frac{1}{5}$$

- For $\{q_1, q_2\} = \{0.3, 0.6\}$:

$$p_{-1} = \frac{1}{5}, p_0 = \frac{1}{3}, p_1 = \frac{4}{15}, p_2 = \frac{1}{5}$$

- For $\{q_1, q_2\} = \{0.8, 0.3\}$:

$$p_{-1} = \frac{1}{5}, p_0 = \frac{1}{3}, p_1 = \frac{4}{15}, p_2 = \frac{1}{5}$$

In some rational starting sets, there were also cases where I could not "come back" to the starting set $\{q_1, q_2\}$. For those starting sets, the program now looks for periodicity in the m_j sequence. And for all starting sets that I described above, even with $\Delta_1 = \Delta_2 = 0.01$, all m_j vectors exhibit a periodic behavior. The most frequent and highest periodicity I found was $n = 30$ for all those starting sets. The periodicities I found were

$$1, 2, 3, 6, 10, 30\,. \tag{9.4}$$

The second important observation was that for irrational starting points, such as $\{q_1, q_2\} = \{\frac{\pi}{6}, \frac{\pi}{8}\}$, even if $N = 20\,000$, the program found no periodicity, neither in the q_j's, nor the m_j sequences. That confirms what Boris mentioned in his previous remark.

Should I try with other numbers? More rational? More irrational?

I guess that the next step is what Boris told Rana in their meeting today: looking for frequencies of sequences of 2 symbols, then sequences of 3 symbols, ...

2016-06-17 Predrag : I assume that you stop your program once a periodic orbit is found, not always go all the way to $N = 1000$?

- [ ] Explain your result for $\{q_1, q_2\} = \{1/5, 0\}$
- [ ] Explain why your results above, for $\{q_1, q_2\} = \{3/10, 3/5\}$ and $\{q_1, q_2\} = \{4/5, 3/10\}$, are wrong for these initial points (but not for their irrational approximations).
- [ ] Derive the $\{p_{-1}, p_0, p_1, p_2\} = \{1/5, 1/3, 4/15, 1/5\}$. Hint: derive the $\{m_j\}$ partition of the unit square that Li Han had shown you.

2016-06-17 Predrag : Determine the possible periodic point denominators, periods for

- [ ] $\{q_1, q_2\} = \{\frac{P_1}{10}, \frac{P_2}{10}\}$
- [ ] $\{q_1, q_2\} = \{\frac{P_1}{100}, \frac{P_2}{100}\}$
- [ ] $\{q_1, q_2\} = \{\frac{P_1}{8}, \frac{P_2}{8}\}$
- [ ] $\{q_1, q_2\} = \{\frac{P_1}{17}, \frac{P_2}{17}\}$

How many decimal digits of accuracy you need to be sure that all periodic orbits close with accuracy of 10^{-4} for

- [ ] $\{q_1, q_2\} = \{\frac{P_1}{10}, \frac{P_2}{10}\}$?
- [ ] $\{q_1, q_2\} = \{\frac{P_1}{100}, \frac{P_2}{100}\}$?
- [ ] $\{q_1, q_2\} = \{\frac{P_1}{8}, \frac{P_2}{8}\}$?
- [ ] $\{q_1, q_2\} = \{\frac{P_1}{7}, \frac{P_2}{7}\}$?

[ ] If the program is computing with double precision accuracy, what is the longest period that can be determined by mindless computation?

Hint: you know Floquet multipliers for all cat map orbits.

2016-06-17 Predrag : Don't let Matlab prevent you from thinking. You know that periodic points are rationals of form $\{q_j, q_{j+1}\} = \{P_j/Q, P_{j+1}/Q\}$, so at every iterate of your trajectory you can correct the 1-step error by replacing your decimal number by the nearest correct rational. This way you can compute any periodic orbit, of any period, as this eliminates the exponential accumulation of errors. Write a program that beats Li Han's zillion digits accuracy :)

[ ] If the computation is done by thinking (+ a computer program), estimate the longest period that can be determined by thoughtful computation.

Of course, all this is a magic of rationals and number theory - the moment the maps go nonlinear, none of this trickery works. Still, it might be useful in tracking the symbolic dynamics for nonlinear maps as well, in the way in which the ChaosBook dike map captures the correct symbolic dynamics of any nonlinear unimodal map. For example, slightly deformed cat map still has the same symbolic dynamics as the (piecewise linear) Arnol'd cat map [1].

2016-06-21: Boris' lecture of today - Adrien We're explaining how the symbolic dynamics, in other words the array of m, relate to the trajectory in the phase space.
For the Arnol'd cat map we know that:

$$\mathcal{D}_n Q_n = m_n \,,$$

with $Q_n = \begin{pmatrix} q_1 \\ q_2 \\ \vdots \\ q_{||} \end{pmatrix}$, $m_n = \begin{pmatrix} m_1 \\ m_2 \\ \vdots \\ m_{||} \end{pmatrix}$ and

$$\mathcal{D}_n = \begin{pmatrix} -3 & 1 & 0 & 0 & 0 & \dots & 1 \\ 1 & -3 & 1 & 0 & 0 & \dots & 0 \\ \vdots & & & & & & \\ 1 & 0 & 0 & 0 & \dots & 1 & -3 \end{pmatrix}$$

For a given n, we define N_n as the total number of orbits with length n. It is pretty clear that $N_n = |\det(\mathcal{D}_n)|$, which also corresponds to $N_n = |\det(\mathbb{1} - A^n)|$ if we follow the first method.

For a given sequence of length p, such as $\{m_1 m_2 \dots m_p\}$, we also define $N_n(m_1 m_2, \dots m_p)$ as the number of periodic orbits of length n that generate the given sequence. The probability of obtaining the sequence $\{m_1, m_2, \dots, m_p\}$ is then:

$$p(m_1 m_2 \dots m_p) = \lim_{n\to\infty} \frac{N_n(m_1 m_2 \dots m_p)}{N_n}$$

1. Let's now do the case $p = 1$, where $m_k = a$ and a is a given symbol. The equations of motion can be rewritten as:

$$\begin{cases} q_{i-1} + q_{i+1} = 3q_i + m_i \quad \forall i \neq k \\ q_{k-1} + q_{k+1} = 3q_k + a \end{cases}$$

$$\begin{cases} q_{i-1} + q_{i+1} = 3q_i + m_i \quad \forall i \neq k, k-1, k+1 \\ q_{k-2} + \frac{1}{3} q_{k+1} = \frac{8}{3} q_{k-1} + \frac{a}{3} + m_{k-1} \\ q_{k+2} + \frac{1}{3} q_{k-1} = \frac{8}{3} q_{k+1} + \frac{a}{3} + m_{k+1} \end{cases}$$

   This system we can write in the matrix form

$$\mathcal{D}_{n-1} Q_{n-1} = m_{n-1} + \frac{a}{3} J$$

   where $\mathcal{D}_{n-1}, Q_{n-1}$, and m_{n-1} are the same as the $\mathcal{D}_n, Q_n$, and m_n, with the k^{th} row removed, and with:

$$J^\top = \left(0, 0, \vdots, 1, 1, 0, \cdots, 0, \right) .$$

   The three inequalities we "collect" from all this mess are then:

$$\begin{gathered} 0 \leq q_{k-1} < 1 \\ 0 \leq q_{k+1} < 1 \\ a \leq q_{k-1} + q_{k+1} < a + 3 \end{gathered}$$

   For $a \in \{-2, -1, 0, 1\}$, it is pretty clear how to derive the regions admissible in the plane defined by q_{k-1} and q_{k+1}

2. For $p = 2$ and $n = 4$, we specify $m_2 = a$ and $m_3 = b$ and we limit our study to orbits of length 4. Indeed, only the outer points of the given sequence (here q_1 and q_4) span the lattice on which we can derive the admissible regions. For such system, the 4 inequalities that help us doing so are:

$$\begin{gathered} 0 \leq q_1 < 1 \\ 0 \leq q_4 < 1 \\ 0 \leq \tfrac{1}{8}(3q_1 + q_4 - 3a + b) < 1 \\ 0 \leq \tfrac{1}{8}(3q_4 = q_1 - 3b - a) < 1 \end{gathered}$$

2016-06-21 Answering Pedrag's questions - Adrien First of all, I modified my m_j vector such that it is made of the symbols$\{-2,-1,0,1\}$. Now answering the questions:

1. For $\{q_1,q_2\} = \{\frac{1}{5},0\} = \{0.2,0\}$ (the decimal or rational notation doesn't make a difference), my program actually computes 1000 iteration since it does not find periodicity through the Q matrix. Nevertheless, it observes a repetition of symbol in the m_j vector as follow:

$$m = \begin{pmatrix} -2 \\ 0 \\ 0 \\ -2 \\ 1 \\ 0 \\ -1 \\ -1 \\ 0 \\ 1 \end{pmatrix}$$

It is then easy to figure that:

$$p_{-2} = \frac{1}{5}, p_{-1} = \frac{1}{5}, p_0 = \frac{2}{5}, p_1 = \frac{1}{5}$$

2. For $\{q_1,q_2\} = \{\frac{3}{10},\frac{3}{5}\}$ the m_j vector is:

$m^T = (0,0,-2,1,-1,-2,1,0,0,-2,1,-1,0,-1,-1,0,-1,1,-2,0,0,1,2,-1,1,-2,0,-1,0,0)$

and for $\{q_1,q_2\} = \{\frac{4}{5},\frac{3}{10}\}$

$m^T = (0,0,1,-2,-1,1,-2,0,-1,0,0,-1,0,-2,1,-1,-2,1,0,0,-2,1,-1,0,-1,-1,0,-1,1,-2)$

For both cases, the periodicity is $n = 30$.
By counting the frequencies of $-2,-1,0,1$, I confirm the probabilities are different than the ones I wrote earlier. I might have wrongly interpreted the fractions given the decimal approximation of Matlab. For $\{q_1,q_2\} = \{0.3,0.6\}$:

$$p_{-2} = \frac{1}{5}, p_{-1} = \frac{7}{30}, p_0 = \frac{11}{30}, p_1 = \frac{1}{5}$$

However, for $\{q_1,q_2\} = \{0.8,0.3\}$, the result is identical:

$$p_{-2} = \frac{1}{5}, p_{-1} = \frac{4}{15}, p_0 = \frac{1}{3}, p_1 = \frac{1}{5}$$

3. I am not so sure about this question. We know now that the following distribution $p_{-2} = \frac{1}{5}, p_{-1} = \frac{4}{15}, p_0 = \frac{1}{3}, p_1 = \frac{1}{5}$ can be generated from the starting set $\{q_1, q_2\} = \{0.8, 0.3\}$. But we obtain such frequencies after 30 iterations, since it's the length of this periodic orbit. If we refer to what Li Han presented over last week, we actually look at 1 iteration but for a GREAT number of starting sets spread over the unit square.
   For $\{q_1, q_2\} = \{i\Delta_1, j\Delta_2\}$ with $\Delta_1 = \Delta_2 = \frac{1}{200}$ and $i, j = 0, 1, 2, \ldots, 199$, we obtain data for m_1 over 40,000 points spread over the unit square:

$$p_{-2} = 0.16583, p_{-1} = 0.33335, p_0 = 0.33310, p_1 = 0.16773$$

   Which should fit with the theoretical values that we get from "Boris inequalities" that lead to admissible areas in the unit square spanned by $\{q_0, q_2\}$:

$$p_{-2} = \frac{1}{6}, p_{-1} = \frac{1}{3}, p_0 = \frac{1}{3}, p_1 = \frac{1}{6}$$

4. For "starting sets" of the form $\{\frac{i}{N}, \frac{j}{N}\}$, we obtain the following periodicities:
   - For $\{q_1, q_2\} = \{\frac{i}{10}, \frac{j}{10}\}$, the periodicities found were: $n = 1, 2, 3, 6, 10, 30$
   - For $\{q_1, q_2\} = \{\frac{i}{100}, \frac{j}{100}\}$, they were: $n = 1, 2, 3, 6, 10, 30, 50, 150$
   - For $\{q_1, q_2\} = \{\frac{i}{8}, \frac{j}{8}\}$, $n = 1, 3, 6$
   - And for $\{q_1, q_2\} = \{\frac{i}{17}, \frac{j}{17}\}$ $n = 1, 18$

   Now if I understand your question carefully, we try to make sure than the final computed value of q_N, or q_n for periodic orbits, is within 10^{-4} from the actual $q_{n,real}$, in the worst case scenario. Let n_{max} the highest periodicity, and ϵ the error; then:

$$q_{n,comp} = q_{n,real} + \epsilon\, \lambda^{n_{max}}, \text{ where } \lambda = \frac{3+\sqrt{5}}{2} = \text{multiplier}$$

   So we want:

$$|\epsilon\, \lambda^{n_{max}}| \leq 10^{-4} \Rightarrow \epsilon \leq 10^{-4}\, \lambda^{-n_{max}}$$

   - For $\{q_1, q_2\} = \{\frac{i}{10}, \frac{j}{10}\}$, $\epsilon \approx 10^{-18}$
   - For $\{q_1, q_2\} = \{\frac{i}{100}, \frac{j}{100}\}$, $\epsilon \approx 10^{-68}$
   - For $\{q_1, q_2\} = \{\frac{i}{8}, \frac{j}{8}\}$, $\epsilon \approx 10^{-8}$
   - And for $\{q_1, q_2\} = \{\frac{i}{17}, \frac{j}{17}\}$ $\epsilon \approx 10^{-12}$

5. If we use double digit accuracy, aka 64 bits but 53 bits for accuracy, it means the error $\epsilon = 2^{-53}$. Following the same logic:

$$|\epsilon\, \lambda^{n_{max}}| \leq 10^{-4}$$

$$\Rightarrow n_{max} \approx \ln(\lambda)\ \ln(\frac{10^{-4}}{\epsilon})$$

$$\Rightarrow n_{max} = 26$$

6. Coming soon...

2016-07-10 Adrien One more thing to add regarding the single Cat Map: the correlation of frequencies. I found interesting how the correlation between future and past symbolic dynamics vanish exponentially.
I pretty much did what Rana had done before, computing frequency of a given sequence $A = [a_1, \ldots, a_u]$ of length u, another one $B = [a_1, \ldots, a_v]$ of length v, as well as the frequency of seeing one repeated a length $space$ (for example $space = 3$) after the other. We then increase the *spacing* and observe how the correlation factor:

$$Correl = p(A, space, B) - p(A)\, p(B) \quad \text{behaves}$$

For the ergodic orbit $\{q_1, q_2\} = \{\frac{\sqrt{5}}{4}, \frac{\sqrt{2}}{2}\}$, $A = [-1, 1]$, and $B = [-2, 0]$ and of length $N = 1,000,000$, we obtain the following:

$$p(A) = 0.1249 \quad p(B) = 0.0623$$

$Spacing$	$P(A, space, B)$	$Correl$
1	0.0085	$7.3567\ 10^{-4}$
2	0.0066	-0.0011
3	0.0073	$-4.6733\ 10^{-4}$
4	0.0080	$1.8867\ 10^{-4}$
5	0.0079	$6.8666\ 10^{-5}$
6	0.0078	$4.6655\ 10^{-6}$

For longer sets $A = [-1, -1, -1, -1]$ and $B = [-2, 1, -1, 0]$, and the same orbit, the probabilities are as follow:

$$p(A) = 0.0178 \quad p(B) = 0.0151$$

$Spacing$	$P(A, space, B)$	$Correl$
1	$2.9400\ 10^{-4}$	$2.4439\ 10^{-5}$
2	$2.2400\ 10^{-4}$	$-4.5561\ 10^{-5}$
3	$2.4900\ 10^{-4}$	$-2.0561\ 10^{-5}$
4	$2.5100\ 10^{-4}$	$-1.8561\ 10^{-5}$
5	$2.7300\ 10^{-4}$	$3.4392\ 10^{-6}$
6	$2.6900\ 10^{-4}$	$-5.6081\ 10^{-7}$

Conclusion: We clearly see that in both scenarios, the Correlation factor diminishes as the separation between the two blocs increases. We also notice that for longer sets A and B, the correlation is small enough (but not zero) even for small spacing...

9.3 Coupled Cat Maps

We now get to more complicated systems by increasing the number of particle N. T will be now known as the period of the orbit, and if it doesn't exist, T will just refer to latest time iteration in the computation of the symbols m's. Another objective of this study is to explain the impact of certain factors such as the trace of the A matrix (that we refer as $s = trace(A)$) on the nature of our alphabet, the frequencies of symbols repetition, the length of periodic orbits. and the admissibility of particular sequences of symbols.

9.3.1 Periodic orbits

We first verify the accuracy of our calculations by checking that rational sets $\{q_{1,1}, p_{1,1}, q_{2,1}, p_{2,1}, \ldots, q_{N.1}, p_{N,1}\}$ belong to periodic orbits. To do so, we perform the iteration:

$$\mathcal{Z}_{t+1} = \mathcal{B}_N \ \mathcal{Z}_t$$

over and over, until we obtain:

$$\mathcal{Z}_{T+1} = \mathcal{B}_N \ \mathcal{Z}_1$$

in which case, the periodicity is T. We first tried with a number of 3 particles ($N = 3$), and picked the same trace $s = 3$ that we used in part 7.2. The initial coordinates of $\mathcal{Z}_1$ are multiples of hundredth, chosen randomly, but above all are **between** $[\frac{-1}{2}, \frac{1}{2}]$. Therefore, our symbolic dynamic $m = \{m^q, m^p\}$ should be symmetric with respect to 0 (which is the case) and our matrix $\mathcal{B}_3$ is:

$$\mathcal{B}_3 = \begin{pmatrix} 2 & 1 & -1 & 0 & -1 & 0 \\ 1 & 1 & -1 & 0 & -1 & 0 \\ -1 & 0 & 2 & 1 & -1 & 0 \\ -1 & 0 & 1 & 1 & -1 & 0 \\ -1 & 0 & -1 & 0 & 2 & 1 \\ -1 & 0 & -1 & 0 & 1 & 1 \end{pmatrix}$$

- for $\mathcal{Z}_1 = \left\{ \ \frac{31}{100} \quad \frac{29}{100} \quad \frac{7}{50} \quad -\frac{13}{100} \quad \frac{31}{100} \quad \frac{3}{100} \ \right\}$

  the periodicity is $T = 60$, and the symbolic dynamics is:

$$\begin{aligned} m = -2, p_{-2} &= 0.011111 \\ m = -1, p_{-1} &= 0.222222 \\ m = 0, p_0 &= 0.536111 \\ m = 1, p_1 &= 0.227778 \\ m = 2, p_2 &= 0.002778 \end{aligned}$$

- for $\mathcal{Z}_1 = \left\{ \ -\frac{3}{20} \quad \frac{43}{100} \quad \frac{37}{100} \quad \frac{1}{20} \quad \frac{3}{25} \quad \frac{2}{25} \ \right\}$

the periodicity is $T = 60$, and the symbolic dynamics is:

$$\begin{aligned} m = -2, p_{-2} &= 0.016667 \\ m = -1, p_{-1} &= 0.222222 \\ m = 0, p_0 &= 0.511111 \\ m = 1, p_1 &= 0.244444 \\ m = 2, p_2 &= 0.005556 \end{aligned}$$

- for $N = 5$ and $\mathcal{Z}_1 = \left\{ \begin{array}{ccccccccc} -\frac{3}{10} & -\frac{1}{5} & -\frac{3}{100} & -\frac{27}{100} & \frac{17}{50} & -\frac{31}{100} & -\frac{7}{25} & -\frac{33}{100} & -\frac{7}{25} & -\frac{7}{100} \end{array} \right\}$

  the periodicity is $T = 60$, and the symbolic dynamics is:

$$\begin{aligned} m = -2, p_{-2} &= 0.007333 \\ m = -1, p_{-1} &= 0.222667 \\ m = 0, p_0 &= 0.540667 \\ m = 1, p_1 &= 0.221333 \\ m = 2, p_2 &= 0.008000 \end{aligned}$$

- And for $N = 7$ and

$$\mathcal{Z}_1 = \left\{ -\frac{19}{100} \; \frac{21}{50} \; -\frac{7}{100} \; -\frac{8}{25} \; \frac{2}{5} \; \frac{47}{100} \; -\frac{7}{100} \; -\frac{39}{100} \; -\frac{1}{4} \; -\frac{1}{10} \; \frac{9}{100} \; -\frac{6}{25} \; \frac{1}{10} \; \frac{21}{100} \right\}$$

  the periodicity is $T = 2790$, and the symbolic dynamics is:

$$\begin{aligned} m = -2, p_{-2} &= 0.012110 \\ m = -1, p_{-1} &= 0.226472 \\ m = 0, p_0 &= 0.526882 \\ m = 1, p_1 &= 0.224014 \\ m = 2, p_2 &= 0.010522 \end{aligned}$$

9.3.2 Ergodic orbits

We now focus on the nature of our symbolic dynamics, by choosing ergodic orbits, running for a very very long time $T = 80,000$. To do so, we start with an irrational set $\mathcal{Z}_1$ but $N = 5$ particles. The trace of the A matrix increases from 3 to 7 in order to obtain a larger alphabet of symbols. Remember that the trace $s = a + b$, so we just set $b = 1$ and $a \in \{2, \ldots, 7\}$ such that $s \in \{3, \ldots, 8\}$. Our initial set is:

$$\mathcal{Z}_1 = \left\{ \begin{array}{ccccccccc} \frac{\sqrt{5}}{6} & 0 & -\frac{\sqrt{3}}{6} & \frac{\sqrt{2}}{8} & \frac{\sqrt{3}}{14} & -\frac{\sqrt{5}}{12} & -\frac{\sqrt{6}}{20} & \frac{1}{17} & \frac{3}{10} & \frac{\sqrt{2}}{10} \end{array} \right\}$$

Observations:

1. The first thing we observe is that the orbit is not periodic. We obviously compute the frequencies of symbol that only appear in our dynamics. The number of particles $N = 5$ clearly has an impact on the nature of our

symbols.
We also compute the frequencies of the *Newtonian* dynamics, defined as:

$$c\,(q_{n,t+1} + q_{m,t-1}) + d\,(q_{n+1,t} + q_{n-1,t}) = -(a+b)q_{n,t} + m_{n,t}$$

The code computes our $\{m^q_{n,t}, m^p_{n,t}\}$ by only referring to the equation $\mathcal{Z}_{t+1} = \mathcal{B}_N\,\mathcal{Z}_t$ and by "capturing" the integer parts of the coordinates q's and p's (similarly to the Single Cat Map code I wrote). Once the orbit has been computed, the Newtonian symbolics $m_{n,t}$ (no upper index) can be derived from the position coordinates $q_{n,t}$.
Let's look at the frequencies of every of those symbols, as a function of the trace s.

- For $s = 3$, the frequencies obtained are:
  $m^{q,p} = -2, p_{-2} = 0.011450$
  $m^{q,p} = -1, p_{-1} = 0.224397$
  $m^{q,p} = 0, p_0 = 0.529401$
  $m^{q,p} = 1, p_1 = 0.223045$
  $m^{q,p} = 2, p_2 = 0.011706$
  And:
  $m = -3, p_{-3} = 0.000850$
  $m = -2, p_{-2} = 0.067293$
  $m = -1, p_{-1} = 0.264819$
  $m = 0, p_0 = 0.332571$
  $m = 1, p_1 = 0.267269$
  $m = 2, p_2 = 0.066364$
  $m = 3, p_3 = 0.000833$

- For $s = 4$, the frequencies obtained are:
  $m^{q,p} = -3, p_{-3} = 0.000444$
  $m^{q,p} = -2, p_{-2} = 0.044169$
  $m^{q,p} = -1, p_{-1} = 0.258639$
  $m^{q,p} = 0, p_0 = 0.394029$
  $m^{q,p} = 1, p_1 = 0.257650$
  $m^{q,p} = 2, p_2 = 0.044615$
  $m^{q,p} = 3, p_3 = 0.000455$
  And:
  $m = -3, p_{-3} = 0.010696$
  $m = -2, p_{-2} = 0.126391$
  $m = -1, p_{-1} = 0.236452$
  $m = 0, p_0 = 0.250635$
  $m = 1, p_1 = 0.239835$
  $m = 2, p_2 = 0.125378$
  $m = 3, p_3 = 0.010613$

- For $s = 5$, the frequencies obtained are:

$m^{q,p} = -3, p_{-3} = 0.005604$
$m^{q,p} = -2, p_{-2} = 0.095479$
$m^{q,p} = -1, p_{-1} = 0.254543$
$m^{q,p} = 0, p_0 = 0.290261$
$m^{q,p} = 1, p_1 = 0.252449$
$m^{q,p} = 2, p_2 = 0.095980$
$m^{q,p} = 3, p_3 = 0.005685$
And:
$m = -4, p_{-4} = 0.000592$
$m = -3, p_{-3} = 0.040080$
$m = -2, p_{-2} = 0.159941$
$m = -1, p_{-1} = 0.198742$
$m = 0, p_0 = 0.199551$
$m = 1, p_1 = 0.201197$
$m = 2, p_2 = 0.159721$
$m = 3, p_3 = 0.039697$
$m = 4, p_4 = 0.000479$

- For $s = 6$, the frequencies obtained are:
  $m^{q,p} = -4, p_{-4} = 0.000255$
  $m^{q,p} = -3, p_{-3} = 0.025382$
  $m^{q,p} = -2, p_{-2} = 0.142405$
  $m^{q,p} = -1, p_{-1} = 0.220257$
  $m^{q,p} = 0, p_0 = 0.224046$
  $m^{q,p} = 1, p_1 = 0.218919$
  $m^{q,p} = 2, p_2 = 0.143320$
  $m^{q,p} = 3, p_3 = 0.025151$
  $m^{q,p} = 4, p_4 = 0.000264$
  And:
  $m = -4, p_{-4} = 0.006921$
  $m = -3, p_{-3} = 0.083823$
  $m = -2, p_{-2} = 0.159604$
  $m = -1, p_{-1} = 0.167262$
  $m = 0, p_0 = 0.165642$
  $m = 1, p_1 = 0.166942$
  $m = 2, p_2 = 0.159625$
  $m = 3, p_3 = 0.083206$
  $m = 4, p_4 = 0.006975$

- For $s = 7$, the frequencies obtained are:

$m^{q,p} = -4, p_{-4} = 0.003830$
$m^{q,p} = -3, p_{-3} = 0.061620$
$m^{q,p} = -2, p_{-2} = 0.160081$
$m^{q,p} = -1, p_{-1} = 0.182371$
$m^{q,p} = 0, p_0 = 0.184342$
$m^{q,p} = 1, p_1 = 0.182932$
$m^{q,p} = 2, p_2 = 0.159601$
$m^{q,p} = 3, p_3 = 0.061515$
$m^{q,p} = 4, p_4 = 0.003706$

And:

$m = -5, p_{-5} = 0.000363$
$m = -4, p_{-4} = 0.028955$
$m = -3, p_{-3} = 0.113895$
$m = -2, p_{-2} = 0.141662$
$m = -1, p_{-1} = 0.142537$
$m = 0, p_0 = 0.144154$
$m = 1, p_1 = 0.142207$
$m = 2, p_2 = 0.142849$
$m = 3, p_3 = 0.114120$
$m = 4, p_4 = 0.028863$
$m = 5, p_5 = 0.000396$

=> One thing that boris emphasized on during our last meeting, is how the frequency of the internal Newtonian symbols (*difference internal/external coming soon*...) should be the same for a given $s = trace(A)$. According to Boris, in all the cases, the external symbols are the 6 outer ones in our alphabet. As you can see, the frequencies of the inner symbols tend be the same for a particular s, but still differ by the $\frac{1}{1000}$. I'm going to run longer simulations ($T = 500,000$) but just for one particular trace $s = 5$ and the same initial conditions. Hopefully, the frequencies will even be closer...

2. The next part is to derive analytically the frequencies for just 1 symbol, by exposing the equations that govern our symbolic dynamics. The number of inequalities we obtain then depends on the system: the number of particle N, the trace of A s and the symbol itself m_0 (that Boris calls a as well). This is something Rana, Li Han and I will discuss in details tomorrow (Tuesday), before our Wednesday meeting.

3. Looking for symmetry between time and space evolution T and N.

9.4 Adrien's blog

2016-01-19 Adrien Here is an example of text edit by me, and here one of a footnote by me[2].

2015-11-20 Adrien (Discussion with Predrag, Kuramoto-Sivashinsky equilibria and relative equilibria project Spring 2016:

- blog the project progress here
- blog whatever I'm reading and learning about dynamical systems here

2016-01-19 Adrien I've been working on reading the ChaosBook materials and doing the online Course 1.

2016-05-13 Report Adrien I am going to upload the tex. version of what I accomplished with Rana and Boris. The code can be copy/paste on Latex to be easily read. Sorry for taking so long, getting used to Latex is kind of a pain..

2016-05-16 Predrag I feel no guilt at all, only pride: you cannot be a physicist and write in `Micro$h!t Word`. What does not kill you will make you stronger :). I'll help with LaTeX - but please, do diff the edited files (Xiong or I can show you how) so I do not have to do the same edits over and over again.

2016-05-26 Predrag My suggestion is in the blog, but you might have not read it: "**2016-05-21 Predrag** Adrien and Rana wondered why are (9.2) and (9.3) the same equation. Have a look at the two forms of the Hénon equation in the ChaosBook Example 3.6. Or see (2.3) (eq. (2.2) in Percival and Vivaldi [4]). Does that help in understanding the relation? Once you do, write it up in your reports."

In any case, looks like you have done that, in deriving (9.3).

2016-06-01 Xiong Equation just above (9.2) may have a typo because there is a factor $1/c$ in the definition of A.

2016-06-02 Predrag : At the start of sect. 9.2 Adrien sets $c = -1$, so I think the rest is correct?

2016-06-06 Adrien : List of things to work through:

1. 14.1 Qualitative dynamics
2. 14.3 Temporal ordering: Itineraries
3. 14.4
4. 14.6 Symbolic dynamics, basic notions

[2] Adrien 2018-01-19: Adrien test footnote

Figure 9.1: Spatiotemporal plots of the ??. (a) this; (b) that. The initial ?? is given by ???.

5. Examples 14.2, 14.3, 14.6, 14.7 and 14.8
6. skip Chapter 15 "Stretch, fold, prune" for now
7. 17 Walkabout: Transition graphs (skip 17.3.1 "Converting pruning blocks into transition graphs" for now)
8. Example 17.1 Full binary shift; 17.2 Complete N-ary dynamics; 17.4 Pruning rules for a 3-disk alphabet; 17.4 Pruning rules for a 3-disk alphabet; 17.7 Complete binary topological dynamics; 17.8 ?Golden mean? pruning;

2016-06-22 Predrag Save your plots in *siminos/figs/* as *AKSmy1stFig.png* and *AKSmy2ndFig.png* (or *AKS*.pdf*), by the names referred to in the (currently commented) parts of figure 9.1.

You can rename the graphical files whatever you find natural, just prefix them by *AKS* and do not use spaces and to many special characters in their names - that might confuse Linux.

Make graphical files modest in size, $\approx 10\,KB$, rather than $\approx 100\,KB$, otherwise the whole repository grows to big and unwieldy. If do not know how to produce small graphical files, ask Xiong for help.

For an example of a table, see table 6.1.

2016-07-11 Adrien :

- Thanks for the heads up to include graphs in our blog. For now though, I have no graph, just results in forms of tables mostly (frequencies for example).
- I will complete the rest of my report on coupled maps once I obtain results for long (very long) computations. Probably will run those through the night...

2016-08-02 Adrien I would like to know how can we mention our references (for me, it will just Gutkin and Osipov [3]) given that we constantly use them? I mentioned his paper at the beginning of my report, but it wasn't more than that. Do you want us to repeatedly mention his publication, or can we mention it just once during the introduction, and make it clear for the rest of the document?

2016-08-02 Predrag Well, if you have not read anything else but the single Gutkin and Osipov [3] paper, I guess there is not much else to refer to.

But they did not invent cat maps, coupled lattices, cat map symbolic dynamics, linear coding, etc., so if you define the project and explain what is

already known (in order to explain what is new in your work) you might need more than one citation. My cat map chapter 1 and spatial lattice chapter 2 have about 30 or so citations, and the common blog chapter **??** has 57. You can see what some of the other student's projects have looked like here.

2017-09-06 Predrag Rana and Adrian reports are in this blog, in `siminos/spatiotemp/chapter/blogCats.tex` (check rev. 5445 message).

2017-09-06 Adrien I am not sure if you guys want me to change the symbol representation in the current figure 8 (current page 30)? I think I could add the numbers in question on top of the colored squares for better visual... but this may become overly 'dense.'

2017-09-06 Predrag I like your colorful figure 8, with the thin and thick square borders around the interior regions, and using both colored tiles and numbered tiles representations, current figures 10 and 12, just to illustrate the two possibilities. Boris and Li Han prefer that all three figures use the number representation. If that is the majority decision, I'm fine with it. We have the old figure 8 numbered tiles in `siminos/figs/AKSs7BlockBorderM1*.*`, can restore them.

2017-09-06 Adrien What do you mean by "integer $s > 4$" is not the correct condition, for $d = 2$ $s = 4$ is already hyperbolic. Give the correct condition on s, explain it."

I believe that we choose $s > 4$ to keep our system hyperbolic and to have a sufficiently large number of internal symbols in our alphabet $\mathcal{A}$. Would that be the reason you're looking for?

2017-09-06 Predrag A cat map is a fully chaotic Hamiltonian dynamical system if its stability multipliers $(\Lambda\,,\ \Lambda^{-1})$, where

$$\Lambda = (s + \sqrt{(s-2)(s+2)})/2\,, \qquad \Lambda = e^{\lambda}\,, \tag{9.5}$$

are real, with a positive stability exponent $\lambda > 0$. The eigenvalues are functions of a single parameter $s = \mathrm{tr}\, A$, and the map is chaotic if and only if $|s| > 2$. Otherwise Λ is on the unit circle in the complex plane, and the map is elliptic.

What is the equivalent statement for the *spatiotemporal cat map*?

I do not know if it is only a coincidence, but $\mathcal{R} = [2\times 2]$ measure inequalities are bounded by $P(s) = s(s-2)(s+2)$.

In your report you look at the linear code for $s = 3$ and numerically compute the block measures (relative frequencies) for that case, figure 7.1, so why are we demanding that $s = 5$ or larger?

2017-09-07 Adrien

- Glad as well than the former figures with numbers weren't deleted, meaning I technically won't have to re-run them unless for my following point.
- From what I see in my Mathematica notebooks, we set our system with $c = d = -1$ and $a + b = s$ and $q_{n,t}, p_{n,t}$ falling in the unit interval [0,1] so that our alphabet $\mathcal{A} = \{0, \ldots, s - 2d\} = \{0, \ldots, s - 4\}$. Since Boris had requested that the switching of 'blocks' in array of symbols $m_{n,t}$ would be done on admissible sequences, and given that internal symbols simply satisfy this condition, we would need to pick an alphabet $\mathcal{A}$ with at least 2 internal symbols; otherwise it's no fun. $s = 5$ has no internal symbols; $s = 7$ has two internal symbols (1 and 2) -> which is why we pick $s \geq 7$ for all these 'switching' experiments.
- In my summer report however, I believe I was using a different set of conditions for the cat map itself:

  $$a = 2\ b = 1 \rightarrow\ s = 3\ c = d = -1 \text{ but } -1/2 \leq q_{n,t}, p_{n,t} \leq 1/2$$

  We picked the unit interval $[-1/2, 1/2]$ for symmetry reasons, but once the summer was over, Boris made it clear that we would now focus on [0,1].

  With such $q_{n,t}, p_{n,t}$ falling in $[-1/2, 1/2]$, the list of admissible symbols was different. I tried to tackle this in my summer report, see sect. 7.3.2.

2017-09-08 Predrag I always prefer the unit interval $[-1/2, 1/2]$ (but not for this paper - that ship is long gone). Asymmetric choice makes both the alphabet and its symmetry under time reversal unnecessarily awkward. You use unit interval, though, in your sect. 7.2.3.

In ref. [2] I write that the $d = 1$ Arnol'd cat map $s = 3$ alphabet has 5 letters $\mathcal{A} = \{\underline{2}, \underline{1}, 0, 1, 2\}$.

I think you meant $d = 2$ spatiotemporal cat map $s = 3$ alphabet on $[-\frac{1}{2}, \frac{1}{2}) \times [-\frac{1}{2}, \frac{1}{2})$ phase space has $s + 4 = 7$ letters? I assume that is what we see in figure 7.1, except that the two exterior letters $\{-3, 3\}$ seem almost totally pruned. Are they, or the little histogram glitches are real? You do not explain how the histogram is ordered, I assume that is as explained in ref. [2].

References

[1] S. C. Creagh, "Quantum zeta function for perturbed cat maps", Chaos **5**, 477–493 (1995).

[2] B. Gutkin, L. Han, R. Jafari, A. K. Saremi, and P. Cvitanović, Linear encoding of the spatiotemporal cat map, In preparation, 2018.

[3] B. Gutkin and V. Osipov, "Classical foundations of many-particle quantum chaos", Nonlinearity **29**, 325–356 (2016).

[4] I. Percival and F. Vivaldi, "A linear code for the sawtooth and cat maps", Physica D **27**, 373–386 (1987).

Chapter 10

Spatiotemporal cat map, blogged

I'm a space and time continuum
— Red Wanting Blue

The latest entry at the bottom for this blog

2016-01-12 PC Literature related to Klaus Richter - Engl *et al.* [22] *Coherent backscattering in Fock space: A signature of quantum many-body interference in interacting bosonic systems*; Engl *et al.* [23] *Boson sampling as canonical transformation: A semiclassical approach in Fock space*

Some of the stuff might already be in Richter [56] book *Semiclassical Theory of Mesoscopic Quantum Systems*.

2016-05-16 Predrag I am putting all stuff about cat maps known to us into sect. 2.1.

2016-05-17 Predrag I have added for the time being chapter 2 *Statistical mechanics applications* from ChaosBook to this blog. Note that there are yet more references to read in the Commentary to the chapter 2.

2016-03-02 Boris Just stumbled upon Lepri, Politi and Torcini [38] *Chronotopic Lyapunov analysis. I. A detailed characterization of 1D systems*.

Are you familiar with this? Somewhere in the direction I thought about.

2016-03-02, 2016-09-03 Predrag Politi and collaborators work is very close to our way of spatiotemporal thinking. See sect. 3.9.3, sect. 3.9.4, sect. 3.9.5 and sect. 3.9.6. If you read that literature, please share what you have learned by writing it up there.

2016-03-02 Predrag Also Pazó *et al.* [47] *Structure of characteristic Lyapunov vectors in spatiotemporal chaos*. Actually (I hesitated to bring it up) this line of inquiry goes smoothly into Xiong Ding's inertial manifold dimension project.

Not sure Li *et al.* [39] *Lyapunov spectra of coupled chaotic maps* is of any interest, but we'll know only if we read it.

Takeuchi and Sano [62] *Role of unstable periodic orbits in phase transitions of coupled map lattices*.

2016-05-17 Boris There has been some progress in the cat maps direction. Li did a simple simulation for single cat map which has confirmed my guesses so far. General question is about 2D symbolic dynamics which we used in our paper with Vladimir [34]. We encoded trajectories by winding numbers so the alphabet is small. This radically differs from standard symbolic dynamics - Markov partitions, etc. which you normally find in the literature.

Question: Given rectangular domain of symbols - what is the probability to find it within a generic N-particle spatiotemporal cat map trajectory of duration T (N and T are large)? To my surprise an answer for this question might be within reach (at least for most of the sequences, small rectangles, etc.) This symbolic dynamics is much nicer then what I thought it would be. If true, this will be a nice project for students. I am writing some notes, will send this crude staff at night today - hopefully it will be digestible.

2016-05-18 Boris To speed up everything I send my notes (click here) on recent progress on cat map symbolic dynamics. Very crude, limited edition (probably barely digestible :). This what I managed to put in latex tonight. More staff and explanations will come on Friday . So far only few things (and only for single cat) were checked numerically.

2016-05-21 Boris The current version of my notes: (click here), with more staff, more or less the same level of disorder. The main news - this symbolic dynamics (for single cat) was investigated a time ago by Percival and Vivaldi [48]. At least some of their results are of relevance for us and maybe overlap with my results. Need some time to digest their paper.

2016-05-21 Predrag For simple linear maps with integer coefficient it might be possible to write explicitly all period points in terms of rational numbers. See Example 11.10 *Periodic points of the full tent map* in ChaosBook.

2016-06-01 Predrag The downside the 'linear code' of Percival and Vivaldi [48] is that the Markov/generating partition is infinite, meaning that for longer and longer orbits there are more and more new pruning (inadmissible blocks) rules, ad infinitum.

As far as I can tell, for N coupled maps this gets harder to describe, as in general there is an coupling strength parameter. Perhaps for rational values of it some miracles might happen.

2016-07-10 Boris The current ver. 5020 of my notes: (click here),

Main atractions:

1. Single cat: Frequencies of sequences which are composed of internal symbols eq. (2.23) - analytic answer.
2. Infinity of cats, pp. 9-11: Results for single symbol frequency. Some results for [2×2] squares - Rana eqs, internal symbols, forbidden sequences. Looks like extendable to general rectangles (Future looks bright gotta wear shades).

To Rana, Adrien and Li - we Skype Wednesday 5pm.

2016-08-15 Predrag : Before I start sounding critical: Rana, Adrien and Li are all good students / postdoc, and the work and what people learned this summer is very good. Now, to my first impressions (Boris still has to chime in, and we should all meet soon to discuss).

Boris was the primary advisor for Adrien and Rana, and he did not push them to write; European style, more hands off than is the American custom. Rana has written too little, not covering all the work that she did (which was good, but only Boris knows what it was). Adrien also has some work to do before the report can be read by anyone other than the members of this team.

For me, what lacks in Rana, Adrien and Li's work is that they did not (on their own initiative) read the literature, or if they did, they never summarized what they learned in their blogs, or cited the original sources in their reports (if it is not recorded, I assume it did not happen). I did an exhaustive literature search for them (for coupled maps, see above in this blog, chapter 10; for cat maps see sect. 1.6 and sect. 2), but they did not pick it up, so I'll have to do that work myself.

2016-08-20 Predrag Might be worth a look - several papers on coupled map lattices, see sect. 3.9.1 on order and chaos in a one-dimensional ϕ^4 model - if you read that literature, please share what you have learned by writing it up there.

Rafael 2016-09-29 I spent a lot of time in the coupled cat maps, but in the regime of small coupling. One thing I did explore numerically is when the conjugacy given by the structural stability breaks down as one turns up the coupling.

Rafael 2016-10-10 The main paper about the coupled maps is the paper with Miaohua Jiang. We show that the local chains of Anosov remain Anosov

under local couplings. The partitions remain the same if you make changes of coordinates that are essentially local.

Of course, the fact that there is a regime of large perturbations in which this does not happen begs the question of studying the transition. Some of this has been studied also by Bastien Fernandez [24].

I have done some preliminary numerics (too crude to show). One possibility is that some of the Lyapunov exponents go to zero. Another is that the Lyapunov exponents remain away from zero but that the angle between the splittings goes to zero. There are heuristic arguments that the second possibility should occur. (Almost a proof when there is a system small coupling to another more massive one).

There were other points of the discussion. The space dynamics for PDE's. This contains references to older papers notably Kirchgassner and Mielke as well as applications to some papers.

I think Weinstein [66] is related.

2016-10-03 Predrag Not quick or easy to explain, but I have a hunch that the spatiotemporal zeta function should be something like the 2D Ising model zeta function described by Aizenman, see chapter 4.

2016-10-30 Predrag I worry a lot about what time-reversibility means - spatiotemporal cat map is both time and space reversible, and then there are Ihara zeta functions for undirected graphs. So I find this interesting: Coppersmith, Kadanoff and Zhang [19] *Reversible Boolean networks I: distribution of cycle lengths*. They write: " We [...] consider time-reversible dynamics of N Boolean variables models, with the time evolution of each depending on K of the other variables, which necessarily have the property that every possible point in the state space is an element of one and only one cycle. The orbits can be classified by their behavior under time reversal. The orbits that transform into themselves under time reversal have properties quite different from those that do not; in particular, a significant fraction of latter-type orbits have lengths enormously longer than orbits that are time-reversal symmetric. For large K and moderate N, the vast majority of points in the state space are on one of the time-reversal singlet orbits. However, for any finite K, the random hopping approximation fails qualitatively when N is large enough (N>22K). When K is large, typical orbit lengths grow exponentially with N, whereas for small enough K, typical orbit lengths grow much more slowly with N. The numerical data are consistent with the existence of a phase transition at which the average orbit length grows as a power of N at a value of K between 1.4 and 1.7. However, in the reversible models, the interplay between the discrete symmetry and quenched randomness can lead to enormous fluctuations of orbit lengths and other interesting features that are unique to the reversible case. "

Need to check also

Toffoli and Margolus [63] *Invertible cellular automata: A review*

D'Souza and Margolus [20] *Thermodynamically reversible generalization of diffusion limited aggregation*

2016-11-06 Predrag Early references on the spatiotemporal invariants and invariant measures:

Grassberger [30] *Information content and predictability of lumped and distributed dynamical systems* " ... we point out the difference between difficulty and possibility of forecasting, illustrating it with quadratic maps. Next, we ask ourselves how this should be generalized to distributed, spatially extended and homogeneous systems. We point out that even the basic concepts of how information is processed by such systems are unknown. Finally, we discuss some intermittency-like effects in coupled maps and cellular automata.

Most interesting systems are spatially extended ("distributed") and have thus, in the infinite-volume limit, an infinite number of degrees of freedom. Nevertheless, concepts developed for dynamical system with few degrees of freedom can be applied.

Let us first consider a system located in a finite space volume V with fixed boundary conditions. For the moment we assume that the field variables (local observables) are continuous, while space and time are discrete.

It is very plausible that the number of excited degrees of freedom in such a system is proportional to the volume, at least in typical situations. More precisely, we expect that both the metric entropy h and the dimension D are extensive quantities. This is supported by overwhelming theoretical [25, 46, 58] and numerical evidence that the Lyapunov exponents (ordered such that 2, decreases with i) scale as

$$\lambda_i \approx f(i/V) \tag{10.1}$$

[...] The limit $\eta = \lim_{V\to\infty}(h/V)$ is called density of metric entropy. [...] more interesting is the information needed to describe a finite part of an infinite system than that needed to describe the system as a whole. "

Politi and Puccioni [52] *Invariant measure in coupled maps* write: " The state of affairs is much less clear when we pass from closed chains (as above) to sub-chains of an-in principle-infinite lattice. This corresponds to the canonical-ensemble picture of statistical mechanics: the system of interest (sub-chain of length E) is coupled with a thermal bath given by the rest of the chain. From the previous considerations, the attractor corresponding to an isolated system would fill, for E sufficiently large, a ρE-dimensional manifold. The main effect of the coupling with the heat bath is to add a sort of "external noise" dressing the manifold along all directions, and thus making the resulting invariant measure to become E-dimensional. "

This paper is lots of hand-waving, so I gave up on reading it.

2016-11-06 Boris Papers to read:

Bardet and Keller [11] *Phase transitions in a piecewise expanding coupled map lattice with linear nearest neighbour coupling* write: " We construct a mixing continuous piecewise linear map on [-1,1] with the property that a two-dimensional lattice made of these maps with a linear north and east nearest neighbour coupling admits a phase transition. We also provide a modification of this construction where the local map is an expanding analytic circle map. The basic strategy is borrowed from Gielis and MacKay (2000 Nonlinearity 13 867-88); namely, we compare the dynamics of the CML with those of a probabilistic cellular automaton of Toom's type; see MacKay (2005 Dynamics of Coupled Map Lattices and of Related Spatially Extended Systems (Lecture Notes in Physics vol 671) ed J-R Chazottes and B Fernandez (Berlin: Springer) pp 65–94) for a detailed discussion. "

de Maere [41] *Phase transition and correlation decay in coupled map lattices* writes: " For a Coupled Map Lattice with a specific strong coupling emulating Stavskaya's probabilistic cellular automata, we prove the existence of a phase transition using a Peierls argument, and exponential convergence to the invariant measures for a wide class of initial states using a technique of decoupling originally developed for weak coupling. This implies the exponential decay, in space and in time, of the correlation functions of the invariant measures. "

Schmitt [59] *Spectral theory for nonanalytic coupled map lattices* write: " We consider weakly coupled strong mixing interval maps on the infinite lattice with finite range couplings. We construct Banach spaces defined by bounded variation conditions such that the transfer operator associated with the full infinite system has a simple eigenvalue 1 (corresponding to a unique natural invariant probability measure) and a spectral gap. "

2017-02-13 Predrag Consider admissible Lagrangian trajectories in the $[x_0, x_{\ell+1}]$ plane. The 1-step Lagrangian map is

$$x_2 = (s\,x_1 - m_1) - x_0\,. \tag{10.2}$$

For $s = 3$ have $m_j \in \{-1, 0, 1, 2\}$, and the partition borders are slope -1 lines defined by $x_1 = 0$ or 1.

$$-\,m_1 - x_0 \le x_2 \le s - m_1 - x_0\,. \tag{10.3}$$

Anything outside $0 \le x_2 \le 1$ is not a constraint.

$$1 - x_0 \le x_2^{(-1)} \le 4 - x_0\,. \tag{10.4}$$

$$-\,x_0 \le x_2^{(0)} \le 3 - x_0\,. \tag{10.5}$$

$$-\,1 - x_0 \le x_2^{(1)} \le 2 - x_0\,. \tag{10.6}$$

$$-2 - x_0 \le x_2^{(2)} \le 1 - x_0 \,. \tag{10.7}$$

So, there is no pruning for $x_2^{(0)}$ and $x_2^{(1)}$; the only pruning constraints are

$$1 - x_0 \le x_2^{(-1)} \,, \tag{10.8}$$

$$x_2^{(2)} \le 1 - x_0 \,. \tag{10.9}$$

2-step Lagrangian map

$$x_3 = (s-1)(x_2 + x_1) - x_0 - m_2 - m_1 \,, \tag{10.10}$$

Eliminate x_2 by (10.2)

$$x_2 + x_1 = ((s+1)x_1 - m_1) - x_0 \,. \tag{10.11}$$

$$x_3 = (s^2 - 1)x_1 - s\,x_0 - m_2 - s\,m_1 \,, \tag{10.12}$$

2016-01-12, 2016-08-04 PC Literature related to Gutkin and Osipov [34] *Classical foundations of many-particle quantum chaos*:

The existence of 2D symbolic dynamics was demonstrated in ref. [51], for a particular model of coupled lattice map.

"In general, calculating periodic orbits of a non-integrable system is a non-trivial task. To this end a number of methods have been developed," and then, for some reason, they refer to ref. [10].

Pethel *et al.* [50] *Symbolic dynamics of coupled map lattices*

Pethel *et al.* [51] *Deconstructing spatiotemporal chaos using local symbolic dynamics*

Amigó, Zambrano and Sanjuán [5] *Permutation complexity of spatiotemporal dynamics* study diffusive logistic coupled map lattices (CML) (3.1). Sun *et al.* [61] *A method of recovering the initial vectors of globally coupled map lattices based on symbolic dynamics* study CMLs with logistic, Bernoulli, and tent chaotic maps. They cite Refs. [50, 51]. Gundlach and Rand [32] study couple circle maps (the results of subsequent papers in this series are claimed to be wrong, see Jiang [37]).

Atay, Jalan and Jost [7] study coupled map networks with multiple time delays; of no current interest for us.

Chen, Chen, and Yuan [18] *Topological horseshoes in travelling waves of discretized nonlinear wave equations* is a mathematical paper. They concentrate on describing relative equilibria of a discretized version of a PDE that has Kuramoto-Sivashinsky, KdV and Burgers as special cases. They define discretized derivatives up to the 5th, if we ever need them They

2CB

write " Applying the concept of anti-integrable limit to coupled map lattices originated from space-time discretized nonlinear wave equations, we show that there exist topological horseshoes in the phase space formed by the initial states of travelling wave solutions. In particular, the coupled map lattices display spatiotemporal chaos on the horseshoes. "

Afraimovich and Pesin [1] *Hyperbolicity of infinite-dimensional drift systems* study the discrete versions of the complex Ginzburg-Landau equation

$$u_{n,t+1} = u_{n,t} + \tau(u_{n,t}, \sigma) + \gamma(u_{n,t} - u_{n,t-1}) + \frac{\epsilon}{2}[u_{n-1,t} - 2u_{n,t} + u_{n+1,t}]\,, \tag{10.13}$$

where $\tau(u_{n,t}, \sigma)$ is local time dynamics, γ is a parameter of "connection", a memory of the previous step, so this has a time evolution component that could be written as a time Laplacian, with remainder presumably playing role of a friction. Not sure why this would be a good idea, as Ginzburg-Landau is the first order in time. Literature worries about the stability of of the space-homogeneous state in chains of maps. They consider a special 'drift' type of perturbation, at which point they lost me.

Elder *et al.* [21] *Spatiotemporal chaos in the damped Kuramoto-Sivashinsky equation*: " A discretized version of the damped Kuramoto-Sivashinsky (DKS) equation is constructed to provide a simple computational model of spatiotemporal chaos in one dimension. The discrete map is used to study the transition from periodic solutions to disordered solutions (i.e., spatiotemporal chaos). The numerical evidence indicates a jump discontinuity at this transition. "

2016-09-28 Predrag Volevich [65] *Kinetics of coupled map lattices* writes: " A simple example of coupled map lattices generated by expanding maps of the unit interval with some kind of diffusion coupling is considered. The author proves that probability measures from some natural class weakly converge to the unique invariant mixing measure under the actions of dynamics. The main idea of the proof is the symbolic representation of his system by two-dimensional lattice model of statistical mechanics. "

Amritkar *et al.* [6, 27] have investigated the stability of spatially and temporally periodic orbits in one- and two-dimensional coupled map lattices. Using the fact that the stability matrices for such solutions are block circulant and hence can be brought onto a block diagonal form through a unitary transformation, they derive conditions for the stability of periodic solutions in terms of the criteria for smaller orbits.

Zhilin*et al.* [68] *Spatiotemporally periodic patterns in symmetrically coupled map lattices* write: " The stability of the deduced orbits is investigated and we can reduce the problem to analyze much smaller matrices corresponding to the building block of their spatial periodicity or to the building block of the spatial periodicity of the original orbits from which we

construct the new orbits. In the two-dimensional case the problem is considerably simplified. "

Giberti and Vernia [14, 28] *Normally attracting manifolds and periodic behavior in one-dimensional and two-dimensional coupled map lattices* study weakly coupled logistic maps in one- and two-dimensional lattices. They show numerically for some classes of coupled map lattices that the stability of a spatial structure is determined by the stability of its pattern with the minimal (spatial) scale, i.e. by the tiniest detail of this structure.

Continued in Livi, Martínez-Mekler and Ruffo [9, 15, 40] *Periodic orbits and long transients in coupled map lattices*

Hopefully something we can ignore as long as we are interested into the "high-temperature" phase.

Isola, Politi, Ruffo and Torcini [36] *Lyapunov spectra of coupled map lattices*

Fontich, de la Llave and Martín [26] *Dynamical systems on lattices with decaying interaction I: A functional analysis framework*,

2016-11-11 Predrag Boris A. Khesin course notes might be helpful if we ever get to Hamiltonian PDEs :)

2016-11-11 Predrag Belykh and Mosekilde [12] *One-dimensional map lattices: Synchronization, bifurcations, and chaotic structures* study

$$\begin{aligned} x_{n,t+1} &= f(x_{n,t}) + \epsilon[x_{n+1,t} - (1+\gamma)x_{n,t} + \gamma x_{n-1,t}] \\ &= f(x_{n,t}) + (1-\gamma)\epsilon\,(x_{n,t} - x_{n-1,t}) + 2\epsilon\,\Box x_{n,t}\,, \end{aligned} \tag{10.14}$$

asymmetrically drifting due to coupling by $(1-\gamma)$. With $g(x) = f(x) - x$, and rescaling the nonlinearity, this is a discretization of a dynamics of extended, non-equilibrium media PDE

$$\frac{\partial x}{\partial t} = g(x) + (1-\gamma)\frac{\partial x}{\partial s} + \frac{\partial^2 x}{\partial s^2}\,. \tag{10.15}$$

Consider the diffusively coupled maps (10.14) for $\gamma = 1$ and $N = 2m$ and assume periodic boundary conditions ($m \to \infty$ when the array is unbounded). As this has a spatial Laplacian (the dynamics is now reflection-symmetry invariant) they construct a pair of new variables $x_{n,t}$, $y_{n,t}$ from x_n with odd or even n, and obtain a 2D lattice symmetric under $(x, y) \leftrightarrow (y, x)$. Then the symmetric and asymmetric spaces behave differently. In particular, the second period-doubling bifurcation for can be changed into a torus bifurcation [55].

2016-11-11 Predrag Belykh and Mosekilde [12] is a descendent of the system previously studied by Reick and Mosekilde [55] in *Emergence of quasiperiodicity in symmetrically coupled, identical period-doubling systems*: " When two identical period-doubling systems are coupled symmetrically, the period-doubling transition to chaos may be replaced by a quasiperiodic

transition. The reason for this is that at an early stage of the period-doubling cascade, a Hopf bifurcation instead of a period-doubling bifurcation occurs. Our main result is that the emergence of this Hopf bifurcation is a generic phenomenon in symmetrically coupled, identica1 period-doubling systems. The whole phenomenon is stable against small nonsymmetric perturbations. Our results cover maps and differential equations of arbitrary dimension. As a consequence the Feigenbaum transition to chaos in these coupled systems - which exists, but tends to be unstable - is accompanied by an infinity of Hopf bifurcations."

The seemingly first remark on this splitting is due to Ruelle [57]. He noted that the symmetry of the coupling results in a splitting into a symmetric solution and a nonsymmetric solution, where for the latter the two subsystems are 180' out of phase. Later Neu [44, 45] specialized the problem to linear coupling and analyzed the stability of the symmetric and nonsymmetric solutions by singular perturbation methods.

All of these might be of importance for Burak's torus birth and destruction [13].

As for the cats crowd, these seem to suggest that spacetime interchange symmetry $t \leftrightarrow n$ of the spatiotemporal cat map [33] should lead to different dynamics (and symbolic dynamics! only positive (n, t) are needed after the decomposition) in symmetrized and anti-symmetrized lattices, with a possible flow-invariant subspace currently invisible. In Gibson, Halcrow and Cvitanović [29] *Visualizing the geometry of state-space in plane Couette flow* we also had a $C_2 \times C_2$ symmetry, with important consequences on types of solutions, and invariant subspaces.

2016-11-23 Predrag Having a variational principle (action (1.37) in case at hand) and a continuous symmetry means that the **Noether's theorem** applies

"To every one-parameter, continuous group of symmetries of a Lagrangian dynamical system there corresponds a scalar, real-valued conserved quantity."

Is there is a version of it for discrete translations? What is the conserved quantity for a single cat map? What is it for the lattice? Internet says many contradictory things:

"The fact that a Lagrangian is unchanged by a discrete transformation is of no significance. There is no conserved quantity associated with the transformation."

"For infinite symmetries like lattice translations the conserved quantity is continuous, albeit a periodic one. So in such case momentum is conserved modulo vectors in the reciprocal lattice. The conservation is local just as in the case of continuous symmetries."

Read about it here.

Mansfield [42] in proceedings and in her talk defines *total difference* and says " Just as an integral of a total divergence depends only on the boundary data, so does the sum over lattice domain of a total difference."

She states the discrete Noether's Theorem, and in Example 1.3.7 she shows that for a discretization of a standard mechanical Lagrangian, time invariance3 yields "energy" as a the conserved quantity.

Hydon and Mansfield [35].

Capobianco and Toffoli [17] Can anything from Noether's Theorem be salvaged for discrete dynamical systems? is fun to read (but ultimately unsatisfactory):

" we take the Ising spin model with both ferromagnetic and antiferromagnetic bonds. We show that—and why- energy not only acts as a generator of the dynamics for this family of systems, but is also conserved when the dynamics is time-invariant."

The *microcanonical Ising model* is strictly deterministic and invertible: on a given step, a spin will flip (that is, reverse its orientation) if and only if doing so will leave the sum of the potential energies of the four surrounding bonds unchanged. The Ising dynamics is a second-order recurrence relation. They define "energy" as the length of the boundary between 'up' and 'down' domains. While the magnetization—number of spins up minus number of spins down—may change with time, that length, and thus the energy, remains constant. The total energy of a system may be defined as

1. A real-valued function of the system's state,
2. that is additive,
3. and is a generator of the dynamics.

In a discrete Hamiltonian dynamics, a state is no longer a "position/momentum" pair $< q, p >$ as in the continuous case, but an ordered pair of configurations $< q_0, q_1 >$.

A second-order dynamical system has an evolution rule of the form

$$x_{t+1} = g(x_t, x_{t-1}) \,.$$

2016-12-10 Predrag Read Akila *et al.* [4] *Semiclassical identification of periodic orbits in a quantum many-body system*

2016-12-12 Predrag Spatiotemporal cat map claim retracted:

On the second thought, spatiotemporal cat map is not radically different from the previous examples of (D+1)-dimensional spatiotemporal symbolic dynamics cited by Boris (Pesin and Sinai [49], Bunimovich and

Sinai [16], Pethel, Corron and Bollt [50, 51]). In all coupled maps literature, the starting point is time evolution of a non-interacting particle at each site, with its 1-dimensional temporal symbolic dynamics, with spatial coupling to D spatial neighbors subsequently tacked on. while the *coordinate* of site is (D+1)-dimensional, its symbolic dynamics is 1-dimensional. In all models the I am aware of, with the exception of zeta functions in $d = 2$, the field being discretized ("particles" at sites) is *scalar*, and so is the spatiotemporal cat map field (I was wrong when I claimed in a conversation with Boris that is a *vector* field). In d spatiotemporal dimensions it is d-dimensional, but its symbolic dynamics alphabet at each site is 1-dimensional set.

The zeta functions in $d = 2$, reviewed in sect. 4.2, are not based on any dynamics, and have problems of their own. In nutshell, for such zeta functions grammars are awkward, while in the spatiotemporal cat map the grammar rules are automatically obeyed by any simulation, and can be explicitly computed as a finite set of rules for any given invariant 2-torus.

2016-12-17 Predrag Read Qin [54] *Bifurcations of steady states in a class of lattices of nonlinear discrete Klein-Gordon type with double-quadratic on-site potential*

2017-02-17 Predrag For a single cat map linear code is simply awkward

1. depends on choice of x_t origin: 4 letters for Boris, 5 for (symmetric) Vivaldi
2. linear code partition areas have no relation to periodic orbit weights
3. linear code pruning rules undercount periodic orbit pruning rules
4. periodic orbits are intrinsic to the flow, so makes more sense to use AW Markov partition

Boris 2017-02-17 Mostly agree, but linear code has its own charm: internal part of the code has trivial grammar rules, it is very homogeneous, i.e., admissible sequences of finite length have volumes either close to zero or close to max (volumes of internal sequences).

Boris 2017-02-17 For p iterations of the map situation rapidly improves - number of internal symbols grows exponentially with p, number of external symbols is fixed (kind of renormalization).
Predrag 2017-03-04 That's just a cheat. For a piecewise linear expanding map of mod 1 variety, it is always the orbit of the outermost critical point (in your language, exterior alphabet) that defines the grammar, in the spirit of the kneading theory, with no grammar rules for the interior alphabet, see ChaosBook chapter *Deterministic diffusion*. If one looks at iterates of the map, of course the number of interior alphabet sequences grows exponentially, but that does not mean that they dominate the topological entropy - that ones is what it is, an irrational number larger than $\ln N_{\mathcal{A}_0}$, the same number for the original map or any of its iterates.

2017-04-29 Predrag Tourigny [64] *Networks of planar Hamiltonian systems* writes things we probably disagree with:

"Hamiltonian systems famously do not admit attractors, but rather families of periodic orbits parameterised by level sets of the Hamiltonian. There have been surprisingly few attempts to study complex networks consisting of coupled Hamiltonian systems. Consequently, in this paper we initiate the study of complex networks whose autonomous units are planar Hamiltonian systems. We choose to focus on planar Hamiltonian systems because already there exists a rich theory that may be identified with the geometry of planar algebraic curves.

Define a weighted graph $\mathcal{G}$ by assigning a vertex to each $i \in V$ and an edge with "weight" $W_{ij} = W(i,j)$ joining vertex i to j. We assume this graph $\mathcal{G}$ is *undirected* (i.e., $W_{ij} = W_{ji}$) and *connected* meaning that there always exists a path from any vertex i to any other vertex j. The network is then defined to be the dynamical system on $\mathbb{R}^{m\times n}$ whose time evolution is governed by the equations

$$\dot{z}_i = F_i(z_i) + \sum_{j=1}^{n} W_{ij} U(z_i, z_j) \ .$$

We will actually only be concerned with networks where the autonomous units are planar ($m = 2$) and the coupling function is *diffusive*, implying $U(z_i, z_j) = U(z_i - z_j)$. We say that a network is an *oscillator network* if each of the underlying systems $\dot{z}_i = F_i(z_i)$ admits at least one periodic solution. "

This work is inspired by Winfree, Kuramoto and Turing (rather than coupled maps lattices). If the dynamics on a node is the same everywhere, the network (graph) is "homogenous", otherwise it is "heterogenous." The diffusive coupling $W_{ij} = W_{ji}$ couples all nodes, in his model with the same strength, but the nodes are assumed heterogenous. After further reading it seems that the networks are not Hamiltonian (coupling destroys that, and that we can safely avoid this literature.

Rest in pacem.

2017-10-10 Boris Our recent [2] *Semiclassical prediction of large spectral fluctuations in interacting kicked spin chains*, arXiv:1709.03601, hides a feline creature in the form of (10.16):

"**Integrable Case**: For $b^x = 0$ all rotations are around the z-axis and therefore commute with the Hamiltonian making the system integrable. As a result the dynamics of the kicked system for arbitrary times is equivalent to one at fixed time, e.g. $T = 1$ with rescaled system parameters $J \to JT$ and $b^z \to b^z T$. Moreover, the flow induced by the Hamiltonian $\hat{H}_I + \hat{H}_K$ for time T is identical to the evolution of the kicked system for T time steps with the same parameters.

For the classical trajectories p_n = const. holds for each n and periodic orbits form L dimensional manifolds. To close a trajectory in phase-space after T iterations it is sufficient that the total change in angles Δq_n is a multiple of 2π,

$$\Delta q_n = 4T\left(J(p_{n-1}+p_{n+1})+2Vp_n\right)+2b^zT = 2\pi\hat{m}_n\,. \tag{10.16}$$

The $\hat{m}_n \in \mathbb{Z}$ is a local winding number for spin n. Since the momenta are bounded, $|p_n| \leq 1$, $\chi_n = p_{n-1}+p_{n+1}$ resides within the interval $[-2,+2]$. Therefore, this equation has no solution if, for instance, $b^z > 4(J+V)$ and $4(J+V)+b^z < \pi/T$. In such cases the system does not posses any classical periodic orbits of period T or shorter. If all parameters (times T) are sufficiently small, the first accessible winding number is necessarily zero. With increasing time T the number of possible $\hat{m}_n$ grows linearly, and with it the number of possible distinct periodic orbits grows algebraically. With respect to L the number of periodic orbits is determined by all admissible combinations of the winding numbers. If there is more than one allowed m_n the growth is thus exponential in L. This exponential growth also holds for non-integrable parameter choices. "

Boris continues: This is the (dual) equation for "spatially" periodic orbits of an integrable spin chain. For $4JT = 2\pi$ it is the cat map

$$p_{n+1} - s\,p_n + p_{n-1} = -m_n\,, \tag{10.17}$$

with the cat map "stretching" parameter $s = -2TV/\pi$, and the winding number $m_n = b^zT/\pi - \hat{m}_n \in \mathbb{Z}$. For other times T, the map is non-symplectic but still linear. The equation says, loudly, that temporally integrable system can be "spatially" chaotic (e.g., number of spatial periodic orbits grows exponentially with the spatial period L (in case at hand, the number of "particles").

On the quantum side the corresponding "dual" evolution is exactly quantum cat map.

2017-10-10 Predrag Thanks for pointing it out, I would have never noticed that the very feline (10.17) is hiding within (10.16). So, whenever one has the nearest neighbor couplings, spatially, spatial translation invariance, a spatial reflection symmetry, and a linear dynamics on the site, one gets a spatial cat map. Your $T = 1$ example is the discrete time analog of the Michelson [43] $T = 0$ study of equilibria on the kneading sequence spatial $L \to \pm\infty$ (described in the parallel `blog.tex`, in this subversion repo directory). This system is not integrable, but, needless to say, the number of equilibria does not grow with increasing T (it is constant).

2017-10-10 Predrag Currently open ends:

1. Finish the Pythagorean tiling of figure **??** in terms of two rectangles. In these coordinates the cat map should again have a linear encoding, but with no pruning rules (the two rectangles are a generating partition).

2. Do the same for $d > 1$.
3. Redo everything with doubly-periodic boundary conditions, where all Green's functions trivial.
4. I have started writing up the spatiotemporal Jacobian and the det $(1-J)$ for d-tori in what is currently called Sect. 1.3.2 *Spatiotemporal stability* in the parallel `blog.tex`. In the discrete spacetime case, that should agree with the determinants that Boris has computed.

2017-10-31 Burak I looked everywhere but could not find the following Politi and Torcini *Towards a statistical mechanics of spatiotemporal chaos* (1992) [53] in this blog or the bib files. The abstract:

> Coupled Hénon maps are introduced to model in a more appropriate way chaos in extended systems. An effective technique allows the extraction of spatiotemporal periodic orbits, which are then used to approximate the invariant measure. A further implementation of the ζ-function formalism reveals the extensive character of entropies and dimensions, and allows the computation of the associated multifractal spectra. Finally, the analysis of short chains indicates the existence of distinct phases in the invariant measure, characterized by a different number of positive Lyapunov exponents.

I skimmed the article quickly, although I think we should all read it very carefully. There is a strange way of inferring spatiotemporal periodic orbits and their symbolic dynamics by introducing a system depending on a continuous fictitious time. The method probably works only for maps but nevertheless seems quite interesting.

I'm not sure if they are using periodic orbits of systems of different chain length in order to guess the statistics of the system at thermodynamic limit $L \to \infty$. If that's the case and the dynamical ζ function is designed for this purpose, then this paper is very similar to what we have in mind, I believe.

2017-11-06 Predrag I'll continue the discussion in this (sub)blog, in case that Boris wants to read the paper as well.

2017-10-31 Matt Read *Towards a statistical mechanics of spatiotemporal chaos* by Politi and Torcini [53].

I find it interesting they introduce a continuous fictitious dynamics for a spatiotemporal system of mappings, and I have a discrete fictitious time (in the form of my spatiotemporal mapping) introduced for continuous (albeit discretized) spatiotemporal equations.

2017-11-08 Matt For a beginning on the subject of Politi and Torcini [53] coupled map lattices, we begin with a description of a single Hénon map, written using the conventions of Chaosbook.

Note: Politi and Torcini say that in the case of $\epsilon = 0$ that the original Hénon map is retrieved, but if you actually do this then indices don't match the original equation.

$$\begin{aligned} x_{n+1} &= 1 - a y_{n+1}^2 + b x_{n-1} \\ y_{n+1} &= x_n \end{aligned} \tag{10.18}$$

Written in terms of a single equation this becomes

$$x_{n+1} = 1 - a x_n^2 + b x_{n-1}$$

In the Hénon map, the parameter a is what quantifies the stretching and b quantifies the contraction.

The deviation of an approximate trajectory from the two step recurrence relation is

$$v_n = x_{n+1} - (1 - a x_n^2 + b x_{n-1})$$

Usually in classical mechanics, specifically a gradient system, we think of force as gradient of potential, so in this system we can view the force as the derivative of a cubic function such that the Hénon map is the derivative of the cubic potential.

$$V_n = x_n(x_{n+1} - b x_{n-1} - 1) + a x_n^3$$

With the cubic potential of a single Hénon map we can start to look for orbits with initial conditions of two points (two point recurrence relation requires this) and make the guess as we iterate in time. A particular guess is to choose a sequence of maxima/minima of the potential.

In order to accurately enumerate the orbit with symbolic dynamics, in order to choose which way you "roll" the potential needs to be modified by ± 1,as when viewed from the perspective of the cubic potential, trajectories roll "downhill", so in order to flip the direction one must apply a flip. The symbolic dynamics is therefore binary and determined by these flips. One can just list the binary sequences and see if the orbit is realized by the system. Chaosbook does this up to sequences of length 13, while it has been done by Grassberger, Kantz and Moenig [31] to symbol length 32. This means that theoretically, there are $\frac{2^{32}}{32}$ possible itineraries.

Making x a complex number you can find non-physical solutions; what we're really doing is finding roots of polynomials. For a cycle of length N, the degree of the polynomial is $\exp^{2N}$? Finding the real roots of these equations is one way of finding these solutions, but this fictitious time is really just a way of finding these solutions.

Now to state the coupled Hénon map equations from [53]. n is the index associated to time, while j is the index associated with space. These are in fact, different, from the equations in the paper; but if we take their claim that in the $\epsilon = 0$ case we should retrieve the classical Hénon equations

very strictly, this is how they should appear I believe. The difference lies in the time index $n+1$ versus n of the y terms.

$$\begin{aligned} x^j_{n+1} &= 1 - a(y^j_{n+1})^2 + bx^j_{n-1} \\ y^j_{n+1} &= (1+\epsilon)x_n + \frac{\epsilon}{2}(x^{j+1}_n + x^{j-1}_n) \end{aligned} \tag{10.19}$$

In the $b = -1$ case there's only one parameter; when it is small some orbits become stable, not everyone is unstable. If there's not strong stretching then there is a mixture as the hyperbolicity isn't dominating. All of these coupled maps, say something wild happens at each site (alternating between 1 and -1 is far in this case), and THEN you couple it weakly to its neighbors. Two adjoining shapes are not coupled at all due to the fact that its so hyperbolic. Usually in chaotic dynamics there is stretching, but due to folding in this case a binary sumbolic dynamics is created.

But when the coupling with neighbors is very strong, its a very different phenomena. The cats have written a Helmholtz in space and time where the Laplacian is weighted by $+1$ as opposed to $1, -1$ in the Minkowski case. Second order operator that has different weights (as determined by some metric) its called the Beltrami operator. Predrag also thinks the sign is different. This is 1992 though, and there's not much there because its Phys. Rev. Lett. so there must be real work somewhere.

If this paper is worth something then other people cite it, there are currently **twenty-two** citations of [53] per Google.

They cite the fact that most people don't use it for invertible dynamics. Then they say the spatially and temporally periodic orbits are extracted using the Newton method. What they actually do, they take $L = 1, 2, 3, 4$ only. They don't elucidate on interesting tricks, like how to use the method for coupled maps. The density of periodic orbits in the invariant measure is stated, but this is only really known for single maps, Predrag doubts this.

[53] is one of the first papers that uses spatiotemporal symbolic dynamics, as seen by Predrag in the literature. Symbol of a torus is really just a lattice label. Politi and Torcini use doubly periodic boundary conditions, with canonical values from Hénon for the parameters.

When you write the equations in diagonal, form you'll likely take a square root of it. Then, they say some orbits are pruned, some exist only with uncoupled case. That helps them because if you can prove you only lose orbits and never gain orbits you can see if certain orbits are realized or not. Slightly mysterious, "need to discard all periodic orbits that do not belong to the attractor". What are those? There is an isolated orbit, corresponding to fixed points, so they do not allow orbits that spend too much time around the isolated region.

Do not allow invariant subspaces? maybe. Depends on how unstable the invariant subspace is because sometimes you can be glued to it. The orbits are found with Newton method.

They discarded all of the cycles that had a sequence, specifically $0\bar{0}\bar{0}$ in symbolic dynamics, is not allowed. The application of the zeta function, "they don't know what they are doing, so ignore it".

They have some intuition about the inertial manifold, if you double the physical length, you should double the number of physical Lyapunov exponents as you go in time. They compute some Jacobian, they are just the normal Jacobians in time. Using these they compute $2J \times 2J$ sized matrices for the spatiotemporal domain, (thinks Bloch theorem doesn't apply, maybe). Maybe this Bloch theorem would be worthwhile in understanding. They also say to take the logarithm and divide it by the size of the domain. They entropy is a sum of Lyapunov and divide it by L. They have an intuition but its hard to check because of the small L. One possible solution is to use the fixed point, as its a representative of the stretching rate in the neighborhood. "Let's just say the typical stretching rate is roughly the same no matter the domain size." I.e. they assume its a frozen state so it doesn't matter how big the domain gets. Grand canonical formalism for the Zeta function, but it can be "safely ignored". Multifractal stuff seems useless, look at this h, instead of plotting everything from infinity to infinity, but can subtract something and it works out and they get a plot. But there seems to be an envelope which may be connected to the quantity they try to claim, maybe.

Different phases, but they notice that different periodic orbits have different number of positive Lyapunov exponents. They interpret periodic orbits with the same number belong to the same 'phase'.

The problem only uses Biham in time; Not clear why they did it because they say its invertible, which makes sense because Hamiltonian. This is different from Cat map because the symmetry imposed makes it same in space and time.

The single Hénon map is nice because the system is not linear, but has binary dynamics.

All symbolic dynamics in the cat map paper, the way the equations work, the 'Laplace' equation (symmetric in space and time) has a stretching rate that depends on the number of neighbors)?(I had this written but I thought it only depended on s).

The source terms on the RHS, make sure that its modulo two pi. They act like symbolic dynamics, and PC has showed that all of these types of maps have to be put back into the torus (unit square in cat map case). Optimistic because it will be a general equation.

For a particular solution, the potential is just a set of numbers, even though it depends on x. It will have to be evaluated at the linearization

of the nonlinear equations and evaluated along the orbit. e.g. stablity of orbits do not look like constant anything. PC Thinks the Jacobian will work out somehow.

Part Two: Discussions from the Invariant Solns Meeting

Ignore the last third of the paper. The one thing PC doesn't understand, is that they are studying coupled Henon maps because they're invertible, but he doesn't understand why they care.

Uses the standard parameter values of Hénon

Fictitious time isn't important, the method is the method of Biham where they derive a cubic potential such that its derivative is the Hénon map.

The people who used coupled map lattices before Gutkin and Osipov, you always assumed weakly coupled with nearest neighbors, such that the coupling takes the form of the Laplacian.

Gutkin and Osipov, PC, impose a symmetry such that the coupling in time is the same as the coupling in space such that there is something like Helmholtz equation in space-time.

The coupling is what determines the type of behavior here, in the weak coupling limit, everything looks unstable on its own, but when the coupling is strong The model is then determined to be an ergodic model, because it is fully developed due to the length scale imposed but no laminar patches (No point where there are a different number of unstable directions).

If we write it carefully, take a Hamiltonian map, rewrite in terms of Beltrami operator (Laplacian with metric). Looking at this operator, its bilinear in derivative, but the derivatives have different weights and can have opposite signs.

Elliptic structure in PC's case, but thinks the Hénon there should be a negative sign.

If you have a spatially periodic chain, (they still think of a chain in space evolved in time, but they change this in the future). They say if you have periodic lattice, you should use Bloch theorem, which is what is done in condensed matter. They write the Bloch theorem, but we don't know why. PC believes it may be because the coupling is weak, so deformations are long wavelength deformations.

Explicitly the stretching parameter, changed from small to large, the problem becomes hyperbolic and sines and cosines change to hyperbolic sines and cosines.

In order to rewrite the equations in one variable that has a spatiotemporal Beltrami operator, we need to modify (10.19). First we write the set of equations as two step recurrence in one variable,

$$x^j_{n+1} + bx^j_{n-1} = 1 - a((1+\epsilon)x^j_n + \frac{\epsilon}{2}(x^{j+1}_n + x^{j-1}_n))^2\,, \tag{10.20}$$

Then we can add and subtract $2x_n^j$ to the LHS of the equation,

$$(\Box\_t - 2)x_n^j = 1 - a((1+\epsilon)x_n^j + \frac{\epsilon}{2}(x_n^{j+1} + x_n^{j-1}))^2\,, \tag{10.21}$$

Because the quadratic nonlinearity is where the spatial part of the Beltrami or Laplacian is, I don't know how to get around this and combine space and time currently. I recall Predrag mentioning something about a square root but it doesn't seem very well motivated because the spatial coupling is completely separated from time coupling unless I'm missing some type of approximation.

2017-11-08 Matt Discussed with Predrag differences between my spatiotemporal code and Jianke Yang's code with Predrag, also about what to do for [53] coupled Hénon maps.

2018-01-20 Predrag Akila, Waltner, Gutkin, Braun and Guhr [3] *Collectivity and periodic orbits in a chain of interacting, kicked spins* is presumably closely related to [2] *Semiclassical prediction of large spectral fluctuations in interacting kicked spin chains*, see **2017-10-10 Boris** post above.

2018-01-20 Predrag Catnipping is taking a delirious turn. Axenides, Floratos and Nicolis [8] *The quantum cat map on the modular discretization of extremal black hole horizons* write: " We present a toy model for the chaotic unitary evolution of infalling black hole horizon single particle wave packets. We construct explicitly the eigenstates and eigenvalues for the single particle dynamics for an observer falling into the BH horizon, with time evolution operator the quantum Arnol'd cat map (QACM). Using these results we investigate the validity of the eigenstate thermalization hypothesis (ETH), as well as that of the fast scrambling time bound (STB). We find that the QACM, while possessing a linear spectrum, has eigenstates which are random and satisfy the assumptions of the ETH. We also find that the thermalization of infalling wave packets in this particular model is exponentially fast, thereby saturating the STB, under the constraint that the finite dimension of the single–particle Hilbert space takes values in the set of Fibonacci integers. "

2018-02-06 Predrag A job candidate Glen Evenbly talked about "Tensor Networks", (also known as "birdtracks", but getting a citation out of computer nerds who do it is harder than pulling teeth - at best I can pass under "Penrose diagrams"). If you want to see a lot of non-birdtracky pictures, Román Orús has them. Basically, if you are solving a 1D lattice problem, the transfer operator is a matrix. However, if you are acting on a 2D or higher lattice, the transfer operator has pairs of more indices replacing each index ow the 1D matrix, hence "tensor." We need to understand that as we go from cat map Toeplitz matrices to their d-dimensional generalizations.

2018-03-28 Predrag Plasma physicists Xiao *et al.* [67] *A lattice Maxwell system with discrete space-time symmetry and local energy-momentum conservation*, arXiv:1709.09593 might of interest to us. By 'Maxwell' they mean EM on a discrete spacetime lattice. Their system has gauge symmetry, symplectic structure and discrete space-time symmetry. They generalized Noether's theorem to discrete symmetries for the lattice Maxwell system, and the system is shown to admit a discrete local energy-momentum conservation law corresponding to the discrete space-time symmetry. These conservation laws make the discrete system an effective algorithm for numerically solving the governing differential equations on continuous space-time.

There is also Stern *et al.* [60] *Geometric computational electrodynamics with variational integrators and discrete differential forms*, They write: " We develop a structure-preserving discretization of the Lagrangian framework for electrodynamics, combining the techniques of variational integrators and discrete differential forms. This leads to a general family of variational, multisymplectic numerical methods for solving Maxwell's equations that automatically preserve key symmetries and invariants. We generalize the Yee scheme to unstructured meshes in 4-dimensional spacetime, which relaxes the need to take uniform time steps or even to have a preferred time coordinate. We introduce a new asynchronous variational integrator (AVI) for solving Maxwell's equations. These results are illustrated with some prototype simulations that show excellent numerical behavior and absence of spurious modes. "

2018-04-05 Boris You show that your Adler-Weiss (Markov) partition can be used to get position of the points in the phase space by linear transformation. So your partiton is good on both fronts = simple grammar rules + easy walk from phase space to symbolic representation and back (as opposed to the linear code of Percival-Vivaldi, where only the second part is true).

Q: Was it known already (I mean simple connection between phase space and symbolic dynamics for Adler Weiss partitions)?

2018-04-08 Predrag The generating partition of figure 5.4 is new.

Newer still is the generating partition of figure 5.16 (a) which incorporates the invariance of the cat map dynamics (1.8) under spatial reflection flip across the $x_1 = -x_0$ anti-diagonal, together with $m_n \to -m_n$ time reversal symmetry, so the full symmetry is $C_2 \times C_2$. This should lead to very simple symbolic dynamics, but sect. 5.3 *Reduction to the fundamental domain* has still to be completed.

2018-04-05 Boris Start from e.g., 5 letter alphabet, then translate admissible sequences (from the transition graph) into tree letter (-1,0,1) LINEAR alphabet (1.9), and use Green's function to get to the phase space points. Right?

2018-04-08 Predrag As explained in ChaosBook.org, in symmetry reduction the *links* of such graphs are not labelled arbitrarily, they have a precise group-theoretic meaning.

Figure 5.4 (d) indeed has 5 links (I prefer not use an arbitrary 'alphabet' to label them), but the important thing is that the links correspond to the symmetry group elements; they enable you to reconstruct from a walk on the torus the corresponding walk in the space tiled by the copies of the torus. In the symmetry reduction of dynamical systems we call that "reconstruction equations". It is these group elements (5.22), (5.23), etc., that are the *alphabet*, as explained in ChaosBook diffusion chapter, and the preceding chapters that deal with discrete symmetry reduction (like the 3-disk billiard).

To repeat: we are reducing translational symmetry. Hence the alphabet are the group elements that reduce global motions to the elementary cell, in this case our 2-rectangle partition.

2018-04-05 Boris If linear refers to linear connection between symbol sequences and phase space points (my definition) then your three letter code is indeed linear, but (probably) not the original 5-letter one.

2018-04-08 Predrag What code? There is no "original 5-letter" code... Maybe you mean link labels in the (5.21) calculation? That just looks like clumsy notation to me. Writing down a transition graph with 5 nodes corresponding to such 'alphabet' would be a mess, I did not do it.

2018-04-05 Boris I would say that under any Adler-Weiss looms a linear code

2018-04-08 Predrag I think so too. While the canonical Thom-Arnol'd cat map (1.1) and the Percival-Vivaldi [48] two-configuration representation (1.5) are related by the anti-symplectic transformation (5.5), the Thom-Arnol'd cat map seems clumsier, as it seems to require 2D translations in figure 1.1 to return subpartitions back into the 2-rectangle partition (have not bothered to work that out). Still a linear code.

2018-04-05 Boris Adler-Weiss code is not linear on its own. Agree?

2018-04-08 Predrag I agree - I have never seen it recast in the group-theoretic symbolic dynamics. Percival-Vivaldi [48] do discuss Adler-Weiss, and do write down the 1D damped Poisson and 1D Green's functions, but they never saw that Adler-Weiss could be combined with their linear code. Would sure have saved a ton of needless work in the subsequent literature.

2018-04-05 Boris The biggest question to me what are you doing/going to do in $d = 2$ case. For me, Adler-Weiss partitions can be (probably) turned to 1D linear code (with a huge alphabet), but not to the 2D linear code. Right, Wrong?

2018-04-08 Predrag Wrong. Why would one turn $d = 2$ Adler-Weiss into 1D linear code? For finite spatial periodicity L that would be stupid, and for $L \to \infty$ (the subject of these papers) impossible. No, for $d = 2$ one has to partition the 4D invariant 2-torus partition hypercube. I'm optimistic about us being able to accomplish that. Symmetries should help. The stupid Percival-Vivaldi [48] hypercube is already working (see Han's examples (5.58), etc.), now we have to find a generating partition.

Just get cracking :)

2017-12-18 Predrag More seriously, what is wrong with the argument so far?

I used the Hamiltonian, evolution-in-time thinking to generate the $d = 1$ generating partition. That will not work in higher dimensions, so the above argument has to be recast in the Lagrangian form.

In principle, it is just a discrete Legendre transform, see sect. 1.4 *Generating functions; action*, but I do not see it yet...

2018-04-05 Boris

2018-04-08 Predrag

2018-04-05 Boris

2017-09-30 Predrag Cats rule.

References

[1] V. S. Afraimovich and Y. B. Pesin, "Hyperbolicity of infinite-dimensional drift systems", Nonlinearity **3**, 1–19 (1990).

[2] M. Akila, B. Gutkin, P. Braun, D. Waltner, and T. Guhr, Semiclassical prediction of large spectral fluctuations in interacting kicked spin chains, 2017.

[3] M. Akila, D. Waltner, B. Gutkin, P. Braun, and T. Guhr, "Collectivity and periodic orbits in a chain of interacting, kicked spins", Acta Phys. Pol. A **132**, 1661–1665 (2017).

[4] M. Akila, D. Waltner, B. Gutkin, P. Braun, and T. Guhr, "Semiclassical identification of periodic orbits in a quantum many-body system", Phys. Rev. Lett. **118**, 164101 (2017).

[5] J. M. Amigó, S. Zambrano, and M. A. F. Sanjuán, "Permutation complexity of spatiotemporal dynamics", Europhys. Lett. **90**, 10007 (2010).

[6] R. E. Amritkar, P. M. Gade, A. D. Gangal, and V. M. Nandkumaran, "Stability of periodic orbits of coupled-map lattices", Phys. Rev. A **44**, R3407–R3410 (1991).

[7] F. M. Atay, S. Jalan, and J. Jost, "Symbolic dynamics and synchronization of coupled map networks with multiple delays", Phys. Lett. A **375**, 130–135 (2010).

[8] M. Axenides, E. Floratos, and S. Nicolis, The quantum cat map on the modular discretization of extremal black hole horizons, 2017.

[9] F. Bagnoli, S. Isola, R. Livi, G. Martínez-Mekler, and S. Ruffo, Periodic orbits in a coupled map lattice model, in *Cellular Automata and Modeling of Complex Physical Systems: Proceedings of the Winter School, Les Houches 1989*, edited by P. Manneville, N. Boccara, G. Y. Vichniac, and R. Bidaux (Springer, Berlin, 1989), pp. 282–290.

[10] M. Baranger, K. T. R. Davies, and J. H. Mahoney, "The calculation of periodic trajectories", Ann. Phys. **186**, 95–110 (1988).

[11] J.-B. Bardet and G. Keller, "Phase transitions in a piecewise expanding coupled map lattice with linear nearest neighbour coupling", Nonlinearity **19**, 2193 (2006).

[12] V. N. Belykh and E. Mosekilde, "One-dimensional map lattices: Synchronization, bifurcations, and chaotic structures", Phys. Rev. E **54**, 3196–3203 (1996).

[13] N. B. Budanur and P. Cvitanović, "Unstable manifolds of relative periodic orbits in the symmetry-reduced state space of the Kuramoto-Sivashinsky system", J. Stat. Phys. **167**, 636–655 (2015).

[14] L. A. Bunimovich, V. Franceschini, C. Giberti, and C. Vernia, "On stability of structures and patterns in extended systems", Physica D **103**, 412–418 (1997).

[15] L. A. Bunimovich, R. Livi, G. Martínez-Mekler, and S. Ruffo, "Coupled trivial maps", Chaos **2**, 283–291 (1992).

[16] L. A. Bunimovich and Y. G. Sinai, "Spacetime chaos in coupled map lattices", Nonlinearity **1**, 491 (1988).

[17] S. Capobianco and T. Toffoli, Can anything from Noether's theorem be salvaged for discrete dynamical systems?, in *Unconventional computation: 10th international conference, uc 2011, turku, finland*, edited by C. S. Calude, J. Kari, I. Petre, and G. Rozenberg (Springer, Berlin, Heidelberg, 2011), pp. 77–88.

[18] Y.-C. Chen, S.-S. Chen, and J.-M. Yuan, "Topological horseshoes in travelling waves of discretized nonlinear wave equations", J. Math. Phys. **55**, 042701 (2014).

[19] S. Coppersmith, L. P. Kadanoff, and Z. Zhang, "Reversible Boolean networks I: distribution of cycle lengths", Physica D **149**, 11–29 (2001).

[20] R. M. D'Souza and N. H. Margolus, "Thermodynamically reversible generalization of diffusion limited aggregation", Phys. Rev. E **60**, 264–274 (1999).

[21] K. R. Elder, H. Xi, M. Deans, and J. D. Gunton, "Spatiotemporal chaos in the damped Kuramoto-Sivashinsky equation", AIP Conf. Proc. **342**, 702–708 (1995).

[22] T. Engl, J. Dujardin, A. Argüelles, P. Schlagheck, K. Richter, and J. D. Urbina, "Coherent backscattering in Fock space: A signature of quantum many-body interference in interacting bosonic systems", Phys. Rev. Lett. **112**, 140403 (2014).

[23] T. Engl, J. D. Urbina, Q. Hummel, and K. Richter, "Complex scattering as canonical transformation: A semiclassical approach in Fock space", Ann. Phys. **527**, 737–747 (2015).

[24] B. Fernandez, "Breaking of ergodicity in expanding systems of globally coupled piecewise affine circle maps", J. Stat. Phys. **154**, 999–1029 (2014).

[25] C. Foias, O. Manley, R. Témam, and Y. Treve, "Asymptotic analysis of the Navier-Stokes equations", Physica D **9**, 157–188 (1983).

[26] E. Fontich, R. de la Llave, and P. Martín, "Dynamical systems on lattices with decaying interaction I: A functional analysis framework", J. Diff. Equ. **250**, 2838–2886 (2011).

[27] P. M. Gade and R. E. Amritkar, "Spatially periodic orbits in coupled-map lattices", Phys. Rev. E **47**, 143–154 (1993).

[28] C. Giberti and C. Vernia, "Normally attracting manifolds and periodic behavior in one-dimensional and two-dimensional coupled map lattices", Chaos **4**, 651–663 (1994).

[29] J. F. Gibson, J. Halcrow, and P. Cvitanović, "Visualizing the geometry of state-space in plane Couette flow", J. Fluid Mech. **611**, 107–130 (2008).

[30] P. Grassberger, "Information content and predictability of lumped and distributed dynamical systems", Phys. Scr. **40**, 346 (1989).

[31] P. Grassberger, H. Kantz, and U. Moenig, "On the symbolic dynamics of Hénon map", J. Phys. A **22**, 5217–5230 (1989).

[32] V. M. Gundlach and D. A. Rand, "Spatio-temporal chaos. I. Hyperbolicity, structural stability, spatio-temporal shadowing and symbolic dynamics", Nonlinearity **6**, 165 (1993).

[33] B. Gutkin, L. Han, R. Jafari, A. K. Saremi, and P. Cvitanović, Linear encoding of the spatiotemporal cat map, In preparation, 2018.

[34] B. Gutkin and V. Osipov, "Classical foundations of many-particle quantum chaos", Nonlinearity **29**, 325–356 (2016).

[35] P. E. Hydon and E. L. Mansfield, "Extensions of Noether's Second Theorem: from continuous to discrete systems", Proc. R. Soc. London A **467**, 3206–3221 (2011).

[36] S. Isola, A. Politi, S. Ruffo, and A. Torcini, "Lyapunov spectra of coupled map lattices", Phys. Lett. A **143**, 365–368 (1990).

[37] M. Jiang, "Equilibrium states for lattice models of hyperbolic type", Nonlinearity **8**, 631 (1995).

[38] S. Lepri, A. Politi, and A. Torcini, "Chronotopic Lyapunov analysis. I. A detailed characterization of 1D systems", J. Stat. Phys. **82**, 1429–1452 (1996).

[39] X. Li, Y. Xue, P. Shi, and G. Hu, "Lyapunov spectra of coupled chaotic maps", Int. J. Bifur. Chaos **18**, 3759–3770 (2008).

[40] R. Livi, G. Martínez-Mekler, and S. Ruffo, "Periodic orbits and long transients in coupled map lattices", Physica D **45**, 452–460 (1990).

[41] A. de Maere, "Phase transition and correlation decay in coupled map lattices", Commun. Math. Phys. **297**, 229–264 (2010).

[42] E. L. Mansfield, Noether's theorem for smooth, difference and finite element schemes, in Foundations of computational mathematics, santander 2005, Vol. 331, London Math. Soc. Lect. Notes (2006), pp. 230–254.

[43] D. Michelson, "Steady solutions of the Kuramoto-Sivashinsky equation", Physica D **19**, 89–111 (1986).

[44] J. C. Neu, "Coupled chemical oscillators", SIAM J. Appl. Math. **37**, 307–315 (1979).

[45] J. C. Neu, "Chemical waves and the diffusive coupling of limit cycle oscillators", SIAM J. Appl. Math. **36**, 509–515 (1979).

[46] B. Nicolaenko, "Some mathematical aspects of flame chaos and flame multiplicity", Physica D **20**, 109–121 (1986).

[47] D. Pazó, I. G. Szendro, J. M. López, and M. A. Rodríguez, "Structure of characteristic Lyapunov vectors in spatiotemporal chaos", Phys. Rev. E **78**, 016209 (2008).

[48] I. Percival and F. Vivaldi, "A linear code for the sawtooth and cat maps", Physica D **27**, 373–386 (1987).

[49] Y. B. Pesin and Y. G. Sinai, "Space-time chaos in the system of weakly interacting hyperbolic systems", J. Geom. Phys. **5**, 483–492 (1988).

[50] S. D. Pethel, N. J. Corron, and E. Bollt, "Symbolic dynamics of coupled map lattices", Phys. Rev. Lett. **96**, 034105 (2006).

[51] S. D. Pethel, N. J. Corron, and E. Bollt, "Deconstructing spatiotemporal chaos using local symbolic dynamics", Phys. Rev. Lett. **99**, 214101 (2007).

[52] A. Politi and G. P. Puccioni, "Invariant measure in coupled maps", Physica D **58**, 384–391 (1992).

[53] A. Politi and A. Torcini, "Towards a statistical mechanics of spatiotemporal chaos", Phys. Rev. Lett. **69**, 3421–3424 (1992).

[54] W.-X. Qin, "Bifurcations of steady states in a class of lattices of nonlinear discrete Klein-Gordon type with double-quadratic on-site potential", J. Phys. A **36**, 9865–9873 (2003).

[55] C. Reick and E. Mosekilde, "Emergence of quasiperiodicity in symmetrically coupled, identical period-doubling systems", Phys. Rev. E **52**, 1418–1435 (1995).

[56] K. Richter, *Semiclassical theory of mesoscopic quantum systems* (Springer, Berlin, 2000).

[57] D. Ruelle, "Some comments on chemical oscillations", Trans. N. Y. Acad. Sci. **35**, 66–71 (1973).

[58] D. Ruelle, "Large volume limit of the distribution of characteristic exponents in turbulence", Commun. Math. Phys. **87**, 287–302 (1982).

[59] M. Schmitt, "Spectral theory for nonanalytic coupled map lattices", Nonlinearity **17**, 671 (2004).

[60] A. Stern, Y. Tong, M. Desbrun, and J. E. Marsden, Geometric computational electrodynamics with variational integrators and discrete differential forms, in *Geometry, Mechanics, and Dynamics: The Legacy of Jerry Marsden*, edited by D. E. Chang, D. D. Holm, G. Patrick, and T. Ratiu (Springer, New York, 2015), pp. 437–475.

[61] L.-S. Sun, X.-Y. Kang, Q. Zhang, and L.-X. Lin, "A method of recovering the initial vectors of globally coupled map lattices based on symbolic dynamics", Chin. Phys. B **20**, 120507 (2011).

[62] K. Takeuchi and M. Sano, "Role of unstable periodic orbits in phase transitions of coupled map lattices", Phys. Rev. E **75**, 036201 (2007).

[63] T. Toffoli and N. H. Margolus, "Invertible cellular automata: A review", Physica D **45**, 229–253 (1990).

[64] D. S. Tourigny, Networks of planar Hamiltonian systems, 2017.

[65] V. L. Volevich, "Kinetics of coupled map lattices", Nonlinearity **4**, 37–48 (1991).

[66] A. Weinstein, "Periodic nonlinear waves on a half-line", Commun. Math. Phys. **99**, 385–388 (1985).

[67] J. Xiao, H. Qin, Y. Shi, J. Liu, and R. Zhang, A lattice Maxwell system with discrete space-time symmetry and local energy-momentum conservation, 2017.

[68] Q. Zhilin, A. Gangal, M. Benkun, and T. Gang, "Spatiotemporally periodic patterns in symmetrically coupled map lattices", Phys. Rev. E **50**, 163–170 (1994).